HYDROLOGICAL RESPONSE OF A PREFERENTIAL INFILTRATION DOMINATED NATURAL HILLSLOPE IN BRAHMAPUTRA RIVER BASIN

Thesis Submitted to the
Indian Institute of Technology Guwahati
for the award of the degree of

Doctor of Philosophy
in
Civil Engineering

By

Rupak Sarkar

Department of Civil Engineering
Indian Institute of Technology Guwahati
Guwahati, Assam – 781039, INDIA

DECEMBER 2011

Dedicated
to
The People of Northeast India

INDIAN INSTITUTE OF TECHNOLOGY GUWAHATI
Guwahati, Assam, India- 781039
Department of Civil Engineering

CERTIFICATE

This is to certify that the thesis entitled **"Hydrological Response of a Preferential Infiltration Dominated Natural Hillslope in Brahmaputra River Basin"** submitted by Rupak Sarkar, Roll No. 06610405 to the Indian Institute of Technology Guwahati, for the award of the degree of Doctor of Philosophy in Civil Engineering is a record of bonafide research work carried out by him under my supervision and guidance. The thesis work, in my opinion, has reached the requisite standard fulfilling the requirement for the degree of Doctor of Philosophy.

The results contained in this thesis have not been submitted in part or full to any other University or Institute for award of any degree or diploma.

(Dr. Subashisa Dutta)
Associate Professor
Department of Civil Engineering
Indian Institute of Technology Guwahati
Guwahati, Assam - 781039, INDIA.

December, 2011

INDIAN INSTITUTE OF TECHNOLOGY GUWAHATI
Guwahati, Assam, India- 781039
Department of Civil Engineering

STATEMENT

I do hereby declare that the matter embodied in this thesis is the result of investigations carried out by me in the Department of Civil Engineering, Indian Institute of Technology Guwahati, Guwahati, Assam, India.

In keeping with the general practice of reporting scientific observations, due acknowledgements have been made wherever the work described is based on the findings of other investigators.

December, 2011

(RUPAK SARKAR)
Department of Civil Engineering
Indian Institute of Technology Guwahati
Guwahati, Assam - 781039, INDIA.

ACKNOWLEDGEMENTS

Every progressive effort in this world is supported by many people. Acknowledgement for a few might be a trifle thing written on a piece of paper. Nevertheless, here I get a great opportunity to express my token of thanks to people who in a way, helped and supported me during the course of this investigation.

I express my deepest sense of gratitude and veneration to my supervisor Dr. Subashisa Dutta, Associate Professor, Department of Civil Engineering, Indian Institute of Technology (IIT) Guwahati, for his meticulous guidance, constructive suggestions, and sustained interest and patience throughout the present investigation.

It is my sublime duty to express my deepest sense of reverence and indebtedness to the Chairman of my Doctoral Committee Dr. S. Sreedeep, Assistant Professor, Department of Civil Engineering, Indian Institute of Technology (IIT) Guwahati, for his constant encouragement and indelible inspiration provided during the study.

I express my sincere thanks to the members of my Doctoral Committee Dr. G. Barua, Associate Professor, Department of Civil Engineering, Indian Institute of Technology (IIT) Guwahati, and Dr. S.K. Dwivedy, Professor, Department of Mechanical Engineering, Indian Institute of Technology (IIT) Guwahati, for their valuable suggestions, eternal encouragements, and timely help provided at various stages of the investigation and compilation of thesis.

Sincere thanks are due to Dr. S. Nandi, Dean, Academic Affairs, Dr. P.S. Robi, Dean, Research and Development, and Dr. S.K. Deb, Head, Department of Civil Engineering, Indian Institute of Technology (IIT) Guwahati, for providing necessary facilities towards successful completion of this endeavor.

This research work has been financially supported by the Remote Sensing Application Mission (RSAM) programme under the Department of Space (DOS), India. I express my sincere thanks to Dr. S. Panigrahy and Dr. J. S. Parihar, Space Applications Centre (SAC), Indian Space Research Organization (ISRO), Ahmedabad, India.

My abstruse regard goes to the administration of my present institute of employment Uttar Banga Krishi Viswavidyalaya, Cooch Behar, India, for allowing me to complete this research.

Thanks are due to all my colleagues, without whose support this work could not have been completed. I hereby acknowledge all the project staffs and the students of Department of Civil Engineering, Indian Institute of Technology (IIT) Guwahati, for their sincere help and assistance provided during the field experiments and data

collection. I am especially thankful to Mr. Amit Dubey, Research Scholar of Department of Civil Engineering, IIT Guwahati, for his help extended to me during the compilation of the thesis.

It is often said good friends are rare to get. In this context I find myself very lucky to have friends like Kamal, Zela, Minaxi, Sandip, Albino, and Sachin. Their friendly affection, timely help, and encouragements never let me feel away from home during my stay at the institute. Words of appreciation are also due for all the fellow members of my IIT Guwahati soccer team. Those moments of victory and defeat are truly unforgettable.

It is not possible to express in words the inspiration from my brother and the noble sacrifice of my parents, whose invaluable love and support have brought me to this position. Last, but not the least, I would like to convey my special thanks and love to my wife Sumita for all her support, patience, and encouragements.

This list is obviously incomplete, but let me submit that the omissions are inadvertent and I once again record my deep felt gratitude to all those who have cooperated with me either directly or indirectly in this endeavor.

IIT Guwahati (RUPAK SARKAR)
December, 2011

TABLE OF CONTENTS

CHAPTER		PAGE No.
	Table of Contents	I
	List of Figures	IV
	List of Tables	VIII
	Abstract	X
	Organization of the Thesis	XII
1.	INTRODUCTION	**1-4**
	1.1 Overview	1
	1.2 Objectives	3
2.	REVIEW OF LITERATURE	**5-33**
	2.1 Infiltration	5
	2.1.1 Water infiltration and soil macroporosity	8
	2.2 Subsurface Water Flow through Soil Macropores	10
	2.3 Overland Flow on Hillslopes	13
	2.4 Subsurface Water Movement	15
	2.4.1 Soil moisture storage and its distribution on hillslopes	16
	2.4.2 Characterization of soil macropores using dye and tracers	18
	2.4.3 Subsurface stormflow	20
	2.4.4 Lateral preferential flow	27
	2.5 Conclusion	31
3.	EXPERIMENTAL INVESTIGATIONS	**34-96**
	3.1 Hillslope Experimental Site	34
	3.2 Soil, Vegetation, and Climate	36
	3.3 Design of the Experimental Setup	37
	3.3.1 Limitations of the sheet flow generation system	40
	3.4 Measurement of Infiltration	43
	3.4.1 Double ring infiltrometer tests	43

3.4.2 Estimation of infiltration from runoff plot experiments 49
3.5 Characterization of Soil Macropores 51
3.5.1 Experimental setup and methodology 52
3.5.2 Image analyses 55
3.5.2.1 Horizontal dye pattern analysis 56
Results of horizontal dye pattern analysis 58
3.5.2.2 Vertical dye pattern analysis 58
Results of vertical dye pattern analysis 59
3.6 Subsurface Soil Moisture Monitoring System 63
3.6.1 Calibration of the profile probe soil moisture meter 63
3.6.2 Study of soil moisture profile in the hillslope plot 66
3.7 Observation of Overland Flow in the Hillslope Plot 73
3.7.1 *In situ* overland flow experiments 73
3.7.1.1 Experimental results of overland flow 74
3.7.2 Observation of overland flow under natural storm events 80
3.7.2.1 Observational setup and instruments 80
3.7.2.2 Runoff generation from the hillslope plot 81
3.7.2.3 Evaluation of the inflow intensity-infiltration rate relationship 86
3.8 Experimental Evidences of Lateral Subsurface Flow 88
3.9 Summary of the Chapter 93

4. MATHEMATICAL MODELING **97-134**

4.1 Overland Flow Modeling 97
4.1.1 Description of the model 97
4.1.2 Overland flow model simulations 101
4.2 Modeling Lateral Subsurface Stormflow 107
4.2.1 Physical concept of the model 108
4.2.2 Mathematical formulation of subsurface stormflow 110
4.2.3 Computation of macropore flow 111
4.2.4 Numerical solution of subsurface stormflow 112
4.2.5 Simulations of the subsurface stormflow model 116

4.2.5.1 Design of soil macropore structure through simulations 117
4.3 Summary of the Chapter 127

5. MODEL APPLICATIONS IN DIFFERENT HILLSLOPE TYPES **135-156**

5.1 Different Types of Hillslopes 135
5.2 Overland Flow Behavior on Hillslopes 137
5.2.1 Effect of relief on overland flow 142
5.2.2 Overland flow in non-macroporous soil 142
5.3 Subsurface Stormflow from Hillslopes 146
5.3.1 Effect of relief on subsurface stormflow 150
5.3.2 Effect of changing lateral macroporosity on subsurface stormflow 151
5.4 Summary of the Chapter 152

6. SUMMARY AND CONCLUSIONS **157-173**

6.1 Summary 157
6.2 Major Conclusions 169
6.3 Scopes for Future Research 172

APPEXDIX 1 **174-190**

REFERENCES **191-209**

LIST OF RELEVANT PUBLICATIONS **210-211**

LIST OF FIGURES

FIGURES	PAGE No.
Chapter 3: Experimental Investigations	
Fig. 3.1 Hillslope experimental plot	35
Fig. 3.2 Map of Brahmaputra River basin	35
Fig. 3.3 Digital elevation map of the experimental plot	35
Fig. 3.4 Schematic diagram of the experimental setup	39
Fig. 3.5 Intensity-Frequency-Duration (IFD) curves of the stations (a) Lakhimpur and (b) Guwahati	42
Fig. 3.6 Double ring infiltrometer	44
Fig. 3.7 Vertical water front movement	44
Fig. 3.8 Infiltration curve obtained from a plane agricultural land having no macroporosity in soil	44
Fig. 3.9 Infiltration measurement points in the hillslope plot	46
Fig. 3.10 Double ring infiltrometer test for dry soil condition	46
Fig. 3.11 Double ring infiltrometer test under wet antecedent condition	47
Fig. 3.12 Spatial variation of recharge for dense vegetation and wet soil condition	48
Fig. 3.13 Infiltration rate from runoff plot experiments under different conditions	50
Fig. 3.14 Collection of soil columns from the plot	54
Fig. 3.15 Laboratory setup for conducting dye infiltration experiments	54
Fig. 3.16 Image correction and classification for a horizontal section	57
Fig. 3.17 Digitally processed images of undisturbed hillslope soil at different depths	57
Fig. 3.18 Depth wise dye coverage distribution of the two soil columns	58
Fig. 3.19 Object width and stained path width (SPW) of dye patterns	60
Fig. 3.20 Depth wise distribution of number of stained paths	62
Fig. 3.21 Correlation of volume density with maximum SPW and number of stained paths	62
Fig. 3.22(a-c) Delta-T soil moisture meter (Type HH2)	64
Fig. 3.23 Schematic diagram of the experimental setup and instrumentation in the hillslope plot	64
Fig. 3.24 Calibration of the profile probe sensors at different soil depths	67

Fig. 3.25(a-d) Temporal variations in soil moisture contents at different depths (b.g.l.) in the hillslope plot during and immediately after runoff experiment 68-69

Fig. 3.26 (a-d) Temporal variations in soil moisture contents at different depths (b.g.l.) in the hillslope plot for prolonged duration after runoff experiment 70-71

Fig. 3.27(a-h) Measured subsurface soil moisture profiles of the hillslope plot at different time steps 72-73

Fig. 3.28(a-f) Outflow hydrographs from the hillslope plot for the overland flow experiments conducted under different conditions 76

Fig. 3.29 Variation of time of concentration (t_c) with inflow intensity (i) 78

Fig. 3.30 Observed runoff coefficients for the overland flow experiments 78

Fig. 3.31 Variation of preferential infiltration rate (f_b) with inflow intensity (i) 79

Fig. 3.32 Scatter plot of total rainfall depth and 7 days API for the year 2010 85

Fig. 3.33 Scatter plot of total rainfall depth and 7 days API for the year 2009 85

Fig. 3.34 Scatter plot of total rainfall depth and 7 days API for the year 2008 85

Fig. 3.35 Scatter plot of maximum rainfall intensity and 7 days API for the year 2010 87

Fig. 3.36 Scatter plot of maximum rainfall intensity and 7 days API for the year 2009 87

Fig. 3.37 Scatter plot of maximum rainfall intensity and 7 days API for the year 2008 87

Fig. 3.38 Observed and estimated hydrographs for the 1st storm event of 12-07-2010 89

Fig. 3.39 Observed and estimated hydrographs for the 2nd storm event of 12-07-2010 89

Fig. 3.40 Location of the piezometers in the experimental plot 91

Fig. 3.41(a-e) Temporal variation of water table depths above impermeable layer observed at different piezometer locations for the experiment E-12 91-92

Chapter 4: Mathematical Modeling

Fig. 4.1 Estimation of Manning's roughness coefficient from model simulations 100

Fig. 4.2(a-f) Observed and overland flow model simulated outflow hydrographs from the hillslope plot for some of the experiments 102

Fig. 4.3(a-c) Variation of simulated overland flow depths for different inflow intensities for moderate vegetation condition of the plot 103-104

Fig. 4.4 Flow accumulation of the experimental hillslope plot 104

Fig. 4.5 Variation of Manning's roughness coefficient (n) with inflow intensity (i) 106

Fig. 4.6(a-b) Definition sketch of a uniform hillslope and its soil moisture capacity; (c) Section A-A' and (d) section B-B' showing the subsurface formations of the hillslope soil 109

Fig. 4.7(a-f) Observed and simulated temporal variations of saturated depth for Set III of the experiment E-12 with f_{avg}= 0.139 m/hr continued for 0.8 hr 119

Fig. 4.8 Temporal variations in no. of hydrologically active macropores with different macropore structures for the experiment E-12 120

Fig. 4.9 Hydrologically active macropores at different time steps with the macropore structures Set III, Set V, and Set VI for the experiment E-12 122

Fig. 4.10 Variation in hydrologically active macropores with time due to change in macropore diameter for the experiment E-12 122

Fig. 4.11 Maximum no. of hydrologically active macropores for different rates of recharge 124

Fig. 4.12 Computed subsurface flow hydrographs through soil matrix and macropores for the experiment E-12 125

Fig. 4.13 Contribution of preferential flow in subsurface stormflow hydrograph for different rates of recharge 126

Fig. 4.14 Peak rate of macropore flow as a function of average rate of recharge 126

Fig. 4.15 Peak rate of soil matrix flow as a function of average rate of recharge 127

Chapter 5: Model Applications in Different Hillslope Types

Fig. 5.1 (a-c) Three different types of hillslope profiles 138

Fig. 5.2 Overland flow hydrographs for the Type 1 hillslope at different intensities 140

Fig. 5.3 Overland flow hydrographs for the Type 2 hillslope at different intensities 140

Fig. 5.4 Overland flow hydrographs for the Type 3 hillslope at different intensities 140

Fig. 5.5 Overland flow hydrographs for H = 10 m and i = 150 mm/hr 143

Fig. 5.6 Overland flow hydrographs for non-macroporous soil (Type 2 hillslope) 144

Fig. 5.7 Overland flow hydrographs for non-macroporous soil (Type 3 hillslope) 145

Fig. 5.8 Macropore flow hydrographs for the Type 1 hillslope 148
Fig. 5.9 Macropore flow hydrographs for the Type 2 hillslope 148
Fig. 5.10 Macropore flow hydrographs for the Type 3 hillslope 148
Fig. 5.11 Matrix flow hydrographs for the Type 1 hillslope 149
Fig. 5.12 Matrix flow hydrographs for the Type 2 hillslope 149
Fig. 5.13 Matrix flow hydrographs for the Type 3 hillslope 149

LIST OF TABLES

TABLES	PAGE No.
Chapter 2: Review of Literature	
Table 2.1 Some definitions of soil macropores and macroporosity	11
Chapter 3: Experimental Investigations	
Table 3.1 Soil profile data of the experimental plot	38
Table 3.2 Different vegetation conditions of the study plot	38
Table 3.3 Design specifications of the experimental setup	39
Table 3.4 Summary of the results of double ring infiltrometer tests	47
Table 3.5 Measured steady infiltration rates in the plot for dense vegetation and wet antecedent conditions	47
Table 3.6 Results of runoff plot experiments	50
Table 3.7 Distribution of average volume density with SPW at a particular transect	61
Table 3.8 Summary of the *in situ* overland flow experiments conducted	74
Table 3.9 Details of the overland flow experiments conducted	75
Table 3.10 Relationships of t_c with inflow intensity (i)	80
Table 3.11 Relationships of f_b with inflow intensity (i)	80
Table 3.12 Description of the observed storm events for the year 2008	82
Table 3.13 Description of the observed storm events for the year 2009	82
Table 3.14 Description of the observed storm events for the year 2010	83
Table 3.15 Experiments conducted for capturing lateral subsurface flow from the hillslope plot (April-May, 2007)	90
Chapter 4: Mathematical Modeling	
Table 4.1 Simulations of the overland flow model for the hillslope plot	105
Table 4.2 Relationships of n with inflow intensity (i)	106
Table 4.3 Computation of average saturated depth in the piezometers at different transects (Fig. 3.40) for the experiment E-12	114-115
Table 4.4 Random soil macropore structures assumed for the experiment E-12	118
Table 4.5 Values of computed performance index at various time steps for different macropore structures	118

Table 4.6 The details of the subsurface runoff experiments conducted on the hillslope 124

Chapter 5: Model Applications in Different Hillslope Types

Table 5.1 Different combinations of possible hillslope types 136

Table 5.2 Three selected hillslope types and their plan and profile parameters 137

Table 5.3 Average preferential infiltration rates for different rainfall intensities 139

Table 5.4 Comparison of overland flow hydrographs for different hillslope types 141

Table 5.5 Effect of change in relief on overland flow hydrographs for i = 150 mm/hr 143

Table 5.6 Peak discharge and saturated depth for non-macroporous hillslope soils 145

Table 5.7 Hydraulically effective soil macroporosity for different rainfall rainfall intensities 147

Table 5.8 Maximum depth of water table above the impermeable bed 150

Table 5.9 Occurrence of saturation excess overland flow with no lateral macropores 151

Table 5.10 Effect of change in relief on matrix flow hydrographs for i = 150 mm/hr 151

Table 5.11 Effect of change in soil macroporosity on subsurface flow 152

ABSTRACT

In Brahmaputra river basin, where the hillslopes are characterized by high degree of soil macroporosity and the area receives extreme rainfall events frequently during the monsoon seasons, rapid lateral preferential flow from the adjacent hilly areas often triggers devastating flash floods in the rivers. Using experimental data and physically based semi-distributed hydrological models, the present study has characterized the overland flow and subsurface stormflow behavior on a macropore dominated vegetated hillslope plot. The plot was instrumented with profile probe soil moisture meter and piezometers for monitoring spatial and temporal variations in soil water contents. Soil moisture storage, movement, and distribution patterns indicated rapid preferential flow behavior of the hillslope soil. It was found that once the soil was saturated, it remained at field capacity for the following 2-3 days. Such antecedent wet conditions are extremely favorable for rapid stormflow generation from hillslopes. Dye infiltration tests were also conducted with undisturbed soil columns collected from the hillslope plot. Form the digital image processing of the observed dye patterns high degree of macroporosity throughout the soil profile was evident. It was also found that 1-2 mm diameter macropores, developed mainly by plant roots, dominated the soil profile. Due to high macroporosity of the hillslope soil point scale infiltration measurements showed significant effect of scale over plot scale measurements.

A simple sheet flow generation system was used to capture the overland flow characteristics on the hillslope plot with some approximation of natural rainfall condition in terms of variation of overland flow depth along the slope length. At the hillslope scale, the relationship between rainfall intensity and preferential infiltration rate was found to be linear, but there was power relation between Manning's roughness coefficient and rainfall intensity. There were three major influences on overland flow: (i) preferential infiltration rate; (ii) rainfall intensity; and (iii) degree of vegetation.

A physical based numerical solution of the subsurface flow equations was given to develop a subsurface stormflow model. The model could be simulated for different user defined macropore structures of the soil. The model was calibrated using the measured experimental data from the hillslope plot. The subsurface stormflow model captured the observed spatial and temporal variations of saturated profile observed over the hillslope plot reasonably well. It was found that lateral

macropore flow dominated subsurface stormflow response from the hillslope. The results showed that the hydraulically effective or hydrologically active lateral macroporosity and peak rates of matrix and macropore flow were primarily controlled by the rate of recharge.

Different topographical shapes and bedrock profiles were found to have significant effect on surface and subsurface flow hydrographs of different theoretical hillslope types. In non-macroporous soils subsurface stormflow was not evident. Even under wet antecedent conditions, hillslope soils having very high lateral macroporosity did not produce any saturation excess overland flow under high intensity storm events. The impact of disturbing the lateral macroporosity of hillslope soil was significant on the surface and subsurface runoff generation processes of the hillslopes.

ORGANIZATION OF THE THESIS

The thesis of the present investigation comprises of six chapters. Chapter 1 contains a brief overview of the problem and the specific objectives taken for the study. Chapter 2 is focused towards understanding the relevant literatures to study the progress in hillslope hydrology. A brief assessment of the hydrological investigations carried out in the study area or in other parts of the world has been made to define the possible solution of the problem. Chapter 3 mainly documents the details of the experiments conducted in the hillslope plot. With the descriptions of the study area, experimental setup and procedures, measurements, and the types of instrumentations used in the hillslope plot the chapter also discusses and summarizes the experimental results. Chapter 4 outlines the mathematical modeling concepts of overland flow and subsurface stormflow. The details of the governing equations and solution techniques are mentioned here. The experimental results of the previous chapter have been used for theoretical concepts and calibration of the models. The chapter also presents the model simulated results, inter-comparisons, and reasoning with detailed discussions. Chapter 5 deals with application of the developed overland flow and subsurface stormflow models in different theoretical hillslope types to observe the behavioral changes in their hydrological response. Chapter 6 finally summarizes the results and lists the major conclusions derived from the present investigation. The scopes for future investigations in line of the present study have also been discussed.

CHAPTER 1 INTRODUCTION

1.1 Overview

The hydrological behavior of natural hillslopes controls both surface and subsurface response of hilly watersheds. The typical nature of hillslopes often causes many adverse situations like flash flooding, slope failures and slides, soil erosion, debris flow, etc. Rainfall-runoff processes in wet tropical and subtropical hilly watersheds mostly follow the concept of variable saturated area. However, infiltration excess runoff generation may also be evident in some cases. Under both the conditions, runoff generation is significantly influenced by storm characteristics, topographic characteristics (slope, length of slope, microtopography, etc.), permeability of the soil, and vegetation cover (Beven, 1981; Beven, 2000a; Liu and Singh, 2004). In humid region, subsurface flow primarily governs hillslope response because of the presence of both micropores and macropores in the soil (Kirkby, 1978). Infiltration rate into the soil is controlled by matrix flow through soil micropores and/or preferential flow through soil macropores, depending upon the hydraulic characteristics of soil layers and physical conditions prevailing in a natural hillslope. The preferential flow, considered as an equivalent flow through a network of non-capillary pores, is influenced by overland flow depth, vegetation characteristics, and antecedent moisture condition. When rainfall intensity exceeds the preferential infiltration rate, overland flow occurs. As a result, the characteristics of the overland flow and preferential infiltration through the soil are interdependent and are influenced by many other factors, such as degree of vegetation, microtopography, rainfall characteristics, etc. At the same time due to presence of dense network of macropores in the soil, the magnitude of subsurface stormflow, both in vertical as

well as lateral directions, can be quite significant in the hydrological response of the vegetated hillslopes.

The landscapes of north-eastern states of India are characterized by the mountains, along with the flood plains of river Brahmaputra. Being the eighth largest river of the world with an average annual runoff of about 510 billion m^3 (Subramanya, 1999), river Brahmaputra has a huge impact on the hydrology as well as the socio-economic status of the region. From the hydrologic point of view, the major sources of runoff and sediment load to the river Brahmaputra are the vast hillslope areas of its basin. These hillslopes generally have deep and permeable topsoil with an impermeable layer at a shallow depth (Vadivelu *et al*., 2004). Study of meteorological data of the region reveals that the area undergoes high intensity storm events quite frequently during the monsoon season (Soja and Starkel, 2007). In general, the hillslopes have dense vegetation cover with highly interconnected macropore network in the subsoil induced mainly by plant roots. A typical combination of all these factors produces less surface runoff with a dominating component of subsurface stormflow under very high intensity storm events over these hillslopes. Therefore, both the phenomena of shallow water overland flow and subsurface stormflow through preferential pathways are considered to be predominant and critical hydrological processes of the region. It is of prime importance to study the hydrological response of natural hillslopes in order to identify and analyze the controlling parameters of the most critical hydrological processes towards understanding the behavior of hillslope hydrology at a large scale, which is a rather complex phenomenon. Negi (2001) emphasized the need of micro-scale (plot scale) and meso-scale (watershed scale) studies in the Himalayan mountainous regions for a better understanding of the hydrological processes. But, no detailed hydrological

studies have been undertaken in the Brahmaputra basin to address the interdependence of overland flow, rainfall intensity, degree of vegetation, preferential infiltration rate, and subsurface stormflow through soil macropores. Keeping these in view, the present investigation has been taken up in the region to explore the hydrological behavior of a preferential infiltration dominated natural hillslope by combining *in situ* experiments with hydrological modeling.

1.2 Objectives

The specific objectives of the present investigation are listed as follows:

- To study the infiltration behavior in a macropore dominated vegetated hillslope soil and to assess the effect of scale on infiltration measurements by conducting point scale and plot scale experiments.
- To collect undisturbed soil columns from the hillslope plot for characterizing soil macroporosity by conducting dye tracer infiltration tests and applying subsequent image processing techniques.
- To design a sheet flow generation system for the experimental hillslope plot to study the overland flow and subsurface stormflow response under different high intensity artificial runoff events.
- To study the soil moisture storage, distribution, and movement in the macropore dominated hillslope soil before, during, and after the artificial runoff events.
- To monitor the overland flow response of the hillslope plot under natural storm events and to evaluate the validity of the experimentally developed rainfall-runoff relationships for natural rainfall events.
- To characterize overland flow behavior on the preferential infiltration dominated hillslope by coupling experimental data with semi-distributed

hydrological model and to study the nonlinear interdependence between overland flow characteristics and its controlling parameters.

- To develop a physically based hydrological model to simulate the subsurface stormflow response from the hillslope plot and to establish the nonlinear interdependency function of subsurface stormflow, lateral macroporosity, and rainfall intensity in relation with changing soil macropore connectivity.
- To study the effect of topographical shapes on the hydrological response of theoretical hillslopes using the functional relationships established from the field experiments and the semi-distributed hydrological modeling.

REVIEW OF LITERATURE

During the past few decades a number of researchers have contributed towards proper understanding of hillslope hydrology in different parts of the world. A number of theoretical and modeling investigations as well as field and laboratory experiments under either natural or artificial rainfall conditions have been carried out towards proper conceptualization of the hydrological behavior of hillslopes. This chapter is focused towards a brief discussion on the relevant research works carried out on different aspects of hillslope hydrology like infiltration, overland flow, soil macropores, preferential infiltation rate, and subsurface stormflow.

2.1 Infiltration

In hydrological modeling infiltration is considered to be an important factor as it controls the spatial and temporal partitioning of rainfall into surface and subsurface runoff and thus affects the subsequent movement in and between these two general components of hydrologic cycle. Several infiltration models have been developed and proposed for simulating infiltration under different conditions. A brief review of some of the popular infiltration models are discussed here.

Green and Ampt (1911) developed an infiltration equation based on the physical approximation that water infiltrates with a sharp wetting front and the soil behind the wetting front is saturated. Thus, the infiltration rate (I) can be written as

$$I = K\left[\frac{h_0 - (-\psi - L)}{L}\right] \tag{2.1}$$

where I is the infiltration rate (m/s), L is the depth of the wetting front below the ground surface (m), h_0 is the depth of ponded water (m), ψ is the soil suction head at the wetting front (m), and K is the vertical hydraulic conductivity (m/s) which is often

taken to be half of the saturated value, for use in the Green-Ampt equation. The wetting front suction is generally considered to be a constant for a given soil. Chow *et al*. (1988) tabulated the values of typical Green-Ampt parameters (ψ, K) for different soil textural classes.

Richards (1931) proposed a flow equation by combining mass balance on an elemental volume of porous media with Darcy's law. It is considered to be the fundamental governing equation for subsurface flow. The Richards equation in three dimensional form for homogeneous soil can be written as

$$\frac{\partial \theta}{\partial t} = \frac{\partial}{\partial x}\left[K(\psi)\frac{\partial h}{\partial x}\right] + \frac{\partial}{\partial y}\left[K(\psi)\frac{\partial h}{\partial y}\right] + \frac{\partial}{\partial z}\left[K(\psi)\frac{\partial h}{\partial z}\right] \tag{2.2}$$

where θ is the volumetric moisture content (cm^3/cm^3), h is the hydraulic head (cm), ψ is the soil suction head (cm), and $K(\psi)$ is the hydraulic conductivity (cm/s) function. In unsaturated soil, both ψ and K are a function of θ. Defining *specific moisture capacity* as $C(\psi)=d\theta/d\psi$, equation (2.2) can be written as

$$C(\psi)\frac{\partial \psi}{\partial t} = \frac{\partial}{\partial x}\left[K(\psi)\frac{\partial \psi}{\partial x}\right] + \frac{\partial}{\partial y}\left[K(\psi)\frac{\partial \psi}{\partial y}\right] + \frac{\partial}{\partial z}\left[K(\psi)\left(\frac{\partial \psi}{\partial z}+1\right)\right] \tag{2.3}$$

The solution of this equation requires the functions $K(\psi)$, $C(\psi)$, and $\theta(\psi)$ to be known. For saturated condition, $C(\psi)$ is zero, and $K(\psi)$ is constant and equal to saturated hydraulic conductivity (K_s). van Genuchten (1980) proposed the following two relationships for computing the values of $\theta(\psi)$ and $K(\psi)$, which are required to solve the Richards equation

$$\theta(\psi) = \theta_r + \frac{\theta_s - \theta_r}{\left(1+|\alpha\psi|^n\right)^m} \qquad \text{when } \psi < 0$$

$$= \theta_s \qquad \text{when } \psi \geq 0 \tag{2.4}$$

$$K(\psi) = K_s S_e^l \left[1-\left(1-S_e^{1/m}\right)^m\right]^2 \tag{2.5}$$

where $m = (1 - 1/n)$ for $n > 1$, $S_e = (\theta - \theta_r)/(\theta_s - \theta_r)$, θ_s is the saturated moisture content (cm^3/cm^3), θ_r is the residual moisture content (cm^3/cm^3), and α (1/cm), l, and n are the van Genuchten model parameters. Using pedotransfer functions Schaap (1999) developed a computer program *Rosetta*, for estimating the van Genuchten model parameters. The program predicts the parameters based on different combinations of soil textural classes; sand, silt, and clay percentages; bulk density; the value of θ at ψ = 33 kPa; and/or the values of θ at ψ = 33 kPa and 1500 kPa.

Kostiakov (1932) gave the following simple equation for determining the infiltration rate

$$f(t) = \alpha\, t^{-\beta} \tag{2.6}$$

where α and β are the constants to be derived from infiltration data. However, there is no efficient way of determining the values of α and β from basic soil properties. Therefore, the equation is not used frequently.

Horton (1933) proposed the following empirical infiltration model

$$f(t) = f_c + (f_0 - f_c)\, e^{-\beta t} \tag{2.7}$$

where f_0 is the initial infiltration capacity (m/s), f_c is the final steady infiltration rate (m/s), and β is a coefficient called the rate constant (s^{-1}). The main limitation of this model is that all the three parameters of the equation are to be determined from infiltration data. It also does not adequately represent the rapid decrease of infiltration rate from its very high initial value.

Philip (1957) developed an equation based on an infinite series solution to the Richards equation for ponded infiltration into a deep soil with uniform initial water content. It can be written as

$$f(t) = 0.5\, S\, t^{-0.5} + K_s \tag{2.8}$$

where S is a parameter known as soil sorptivity ($m/s^{0.5}$).

Holtan (1961) suggested an empirical infiltration equation which is explicitly dependent on soil water conditions in the form of available pore space for moisture storage. The model can be given as

$$f(t) = a\, b\, (\theta_d - I)^{1.4} + f_c \qquad (2.9)$$

where a is a constant related to the surface conditions (0.25-0.8), b is a scaling factor, θ_d is the initial moisture deficit or the pore space per unit area of cross section initially available for water storage (cm), I is the cumulative infiltration (cm) at time t (s).

2.1.1 Water infiltration and soil macroporosity

The infiltration equations mentioned in the previous section are either empirical or derived from Darcy's law (Green and Ampt, 1911; Richards, 1931; Philip, 1957). Though some of these models have been popularly used, but their main limitation is that they are conceptually valid for water flow through the soil matrix only. When a significant amount of water flows through the preferential pathways (macropores) of soil bypassing the soil matrix, the assumptions of homogeneity of the soil hydraulic properties over some representative cross-sectional area is no longer valid and thus the flow concept based on an average hydraulic gradient is expected to fail (Beven and Germann, 1982). A number of studies have reported that the results obtained from Darcy-type infiltration models failed to represent the irregular patterns of infiltration observed in macropore dominated soils (Blake *et al*., 1973; DeVries and Chow, 1978; Bouma *et al*., 1980; Rogowski and Weinrich, 1981). The presence of macropores generally leads to heterogeneity of flow within the soil (Ligon *et al*., 1977; Germann, 1981). The size of macropores as well as their connectivity, which may change within a few centimeters as well, also influences the infiltration behavior

of soil (Beven and Germann, 1982). Under such conditions a combined experimental and modeling approach for predicting infiltration has been adopted by many researchers (Hoogmoed and Bouma, 1980; Weiler, 2001; Ticehurst *et al*., 2003; Rajot *et al*., 2004; Weiler, 2005). But the performance of the physical based infiltration models largely depends on the accuracy of actual infiltration measured in the field. Parr and Bertrand (1960) classified infiltration measurement procedures as: (a) estimation of infiltration over a plot from runoff data obtained using rainfall simulators; (b) point measurement of infiltration using infiltrometers; and (c) estimation of infiltration from natural rainfall data. But the selection of a particular method is critical as the error involved in the estimation largely depends on scale of measurement (Dagan, 1986; Lauren *et al*., 1988; Lischeid *et al*., 1998; Wagenet, 1998) and also the physical conditions of the site which largely influence the infiltration rate. Haws *et al*. (2004) studied the spatial variability of infiltration and effect of measurement scale on steady state infiltration rate on an agricultural landscape considering local scale, hillslope scale, and landscape scale measurements. They had reported a representative measurement area (RMA) of about 400 cm^2, above which the scale effect of infiltration was not evident. Infiltration measurement particularly on a steep hillslope is complex as the lateral gravity component influences the soil wetting pattern considerably. The presence of macropores also significantly influences the hydrological response of hillslopes (McDonnell, 1990; Smettem *et al*., 1991; Návar *et al*., 1995; Bronstert, 1999). The preferential features are known to strongly affect the watershed hydrology at different scales and practical measurement of preferential infiltration is difficult. Therefore, in macropore dominated hillslopes

the selection of a particular infiltration measurement technique and measurement scale is critical. In macroporous soils plot scale measurements should be preferred over point measurements (Sarkar *et al.*, 2008a). van Schaik (2009) studied the spatial variability of infiltration patterns related to the site characteristics at the catchment scale. In addition to the dye-tracer experiments additional site measurements of soil type, vegetation, and soil physical parameters were performed in a 1 km^2 catchment. The spatial variability of infiltration was explained with the site characteristics and sub-areas within the catchment were delineated to represent different infiltration patterns.

2.2 Subsurface Water Flow through Soil Macropores

Macropore flow is defined as the rapid movement of water through soil structural voids like plant root channels, wormholes, or cracks in soils. Actual definition of macropores or soil macroporosity is rather difficult to specify. Table 2.1 enlists some of the definitions of macropores based on capillary potential or size of the macropores. However, Beven and Germann (1982) stressed on the fact that size alone is not a sufficient criterion for defining a pore as macropore. The hydraulic effectiveness of the pore as influenced by its network connectivity and dynamics of pore structures are crucial towards defining a pore as macropore.

The influence of soil macropores in hillslope hydrology has been studied in detail (Kitahara *et al.*, 1988; Jones, 1997; Jones and Connelly, 2002). Macropores in soil can develop by the activities of soil fauna, pore formed by plant roots and decayed root holes, cracks and fissures in the soil formations, and natural soil pipes formed by the erosive action of subsurface flow. The macroporosity of a soil is a

Table 2.1 Some definitions of soil macropores and macroporosity

References	Capillary Potential (kPa)	Equivalent Diameter (μm)
Nelson and Baver (1940)	>-3.0	-
Marshall (1959)	>-10.0	>30
Brewer (1964)	-	75 – 5,000
McDonald (1967)	>-6.0	-
Ranken (1974)	>-1.0	-
Bullock and Thomasson (1979)	>-5.0	>60
Reeves (1980)	-	200-10,000
Luxmoore (1981)	>-0.3	>1,000
Beven and Germann (1981)	>-0.1	>3,000

dynamic property as it is influenced by existing soil-plant-animal community (Beven and Germann, 1982). Seasonal or yearly variations in these conditions can significantly influence the macropre flow characteristics. Hydrologically effective macropores, developed by plant roots, soil fauna or piping, can be produced in 1 or 2 years time and in undisturbed conditions can last for considerable time periods (van Schaik, 2010).

A number of studies have been conducted towards understanding the nature of flow through soil macropores. Some of the studies related macropore flows based on pore size alone (Wilkins *et al*., 1977; Hewitt and Dexter, 1980). But these are not reliable as the concept of hydraulic effectiveness is an important factor as it has been shown clearly that different numbers and sizes of macropores may be effective under different conditions (Bouma *et al*., 1977). Dye and tracers experiments have popularly been used for studying water flow through soil macropores (Kissel *et al*., 1973;

Ehlers, 1975; Bouma and Dekker, 1978; Bouma and Wosten, 1979; Bouma *et al*., 1979; Omoti and Wild, 1979; Flury *et al*., 1994; Weiler, 2001).

To address the heterogeneity in macroporous soils a domain concept is often used to model macropore-matrix system (Muskat, 1946; Wakahama, 1974; Duguid and Lee, 1977; Scotter, 1978). In these models the soil matrix is considered as one domain and is described by hydraulic principles based on Darcy's laws and the macropores as the other domain. However the dual porosity models should consider the nature of flows in matrix and macropore domains, spatial and temporal variation of flow network, initiation of macropore flow, and interaction between the two domains at different stages of flow. Incorporating all these complicated processes accurately in a single model is difficult. Weiler (2001) developed a macropore infiltration model called INfiltration-INitiation-INteraction Model (IN^3M) using dye tracer experiments for describing flow through a simple macropore pathway. The model was tested for simulating observed dye patterns obtained from laboratory experiments. Larsbo and Jarvis (2003) developed a physically-based, one-dimensional, numerical model for water and solute transport in macroporous soils. In this dual domain model Richards' equation and the convection-dispersion equation were used to model water and solute movement in soil matrix. A simple capacitance type approach was used for macropore flow. Kroes *et al*. (2008) included a concept for water and solute movement in cracked or macroporous soils in the SWAP (Soil Water Atmosphere Plant) model. The model has a provision of defining advanced macropore flow descriptions. The macropore geometry can be defined as a depth dependent function of macropore volume. Using this function the fraction of macropores ending in a soil layer can be calculated and the water entering those macropores is infiltrated in that soil layer.

2.3 Overland Flow on Hillslopes

Over the last four decades, several investigations have been conducted on many aspects of overland flow on hillslopes, including field observations (Lima, 1989; Kadlec, 1990; Abrahams *et al.*, 1992), experimental studies (Chen, 1975; Hirsch, 1992), theoretical analyses and mathematical modeling (Govindaraju *et al.*, 1992; Chen *et al*., 2001; Wang *et al*., 2002). The investigations have primarily been focused to differentiate between the overland flow characteristics of semiarid and humid regions. In semiarid regions, overland flow occurs in less-vegetative hillslopes with non-significant preferential flows. Based on soil type and surface roughness, Huggins and Monke (1966) related overland flow behavior to a single parameter, *i.e.*, Manning's roughness coefficient. Emmett (1970) studied the hydraulics of overland flow on hillslopes using rainfall simulators and computed the roughness coefficient values. Chen (1975) studied the resistance coefficient for sheet flow on natural turf surfaces in the laboratory. Wu *et al*. (1999) studied the variation of the vegetative roughness coefficient with flow depth. Experiments were conducted with different simulated vegetation conditions in the watercourse to study the variation of roughness coefficient for unsubmerged and submerged overland flow. It was reported that the roughness coefficient reduced with increasing depth under unsubmerged condition. However, when fully submerged, the vegetative roughness coefficient tends to increase at low depths but then decreased to an asymptotic constant as the water level continued to rise. They developed a simple model based on force equilibrium to predict the roughness coefficients corresponding to different flow depths. The experimental data were in good agreement with the model predictions. Tsihrintzis (2001) further concluded that the experimental roughness follows a power law relationship with overland flow depth. Liu and Singh (2004) studied the effect of

microtopography, slope length and gradient, and vegetative cover on overland flow. They used a one-dimensional kinematic wave model in conjunction with a revised form of the Green-Ampt infiltration equation to evaluate the effect of different surface conditions on overland flow. The effect of microtopography and vegetation cover on overland flow was treated through grain resistance, form resistance, and wave resistance. The length and gradient of slope also affected the process of runoff generation and other hydraulic characteristics of overland flow. It was also reported that the microtopography has little effect on overland flow discharge at the outlet, but affects other hydraulic characteristics like flow velocity, depth, and shear stress. The vegetative cover slightly influences the outlet discharge, but has pronounced effect on some other parameters. With increasing percentage of vegetation cover, the velocity of overland flow decreases, but the water depth and flow shear stress increase. They reported these influences to be nonlinear in nature. Liu *et al.* (2004) developed a two-dimensional kinematic wave model for simulating runoff generation and flow concentration on an experimental infiltrating hillslope receiving artificial rainfall. Experimental observations of runoff generation and flow concentration on irregular hillslopes showed that the topography of the sloping surface controlled the direction and flow lines of overland flow. The model-simulated results satisfactorily compared with the experimental observations. The erosive ability of the concentrated flow was found to be mainly dependent on the ratio of the width and depth of confluent grooves. Adams *et al.* (2005) used a system of large rainfall simulators to generate runoff from a large hill pasture and determined the surface roughness coefficient by simulating the observed conditions with the help of a fully distributed hydrologic model, HILLS (Smith and Hebbert, 1983; Ticehurst *et al.*, 2003). In one of the recent studies, Jain *et al.* (2005) used a depth-dependent roughness coefficient for simulating

overland flow process in watershed modeling. Helmers and Eisenhauer (2006) modeled overland flow in a vegetative filter considering non-planar topography and spatial variability of soil hydraulic properties and vegetation density. They used the physically based, distributed hydrological model MIKE SHE to develop a two-dimensional overland flow model. They quantified the physical roughness of vegetative cover based on the stem density over the plot. A good agreement between field measured data and model predictions was found. They concluded that the non-planar topography significantly affected the overland flow, but the spatially variable roughness and variable soil hydraulic properties had a lesser impact on two-dimensional overland flow. Scherrer *et al*. (2006) studied the process of runoff generation at the hillslope scale under intense precipitation. They conducted a total of 48 high intensity sprinkling experiments on 60 m^2 hillslope plots at 18 grassland locations in Switzerland. The intensity of the applied rainfall was in the range of 50-100 mm/hr with duration between 3 and 6 hr. Subsequent measurements of overland flow and subsurface flow in 0.5-1.3 m below the surface were taken. They found that the runoff coefficient varied in a wide range of 2 to 90%. It was reported that at the majority of the sites, runoff was mainly in the form of overland flow, though in some locations subsurface flow through macropores was dominant.

2.4 Subsurface Water Movement

Subsurface water movement is one of the key processes of hillslope hydrology. The fate of infiltrated water in hillslope soil can be described by two main processes: storage and redistribution of moisture in the soil matrix and quick vertical and lateral movement of water through preferential pathways commonly known as subsurface stormflow.

2.4.1 Soil moisture storage and its distribution on hillslopes

The storage and redistribution of soil moisture on a hillslope is a dynamic process and depends on several factors like topography (Burt and Butcher, 1985; Petch, 1988; Moore *et al*., 1988; Nyberg, 1996), climate, vegetation (Lull and Reinhart, 1955; Hawley *et al*., 1983; Francis *et al*., 1986), and soil properties (Helvey *et al*., 1972; Afyuni *et al*., 1993). The top layer of the hillslope soil, which is also termed as plant root zone, is the most dynamic part as it passes through seasonal variations (Gómez-Plaza *et al*., 2001) due to activities of both plants and soil organisms. Van't Woudt (1955) reported increase in soil moisture from the top to the base of a hillslope and the greater wetting depth at the bottom of the slope was ascribed to surface and subsurface lateral flow, greater moisture retention, and lower evaporation. Stoeckeler and Curtis (1960) showed that the moisture content of the top 2 ft of the soil slope is inversely related to distance above the stream channel. Helvey *et al*. (1972) studied the spatial and temporal variation of soil moisture on hillslopes in greater detail. The dynamics of root zone soil moisture content was found to be influenced by plant evapotranspiration losses and seepage of soil water through the soil matrix. Therefore, seasonal variations of vegetation on hillslopes significantly affect the process of moisture distribution. In soil water budgeting, the evapotranspiration losses are often accounted for by incorporating a sink term (Jarvis, 1989). Yeakley *et al*. (1998) studied the effect of topography and soil properties on soil moisture gradients along hillslopes in humid watersheds. It was reported that the topographic factors assert more control over hillslope soil moisture during drier periods as drainage progresses, while variations in soil water storage properties are more important during wet periods. Hillslope soil moisture gradients in southern Appalachian watersheds appeared to be restricted to upper soil layers, with deeper

hillslope soil moisture gradients occurring only with sufficient drought. Famiglietti *et al*. (1998) studied spatial and temporal variability in surface moisture content along a hillslope transect. The study was aimed at characterizing variations in moisture content in the 0–5 cm surface soil layer along a hillslope transect by means of intensive sampling in both space and time; and to make inferences regarding the environmental factors that influence this variability. It was concluded that while topographic and soil attributes operate jointly to redistribute soil water following storm events, under wet conditions, variability in surface moisture content is most strongly influenced by porosity and hydraulic conductivity, and under dry conditions, correlations are strongest to relative elevation, aspect, and clay content. Consequently, the dominant influence on soil moisture variability gradually changes from soil heterogeneity to joint control by topographic and soil properties as the transect dries following significant rain events. Gómez-Plaza *et al*. (2001) determined the factors which controls soil moisture patterns in semiarid hillslopes. It was reported that upslope contributing area, aspect, soil profile curvature, and soil depth best explained the spatial variability of soil moisture in the vegetated zones. The influence of these factors showed marked seasonal variations due to changes in the physiological activities of the vegetal cover. New topographic indices considering the hillslope aspect were proposed to improve Beven and Kirkby's topographic index (Beven and Kirkby, 1979) for the prediction of soil water content patterns in semiarid areas. Rezzoug *et al*. (2005) investigated the effect of plane and profile curvatures on soil moisture distributions and related fluxes by conducting experiments on a hillslope. The soil moisture dynamics were simulated using a kinematic wave model in case of a convergent hillslope. Venkatesh *et al.* (2011) analyzed the observed variability of soil moisture contents under different land covers in the hilly tracts of Western Ghats,

India. The results of this study indicated that the nature of land cover had an influence on the spatio-temporal variability of soil moisture. The other variables related to topography might also have a more dominant effect.

2.4.2 Characterization of soil macropores using dye and tracers

A major constraint in modeling the impacts of preferential flow is the quantitative measurement of the indicators of preferential flow. Most of the methods are labour intensive and destructive. The spatial and temporal scales of measurements are often a serious disadvantage considering the wide spatio-temporal variability of the preferential flow features. Therefore, a consistent measurement method is not yet achieved (Droogers *et al.*, 1998; Perret *et al.*, 1999). In spite of their limitations dye and tracer experiments have popularly been used to study infiltration and preferential flow of water through soil macropores (Bouma and Dekker, 1978; Bouma and Wosten, 1979; Bouma *et al*., 1979; Omoti and Wild, 1979; van Stiphout *et al*., 1987; Ghodrati and Jury, 1990; Flury *et al*., 1994; Natsch *et al*., 1996; Forrer *et al*., 1999; Perillo *et al*., 1999; Weiler, 2001; Weiler and Naef, 2003; Morris and Mooney, 2004; Wang *et al*., 2006; Alaoui and Goetz, 2008; Anderson *et al*., 2008). This method can be a reliable indicator of active continuous macropore flow pathways which can easily be detected and quantified from laboratory experiments conducted with undisturbed soil columns collected from the field. As these continuous macropore pathways are essentially related to preferential flow, the degree of macroporosity obtained can be used effectively as a descriptive tool for comparing the effects of soil management on soil structure (Cattle *et al*., 1994). Several studies have suggested that, in addition to surface connected macropores, subsurface macropores can also play an important role in the preferential flow of water and solutes (Quisenberry and Phillips, 1976; Li and Ghodrati, 1997). In one of the significant studies, van Stiphout *et al*. (1987) used dye

tracer and soil moisture measurements to study infiltration behaviour in macroporous soil at the plot scale with both dry and wet initial soil moisture conditions. Droogers *et al*. (1998) used dye staining technique with subsequent digital image processing to quantify parameters for describing macroporosity in soils under different management practices. It was reported that the number of pores, the average area per pore, and the pore-shape were the most appropriate parameters to describe soil macroporosity. Weiler *et al.* (1998) conducted artificial rainfall and tracer experiments on two hillslope sites to identify runoff processes and to test a dual porosity physical based numerical model (QSOIL). The results showed good agreement between the observed and predicted runoff, water content, and matric potential. One of the two hillslopes showed higher subsurface flow response due to the presence of soil micropores and mesopores developed by plant roots. To understand the specific processes involved in macropore flow Ghodrati *et al*. (1999) conducted a dye tracer experiment with a Split Macropore Column (SMC) in the laboratory. With a single macropore in a cylindrical soil sample the effect of the physical parameters such as size, density, and continuity of macropores were investigated and the results suggested that the macropore flow was mostly influenced more by matrix-macropore size ratio than by the macropore size alone. Öhrström *et al.* (2002) carried out a field investigation in semiarid Tunisia to investigate spatial variability of preferential pathways in both hillslope and plot scales. Analysis of dye distribution patterns indicated that the preferential pathways were randomly distributed. The results also showed that the physiographic features of the watersheds such as nose, slope, and hollow significantly influenced the dye infiltration patterns. Wahl *et al.* (2003) conducted dye tracer experiments on confined irrigation plots and the stained and unstained areas at different depths were analysed using GIS-software to study the infiltration capacity and macroporosity of soil under

different tillage systems. van Schaik *et al.* (2010) used dye tracer infiltration patterns for physical based parameterization of macropore flow. A physically based macropore concept was embedded in the SWAP model by using dye infiltration patterns to parameterize macropore infiltration at three locations of a catchment. The model with the calibrated parameters was validated under natural field conditions with measured data. It was found that runoff production could be better simulated using the macropore component of the model. Bachmair *et al.* (2010) evaluated the performance of two dual-permeability models under different land use and land cover (LULC). Dye tracer sprinkling experiments were conducted in five sites with similar soils but different LULC. Measurements of water contents were taken at different depths using time domain reflectometers. The experimental data were compared with model simulations to study water content changes, solute distribution profiles, and maximum infiltration depths. The results suggested that LULC effects need to be better incorporated into the conceptualization and parameterization of infiltration and percolation in hydrologic models for better predictions regarding water quality and quantity.

2.4.3 Subsurface stormflow

Subsurface stormflow is the quick interflow through the upper soil layer mainly through the preferential pathways of soil. The lateral movement of water through non-capillary pores and concentrated flow in soil pipes and fissures (Gregory and Walling, 1973) has gained the attention of many researchers. Hursh and Brater (1941) suggested that in small forested catchments subsurface stormflow along soil layers together with groundwater movement near stream channels could account for a major portion of the hydrograph peak. However, overland flow seemed of much less importance in this regard. Roessel (1950) and Fletcher (1952) observed that

subsurface stormflow through large non-capillary pores accounted for the major part of storm runoff from undisturbed forested watersheds. Subsurface stormflow can be significant under both saturated (Kirkby and Chorley, 1967; Kirkby, 1969; Kirkby, 1978; Calver *et al*., 1972) and unsaturated (Whipkey, 1969; Jones, 1971) conditions. Subsurface stormflow response from hillslopes are influenced by several factors like antecedent moisture condition, rainfall intensity, rainfall depth, topography, and the physical characteristics of preferential flow network (Tsuboyama *et al.*, 1994; Sidle *et al.*, 1995 and 2000; Uchida *et al.*, 2005; Tromp-van Meerveld and McDonnell, 2006a). van Schaik *et al.* (2008) studied the influence of preferential flow on hillslope hydrology in semi-arid region. It was found that the hillslope hydrological system consists of soil matrix and macropore domains, which can interact depending on water contents. It was also reported that based on storm characteristics the contribution of macropore flow in total subsurface runoff ranged from 13 to 80 percent.

Direct field measurements of subsurface stormflow by intercepting the flow digging a trench or pit, have been reported by many researchers (Tsukamota, 1961; Hewlett and Hibbert, 1963; Whipkey, 1965; Dunne and Black, 1970; Knapp, 1973). However, excavation of such pits may distort the flow net upstream to the face of the pit and thus the flow hydrograph may get affected (Knapp, 1973). Under extreme magnitudes of lateral preferential flows, the stability of the face of the pit may also be a matter of concern. In this regard, piezometers and soil profile moisture monitoring systems may be a better alternative. Hydrometric studies using dye tracing and subsurface flow measurements (Mosley, 1979 and 1982) concluded that rapid flow of new water through soil macropores was capable of accounting for storm period streamflow. However, some of the researchers have emphasized on the fact that the

rapid discharge of water through the soil macropores is mainly the 'old water' which is stored in the soil from the antecedent storm events (Abdul and Gillham, 1984; Stauffer and Dracos, 1986; McDonnell, 1990). Montgomery *et al*. (1997) demonstrated the importance of flow through near-surface bedrock on runoff generation and pore pressure development in shallow colluvial soil on a steep, unchanneled zero-order catchment under natural rainfall and sprinkling experiments. Freer *et al*. (1997) highlighted the importance of understanding the dominant downslope hydraulic gradients at the hillslope scale, which may not necessarily be represented by surface topography. This is important for the evaluation of spatial model predictions where the underlying subsurface topography is significantly different from that of the surface and, therefore, would significantly alter the spatial pattern of any topographic indices derived from digital terrain models. It was emphasized that if the surface and subsurface hydraulic gradients and dominant flow paths are correlated then it is not necessary to document the subsurface topography. Negishi et al. (2004) studied stormflow generation in a tropical headwater zero-order basin characterized by steep slopes and shallow soils in peninsular Malaysia. Kienzler and Naef (2006) investigated the interdependency of spatially and temporally variable factors towards preferential subsurface stormflow generation in shallow soil layers.

Modeling subsurface flow in macroporous soils is a critical task as the flow geometry through soil macropores can change even within very short distances (Beven and Germann, 1982). Preferential flow models have been developed for a single pipe (Tsutsumi *et al.*, 2005), for hillslopes (Faeh *et al.*, 1997; Weiler and McDonnell, 2007), and for watersheds (Beckers and Alila, 2004). Both analytical and computational techniques have been adopted for modeling subsurface stormflow. For modeling high velocity of flow through soil macropores Mosley (1979) used an

effective hydraulic conductivity calculated based on tracer velocity, effective porosity, and a hydraulic gradient equal to the bed slope. Sloan *et al*. (1983) suggested the use of an effective hydraulic conductivity based on a baseline hydraulic conductivity obtained from direct measurement of soil samples collected from hillslopes. The lower limit of effective hydraulic conductivity is the baseline hydraulic conductivity and higher order values as a multiple of this can be adopted to account for higher flow rates owing to the effect of soil macropores. Smith and Hebbert (1983) used mathematical simulation for interdependent surface and subsurface hydrologic processes. Beven (1982) provided analytical solutions for some simple cases of subsurface stormflow with simple kinematic theory for saturated and unsaturated flows. Solutions for rising, falling, and partial equilibrium hydrographs were given. Sloan and Moore (1984) evaluated five mathematical models for predicting subsurface flow. The models included one- and two-dimensional finite element models based on Richard's equation, a kinematic wave model, and two simple storage discharge models based on kinematic wave and Boussinesq assumptions. They reported that the performance of simple storage-discharge models were comparable to that of complex finite element models. Germann and Beven (1985) approximated infiltration behavior into soils with sorbing macropores considering a two-domain flow. The matrix domain, where the water is subjected to capillarity, the infiltration was approximated by Philip's sorptivity concept (Philip, 1957). In macropore domain water was assumed to move only under gravity and the flow was approached by kinematic wave theory. A sink function was introduced to account for water sorption by the soil matrix. The model was tested for infiltration into an undisturbed block of soil containing macropores. Germann *et al*. (1986) demonstrated the importance of saturated layers on the initiation of subsurface

stormflow in a sloping forest soil. The kinematic wave theory was applied in the model and the distribution of flow parameters (macropore conductance and sorbance), that were used to represent macropore flow processes within a given soil, were derived. The model successfully reproduced the hydrograph peaks for a number of experiments. Germann and Beven (1986) used a distribution function approach to model water flow in soil macropores based on kinematic wave theory. Fisher (1997) developed a one-dimensional finite difference model for saturated subsurface flow within a hillslope by solving Boussinesq equation. The model uses rainfall, elevation data, a hydraulic conductivity, and a storage coefficient to predict the saturated thickness in time and space. But the model was limited in its ability to reproduce historical piezometric responses. Fan and Bras (1998) presented analytical solutions to hillslope subsurface stormflow and saturation overland flow. Combining continuity equation with a kinematic form of Darcy's law, a quasi-linear wave equation was obtained and it was solved applying the method of characteristics to develop a one-dimensional model. Troch *et al*. (2002) produced a more general analytical solution to the hillslope-storage kinematic wave equation for subsurface flow. Weiler and McDonnell (2004) studied in detail about the actual structures in the soil that promote and conduct a lateral water transfer. They used a new virtual experiment approach to identify the control of water flow and solute transport at the hillslope scale for two hillslopes in New Zealand and Japan. Their investigations revealed threshold behavior observed at these and other experimental hillslope sites around the world.

Some catchment scale models have also shown significant improvements after incorporating rapid subsurface flow component into them. Vertessy and Elsenbeer (1999) described a process-based distributed model (Topog_SBM) for storm flow generation consisting of a simple bucket model for soil water accounting,

a one-dimensional kinematic wave overland flow scheme, and a contour-based element network for routing surface and subsurface flows. Scanlon *et al*. (2000) used a modified version of TOPMODEL to simulate the observed catchment dynamics. The model considered macroporous subsurface stormflow zone as a hydrological pathway for rapid runoff generation. Further, a generalized topographic index theory was applied to the subsurface stormflow zone to account for logarithmic storm flow recessions, indicative of linearly decreasing transmissivity with depth. Walter *et al*. (2002) extended the TOPMODEL theory to develop a model (STOPMODEL) for shallow-soil subsurface flow. The common TOPMODEL theory implicitly assumes a water table below the entire watershed and this does not conceptually apply to systems hydrologically controlled by shallow interflow of perched groundwater. STOPMODEL provides an approach for extending TOPMODEL's conceptualization to apply to shallow, interflow-driven watersheds by using soil moisture deficit instead of water table depth as the state variable. STOPMODEL equations are derived using a hydraulic conductivity function that changes exponentially with soil moisture content. Zhang *et al*. (2006) introduced the macropore domain in Representative Elementary Watershed (REW) model for describing preferential flow of water in both vertical as well as lateral directions. The lateral macropores were assumed parallel to the soil surface and no exchange between macropores and matrix was considered. The mass balance equation of the model had been reformulated to account for the quick subsurface stormflow. It was clearly demonstrated that subsurface stormflow contributed considerably to stream flow in the study area.

More recently, Tromp-van Meerveld and Weiler (2008) stressed on the need of including bedrock leakage, variable soil depth, and preferential flow to model subsurface flow response from the hillslopes. Graham *et al.* (2010) applied a forensic

approach by combining irrigation and excavation experiments in the Maimai hillslope to determine typology and morphology of lateral subsurface flowpaths. The controls of topography and bedrock permeability on these flowpaths were also studied. The experiments showed that downslope flow was concentrated at the soil bedrock interface, with flowpath locations controlled by small features in the bedrock topography. Lateral subsurface flow was characterized by high velocities, several orders of magnitude greater than predicted by Darcy's Law, using measured hydraulic conductivities at the site. It was found that the bedrock was moderately permeable and the vertical percolation of water into the bedrock was a potentially large component of the hillslope water balance. The experimental findings were incorporated in a conceptual model of hydrological processes to address the threshold response of hillslopes to rainfall (Graham and McDonnell, 2010). Vogel *et al.* (2010a) reported that the formation and intensity of preferential flow depends on the contrast between the hydraulic properties of the two flow domains as well as the properties of their interface. Physical coupling and numerical coupling of the respective governing equations were targeted. The governing equations were solved using sequentially coupled and fully coupled approaches. It was found that fully coupled approach was a numerically more robust alternative. Vogel *et al.* (2010b) studied soil moisture dynamics at an experimental hillslope site using a one-dimensional dual-continuum model. The water present in soil matrix and the one flowing through the preferential pathways were treated as two separate but mutually communicating soil water continua. The ^{18}O isotope was used as a natural tracer to study the role of preferential flow in the formation of shallow subsurface runoff. It was found that the dual-continuum model could explain the observed process of subsurface hillslope discharge.

2.4.4 Lateral preferential flow

At field scale or catchment scale the influences of preferential flow mainly depend on the connection of vertical and lateral preferential flow paths (van Schaik, 2010). The process of vertical infiltration in macroporous soils has widely been addressed by many researchers (Germann and Beven, 1985; Beven and Clarke, 1986; Ruan and Illangasekare, 1998; Weiler and Naef, 2003; Weiler, 2005). But, in many instances lateral preferential flow through the macropores as gravity flow or flow through areas with higher permeability than the surrounding soil matrix, can become significant (Weiler *et al.*, 2005). Many studies have reported lateral preferential flow to be an important component for soil water balance, mainly in forested hilly areas (Jones, 1997; Uchida *et al.*, 2005; Tromp-van Meerveld and McDonnell, 2006b; Negishi *et al.*, 2008). In humid forested hillslopes the preferential flow features can be relatively short (Noguchi *et al.*, 1999; Terajima *et al*., 2000). However, in some steep forested hillslopes large preferential flow features have been reported (Roberge and Plamondon, 1987; Kitahara, 1993; Uchida *et al.*, 1999). Even if the preferential pathways are short, due to their network and connectivity they can impart high subsurface flow velocity to result in quick runoff response (Peters *et al.*, 1995; Tani, 1997; Hutchinson and Moore, 2000). Saturated soils are also known to provide connectivity between the preferential pathways (Steenhuis *et al.* 1988; Sidle *et al.* 2001). Therefore, in vegetated hillslopes of wet tropical and sub-tropical watersheds, well connected macropore network is primarily responsible for generating rapid lateral stormflow response during high intensity storm events.

The role of soil macropores in generating rapid subsurface flow in forested hilly watersheds has been identified long back (Mosley, 1979) and a number of investigations have reported on different aspects of preferential flow and their

modeling (Beven, 1982; Germann *et al*., 1986; McDonnell, 1990; Faeh *et al*., 1997; Bronstert, 1999; Beckers and Alila, 2004). Considering the wide spatial and temporal variability of soil macropores and their functional behavior (Weiler and McDonnell, 2007), there are a number of areas to be addressed for better conceptualization of lateral preferential flow at the hillslope scale. Therefore, in the recent trend of studies on macropore dominated lateral flow generation in hillslopes, due importance has been given on extensive field investigation for better understanding of the processes and subsequent development of physical based models (Bronstert and Plate, 1997; Faeh *et al*., 1997; Beven, 2000b; Weiler and McDonnell, 2007; Anderson *et al*., 2008).

Some preferential flow models used at hillslope or catchment scale do not actually include lateral preferential flow. The rapid subsurface stormflow is described mainly with vertical preferential flow connected to shallow lateral groundwater flow on the bedrock surface (Zehe *et al.*, 2001; Christiansen *et al.*, 2004; Beckers and Alila, 2004). Sidle *et al*. (2000) reported that subsurface flow contributes more to storm runoff than overland flow in steep forested catchments. However, the flow domain in a forested hillslope soil can be subdivided in two different components viz. matrix flow and preferential flow through well connected macropore network (Uchida *et al*., 2002). The lateral flow velocity through the soil macropores is expected to be very high as compared to that of the surrounding soil matrix. However, in the process of rapid subsurface stormflow generation soil macropores are supposed to contribute the major portion of subsurface runoff occurring within first few hours of high intensity storm events (Sloan and Moore, 1984). To incorporate this behavior some researchers introduced a dual-porosity concept (Gerke and van Genuchten, 1993; Ray *et al*., 1997; Larsson and Jarvis, 1999) or considered different flow velocities in soil

matrix and macropores (Beckers and Alila, 2004). However, some of the models suggested the adoption of an effective lateral hydraulic conductivity, which can be several times higher than the actual saturated hydraulic conductivity of the soil matrix, to account for the higher subsurface flow rates (Sloan *et al*., 1983; Fan and Bras, 1998; Troch *et al*., 2002; Rezzoug *et al*., 2005). Such approximations might give a reasonable correlation with the total subsurface flow hydrograph, but the bifurcation of runoff hydrograph into soil matrix and macropore flow is not addressed thoroughly. The actual contribution of macropores in total subsurface stormflow can be one of the important aspects that need to be evaluated. Beven and Germann (1982) in their famous review paper suggested that the size of macropores and their numbers do not necessarily indicate the generation of active preferential flow; but it is the connectivity of the mocropores that imparts the hydraulic effectiveness. Different number of macropores can be effective under different hydro-geologic conditions. The process of water supply to macropores is a function of antecedent moisture condition, rainfall intensity, rainfall amount, hydraulic conductivity of soil matrix, and surface contributing area (Trojan and Linden, 1992; and Léonard *et al*., 1999).

Bronstert and Plate (1997) proposed a comprehensive hillslope model (Hillflow 3D) to simulate the hydrological processes like interception, evapotranspiration, infiltration into soil matrix and macropores, lateral and vertical water flow in soil matrix and preferential flow paths, surface runoff, and channel discharge. Jones and Connelly (2002) presented a semi-distributed physically based pipe flow model to simulate ephemeral and permanent flow in soil pipes. The water flow in pipes was calculated as a function of wetted perimeter of soil pipe, length of pipe, and velocity at which water enters the pipe. The complexity of a branching network was also taken into account. Herbst and Diekkruger (2003) developed a

simplified finite element approach to model the spatial variability of soil moisture in a micro-scale catchment. The surface runoff and macropore flow processes were conceptualized in the model. The model performed reasonably well to predict the measured hydrograph. But, the subsurface flow response was underestimated by the model. Brooks (2003) reported that the bulk lateral hydraulic conductivity of a soil greatly depends on depth of saturation. For macroporous soils the use of a double exponential relationship between saturated hydraulic conductivity and depth was suggested. This approach was similar to the dual porosity approach, where the lateral saturated hydraulic conductivity is raised exponentially when the topsoil becomes saturated. The model could account for rapid lateral flow under saturated soil conditions, but the process of rapid subsurface flow in unsaturated conditions were not addressed. In one of the recent studies Ticehurst *et al*. (2003) used a physically based model to conduct a sensitivity analysis of subsurface lateral flow in south-east Australia. Uchida *et al*. (2005) reported that lateral preferential flow is highly threshold dependent and a certain amount of rainfall threshold is required to activate lateral preferential flow. Therefore, it seems to be more realistic to develop a model which can compute the contribution of lateral subsurface flow through soil matrix and macropores separately and also can indicate the number of macropores which are hydraulically effective under different hydrologic conditions. Weiler and McDonnell (2007) presented a new approach to formalize the qualitative explanation of complex preferential flow into a numerical model structure. Field observations were used to evaluate the model for its ability to capture flow and hydrograph composition. Model outputs were generated with different pipe network geometries for its calibration and validation. It was suggested that preferential flow can be parameterized within a process-based model structure. Anderson *et al*. (2009) conducted tracer experiments

in a preferential flow dominated hillslope to measure the subsurface flow velocities. It was reported that the subsurface flow velocities were more closely related to the 1-h rainfall intensity than to the antecedent moisture conditions. Very little water table response of the plot indicated that preferential flow operated independently from soil matrix and the majority of flow was carried through the preferential pathways during the storms. It was also found that the subsurface flow velocities were more for shorter length of slopes. It was concluded that the preferential flow network of the hillslope was an important factor to control the subsurface flow velocity. Anderson *et al.* (2010) characterized the subsurface flow processes in a watershed by monitoring water table dynamics using piezometers. The study was focused to characterize water table-runoff relationship, to identify the existence of preferential flow, and to test the feasibility of identifying areas within the watershed that are dominated by lateral preferential flow. Tang *et al.* (2011) studied lateral subsurface flow generation to quantify its contribution in nutrient loading in streams. Hillslope hydrology and stream hydrology were simultaneously monitored and the subsurface flow was separated from observed storms by chemical mixing model. It was found that lateral subsurface flow mainly delivered nitrates to the stream. Therefore, it was suggested to put more attention on lateral subsurface flow generation processes of hillslopes to control non-point source surface water pollution.

2.5 Conclusion

From the above discussions on the available literatures related to different aspects of hillslope hydrology it was clear that the preferential pathways have significant control on both surface and subsurface runoff generation processes in hillslopes under different hydro-geologic conditions. Preferential flow is also known to trigger the hydrological problems like occasional flash flood, accelerated soil

erosion, slope failure and landslides, surface and groundwater pollution in many watersheds around the world. For better assessment of the short and long term hydrological impacts of these issues it is extremely important to identify the dominating processes at the field level to have more clarity in understanding. Considering the large spatial and temporal variability of the preferential flow features and the extent of physical complexity of the controlling flow processes, it is difficult to conceptualize and model preferential flow processes to full satisfaction. Most importantly, from the studies conducted in different parts of the world for the past few decades it has been quite clear that in general the dominance and extent of preferential flow processes show wide variations. In a given region, not only the dynamic physical structures of the macropores may be different, but also the degree of its influence on the flow processes may vary widely. Therefore, in the present scenario before we provide a generalized solution for preferential flow dominated hydrological response of watersheds, it is important to have practical assessment of these flow processes in different parts of the world. The reports and experimental evidences about preferential flow from plot scale or catchment scale studies conducted in different watersheds around the world should help to have a better insight to the problem in our hand.

In the above context, the Brahmaputra river basin of India, being one of the largest river basins of the world, present a wide scope of hydrological assessment of its dominating flow processes. The neighboring area of the basin is also known to receive the largest depth of rainfall in the world. Under very high rainfall conditions the vast undisturbed forested hillslopes of the river basin have significant hydrologic impact on the region. The issues like devastating flash floods, accelerated soil erosion, slope failure and landslides are very common in the river basin. But, the literature survey shows that no detailed hydrological investigation has been carried out in the

river basin to assess the role of preferential flow on the hydrological response of its vegetated hillslopes. However, the outlook of the hydrologic condition prevailing in the basin gives strong indications of the existence of extreme preferential flow condition in the hillslopes. Therefore, the present study has been taken up in the Brahmaputra river basin with the specific objectives mentioned in the previous chapter to experimentally establish and model the hydrological response of a vegetated hillslope plot in the river basin.

CHAPTER 3 EXPERIMENTAL INVESTIGATIONS

This chapter presents a description of the study area and the selected experimental hillslope plot in the Brahmaputra river basin. A detailed description of the experimental setup and the methodologies for the *in situ* experiments are provided herein. The typical characteristics of the hillslopes, climate, and hydro-geologic conditions prevailing in northeast India have been elaborated in order to justify the adoption of the experimental techniques. The descriptions of the laboratory setup and the experimental procedures have been outlined. Detailed instrumentation used in the hillslope plot and the data captured from natural and artificial storm events have been presented. The observed field data and the results obtained from the experimental investigations have been discussed in detail to draw suitable inferences about the hydrological response of the hillslope plot.

3.1 Hillslope Experimental Site

An *in situ* field plot of 18 m × 6 m size on a natural hillslope, shown in Fig. 3.1, was selected in the Brahmaputra river basin (Singh *et al.*, 2004). The geographic location of the site is 26°12′ N latitude and 91°42′ E longitude with an elevation of about 55 m above mean sea level. Fig. 3.2 shows the location of the experimental plot in the Brahmaputra river basin. In order to quantify its topographic characteristics, a detailed topographic survey was conducted with a uniform grid of 0.25 m, using a total station of (±5 mm + 2 ppm) accuracy in all the directions. Fig. 3.3 shows the digital elevation map of the experimental site. The average slope in the main sloping direction is 20 percent whereas coefficient of variation of slope is 10.49% within the plot. Therefore, the microtopographic variations within the plot can be considered insignificant.

Fig. 3.1 Hillslope experimental plot

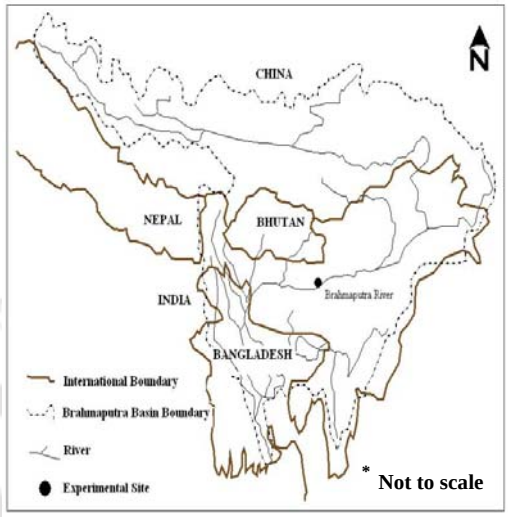

Fig. 3.2 Map of Brahmaputra River basin

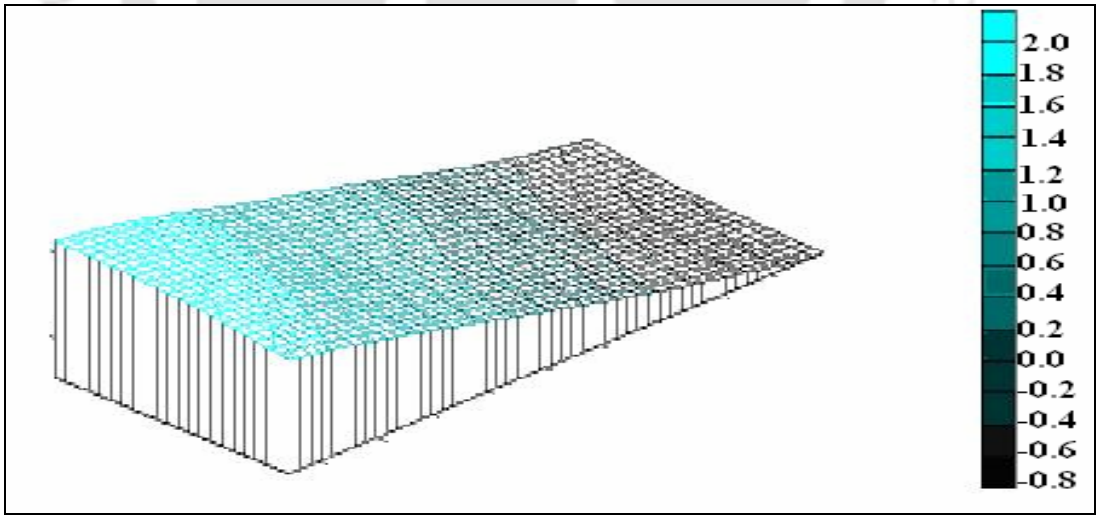

Fig. 3.3 Digital elevation map of the experimental plot

3.2 Soil, Vegetation, and Climate

The plot under study is reported to have deep, coarse loam soils, classed under the hyperthermic family of *Aquic Udifluvents* (Vadivelu *et al.*, 2004). The undisturbed soil samples were collected from different locations of the plot. Five samples each were collected from the top soil layer (0 – 40 cm) and the bottom soil layer (40 – 100 cm). Soil textural analyses were carried out using dry and wet sieving methods to determine the sand, silt, and clay percentages. The bulk density, porosity, and saturated hydraulic conductivity of the collected soil samples were also estimated. It can be observed from the results (Table 3.1) that a coarse textured soil overlay a fine textured soil layer in the subsurface profile. The upper soil layer with an organic top layer of approximately 10 cm depth stores the soil moisture for the growth of vegetation. The depth of the impermeable layer was about one meter below the ground surface. Under saturated condition such a formation is known to be highly conducive for rapid subsurface stormflow generation (Whipkey, 1965; Weyman, 1973; Kirkby, 1978). The range of bulk density was found to be 1.095 g/cc to 1.245 g/cc, whereas saturated hydraulic conductivity of the soil samples varied between 37 mm/hr and 70 mm/hr.

Sparse, moderate, and dense natural vegetation consisting of close growing grasses and shrubs (*Cynadon dactylon, Saccharum spontaneum, Mimosa pudica, Ageratum conyzoides, Ageratum haustonianum, Lantana camara, Mikania micrantha, Parthenium hysterophorus*, etc.) covered the plot throughout the year. However, degree of vegetation varied seasonally, depending upon climatic conditions. Table 3.2 lists different observed vegetation conditions of the hillslope plot.

The climate of the region may be divided into four primary seasons, namely, winter (December - February), pre-monsoon (March – April), monsoon (May –

September), and retreating monsoon (October – November). The average annual rainfall of the study area is 1611.9 mm (Singh *et al.*, 2004).

3.3 Design of the Experimental Setup

A hillslope experimental setup was designed for the study plot for conducting plot scale runoff experiments. The setup was designed keeping in view the natural hillslope conditions prevailing in northeast India, where very high intensity storm events occur frequently. The main design criteria were as follows:

a) The experimental setup should have proper size, so that the continuum behavior of a hillslope can be studied.

b) It should be a mobile and flexible system so that it can be easily installed on a natural hillslope.

c) The design should be simple and cost effective.

d) Unlike rainfall simulators, the installation of the setup should not be affected by the presence of dense vegetation canopy and tree branches that are quite common in the natural hillslopes of the region.

e) The setup should be able to produce high intensity storm events, which frequently occur in the Brahmaputra river basin.

f) The setup should be feasible to operate in steep hilly areas and should have both surface and subsurface flow measurement systems with minimum disturbance to the natural flow paths.

Keeping the above criterion in view, a sheet flow generation system has been set up at the hillslope site (Fig. 3.1) to generate overland flow under various high-intensity storm events. It consists of an upper channel on the upstream end of the slope and one lower channel at the downstream end. Both the channels are of rectangular cross section (Table 3.3). Fig. 3.4 shows the schematic diagram of the

experimental set up. A centrifugal pump with a capacity of delivering about 40,000 l/hr at the required head of 28 m is used to feed water in the upper channel. Once the channel is filled, water starts to spill from it and spreads over the entire plot in the form of sheet flow. Two side plates were used to guide the overland water to the lower channel where it was collected and discharged by another pump. Using venturimeter as well as volumetric method, discharge measurement in both the channels were carried out to obtain the inflow and outflow rates. Flow regulation valves were used to regulate the inflow discharge.

Table 3.1 Soil profile data of the experimental plot

Soil Layer	Bulk Density (g/cc)	Saturated Hydraulic Conductivity (K_s) (mm/hr)	Average Porosity	Average Sand (%)	Average Silt (%)	Average Clay (%)
Top Layer (0 - 40cm)	Range: 1.095 - 1.188 Average: 1.139	Range: 53 - 70 Average: 62.48	0.57	69.55	18.03	12.42
Bottom Layer (40 – 100 cm)	Range: 1.212 - 1.245 Average: 1.240	Range: 37 - 46 Average: 42.43	0.53	59.08	29.83	11.09

Table 3.2 Different vegetation conditions of the study plot

Month	Vegetation Degree	Stem Density per m^2	Range of Plant Height (cm)	Maximum Root Depth (cm)	Ground Cover (%)
August, 2005	Sparse	< 800	< 15	44	< 60
November, 2005	Moderate	800 - 2000	15 - 30	60	60-80
May, 2006	Dense	> 2000	> 30	100	80-100

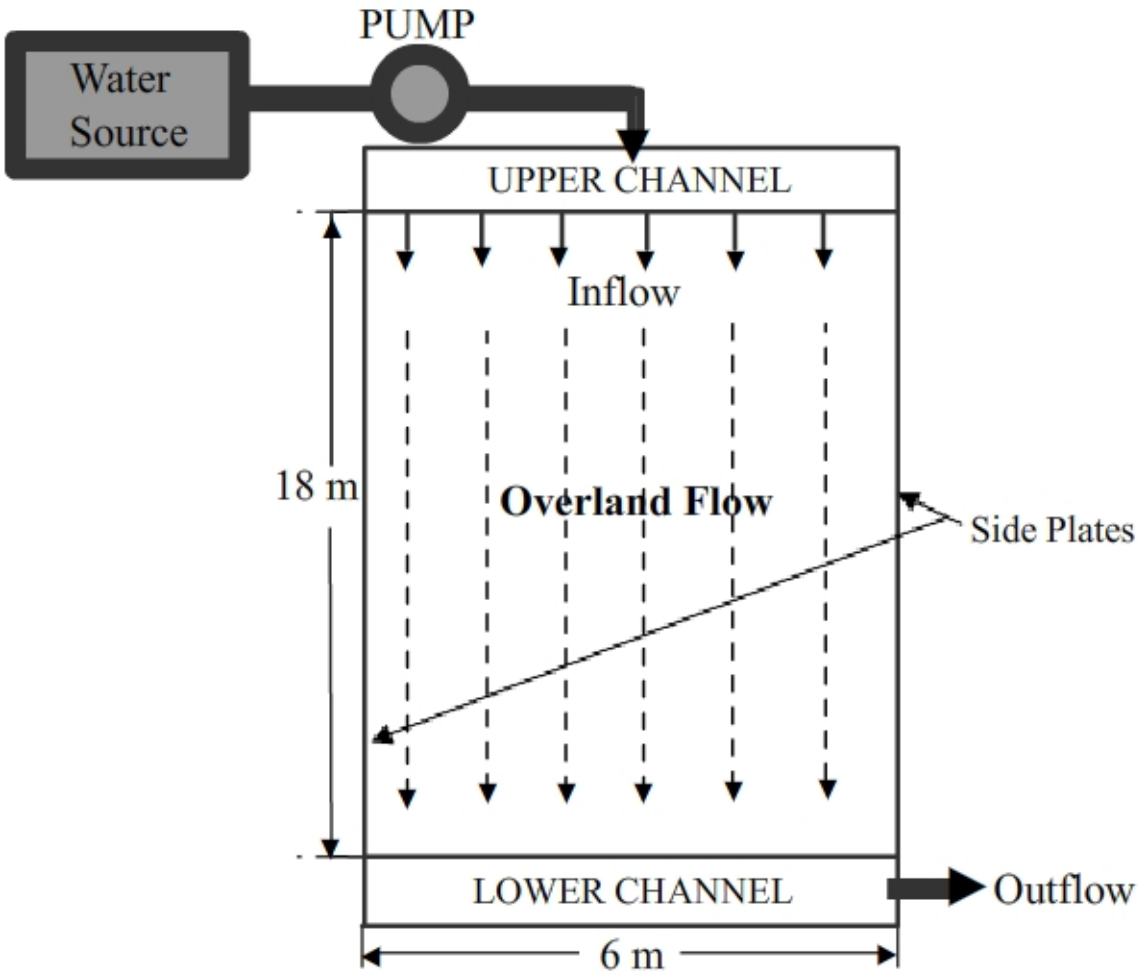

Fig. 3.4 Schematic diagram of the experimental setup

Table 3.3 Design specifications of the experimental setup

Items	Area (m^2)	Height (cm)	Thickness of metal sheet
Upper channel	0.7 × 6	60	3 mm
Lower channel	0.5 × 6	40	3 mm
Side plate	15 cm depth; 15 cm height; 3 mm thickness		
GI Pipe	100 mm diameter, length 43 m, each section of 2 m.		
Pump	10 hp diesel engine centrifugal pump (Kirloskar)		

The main objective of this kind of setup was not to disturb the natural conditions prevailing in the hillslope. Even the depths of side plates were kept only 15 cm, so that they should not affect the free lateral dispersion of infiltrated water significantly. The inflow intensity (i) for the runoff events can be computed as

Inflow Intensity (i) = [Inflow Discharge / Area of the Plot]

The system was capable of simulating a wide range of extreme storm runoff conditions. The setup was found to generate inflow intensities approximately in the range of 50 mm/hr to 400 mm/hr. Steady overland flow conditions could be attained with varying storm durations (15 – 120 minutes).

3.3.1 Limitations of the sheet flow generation system

As explained in the previous section, the designed experimental setup can be used to generate controlled overland flow across a relatively less steep hillslope plot having little micro-topographic variations. However, adopting such a system involves some level of approximations. In case of the sheet flow generation system, inflow enters the plot from the upslope part and gradually flows down the slope. As water moves down the slope, it is slowly infiltrated into the soil below the overland flow surface. As a result, the depth of flow should gradually decrease along the downslope direction. However, in case of a natural rainfall event, the overland flow depth on a hillslope increases in the downslope direction. Essentially there are some differences between the reservoir based approach of controlling the flow over a hillslope and a natural rainfall based event. But, it is obvious that a hillslope having high macroporosity in the subsoil, generates very thin sheet of overland flow due to high preferential infiltration. Practical measurement of such a low depth of overland flow, on a hillslope, is difficult. In the present investigation, for the field observation of overland flow depth wooden pegs painted with washable chalk were placed at

different locations of the plot. At the end of the runoff experiments the approximate maximum flow depths at those points were observed from the washed out paint of the pegs. These observed flow depths over the plot were less than 10 mm for different runoff events. Though, these can be considered as very coarse observations, they indicate the generation of shallow overland flow on the experimental hillslope plot which showed strong evidences of very high degree of active soil macroporosity. Moreover, with such low depths of flow, the variation in overland flow depth over a relatively small slope length of 18 m should not be significant. Apart from these, there are strong evidences of frequent occurrence of extreme rainfall events in the Brahmaputra river basin (Soja and Starkel, 2007), which generates large flood waves in the main river and its tributaries (Karmaker and Dutta, 2010). Fig. 3.5 (a-b) shows the Intensity-Frequency-Duration curves of two rainfall stations (Lakhimpur and Guwahati) of the region. These curves also depict that for durations 15-60 minutes, high intensity storm events are quite frequent in Northeast India. It is important to point out that the main target of the present study is to investigate surface and subsurface flow generation processes under extreme rainfall events. Such high intensity storm events are difficult to be generated on a plot size of 18 m × 6 m using rainfall simulators. Due to very high rate of preferential infiltration of soil, rainfall simulators may not generate any surface runoff from the plot. Not only the large systems of rainfall simulators are costly, but also the installation of such a system on the densely vegetated natural hillslopes of the region is difficult. On the other hand, the sheet flow generation system, used in the present investigation, is capable of producing extreme runoff conditions in such plots with reasonable flow depths and their variations within the plot. The sheet flow generation system produces a spatially averaged overland flow response of the hillslope plot, as the average inflow intensity

is calculated based on the inflow discharge and the area over which the overland flow spreads. The present investigation is focused on observing the lumped surface and subsurface flow response of the hillslope plot under steady infiltration and wet antecedent condition. Therefore, under the given circumstances the adoption of the proposed sheet flow generation system seems to be technically acceptable.

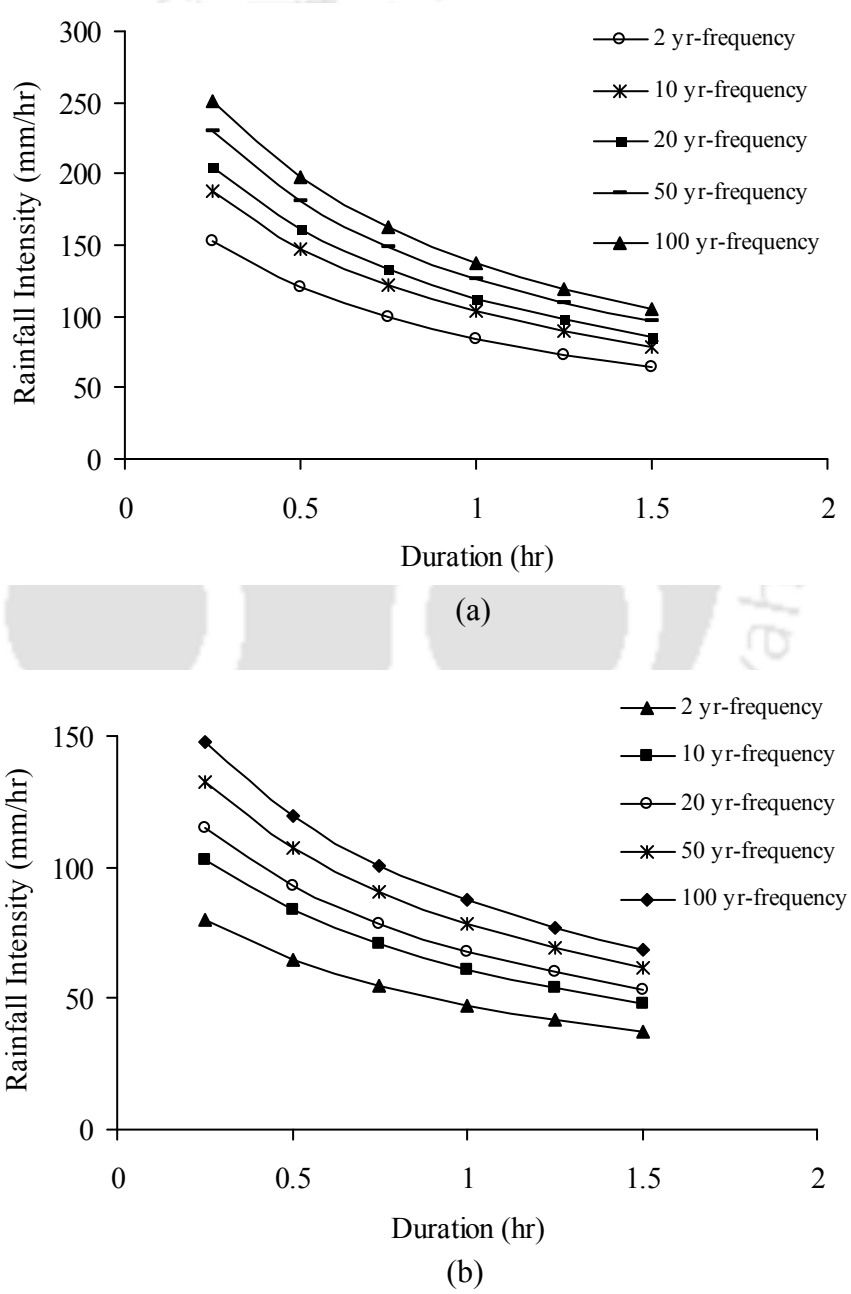

Fig. 3.5 Intensity-Frequency-Duration (IFD) curves of the stations (a) Lakhimpur and (b) Guwahati

3.4 Measurement of Infiltration

The phenomenon of entry of water into soil is known as infiltration. The process of infiltration and the subsequent movement of water through the soil profile play a significant role in the runoff generation process by affecting the timing, distribution, and magnitude of surface and subsurface flow. Infiltration characteristics of soil at a given location can be obtained by conducting controlled experiments on small plots, whereas local scale or point measurement of infiltration can be done by using an infiltrometer.

3.4.1 Double ring infiltrometer tests

Double ring infiltrometer is a simple and inexpensive method of determining point infiltration in soils and its specifications are standardized by the Environmental Protection Agency (EPA). Figs. 3.6 and 3.7 show a double ring infiltrometer and its vertical wetting front movement, respectively. The instrument has two concentric cylinders, which are filled with water during the experiment. The water in the outer ring helps to maintain a vertical wetting front for the downward movement of water below the inner cylinder. The measurement of infiltration is made in the inner cylinder only. Fig. 3.8 shows the infiltration curve derived from double ring infiltrometer test conducted on a plane agricultural land having nearly homogeneous soil. However, this curve can significantly differ in case of infiltration measurements using double ring infiltrometer on very steep vegetated hillslopes. In such cases, due to the effect of gravity, the assumption of vertical movement of waterfront remains no longer valid. Therefore, the subsurface flow pattern gets distorted and the infiltration curve differs from the theoretical curve.

In the hillslope plot local scale infiltration measurements were carried out using a double ring infiltrometer having an inner cylinder diameter of 30 cm. The

diameter of the outer cylinder was 45 cm. To measure infiltration, the two cylinders were inserted concentrically and a constant ponding depth of 15 cm was maintained in both the cylinders while infiltration measurements were carried out in the inner cylinder. This gives a measurement area of about 700 cm^2 for each set of experiment. Infiltrations were measured in 10 locations of the plot (Fig. 3.9) under dry (unsaturated) as well as wet (saturated or at field capacity) antecedent conditions (Table 3.4). The infiltration tests under dry soil conditions showed no particular trends

Fig. 3.6 Double ring infiltrometer

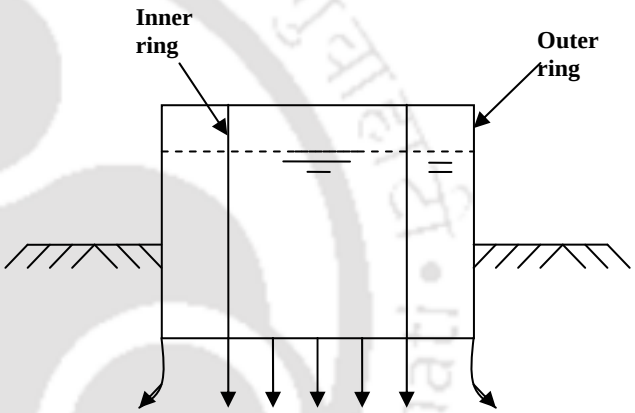

Fig. 3.7 Vertical wetting front movement

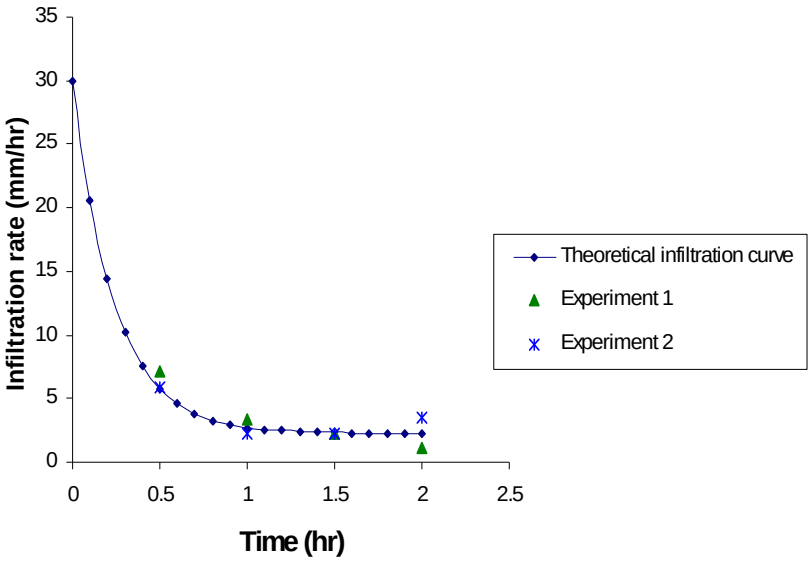

Fig. 3.8 Infiltration curve obtained from a plane agricultural land having no macroporosity in soil

or patterns (Fig. 3.10). Moreover, even after more than 1.5 hrs since the start of the experiment, the infiltration rate did not reach steady state condition for dry soil. These behaviors are quite similar for infiltration in preferential flow dominated soils under dry antecedent conditions (Blake *et al*., 1973; DeVries and Chow, 1978; Bouma *et al*., 1980; Rogowski and Weinrich, 1981). The average infiltration rate varied within a wide range of 18-256 mm/hr. However, under wet soil conditions the infiltration rate tends to reach a near steady state condition after about one hour since the start of the test (Fig. 3.11). The near steady state infiltration rate varied in the range of 42-130 mm/hr (Table 3.5). Macropore flow results in a large spatial variability of infiltration and hydraulic conductivity within a soil profile (Zehe and Flühler, 2001). The results can be explained from the fact that under dry conditions soil suction pressure was very high to result in higher rates of infiltration. The water flowing through the macropores passed through different irregular paths of active soil macropore network with significant interaction with the soil matrix. As a result, the irregular patterns of infiltration were evident. But, under wet conditions soil suction was less and all the macropores were primed for water flow and therefore, after sometime, a near steady state infiltration condition was attained. However, from the wide range of infiltration rates in both the cases it was clear that even within a small plot the effect of local scale was dominating. Infiltration rates in the upslope locations were higher than the downslope locations because of higher lateral gravity component at the upslope points and probably also due to higher degree of active soil macroporosity.

It is worth mentioning here that the present investigation is focused on studying hydrological response of the hillslope under high intensity storm events for wet antecedent conditions only. Therefore, unsaturated flow behaviors were not

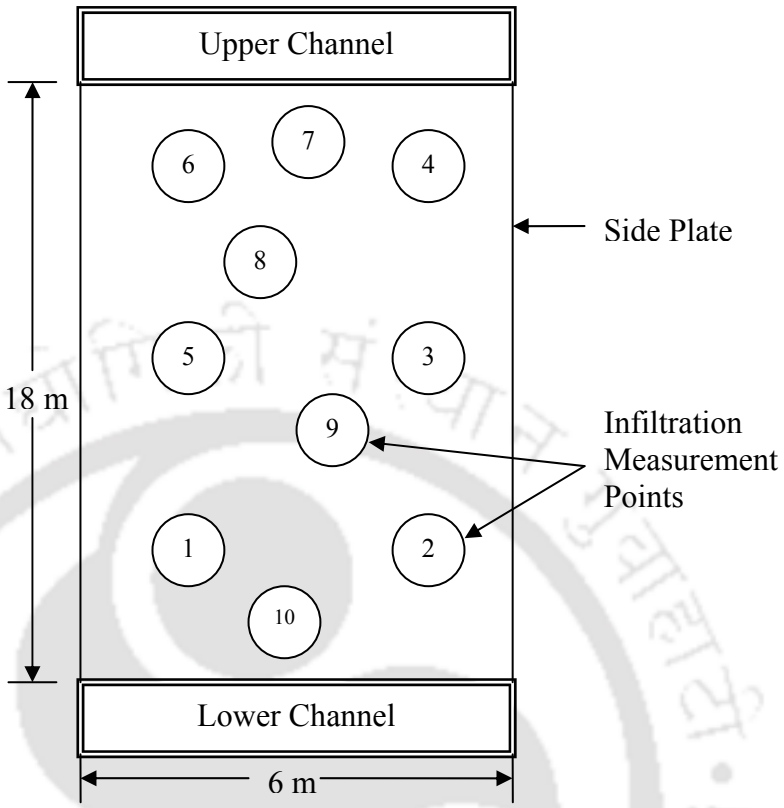

Fig. 3.9 Infiltration measurement points in the hillslope plot

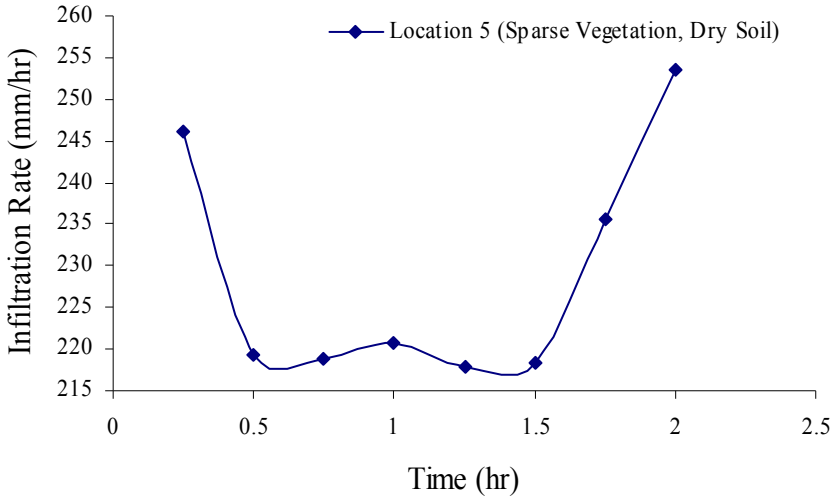

Fig. 3.10 Double ring infiltrometer test for dry soil condition

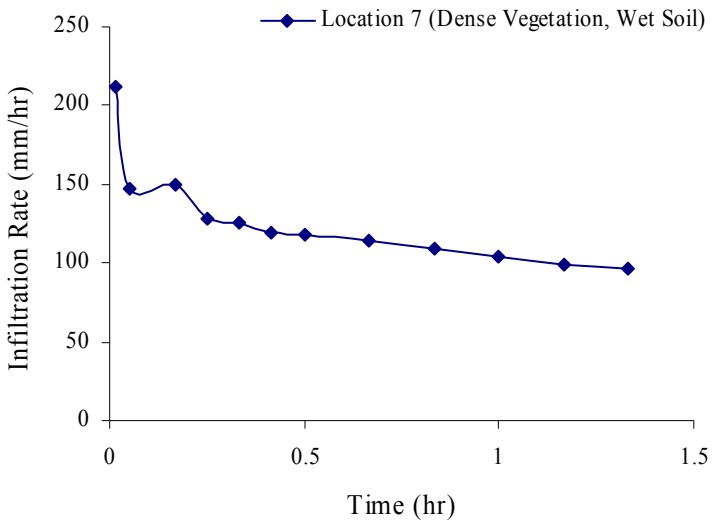

Fig. 3.11 Double ring infiltrometer test under wet antecedent condition

Table 3.4 Summary of the results of double ring infiltrometer tests

Location	Antecedent Moisture Condition	Degree of Vegetation	Range of Infiltration Rate (mm/hr)	Mean (mm/hr)	Coefficient of Variation (%)
Locations 1-5	Dry	Sparse	18-256	156	49
Locations 6-10	Wet	Dense	42-130	85	37

Table 3.5 Measured steady infiltration rates in the plot for dense vegetation and wet antecedent conditions

Infiltration Measurement Point	Distance from Upstream End of the Plot (m)	Measured Steady Infiltration Rate (mm/hr)	Average Rate of Infiltration, f_{avg} (mm/hr)
6	3	130	
7	2	97	
8	8	86	85
9	10	68	
10	16	42	

considered in this study for detailed analysis. Expectedly, the infiltration patterns under dry soil conditions did not show any particular trend to indicate the presence of high macroporosity in the hillslope soil. On the other hand, the local scale infiltration data under wet antecedent conditions indicated that after some time a near steady infiltration condition can be attained on the hillslope. Therefore, the steady infiltration rate data for wet antecedent conditions were used to derive the functional relationship to represent the spatial variation of steady infiltration rate over the plot. It was found that the following linear function quite reasonably represented the variation of steady infiltration rates along the length of the plot for wet antecedent conditions and dense vegetation (Fig 3.12)

$$f(x) = f_{avg}\left[1.9 - \frac{1.8x}{L}\right] \tag{3.1}$$

where L is the length of the plot (m), x is the distance from upstream end of the plot (m) and f_{avg} is the average steady recharge rate (mm/hr) over the plot.

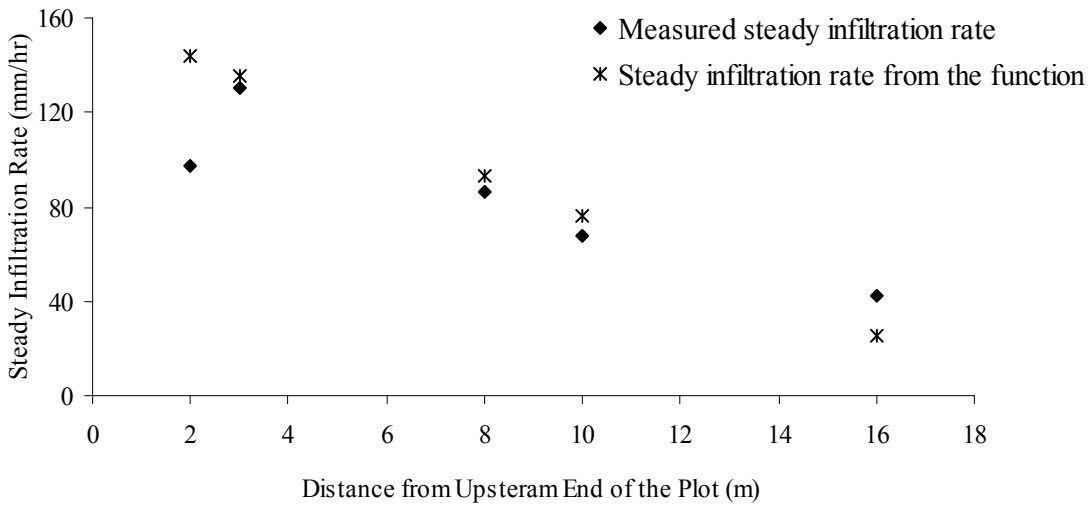

Fig. 3.12 Spatial variation of recharge for dense vegetation and wet soil condition

3.4.2 Estimation of infiltration from runoff plot experiments

As local scale measurements of infiltration showed wide range of variation, spatially averaged infiltration rates over the hillslope plot were estimated by conducting runoff experiments using a sheet flow generation system (Fig. 3.4). Knowing the inflow and outflow hydrographs, the spatially averaged infiltration rate over the plot was computed. The sheet flow generation system was preferred over rainfall simulators as it was more suitable for simulating a wide range of high intensity (50-400 mm/hr) storm events, which may be critical in terms surface and subsurface hydrological response in macropore dominated hillslopes.

The runoff plot experiment results showed that steady state infiltration conditions were attained much earlier (about 15 minutes) than the double ring infiltrometer tests (Fig. 3.13). The results indicate (Table 3.6) lower average steady infiltration rate values for sparse vegetation condition and higher values for dense vegetation. This is in agreement with the fact that under dense vegetation higher root density would enhance the macropore connectivity and thus result in higher infiltration rate. However, double ring infiltrometer tests under dry condition produced higher average infiltration rate (156 mm/hr) and under wet condition produced much lower average infiltration rate (85 mm/hr). These can be attributed to the local scale effects of measurement. It is also worth noting that Haws *et al*. (2004) reported a Representative Measurement Area (RMA) of 400 cm^2, above which the scale effect on infiltration measurement was not significant. But, in the present investigation even with a measurement area of about 700 cm^2 the local scale effect was clearly evident in double ring infiltrometer results. At smaller scales of measurement such spatial variability of preferential infiltration is well reported in literature (van Schaik, 2010).

Table 3.6 Results of runoff plot experiments

Degree of Vegetation	Antecedent Moisture Condition	Range of Simulated Inflow Intensity (mm/hr)	Range of Steady Infiltration Rate (mm/hr)	Mean (mm/hr)	Coefficient of Variation (%)
Sparse	Wet	59-361	33-139	62	45
Dense	Wet	89-310	83-245	135	36

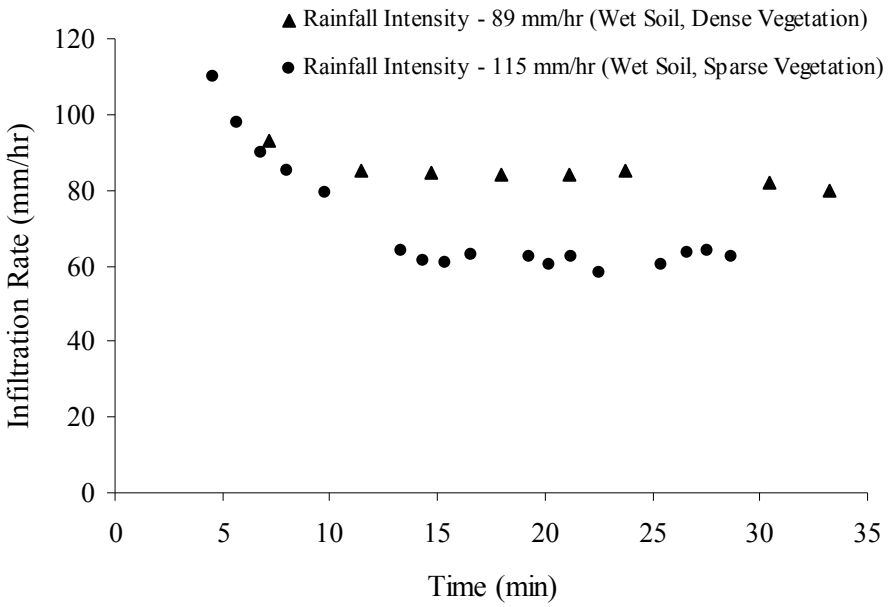

Fig. 3.13 Infiltration rate from runoff plot experiments under different conditions

The infiltrations measured from runoff plots seems to be more accurate as they represent infiltration rate spatially averaged over a larger area and thus considers the soil continuum behavior by taking into account the macropore connectivity within the soil (Sarkar *et al.*, 2008a). Further, it can be noted that the saturated hydraulic conductivity (Table 3.1) of soil matrix, as computed from soil textural data (Schaap *et al*., 1998; Schaap, 1999), is much lower than the spatially averaged steady preferential infiltration rate computed from runoff plot experiments. This clearly indicates the high variability of infiltration rate due to the presence of macropores in the hillslope soil.

3.5 Characterization of Soil Macropores

The process of infiltration into macroporous soils is primarily controlled by size, network, density, connectivity, depth-wise distribution of macropores, and saturation of surrounding soil matrix. It is important to quantify soil macroporosity and trace the dominating flow paths within continuous soil macropores to elucidate the underlying flow mechanisms. To understand the flow behavior in active macropore structures of saturated undisturbed soil columns, dye tracing experiments and subsequent digital image processing techniques were employed. The method provided quantitative information about number of macropores, average number of macropores, maximum and minimum size of macropores, and volume density in terms of stained path width with depth as an explanatory variable. These parameters can be used to compare, evaluate, and quantify the differences in macroporosity under different land use and land cover and management practices. The experimentally derived quantitative data of soil macroporosity can have wide range of applications in the region such as water quality monitoring and groundwater pollution assessment due to preferential leaching of solutes and pesticides, study of soil structural properties and infiltration behaviour of soils, investigation of flash floods in rivers, and hydrological modelling of the watersheds (Shougrakpam *et al.*, 2010).

Similar to the present investigation, dye staining techniques have been used widely by many researchers for characterizing soil macroporosity. It is worth mentioning that for future studies the use of ion tracers for conducting infiltration tests can be more useful, as in dye tests the soil columns are destroyed and no information about the flow velocity through soil macropores can be obtained. Small scale tracer experiments can be used to explore the preferential flow velocity distribution (Weiler and Naef, 2003). Use of ion tracers can also provide spatial and

temporal data on solute transport and their travel time. Elçi and Molz (2009) used bromide tracer to measure actual travel time of water flow in macroporous soils. They found that the soil matrix permeability was much less than the measured soil matrix plus macropore permeability. The use of the measured higher value of permeability resulted in better simulation of their numerical subsurface flow model (MODFLOW). Buttle and McDonald (2000) suggested that tension infiltrometry can be a rapid and non-destructive method of assessing spatial variations in the relative contribution of macropore flow to the infiltration process. For monitoring and understanding the soil water processes, geophysical methods can also be helpful as they are non-invasive and do not disturb either the structure or the water dynamics of the soil. Batlle-Aguilar *et al.* (2009) used electrical resistivity tomography (ERT) for imaging water infiltration dynamics in soil with a tension infiltrometer using Cl^- and Br^- solution as tracer. The method was used to determine soil hydraulic conductivity and sorptivity values. A similar method of determining bulk density and macroporosity of soil is computer tomography (CT). It is also a non-destructive method of obtaining spatial density distribution of macropores and visualizing solute infiltration in soils (Olsen and Børresen, 1997). Thus, the information about size and density distribution of soil macropores, active flow network, flow velocity, and distribution of pore water pressure can be used to better describe the infiltration process, which can help in the process based modeling approach in hillslope hydrology (Weiler and McDonnell, 2004).

3.5.1 Experimental setup and methodology

In order to characterize the macropore structure of the hillslope soil, two undisturbed soil columns were collected from the experimental plot. Each column having a dimension of 25 × 25 × 50 cm, were carved from a pedestal of soil block. A

rectangular chamber made of 6 mm thick Plexiglas sheet, was inserted from the top of the soil column by careful trimming of the excess soil around the sides of the column (Fig. 3.14). The samples were taken to the laboratory for the infiltration experiments. The laboratory experimental setup consisted of a soil infiltrometer chamber, a square overhead water tank, a square tray mounted on a stand, a hollow cylinder, and an outlet for excess water flow (Fig. 3.15). The Plexiglas collection chamber was used as infiltrometer chamber. The chamber containing the soil column was placed over the tray and the tank was securely attached above the soil column with screws. Rubber linings were used between the soil column and the Plexiglas chamber to minimize the leakage of dyed water. A one meter long and 2.5 cm diameter profile probe soil moisture meter (Delta T), equipped with a hand held data logger (Delta T), was inserted through the middle of the soil column down to the bottom of the hollow cylinder for monitoring the volumetric moisture content of soil. The instrument has multiple sensors to capture, display, and store the moisture contents at different depths. To minimize the damage to the soil column a sharp soil auger was used to drill the 2.5 cm diameter hole.

In order to establish a wet initial condition each soil column was subjected to infiltration with clear water for a period of 3 hours with a ponding depth of 2 cm maintained at the overhead water reservoir. By this time the profile probe readings indicated a steady saturated condition of the soil column. Then the column was left for 4-5 hours to allow the soil attain field capacity. Dye infiltration experiments were then conducted. Brilliant Blue FCF ($C_{37}H_{34}N_2Na_2O_9S_3$) is commonly used as a dye tracer and considered as one of the best available (Flury *et al.*, 1994; German-Heins and Flury, 2000). It has low toxicity, high mobility, and high visibility even after dilution and adsorption (Weiler, 2001). In the present study, Brilliant Blue R250

Fig. 3.14 Collection of soil columns from the plot

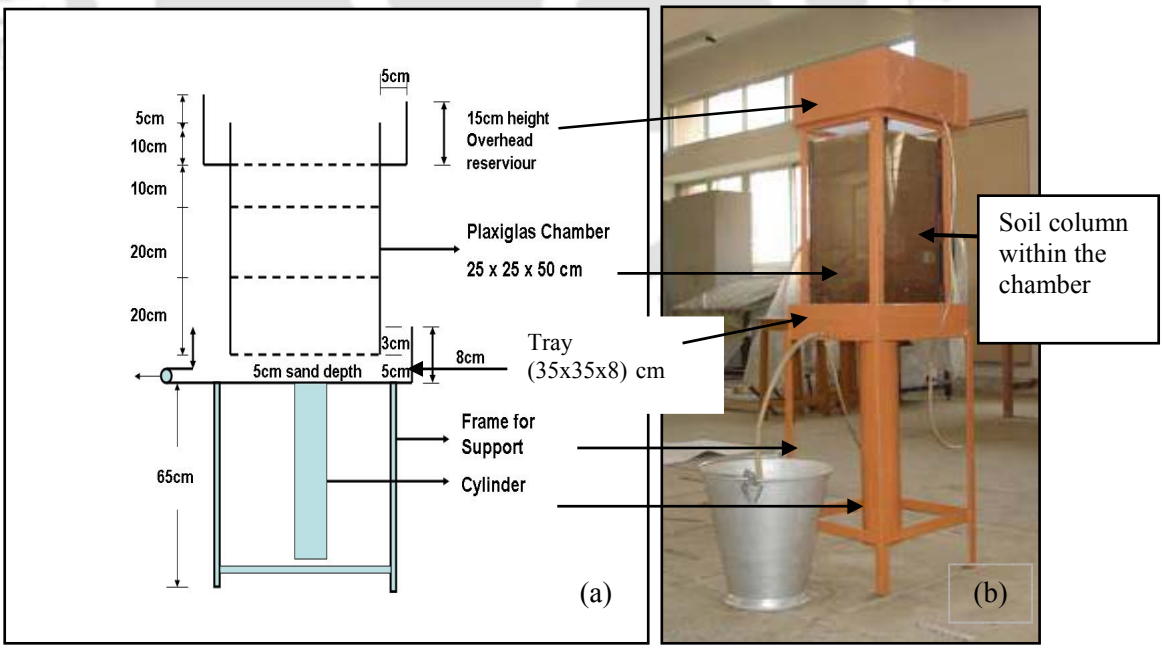

Fig. 3.15 Laboratory setup for conducting dye infiltration experiments

($C_{47}H_{50}N_3O_7S_2$+; C.I. 42660) dye, which belongs to the same family of Brilliant dyes and has similar staining characteristics like Brilliant Blue FCF, was used. Brilliant Blue R250 is also known to have better resolution of the stained objects (Merril, 1990). The dye was applied at the rate of 4 g/l which was sufficient for clear visibility of the stained macropore flow paths in soil.

Infiltration experiments were conducted with dye solution for each of the wet soil sample by maintaining a ponding depth of 2 cm in the overhead tank. This consideration is reasonable as the frequent high intensity storm events of the region can result in such depth of ponded water on the soil surface. After 3 hours, supply of dye solution was stopped and the soil was left for 4-5 hours for allowing proper distribution of dye. Then the overhead tank and the Plexiglas chamber were removed and the soil column was sliced horizontally by a sharp edged thin plate at 1 cm intervals from the top to analyze the dye distribution patterns. The distortions in dye patterns due to slicing were negligible as the soils were not cohesive and had low water holding capacity. A graduated frame was placed on the soil surface to provide a reference for the image analysis. Serial images of the horizontal slices were taken using a digital SLR camera (Canon EOS 400D, 10 Mega Pixels resolution) for digital image analysis of the dye patterns.

3.5.2 Image analyses

For accurate measurement of stained areas, the serial images were color corrected, digitally rectified, and scaled (Fig. 3.16) to a resolution of one square millimetre per pixel (Weiler and Flühler, 2004). These corrected images were analysed to determine the characteristics of macropore flow for the soil samples collected from the hillslope plot. The stained paths indicated flow paths with continuous macropore connectivity. The unstained pores that are visible on a

horizontal slice are the macropores for which the connectivity has been disturbed. Therefore, in relation to active macropore flow, the main area of interest was to quantify the stained path width and their distribution in both horizontal and vertical faces. Besides size of the stained paths, the distribution of these pores along different sections has been described by means of spatial statistical parameters. The horizontal and vertical dye patterns analyses of the images were conducted as follows (Weiler, 2001; Weiler and Flühler, 2004).

3.5.2.1 Horizontal dye pattern analysis

Image analyses of the horizontal dye patterns were conducted to find the percentage dye coverage of the stained patterns for each horizontal section. The stained flow pathways obtained from dye tracer experiments were used to describe the preferential flow behavior in soils. Quantitative parameters can be subdivided into basic and morphometric parameters such as the total stained area or a geometric description of stained objects and their spatial statistics. The objective of the horizontal dye pattern analyses was to find out the depth function of the percentage dye coverage area. The maximum likelihood algorithm available in Geomatica 10.0 software, was used to cluster the percentage dye coverage area of each horizontal image. This algorithm is a probabilistic classification technique of the pixels into different classes (Foody *et al.*, 1992). A classification report after every image analysis was generated as percentage coverage area of the identified objects. Finally, classified images were compared with the original photographs to identify potential errors. The results of the percentage dye coverage area were summarized to indicate the percentage of stained flow path through each horizontal layer. Fig. 3.17 shows the digitally processed horizontal dye patterns at various depths for a hillslope soil column.

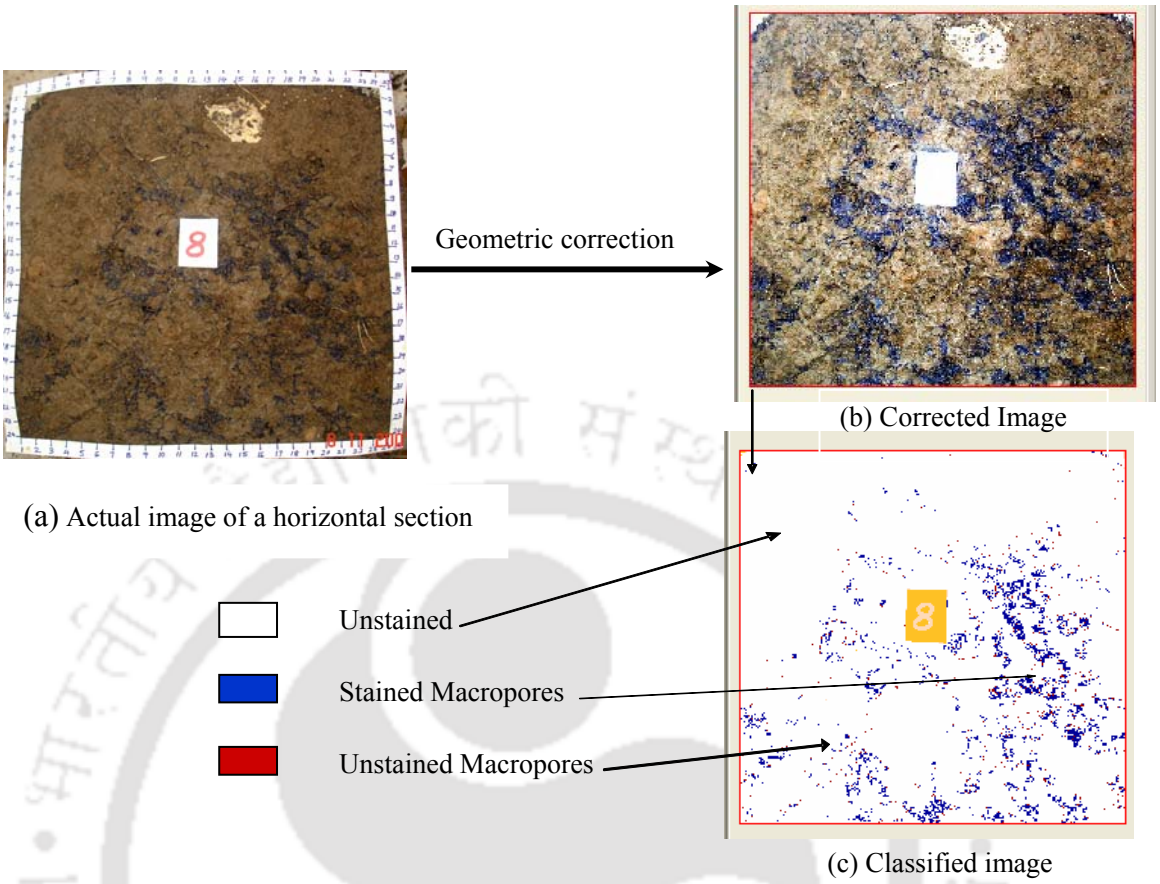

Fig. 3.16 Image correction and classification for a horizontal section

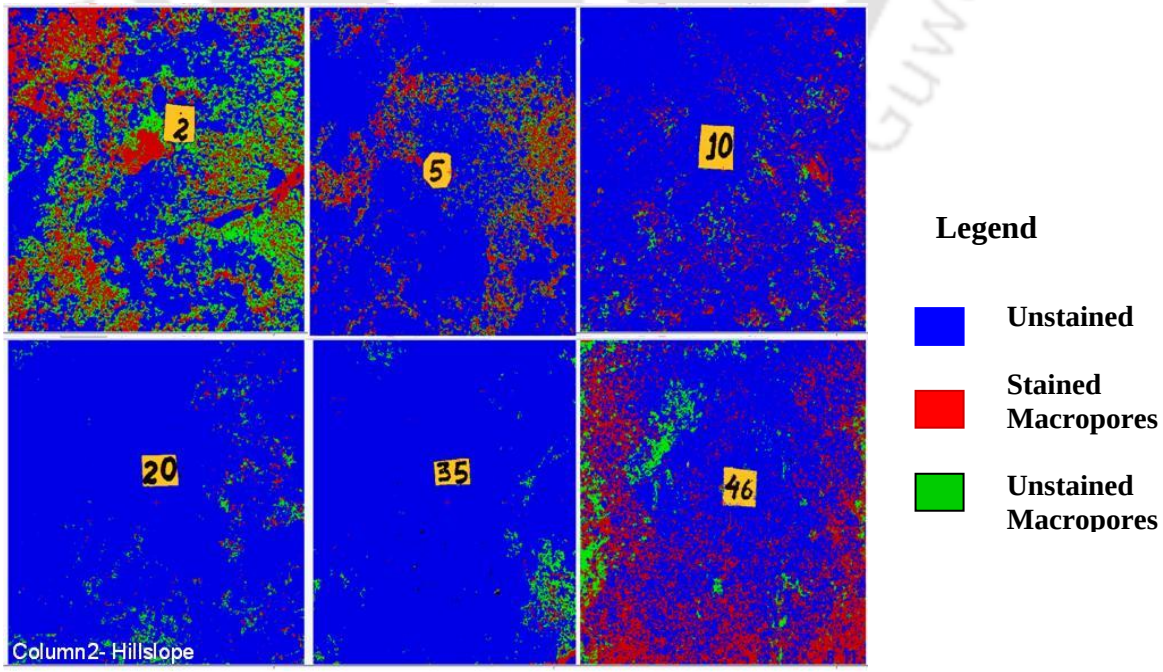

Fig. 3.17 Digitally processed images of undisturbed hillslope soil at different depths

Results of horizontal dye pattern analysis

The horizontal dye patterns provided detailed information about the maximum depth of dye penetration and percentage dye coverage of the sections. For both the soil columns percentage dye coverage versus depth was plotted. Fig. 3.18 shows the depth wise distribution of percentage dye coverage for the two hillslope soil columns (Column 1 and 2). Column 1 had maximum dye coverage of 9.91% at 5 cm depth and an average of 3.71%, whereas Column 2 had maximum dye coverage of 7.42% at 9 cm depth and an average of 2.77%. In both the columns the color dye penetration was clearly visible up to the last soil layer. This indicates the presence of continuous macropores throughout the soil column. Such distribution of macropores can be expected from densely vegetated undisturbed hillslope soils where growth of plant roots provides connectivity to preferential pathways for water movement. The occurrence of maximum dye coverage within 10 cm depth also represents higher root density and activity of soil fauna and flora in the top soil layer. From the average dye coverage, it can be noted that most of the flow pathways were concentrated to 3.71% and 2.77% of total area in Column 1 and Column 2, respectively.

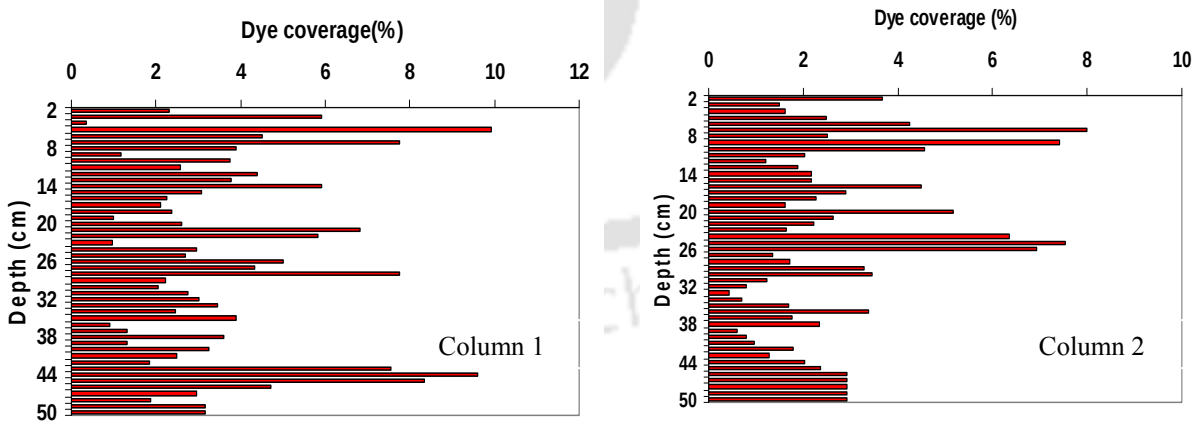

Fig. 3.18 Depth wise dye coverage distribution of the two soil columns

3.5.2.2 Vertical dye pattern analysis

The percentage dye coverage areas of horizontal images were used to calculate the statistical parameters of the vertical dye patterns. The vertical dye patterns provide

a clear picture of the macropore flow processes at different depths. The basic parameter called volume density has been frequently used by the researchers for vertical dye pattern analyses (Weiler, 2001; Weiler and Flühler, 2004; Bachmair, *et al.*, 2009). It is similar to the dye coverage area and can be derived by stereological methods. Stereology is a mathematical procedure used for relating three-dimensional parameters defining a structure to two-dimensional measurements obtained from the sections of the structure (Weibel, 1979). The volume density (Vv) can be derived from one or two-dimensional information, as Vv can be related to the area density (A_A) and length density (L_L) as (Weiler, 2001)

$$Vv = A_A = L_L \tag{3.2}$$

The depth functions of the volume density with a vertical resolution of 1 cm were derived from the observed dye patterns. Four transect lines were taken at each depth to calculate volume density as the ratio of sum of the widths of intercepted stained objects to the total transect length (Equation 3.3).

$$\text{Volume density} = \frac{\sum SPW}{T_L} \tag{3.3}$$

where $\sum SPW$ = sum of the widths of intercepted stained objects, and

T_L = total transect length

The other important parameter that can be useful to describe preferential flow from vertical dye pattern analysis is the stained path width (SPW), which is the width of the stained objects for each soil depth. The one-dimensional intercept length can estimate the area of the object in two dimensions, if the object is isotropic (Weibel, 1979). Therefore, the object width for a given depth of the vertical dye pattern was used as an indicator for the size of the object at that soil depth (Weiler, 2001). As it may not be feasible to calculate the stained path widths for the entire horizontal slices at each depth, it is done in four transect lines. The resulting SPW was also used to derive statistical parameters such as maximum SPW and number of stained paths at

each soil depth. Fig. 3.19 shows the concept of transect lines and stained path widths taken on a horizontal surface and an arbitrary distribution of macropore pathways as may be visible on a vertical section. Here the object widths are referred to as stained path widths. After counting the number of stained paths they were grouped into five SPW classes. Then the depth distribution of number of stained paths in each group was taken to calculate the volume density. For a particular section, volume density was calculated as the total number of stained paths divided by the width of the section. Thus from the frequency distribution of the SPW at each section the volume density related to the SPW classes were determined. The depth function of stained path width was derived by combining all vertical dye patterns.

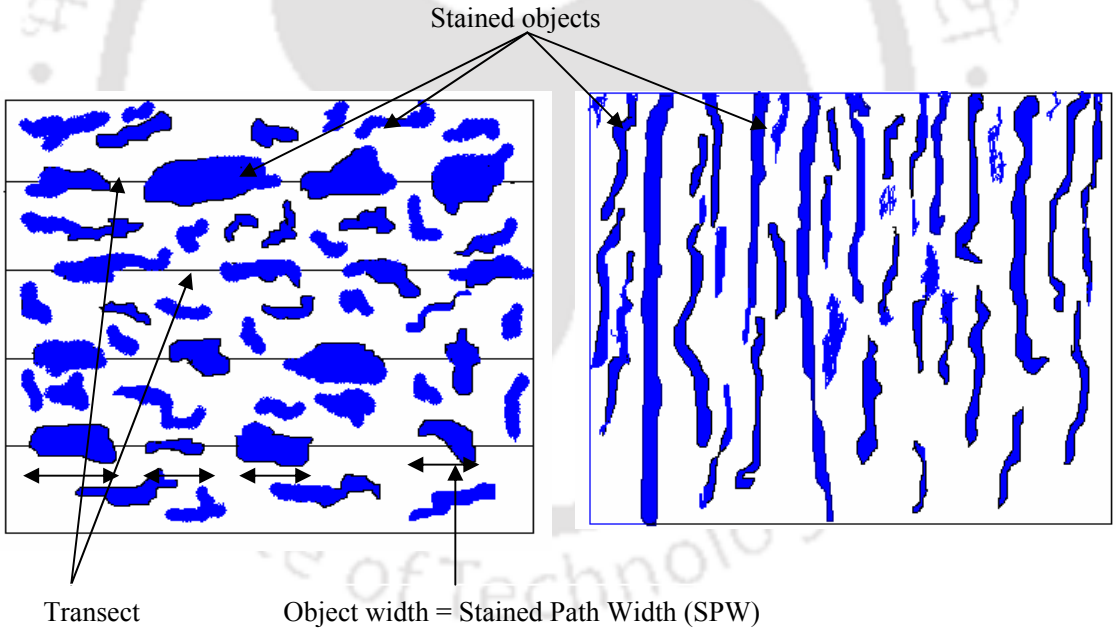

Fig. 3.19 Object width and stained path width (SPW) of dye patterns

Results of vertical dye pattern analysis

Vertical dye pattern analysis was carried out to derive the parameters volume density, stained path width, depth wise distribution of SPW, and maximum SPW at

the transects. These parameters were analyzed to interpret the soil macropore structure and the process of water movement through the hillslope soil columns. A clear indication of soil macroporosity in terms of their size and depth wise distribution could be derived from the analysis.

The SPWs determined at each transect were classified into five groups based on their size. Table 3.7 enumerates average volume densities of different SPW classes at a particular transect for the two soil columns. The SPW classes 1-2 mm and 3-4 mm are clearly dominating, which indicates that most of the macropores present in the soil have sizes in the range of 1-4 mm. Macropores greater than 4 mm in diameter are comparatively much less in number.

Table 3.7 Distribution of average volume density with SPW at a particular transect

SPW Range (mm)	Column 1	Column 2
1-2	0.027333	0.024015
3-4	0.020500	0.021913
5-7	0.010583	0.009371
8-10	0.004583	0.00172
> 10	0.001444	0.00049

Fig. 3.20 depicts the depth wise distribution of number of stained paths encountered at a particular transect for the two soil columns. Column 1 had the highest number of stained paths of 27 at 45 cm depth, whereas Column 2 had a maximum of 24 stained paths at 25 cm depth. These clearly indicate the significant number of the macropores present in the soil profile at the given vertical transects. The maximum sizes of SPWs found at different depths were in the range of 2-23 mm. Overall it was found that the 1-2 mm diameter macropores were present in maximum

numbers throughout the soil profile of the hillslope plot. Such small diameter macropores are mainly formed due to the growth of dense plant root network.

Fig. 3.21 shows that the volume density has a better correlation with the number of stained paths than with the maximum width of the stained paths. This is because the large diameter macropores are very few in numbers and therefore the volume density is mostly influenced by the smaller macropores which are significantly more in numbers.

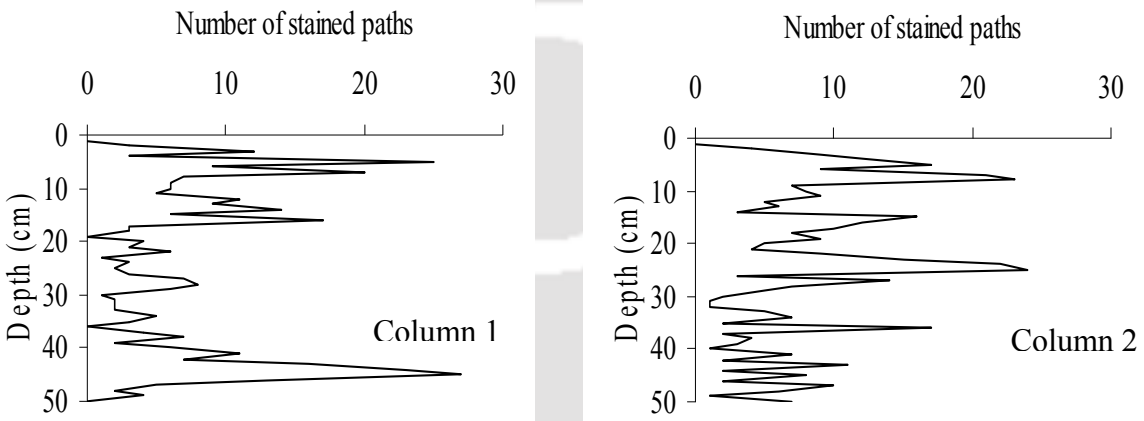

Fig. 3.20 Depth wise distribution of number of stained paths

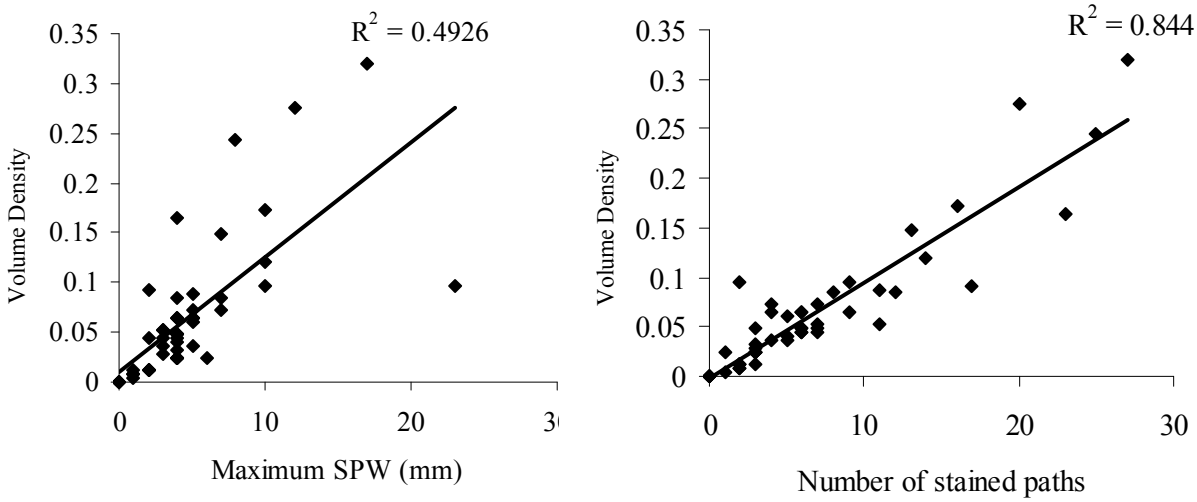

Fig. 3.21 Correlation of volume density with maximum SPW and number of stained paths

3.6 Subsurface Soil Moisture Monitoring System

As discussed in the previous sections, for conducting the *in situ* field experiments in the hillslope plot, a wet antecedent soil moisture condition was required to be established before the start of each experiment. To measure the spatio-temporal variations of moisture content in the subsurface soil a reliable, quick, and accurate soil moisture measurement device was required. Therefore, Delta-T soil moisture profile probe (Fig. 3.22) was used for monitoring the soil moisture conditions of the hillslope plot before, during, and after the experiments. The HH2 type moisture meter is a versatile unit for use with Delta–T moisture devices. The instrument is especially designed for quick measurements in field. It can give instantly the soil moisture data in volume basis (cm^3/cm^3) or millivolt (mV) and can store up to 1100 readings with multiple user defined soil types. The accuracy of the instrument is ± 3%. This instrument is not only simple and versatile in operation, but also permits up to 5 extra user defined soil calibrations to be characterized and stored for later use. The active soil type can be switched at any time during the collection of data, and can be specified separately for each sensor position on a single profile probe. Moreover, it can automatically calculate the water deficit, based on data from the individual sensors. Fig. 3.23 shows the detailed instrumentation of the experimental hillslope plot. In the present investigations, soil moisture contents at 100, 200, 300, 400, and 1,000 mm from the ground surface were monitored at four different locations (P1, P2, P3, and P4) of the plot (Fig. 3.23).

3.6.1 Calibration of the profile probe soil moisture meter

Before use, the profile probe soil moisture device was required to be calibrated for the soil of the experimental hillslope plot. As the measurements were to be taken at five different depths (100, 200, 300, 400, and 1,000 mm), at each depth the sensors

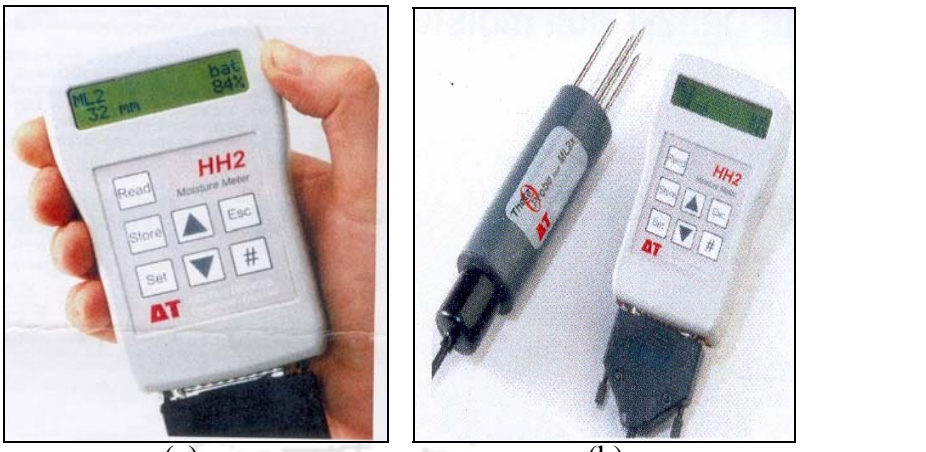

Fig. 3.22(a-c) Delta-T soil moisture meter (Type HH2)

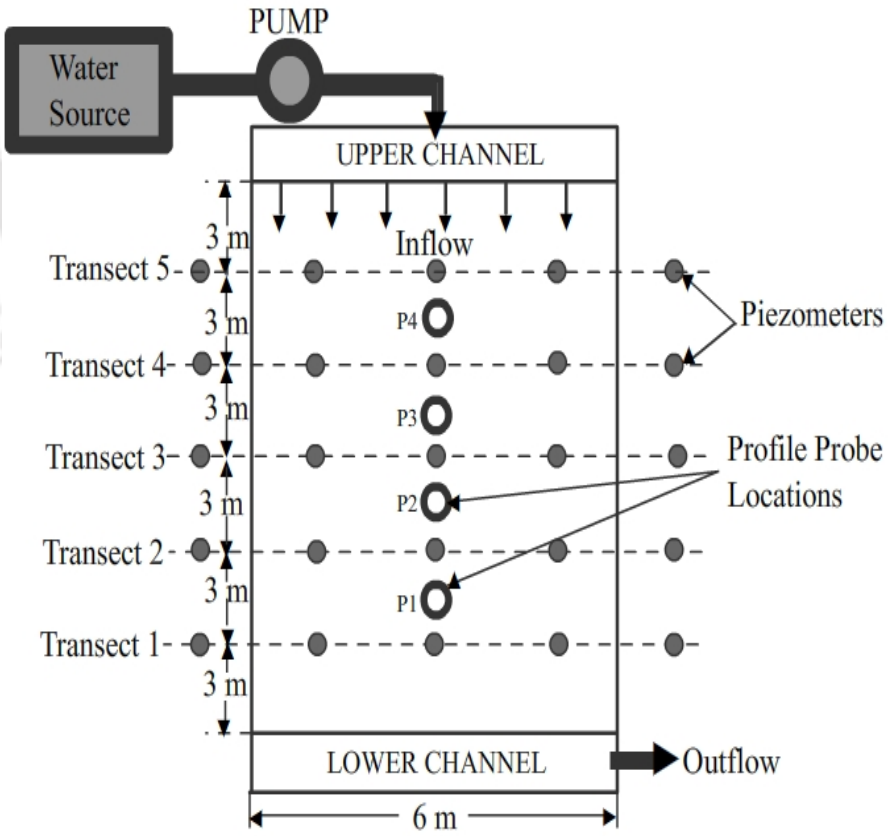

Fig. 3.23 Schematic diagram of the experimental setup and instrumentation in the hillslope plot

were calibrated. For this purpose undisturbed soil samples were collected from each depth using soil core samplers. A simple calibration method (Miller and Gaskin, 1997) has been used for calibrating the instrument. The detailed calibration procedure illustrated hereunder has also been used by Singh (2006).

Theory

The profile probe soil moisture device uses the concept of converting the measured output of the sensor in millivolt (mV) to volumetric soil moisture content (cm^3/cm^3). The measured sensor output (mV) can be directly related to the square root of apparent dielectric constant ($\sqrt{\varepsilon}$) of the soil. If V is the measured sensor output then it can be related to $\sqrt{\varepsilon}$ by either of the following two equations:

$$\sqrt{\varepsilon} = 1.07 + 6.4V - 6.4V^2 + 4.7V^3 \quad \text{with } (R^2 = 0.998) \tag{3.4}$$

$$\sqrt{\varepsilon} = 1.1 + 4.44V \quad \text{with } (R^2 = 0.99) \tag{3.5}$$

For soil specific calibration there is a simple linear relationship between the complex refractive index (which is equivalent to $\sqrt{\varepsilon}$) and volumetric water content (θ) given as (Whalley, 1993)

$$\sqrt{\varepsilon} = a_o + a_1 \times \theta \tag{3.6}$$

where a_o and a_1 are the coefficients required to be determined for a particular type of soil.

Procedure

The collected undisturbed moist soil samples were immediately taken to the laboratory and the sensor output (V_w) for all the soil samples were noted. Knowing the value of V_w, the value of $\sqrt{\varepsilon_w}$ was calculated from Equation 3.5. The moist weight (W_w gm) and volume (V_v cm^3) of the soil were noted before oven drying the samples.

For oven dried samples (i.e. $\theta = 0$) the sensor outputs (V_0) were observed and finally the dry weight (W_0 gm) of the samples were taken. As V_0 is known, using Equation 3.5 the value of $\sqrt{\varepsilon_0}$ were calculated for all the soil samples. For oven dried samples moisture content (θ) is zero. Thus, we get

$$a_0 = \sqrt{\varepsilon_0} \tag{3.7}$$

The volumetric water content of the samples can be determined from the following equation:

$$\theta_w = \frac{(W_w - W_0)}{V_v} \tag{3.8}$$

Now from Equation 3.6 we get

$$a_1 = \frac{\sqrt{\varepsilon_w} - \sqrt{\varepsilon_0}}{\theta_w} \tag{3.9}$$

Finally, knowing the values of the two coefficients a_o and a_1 for each sensor depth the actual volumetric soil moisture content (θ_a) can be computed as

$$\theta_a = \frac{[1.1 + 4.44V] - a_0}{a_1} \tag{3.10}$$

where V is the measured sensor output in mV at a particular sensor depth.

Following the above calibration procedure the sensors of the probe were calibrated for the five different depths of soil (Fig. 3.24). The average values of the coefficients a_o and a_1 determined for the hillslope experimental plot soil are 2.4 and 8.6, respectively. These values were used to convert the measured sensor output at a particular depth to the actual volumetric soil water content.

3.6.2 Study of soil moisture profile in the hillslope plot

Spatial and temporal variations of soil moisture profile within the hillslope plot before, during, and after the runoff experiments were precisely monitored using

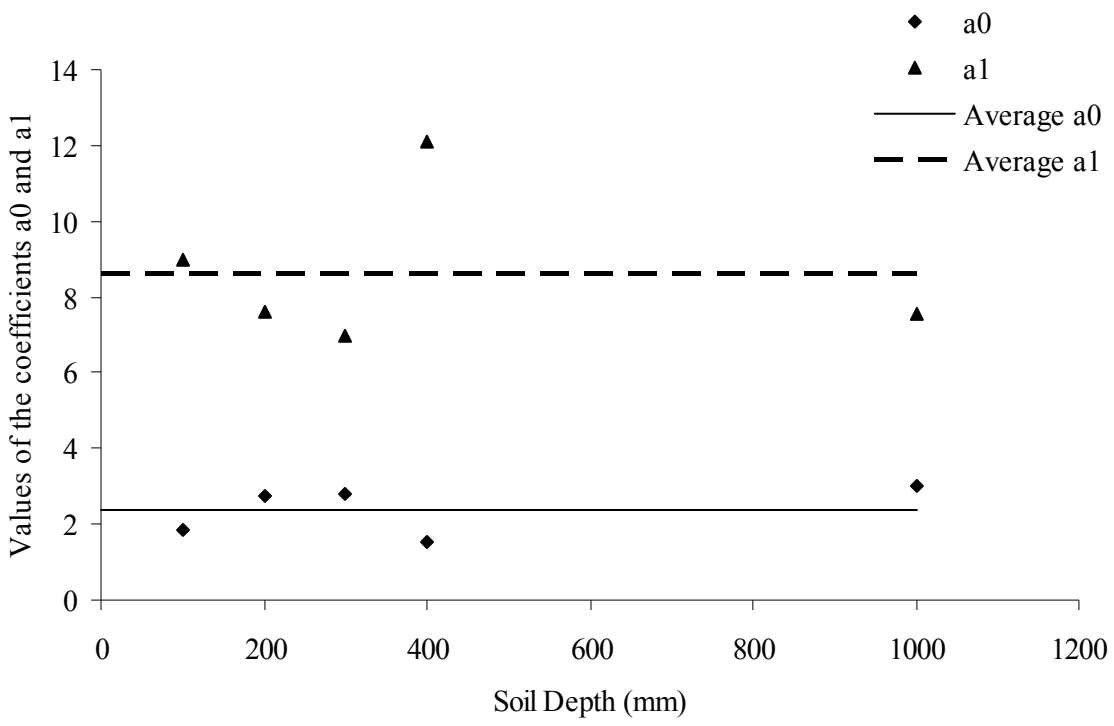

Fig. 3.24 Calibration of the profile probe sensors at different soil depths

the profile probe soil moisture sensor. Interesting observations could be made from the soil moisture distribution patterns in the hillslope soil. After establishing a wet antecedent moisture condition in the plot, runoff events were simulated using the sheet flow generation system. Fig. 3.25 (a-d) shows the temporal variations of the volumetric moisture contents of soil at different depths at the four selected locations (P1, P2, P3, and P4) of the plot. With a wet antecedent condition, the plot was subjected to a runoff event having inflow intensity 250 mm/hr for 30 minutes duration. The graphs clearly show that once a wet antecedent moisture condition is attained, the moisture content of soils at different depths remains almost constant during the runoff events as well as after the cessation of surface runoff. It can be observed that the constant soil moisture conditions over the plot have been attained very quickly during the runoff event. It also indicates that under wet antecedent condition, a steady infiltration/recharge condition has been attained in the hillslope plot within a very short time. It is a very important finding related to the present

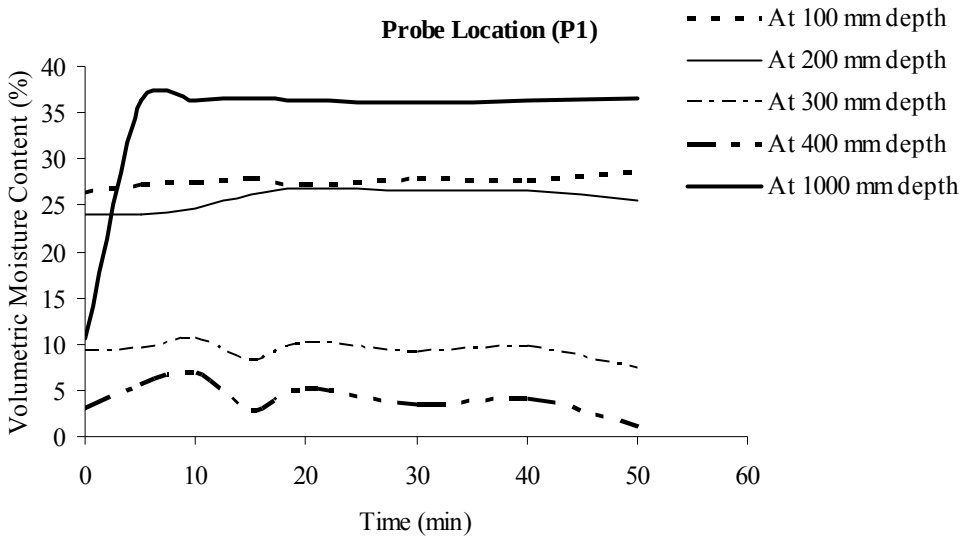
Probe Location (P1)
Volumetric Moisture Content (%)
Time (min)
At 100 mm depth
At 200 mm depth
At 300 mm depth
At 400 mm depth
At 1000 mm depth

(a)

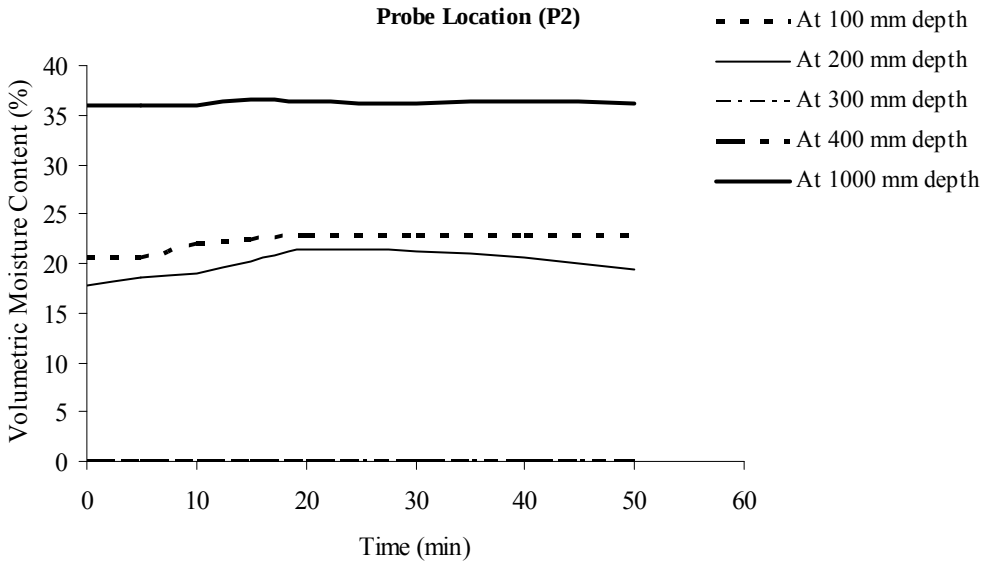
Probe Location (P2)
Volumetric Moisture Content (%)
Time (min)
At 100 mm depth
At 200 mm depth
At 300 mm depth
At 400 mm depth
At 1000 mm depth

(b)

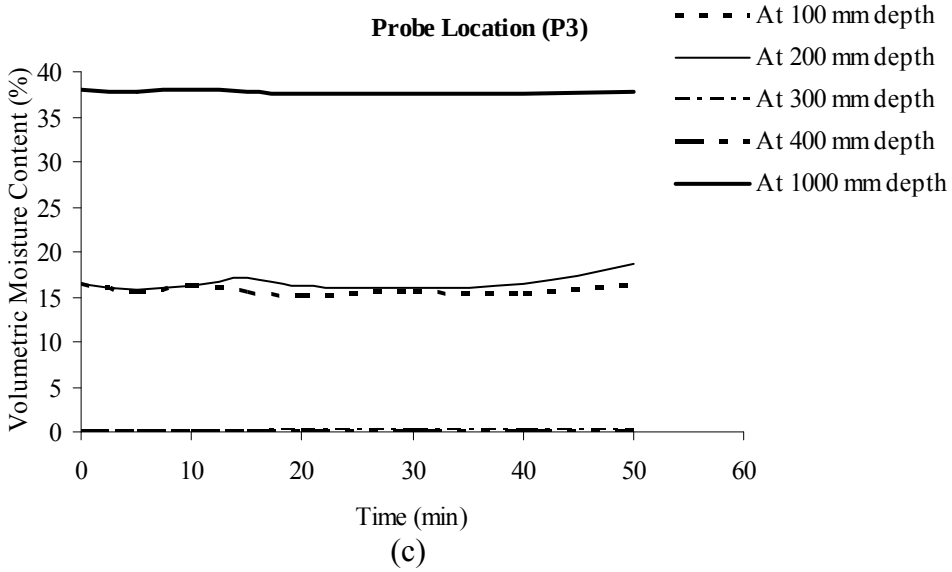
Probe Location (P3)
Volumetric Moisture Content (%)
Time (min)
At 100 mm depth
At 200 mm depth
At 300 mm depth
At 400 mm depth
At 1000 mm depth

(c)

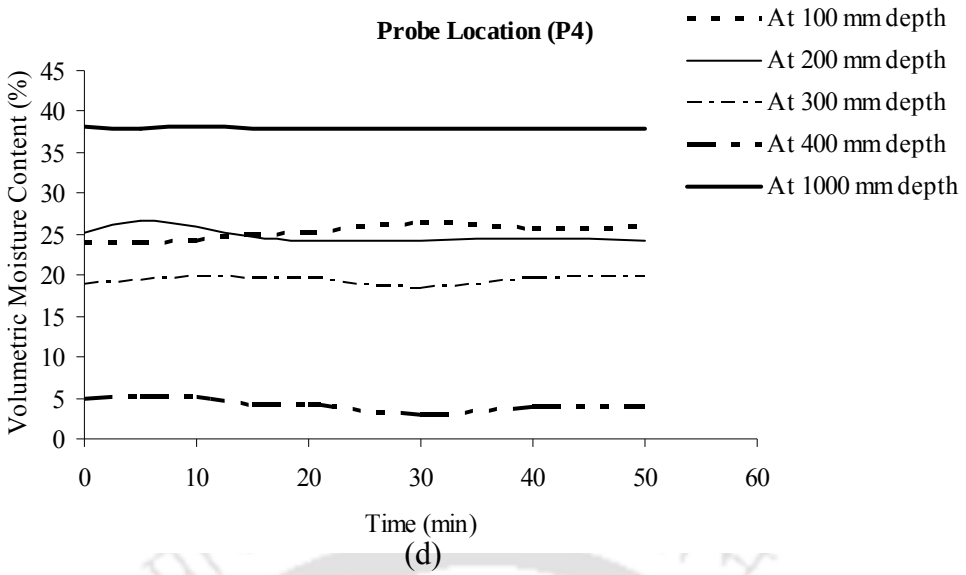

(d)

Fig. 3.25(a-d) Temporal variations in soil moisture contents at different depths (b.g.l.) in the hillslope plot during and immediately after runoff experiment

investigation. Here the main focus is to capture and understand the flow processes under initially wet soil condition. The unsaturated flow processes related to the buildup of soil moisture content from its initial dry condition is beyond the scope of this study.

Soil moisture content measurements were also done for prolonged periods after the runoff experiments. Fig. 3.26(a-d) shows the depth-wise variations of soil moisture contents in the hillslope plot recorded for a long duration of about 35 hours since the completion of runoff experiment. These figures also suggest that once a wet antecedent moisture condition is attained, soil moisture contents remains almost stable for a long duration. Therefore, once the soil was wetted, it remained at field capacity for 2-3 days even if there was no artificial runoff or natural rainfall. This is a significant finding, because from the early monsoon showers the topsoil of the hillslopes is expected to be wet and then it remains at field capacity for a significant period. Therefore, the subsequent storm events are extremely critical for the generation of rapid subsurface stormflow from these hillslopes.

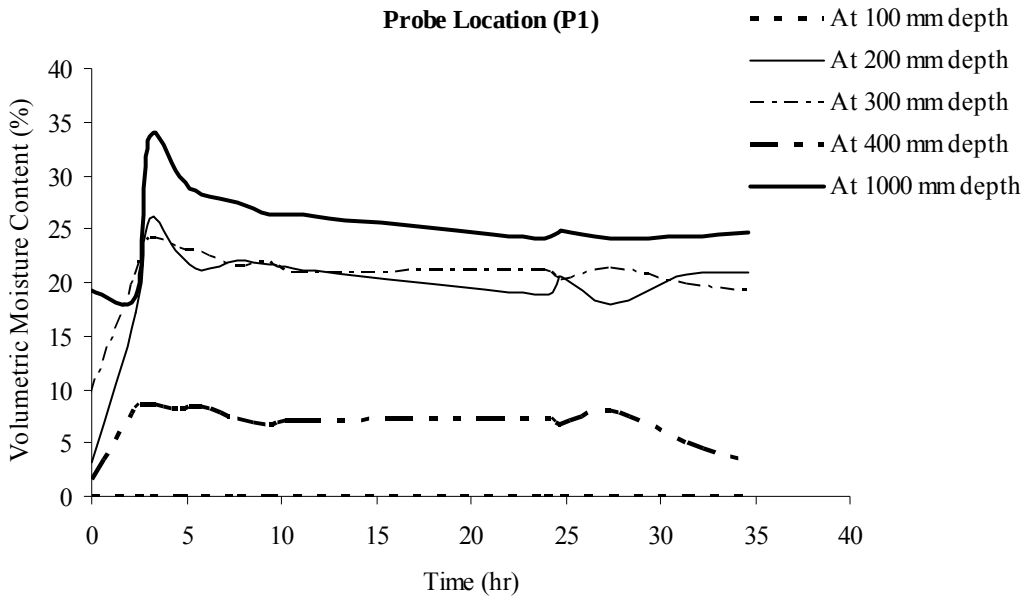
Probe Location (P1)
At 100 mm depth
At 200 mm depth
At 300 mm depth
At 400 mm depth
At 1000 mm depth
Volumetric Moisture Content (%)
Time (hr)

(a)

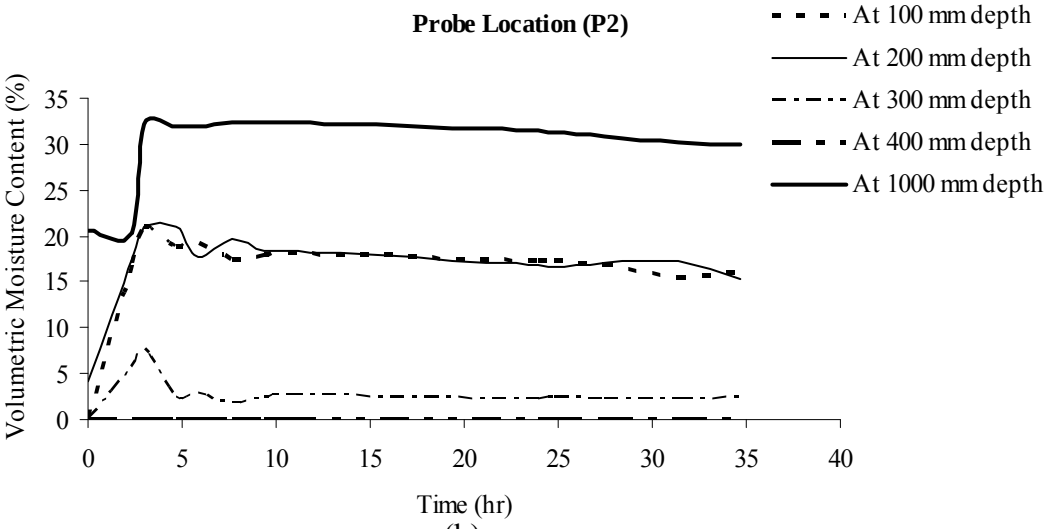
Probe Location (P2)
At 100 mm depth
At 200 mm depth
At 300 mm depth
At 400 mm depth
At 1000 mm depth
Volumetric Moisture Content (%)
Time (hr)

(b)

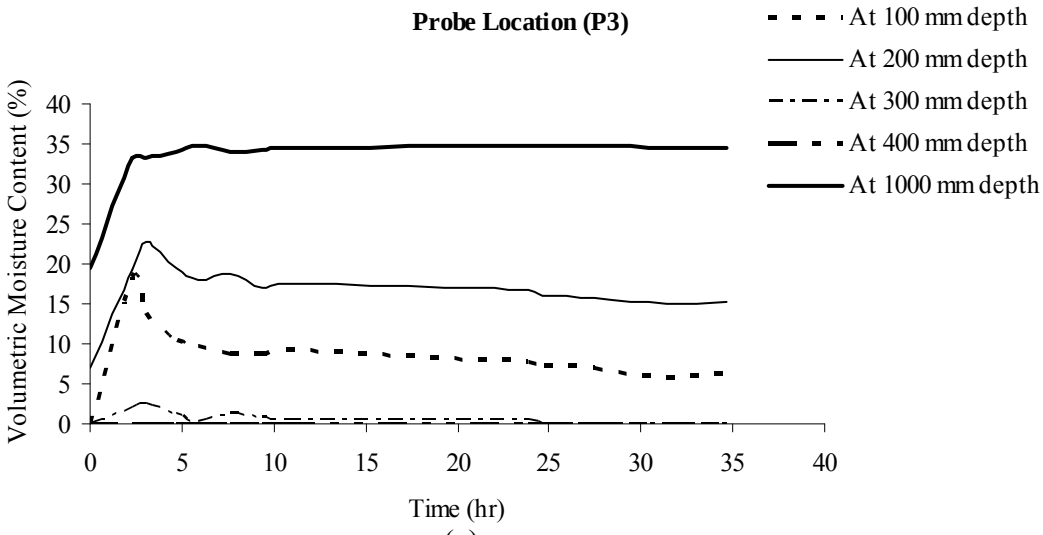
Probe Location (P3)
At 100 mm depth
At 200 mm depth
At 300 mm depth
At 400 mm depth
At 1000 mm depth
Volumetric Moisture Content (%)
Time (hr)

(c)

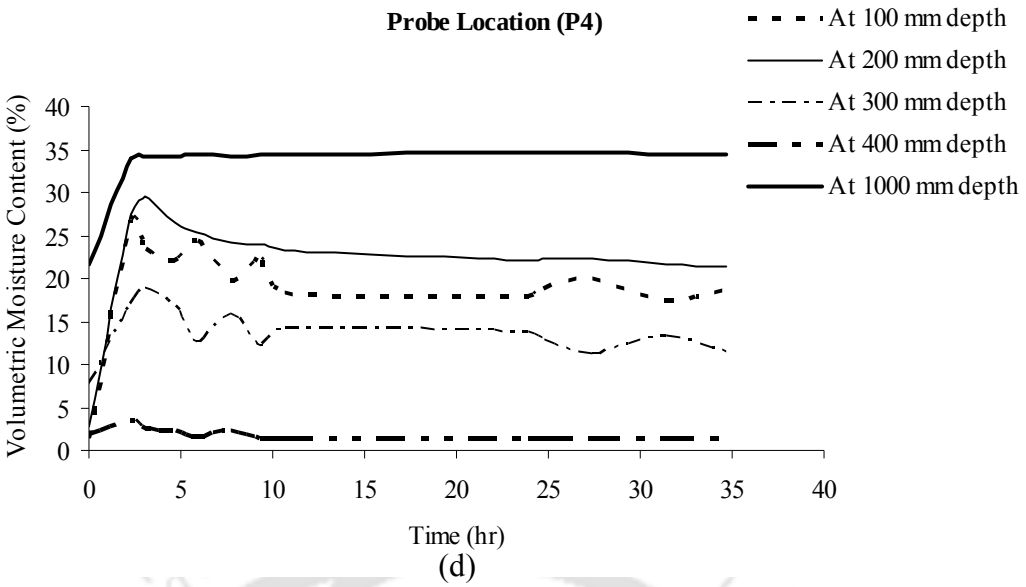

(d)

Fig. 3.26(a-d) Temporal variations in soil moisture contents at different depths (b.g.l.) in the hillslope plot for prolonged duration after runoff experiment

The spatio-temporal variations in the soil moisture profile along the centre line of the hillslope plot can also be studied from the profile probe measurements taken before, during, and after the runoff experiments. Fig. 3.27(a-h) shows the distribution of soil moisture at different time steps along the central transect of the plot for a simulated inflow intensity of 305 mm/hr continued for 40 minutes duration. The figures clearly depict that after a wet antecedent condition has been established, the moisture content in the top soil layer does not vary. The middle layer soil (300-400 mm) has relatively low but stable moisture content. Temporal variations of the soil moisture profiles indicate that the infiltrated water bypasses this layer to reach the bottom layer where the build up of water table takes place over the impermeable bed and causes lateral diversion of water in the form of subsurface stormflow. Such bypassing flow patterns within the soil combined with rapid buildup and recession of water table in the hillslope soil profile strongly indicates the existence of highly active lateral preferential pathways in the subsoil.

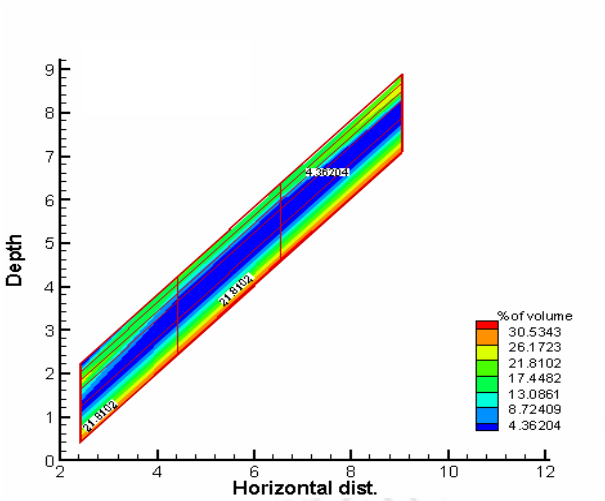

(a) Initial soil moisture distribution

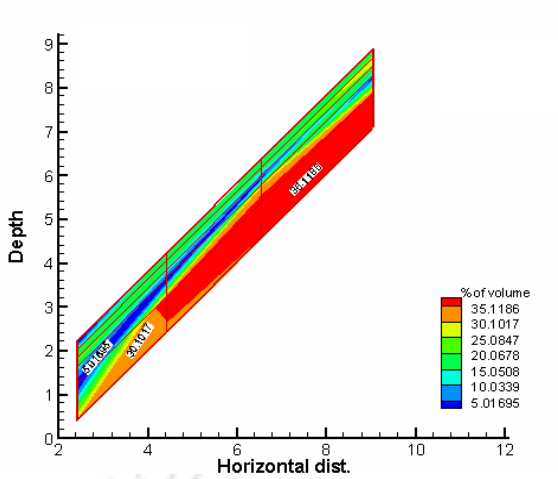

(b) Water table buildup at t = 18 min.

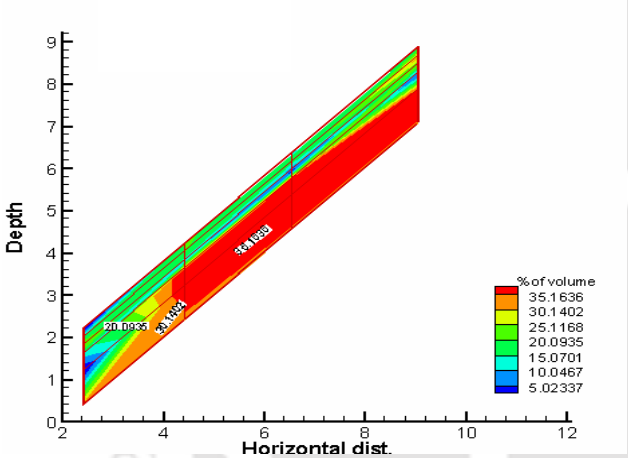

(c) Subsurface flow initiation at t = 22 min.

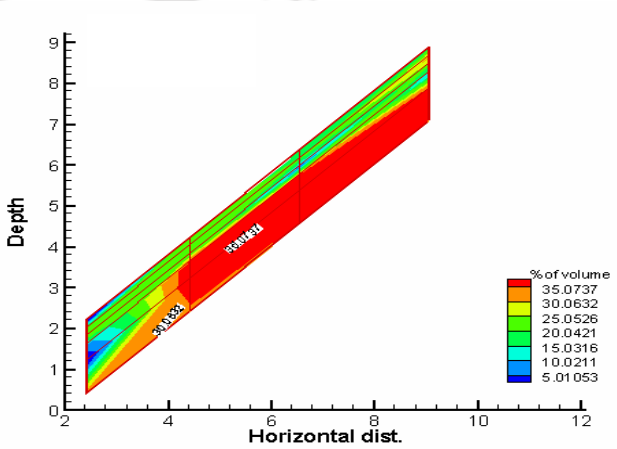

(d) Soil moisture profile at t = 42 min. (Overland flow ceased)

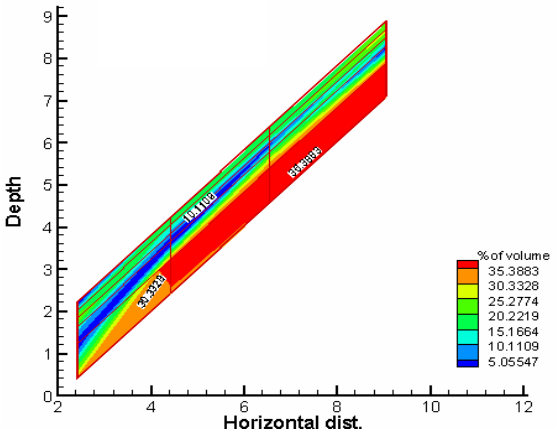

(e) Recession of water table at t = 68 min.

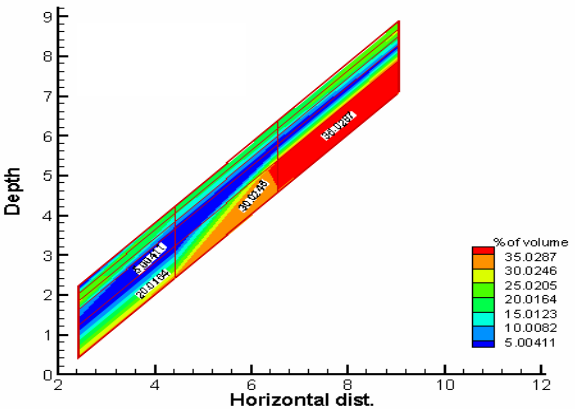

(f) Recession of water table at t = 85 min.

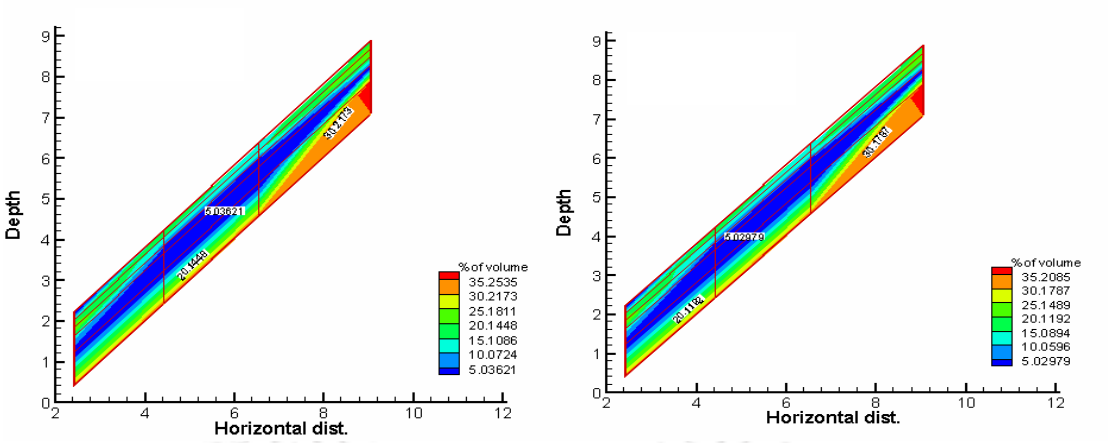

(g) Recession of water table at t = 90 min. (h) Soil moisture profile at t = 120 min.

Fig. 3.27(a-h) Measured subsurface soil moisture profiles of the hillslope plot at different time steps

3.7 Observation of Overland Flow in the Hillslope Plot

3.7.1 *In situ* overland flow experiments

To study the overland flow behavior on the experimental hillslope plot a number of runoff experiments were conducted with a wide range of inflow intensity and duration. From dye tracing experiments it has been identified that the hillslope soil has a highly connected active preferential flow network. Furthermore, from the previous experimental evidences it is well understood that in the process of preferential flow generation, moisture content at the top-soil layer initially increases from its antecedent condition to its field capacity, where it then remains fairly constant. But, as another successive storm event follows, a saturated layer is developed over the impermeable bed and then it gradually grows towards the top and due to lateral preferential flow and gravity effect it tends to flow in the lateral direction (Kirkby, 1978). A similar kind of initial wet antecedent conditions were established before the start of the *in situ* experiments.

The overland flow experiments were conducted in three different seasons representing three distinct vegetation conditions to study the effect of change in physical condition of the plot on infiltration and overland flow behavior. After saturating the hillslope in order to establish a wet initial condition, a constant inflow discharge from the upper channel was maintained to establish steady recharge condition over the slope. Table 3.8 lists the summary of the runoff experiments conducted.

Table 3.8 Summary of the *in situ* overland flow experiments conducted

Month and Year	Vegetation Condition	No. of Experiments Conducted	Range of Inflow Intensity (mm/hr)	Average Seasonal Temperature (°C)	Antecedent Moisture Condition
August, 2005	Sparse	10	59 to 361	28	Wet
November, 2005	Moderate	11	80 to 406	20	Wet
May, 2006	Dense	13	87 to 310	26	Wet

3.7.1.1 Experimental results of overland flow

A total of 34 overland flow experiments were conducted on the hillslope plot varying the inflow intensities in the range of 59 to 406 mm/hr. Out of these 10, 11, and 13 experiments were conducted under sparse, moderate, and dense vegetation conditions, respectively. Duration of the runoff events were between 15 and 120 minutes. Table 3.9 enumerates details of the overland flow experiments conducted and the different estimated parameters. In each of the runoff events time of concentration and the resulting outflow at the downstream channel were recorded. Fig. 3.28(a-f) shows the typical nature of the outflow hydrographs obtained from the experiments conducted under different conditions. The initial time lag in the hydrographs represent the time of concentration (t_c). Within a very short time the

Table 3.9 Details of the overland flow experiments conducted

Experiment No.	Vegetation Condition	Constant Inflow Intensity (mm/hr)	Runoff Duration (min)	Steady Preferential Infiltration Rate (mm/hr)	Runoff Coefficient
1	Sparse	128	25	65	0.49
2		59	42	33	0.44
3		115	30	55	0.52
4		167	20	77	0.54
5		361	15	139	0.61
6		85	32	43	0.49
7		136	25	67	0.51
8		72	45	37	0.49
9		158	35	74	0.53
10		79	60	36	0.54
11	Moderate	121	25	62	0.49
12		406	19	177	0.56
13		298	30	130	0.56
14		276	60	135	0.51
15		103	30	48	0.53
16		229	30	105	0.54
17		80	30	52	0.35
18		241	30	90	0.63
19		339	24	150	0.56
20		174	25	80	0.54
21		270	30	90	0.67
22	Dense	132	51	112	0.15
23		190	120	167	0.12
24		300	15	175	0.42
25		310	27	245	0.21
26		87	62	86	0.01
27		214	63	172	0.20
28		95	42	87	0.08
29		305	60	214	0.30
30		89	36	84	0.06
31		91	48	83	0.09
32		134	57	98	0.27
33		97	51	93	0.04
34		184	41	145	0.21

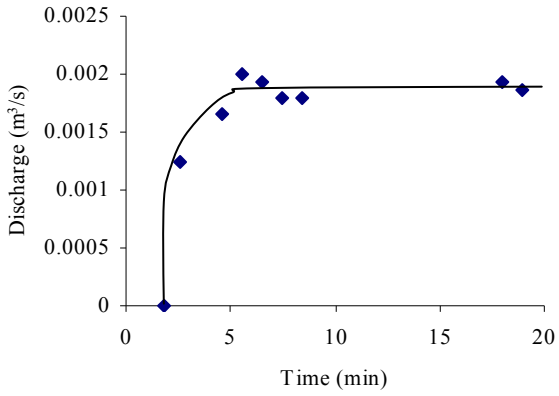

(a) Experiment No. 1

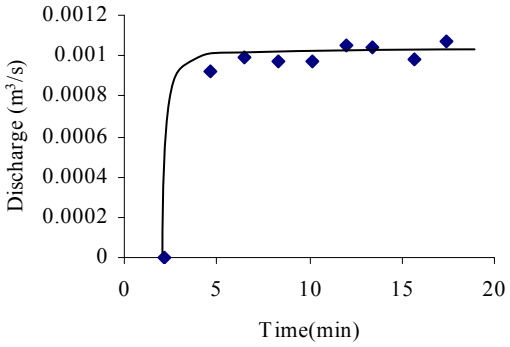

(b) Experiment No. 8

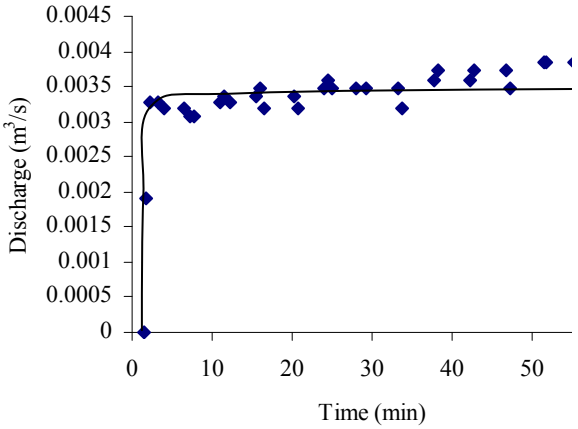

(c) Experiment No. 14

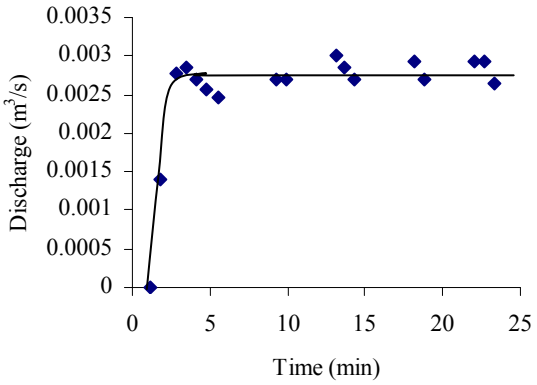

(d) Experiment No. 20

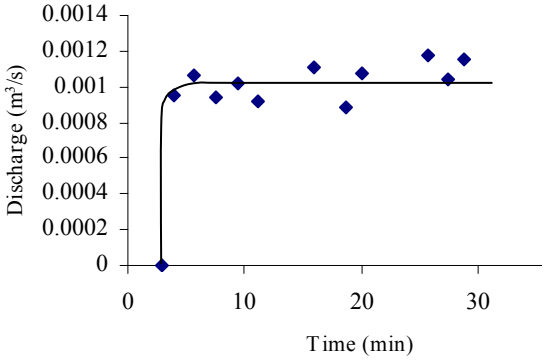

(e) Experiment No. 22

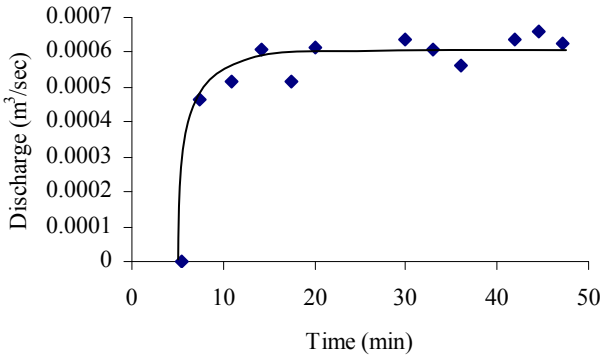

(f) Experiment No. 33

Fig. 3.28(a-f) Outflow hydrographs from the hillslope plot for the overland flow experiments conducted under different conditions

outflow becomes almost steady, only with some minor fluctuations, which in general occur in experimental observations. This phase represents a constant and steady infiltration condition of the soil, referred as preferential infiltration rate (f_b). The steady discharge in the outflow hydrographs and constant soil moisture profile conditions during this stage, measured by the profile probe sensor, also indicates the attainment of steady recharge/infiltration condition over the hillslope plot. The values of f_b have been computed from the *in situ* field experiments knowing the inflow and outflow hydrographs (Table 3.9). This f_b is basically the spatially averaged steady infiltration rate over the hillslope plot.

Fig. 3.29 represents the relationship between t_c and inflow intensity (i) under different degrees of vegetation in the experimental plot. It shows that t_c is dependent on both inflow intensity and degree of vegetation. Vegetation roots are known to create new preferential flow paths as well as establish connectivity between the existing soil macropores to make them hydrologically active. Therefore, the rooting characteristics of surface vegetation under different conditions are closely associated with the seasonal dynamics of preferential pathways in soil (Beven and Germann, 1982; Ziegler *et al.*, 2004; Scanlan and Hinz, 2007; Sarkar *et al.*, 2008b; Shougrakpam *et al.*, 2010). It can be observed from the figure that the t_c curves representing sparse and moderate vegetation conditions are close to each other but under dense vegetation the curve is distinctly separated. As between different seasons there were almost no apparent change in the physical conditions of the plot except vegetation density, one possible reason can be that under sparse and moderate vegetation densities the response of active macropore network in the subsoil, as indicated by the preferential infiltration rates (Table 3.9), were similar. But, under dense vegetation higher root density may have created more active preferential flow

network within the subsoil. Lower values of runoff coefficients were also observed under dense vegetation condition compared to sparse and moderate vegetations (Fig. 3.30). As a result, higher values of t_c were evident for dense vegetation with similar power relation with inflow intensity.

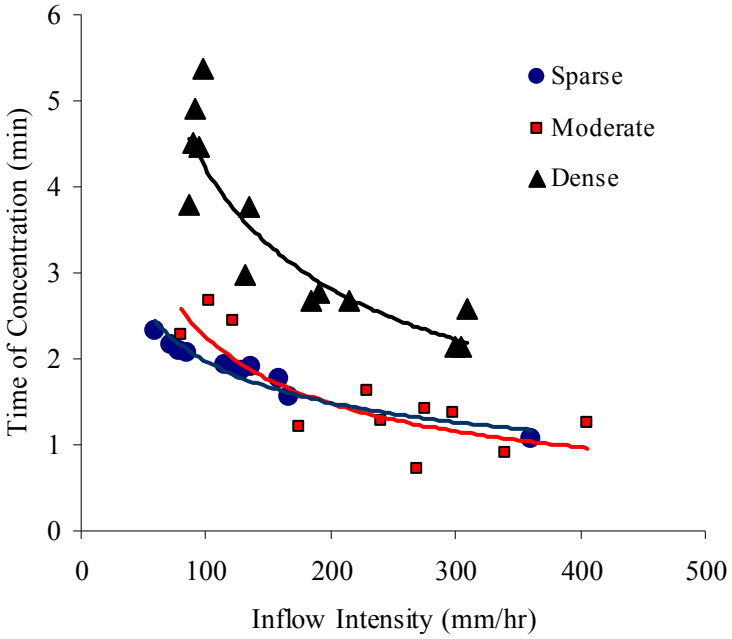

Fig. 3.29 Variation of time of concentration (t_c) with inflow intensity (i)

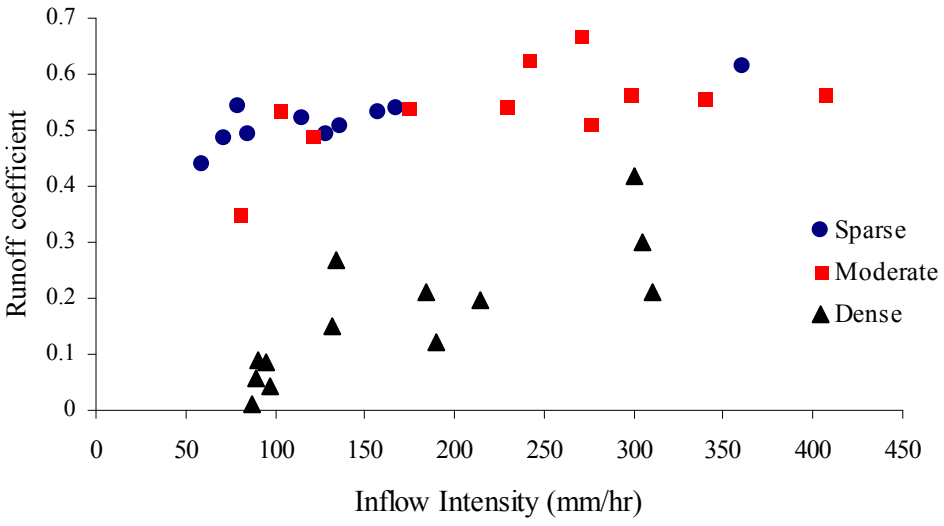

Fig. 3.30 Observed runoff coefficients for the overland flow experiments

The experimental results revealed that in most of the cases the preferential infiltration rate is higher than the average saturated hydraulic conductivity of the soil matrix (50 mm/hr), which was approximated from the USDA (United States Department of Agriculture) soil textural classes and bulk density of soil samples collected from the plot (Schaap *et al.*, 1998). This typical observation leads to the conclusion that preferential infiltration was more dominating over matrix flow in the hillslope plot. Fig. 3.31 depicts the relationships of f_b and i for different degrees of vegetation. The relationships found are linear and vary with degree of vegetation. Possibly, dense vegetation on the hillslope allowed a higher preferential infiltration rate. This may be attributed mainly to the active macropore network, developed by plant roots under high density of vegetation, which created a favorable hydraulic condition for macropore flow by establishing their connectivity. It is also interesting to observe that even under an extreme inflow intensity of 406 mm/hr; constant maximum preferential infiltration rate was not attained. It is an indication of high preferential infiltration characteristics of the plot. Tables 3.10-3.11 list the relationships derived on the basis of *in situ* overland flow experiments.

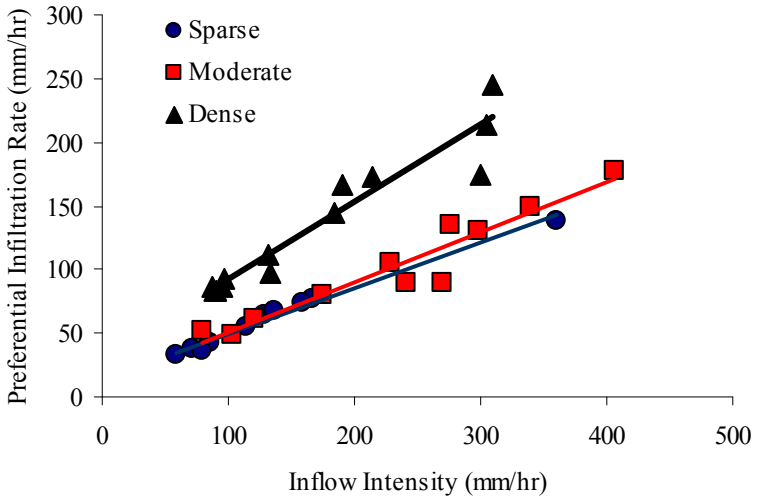

Fig. 3.31 Variation of preferential infiltration rate (f_b) with inflow intensity (i)

Table 3.10 Relationships of t_c with inflow intensity (i)

Vegetation Condition	Range of t_c (min)	Relationship of t_c with Inflow Intensity, (i)	R^2
Sparse	1.08 – 2.33	$t_c = 12.679\ i^{-0.4043}$	0.93
Moderate	0.73 – 2.68	$t_c = 36.668\ i^{-0.6059}$	0.61
Dense	2.15 – 5.38	$t_c = 60.713\ i^{-0.5796}$	0.85

Table 3.11 Relationships of f_b with inflow intensity (i)

Vegetation Condition	Range of f_b (mm/hr)	Relationship of f_b with Inflow Intensity, (i)	R^2
Sparse	33 - 139	$f_b = 0.3574\ i + 14$	0.98
Moderate	48 - 177	$f_b = 0.3924\ i + 11.216$	0.92
Dense	83 - 245	$f_b = 0.6052\ i + 31.737$	0.92

3.7.2 Observation of overland flow under natural storm events

3.7.2.1 Observational setup and instruments

Overland flow responses of the hillslope plot under natural storm events were monitored using an automatic rainfall recorder and a digital water level recorder. These instruments were installed at the hillslope plot in June, 2008. The rainfall recorder has a rainfall sensor (Tipping Bucket Type; Accuracy: 0.025 mm), in-built data logger, solar panel, and power supply unit. The instrument also has a pocket-size device for easy download and transport of data to computers. The digital water level recorder has a weatherproof enclosure which contains a data logger and power supply.

An integral solar panel can keep the battery charged throughout the year. A shaft encoder type water level sensor measures and stores the data in the system memory with date and time record, as per user defined logging period. The overland flow produced from the hillslope plot is collected in the lower channel (Fig. 3.23) and diverted to a collection pit of 0.62 m width and 0.72 m length, through a pipe. To measure the water level in the pit the pressure transducer was installed and synchronized with the time setting of the rainfall recorder unit. The measurements were stored in a data logger with the observation time interval of 5 minutes. Every month the recorded readings from the data logger were downloaded and analyzed to study the runoff generation patterns of the hillslope plot under natural storm events.

3.7.2.2 Runoff generation from the hillslope plot

In Northeast India high intensity storm events occur mainly during the period April to October. The three year (2008-2010) observations of rainfall and the resulting runoff generated from the experimental plot are given in Tables 3.12, 3.13, and 3.14. Compared to the typical pattern of monsoon rainfall in Northeast India, relatively dry monsoons were observed during the years 2008 and 2009. In the year 2008 there were a total of 12 major storm events. Out of these only four storm events generated surface runoff from the hillslope plot (Table 3.12). It may be noted that the maximum rainfall intensity of these runoff generating events were in the range of 21-85 mm/hr. But, the common feature among these events was that they continued for prolonged durations (175-220 minutes). From April to October, 2009 there were only two runoff generating events out of 12 observed storm events (Table 3.13). The year 2010 was the wettest of the three years for which rainfall-runoff observations were made. It produced 24 storm events of varying durations and intensities (Table 3.14). Out of these, only five events generated overland flow from the plot. The two high runoff

Table 3.12 Description of the observed storm events for the year 2008

Date	Total Event Rainfall (mm)	Storm Event Duration (min)	Maximum Rainfall Intensity (mm/hr)	7 Days API (mm)	Runoff Coefficient
02-06-2008	28.19	66	85.34	8.38	0
09-08-2008	32.25	90	60.96	32.26	0
11-08-2008	37.08	220	21.34	46.99	0.75
15-08-2008	22.86	15	25.63	105.92	0
18-08-2008	12.15	20	79.25	144.51	0
21-08-2008	12.95	65	67.06	32.26	0
27-08-2008	5.33	40	21.34	39.37	0
28-08-2008	37.59	175	60.96	21.08	0.05
30-08-2008	5.33	15	27.43	46.48	0
31-08-2008	9.90	30	21.32	1.27	0
31-08-2008	46.48	175	57.91	29.21	0.22
09-09-2008	25.90	180	85.34	50.04	0.27

Table 3.13 Description of the observed storm events for the year 2009

Date	Total Event Rainfall (mm)	Storm Event Duration (min)	Maximum Rainfall Intensity (mm/hr)	7 Days API (mm)	Runoff Coefficient
20-04-2009	19.56	10	188.98	0.00	0.22
09-05-2009	35.05	35	146.30	37.34	0
03-06-2009	20.32	50	57.91	3.81	0
02-07-2009	9.14	140	6.10	18.26	0
28-07-2009	15.26	95	27.43	26.16	0
29-07-2009	4.06	70	6.10	46.99	0
30-07-2009	19.56	55	42.67	65.28	0
04-08-2009	63.75	60	149.35	42.42	0.70
16-08-2009	6.10	45	24.38	32.26	0
17-08-2009	16.51	70	27.43	40.89	0
07-10-2009	4.57	55	9.14	16.26	0
08-10-2009	20.57	85	12.19	43.94	0

Table 3.14 Description of the observed storm events for the year 2010

Date	Total Event Rainfall (mm)	Storm Event Duration (min)	Maximum Rainfall Intensity (mm/hr)	7 Days API (mm)	Runoff Coefficient
05-04-2010	3.05	20	12.19	0	0.00
12-04-2010	9.90	15	57.91	6.85	0.00
17-04-2010	12.70	55	42.67	127.20	0.00
19-04-2010	6.35	35	21.34	164.08	0.00
09-05-2010	14.00	65	12.19	16.00	0.00
16-05-2010	21.08	65	48.77	80.77	0.00
31-05-2010	3.56	80	6.10	16.26	0.00
01-06-2010	7.34	55	18.29	25.90	0.00
02-06-2010	4.83	75	15.24	58.15	0.00
04-06-2010	18.03	55	39.62	79.50	0.00
26-06-2010	10.41	75	24.38	29.97	0.00
28-06-2010	35.31	130	51.82	57.15	0.00
01-07-2010	5.08	100	4.57	98.04	0.00
04-07-2010	43.18	450	73.15	77.72	0.05
10-07-2010	25.15	130	79.25	48.76	0.00
11-07-2010	17.53	50	25.91	37.59	0.00
12-07-2010	30.48	60	57.91	55.12	0.20
12-07-2010	28.19	90	57.91	81.28	0.10
19-07-2010	45.21	120	80.77	38.61	0.04
20-07-2010	36.83	160	67.06	52.83	0.07
29-07-2010	6.10	80	10.67	15.49	0.00
13-08-2010	14.73	70	25.91	2.54	0.00
15-08-2010	5.08	80	6.10	17.78	0.00
18-08-2010	24.38	120	47.24	27.68	0.00

generating events occurred on 12th July 2010, had moderate intensity, high rainfall depth, and wet antecedent conditions.

From the natural observations it can be said that a favorable combination of rainfall depth, storm duration, maximum intensity, and antecedent moisture condition primarily controlled the runoff generation process from the hillslope plot. To

understand the major controlling parameters for runoff generations at the plot scale, three variables namely, 7 days Antecedent Precipitation Index (API), total event rainfall depth, and maximum rainfall intensity were considered. For the storm events in the year 2010, a scatter plot between storm event rainfall depth and 7 days API was prepared (Fig. 3.32). All the runoff generating events had total event rainfall depth more than 28 mm, 7 days API greater than 38 mm, and maximum rainfall intensity more than 57 mm/hr. It can be observed from the figure that the runoff generating events cluster in the upper region of the plot. Non-runoff generating storm events are well separated in the scatter plot from the runoff producing events. This indicates that higher 7 days API and higher total event rainfall depths provided more favorable conditions for surface runoff generation from the hillslope plot.

Similar scatter plots between total event rainfall depth and 7 days API for the years 2009 and 2008 are shown in Figs. 3.33 and 3.34, respectively. In the year 2009, for an exceptional event (Date: 20-04-2009) it can be observed that a very intense precipitation (about 189 mm/hr) occurring for a small duration (10 minutes) generated surface runoff from the plot even under dry antecedent condition and lower depth of event rainfall. The other runoff producing event had the highest rainfall depth (64 mm) and 7 days API value (42 mm). In the year 2008, all the four runoff producing events showed total rainfall depths more than 25 mm and 7 days API values greater than 20 mm.

To study the effect of maximum rainfall intensity on runoff generation, the scatter plots between maximum rainfall intensity and 7 days API were prepared. These plots for the years 2010, 2009 and 2008 are shown in Figs. 3.35, 3.36 and 3.37, respectively. These figures reveal that in 2010 the runoff generating events are clustered in the plot. Comparatively higher intensity storms produced surface runoff.

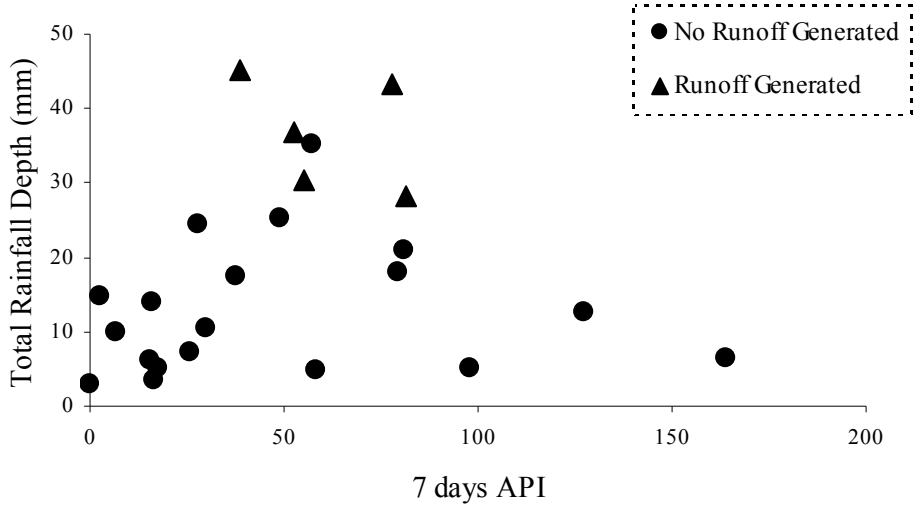

Fig. 3.32 Scatter plot of total rainfall depth and 7 days API for the year 2010

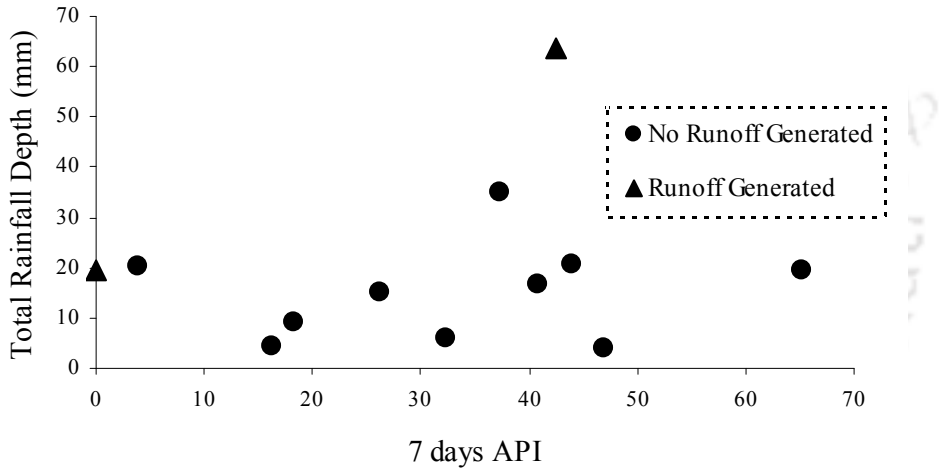

Fig. 3.33 Scatter plot of total rainfall depth and 7 days API for the year 2009

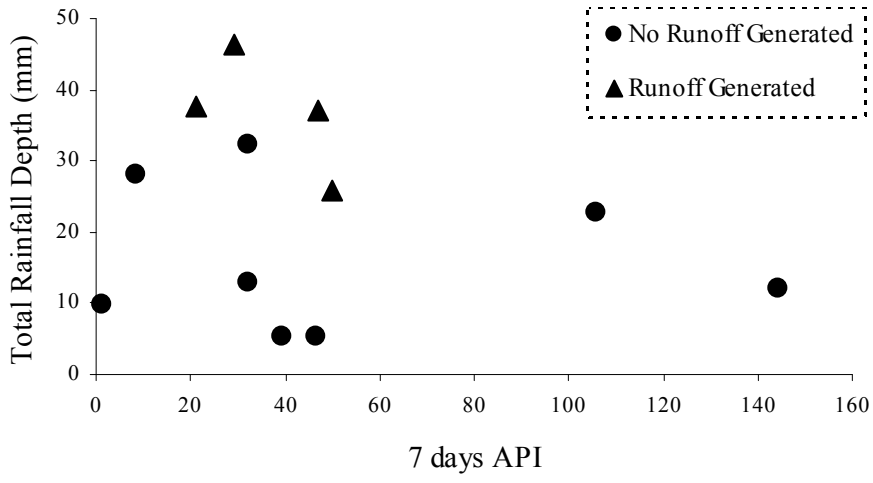

Fig. 3.34 Scatter plot of total rainfall depth and 7 days API for the year 2008

Similarly, in the year 2009 only high intensity storm events produced runoff. But, for the year 2008, the runoff generating and non runoff generating events are scattered together. Some of the high intensity storm events did not produce any surface runoff in spite of having similar 7 days API values. It can be observed that only high intensity events continuing for prolonged durations and having a threshold 7 days API value (Table 3.12) produced overland flow. Therefore, the runoff generation process from the hillslope plot under natural rainfall events showed threshold behavior depending on rainfall depth, duration, intensity, and antecedent moisture condition. In general it has been observed that most of the runoff producing events have total rainfall depths more than 25 mm and 7 days API values higher than 30 mm. Short duration cloudburst events as well as low intensity events continuing for prolonged durations can also produce surface runoff.

3.7.2.3 Evaluation of the inflow intensity-infiltration rate relationship

The relationships between inflow intensity (i) and lumped steady preferential infiltration rate (f_b) developed from the overland flow experiments (Table 3.11) have also been evaluated for the natural events recorded over the hillslope plot. These relationships are valid for wet antecedent conditions only. As the years 2008 and 2009 had relatively dry monsoons, the observed runoff producing events of 2010, having wet antecedent moisture conditions were considered. The two highest runoff producing events occurring on 12-07-2010 have been selected for evaluation. Moderate to sparse vegetation condition was evident in the plot during those rainfall events. Knowing the rainfall intensity values for every 5 minutes time interval, the infiltration rates have been computed using the relationships for both sparse and moderate vegetation conditions (Table 3.11). After satisfying infiltration the excess precipitation generates the surface runoff. Thus, the overland flow generated from the

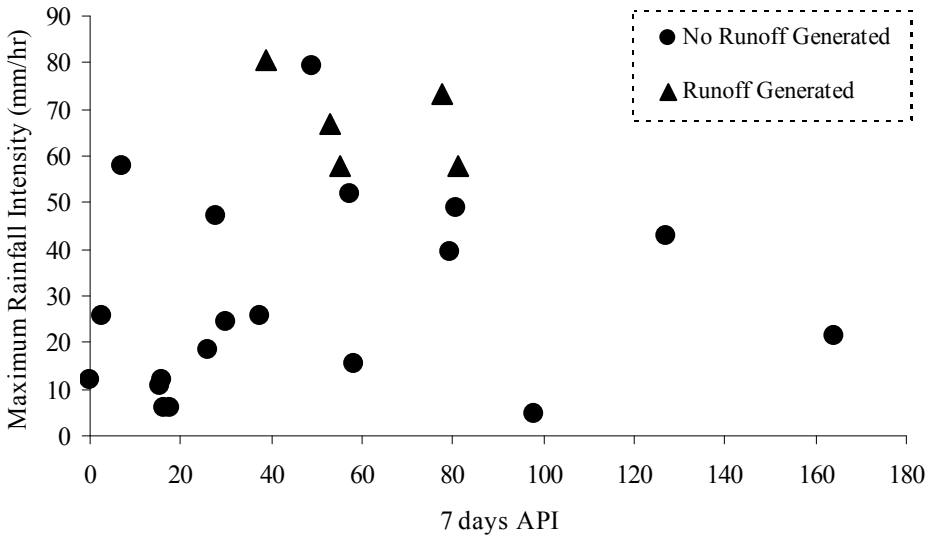

Fig. 3.35 Scatter plot of maximum rainfall intensity and 7 days API for the year 2010

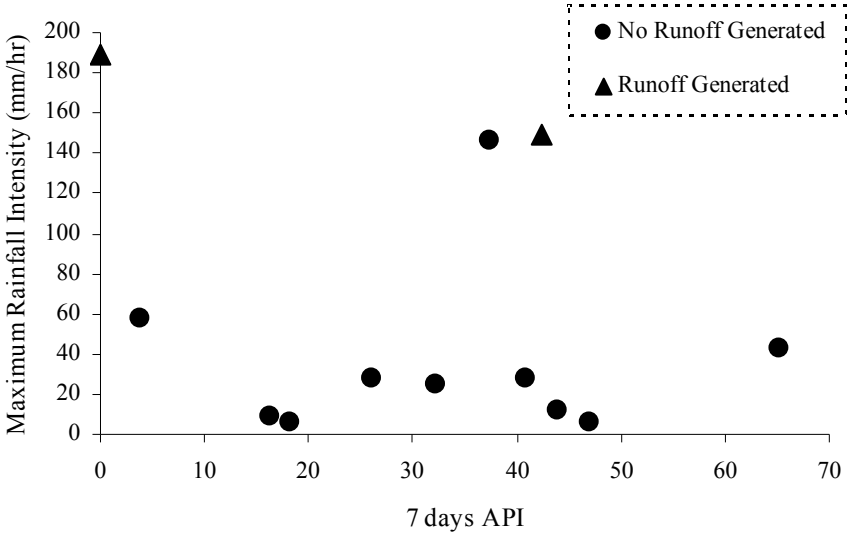

Fig. 3.36 Scatter plot of maximum rainfall intensity and 7 days API for the year 2009

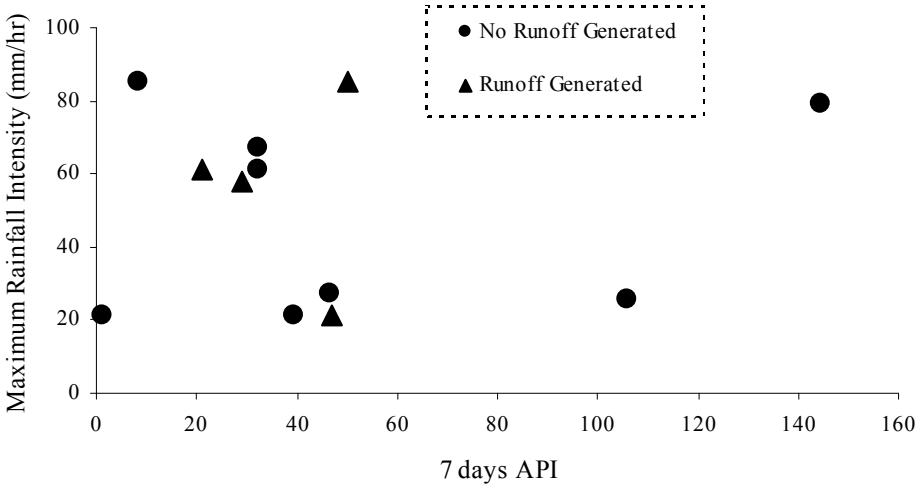

Fig. 3.37 Scatter plot of maximum rainfall intensity and 7 days API for the year 2008

plot has been estimated. The estimated discharge is plotted with the observed hydrograph (Figs. 3.38 and 3.39) for the two selected events under both sparse and moderate vegetation conditions. The hyetograph of the storm events are also shown in the graphs. It can be observed that for the first event the total runoff volumes estimated from the experimentally developed relationships are in close agreement with the observed runoff volume (Fig. 3.38). For the second storm event (Fig. 3.39) the runoff volumes estimated from the experimental relationships are found to be over predicted. However, the peak runoff rate is captured quite reasonably. Thus, the experimentally derived relationships were found to be approximately valid for the observed natural storm events under wet antecedent moisture conditions of the plot. The observed deviations may be due to the differences in antecedent moisture conditions and varying rainfall intensities for natural storm events. Moreover, the experimental relations are valid for high intensity events which produce significant durations of overland flow. For shorter durations, overland flow process should be controlled primarily by the preferential flow network within the soil. The long duration (20 to 30 minutes or more) overland flow processes might follow the hydrological behavior obtained from the artificial runoff experiments more closely. Such long duration runoff events with significant surface and subsurface stormflow generations are more critical and thus require detailed analysis by the hydrologists for predicting flash floods, soil erosion, and assessing their long term eco-hydrological impacts.

3.8 Experimental Evidences of Lateral Subsurface Flow

The plot was instrumented with 25 piezometers to keep track of temporary water table buildup and recession above the impermeable layer. The piezometers were installed along five transects of the plot (Fig. 3.40). The depth of the piezometers

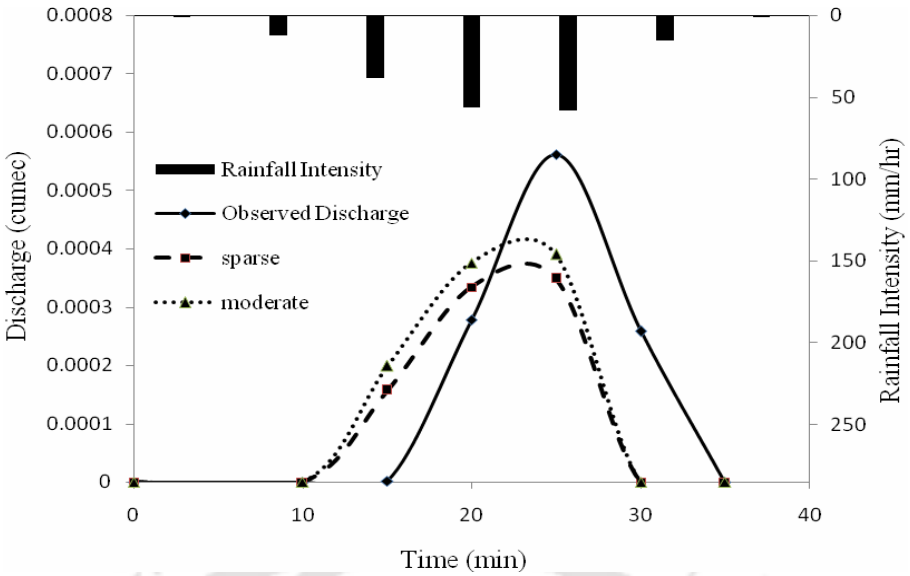

Fig. 3.38 Observed and estimated hydrographs for the 1st storm event of 12-07-2010

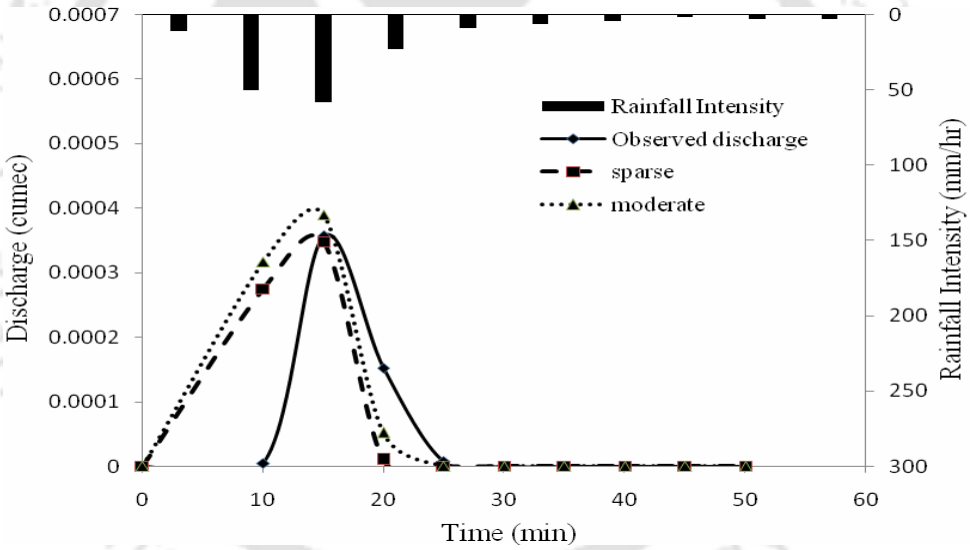

Fig. 3.39 Observed and estimated hydrographs for the 2nd storm event of 12-07-2010

extended up to the impermeable layer (i.e. 1 m) from the ground surface. The piezometers were installed inside as well as outside of the plot (e.g. piezometer nos. 1, 5, 6, 10, 11, 15, 16, 20, 21 and 25) to capture the subsurface flux of water in lateral as well as along the major surface gradient of the plot. A float was used to measure the depth of water above the impermeable bed in each piezometer tube. Additional fifteen runoff experiments were conducted to study the lateral subsurface flow generated

from the hillslope plot (Table 3.15). Measurements of water table in all the piezometers were taken before, during, and after the completion of the runoff experiments. Fig. 3.41 depicts the temporal patterns of water table build up and recession at different piezometer locations for the experiment E-12. From the observations it is clear that there was no lateral flux to the left side of the plot. Very little lateral dispersion of water was evident to the right side of the plot. The subsurface flux of water mainly followed the direction of major surface gradient of the hillslope plot. All the experiments conducted on the hillslope plot showed similar patterns of water table rise and fall. In no case saturation excess overland flow was evident. The quick buildup and recession of water table above the impermeable bed also indicates the existence of highly active lateral preferential flow from the hillslope plot. Because, with a very slow matrix flow velocity ($K_s \approx 50$ mm/hr) through the hillslope soil, such rapid buildup and recession of water table can not be expected (Singh, 2006).

Table 3.15 Experiments conducted for capturing lateral subsurface flow from the hillslope plot (April-May, 2007)

Experiment No.	Vegetation Condition	Constant Inflow Intensity (mm/hr)	Runoff Duration (hr)	Steady Preferential Infiltration Rate (mm/hr)	Runoff Coefficient
E-1	Moderately Dense	245	1.50	184	0.25
E-2		94	1.08	79	0.16
E-3		408	0.75	257	0.37
E-4		121	0.83	71	0.41
E-5		181	0.78	90	0.50
E-6		193	1.57	109	0.43
E-7		337	1.03	195	0.42
E-8		143	1.03	76	0.47
E-9		217	1.00	135	0.38
E-10		216	0.75	123	0.43
E-11		249	1.00	126	0.49
E-12		252	0.80	139	0.45
E-13		296	1.00	176	0.41
E-14		185	0.92	110	0.40
E-15		188	0.85	106	0.44

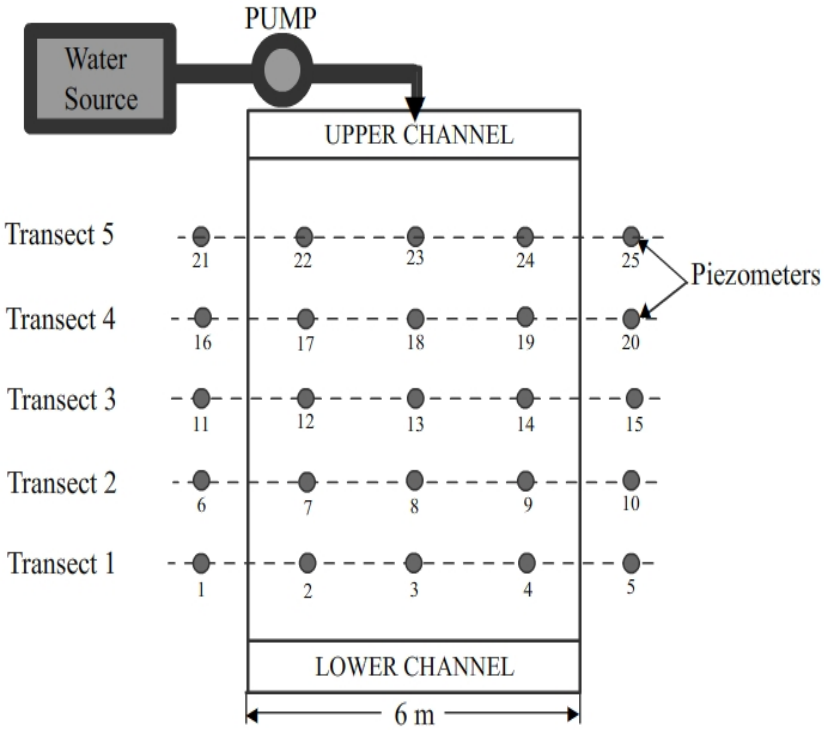

Fig. 3.40 Location of the piezometers in the experimental plot

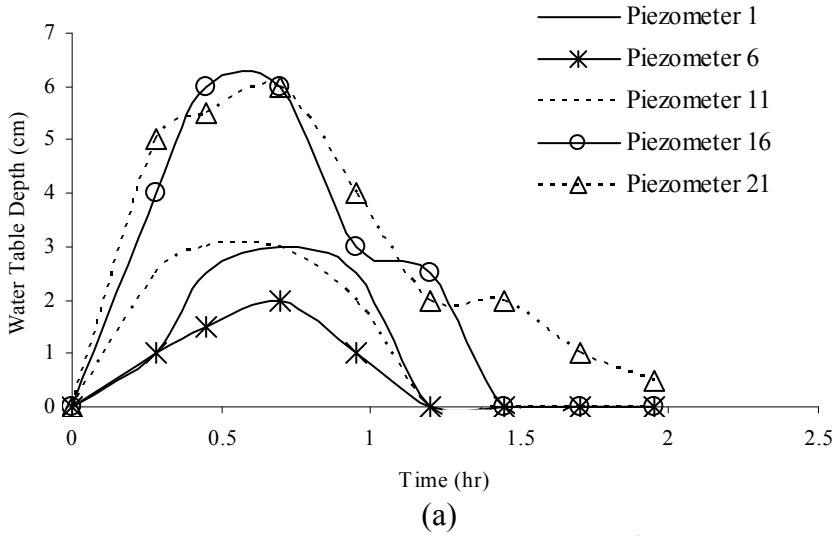

(a)

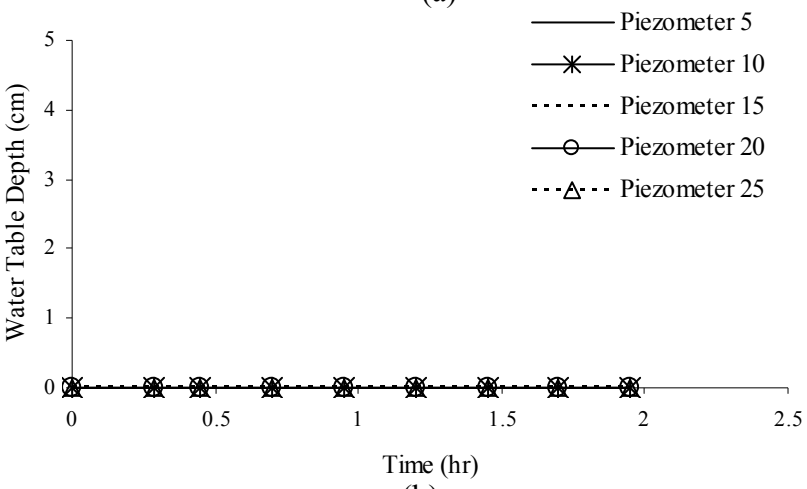

(b)

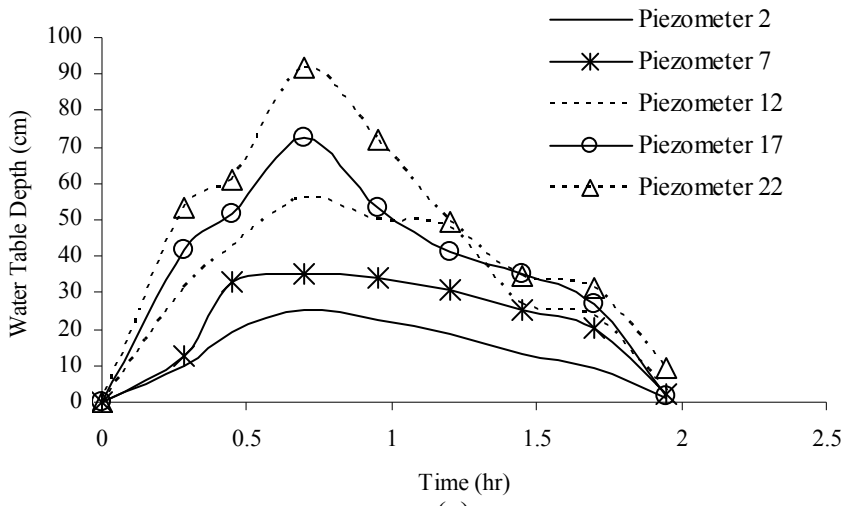

(c)

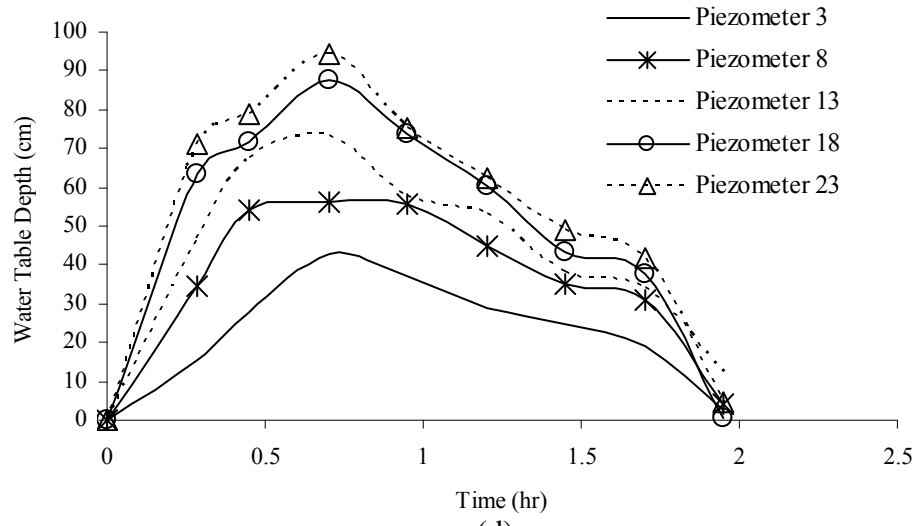

(d)

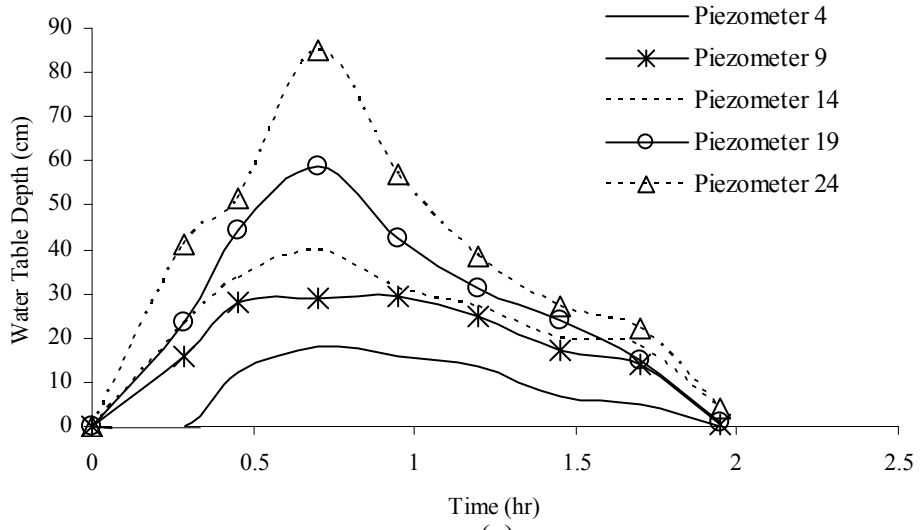

(e)

Fig. 3.41(a-e) Temporal variation of water table depths above impermeable layer observed at different piezometer locations for the experiment E-12

3.9 Summary of the Chapter

The experiments conducted on the hillslope plot revealed some of its typical hydrological behaviors. On the basis of the experimental evidences the following important findings can be summarized.

- The hillslope plot selected for the present investigation has natural vegetation, mainly consisting of close growing grasses and shrubs. The degree of vegetation showed significant seasonal variations viz. sparse, moderate, and dense, depending on climatic conditions.
- The soil profile of the plot showed a two layer formation with a coarse soil layer overlaying a fine textured soil layer. An impermeable bed has been found at about 1 m depth below ground level. The analysis of the collected soil samples revealed that the average saturated hydraulic conductivity of the soil is 50 mm/hr for water movement through the soil matrix.
- Keeping in view the rainfall patterns and physical conditions of the hillslopes in northeast India, a simple sheet flow generation system has been designed for studying the hydrological behavior of the hillslope plot under extreme runoff events for prolonged durations.
- Infiltration behavior of the plot has been studied by conducting point scale double ring infiltrometer tests. The results showed wide range of variation in infiltration rate. For dry soils the irregular patterns of infiltration rate indicated existence of preferential flow network in the soil. Under wet antecedent conditions, a near steady infiltration condition could be attained after a long time. In general, the point scale measurements of infiltration clearly showed the effect of scale. Using the measured steady infiltration rate data for the plot under wet antecedent conditions, a simple linear

function has been developed to represent the spatial variation of infiltration along the length of the plot.

- Runoff experiments were conducted at the plot scale using the sheet flow generation system to compute the spatially averaged lumped infiltration rate over the hillslope plot. The infiltration rate data indicated the attainment of a steady infiltration condition over the plot after some time.
- To characterize the macroporosity of the hillslope soil, dye infiltration tests and subsequent image processing techniques were employed with the undisturbed soil columns collected from the plot. The analysis of the observed dye patterns revealed the existence of highly connected macropores throughout the soil profile. The small diameter macropores (1-2 mm), developed mainly by the plant roots, were dominating.
- Spatial and temporal variations in soil moisture distribution in the hillslope plot were monitored using a profile probe soil moisture meter. The analysis of the data revealed that the moisture content in the hillslope soil at different depths remained fairly constant during, as well as for a prolonged period after the runoff events, if a wet soil moisture condition was established initially. For such antecedent conditions, the moisture content in the top soil layer remained almost constant. Such steady nature of soil moisture profile indicated the steady infiltration/recharge condition of the hillslope plot. Spatial distribution of moisture content at the bottom layer also indicated rapid buildup and recession of water table above the impermeable layer.
- To study the overland flow behavior on the hillslope plot under intense storm events, 34 runoff experiments were conducted with varying intensities and durations for sparse, moderate and dense vegetation conditions of the

plot. Under wet antecedent moisture conditions, within a very short time the observed outflow hydrographs measured at the downstream end of the plot attained a constant discharge. Such patterns of the outflow hydrographs and the constant soil moisture profiles observed during this stage, represents a near steady infiltration condition over the plot. From the dye tracing investigations it was evident that the macroporosity of the hillslope soil was mainly due to the growth of the plant roots. Thus, vegetation density was found to be closely related to the infiltration-runoff relationships of the hillslope plot. On the basis of the experimental results functional relationships of inflow intensity (i) with steady preferential infiltration rate (f_b), and time of concentration (t_c) were developed for the three vegetation conditions of the plot. These relationships are valid for wet antecedent condition of the plot under high intensity storm events occurring for long durations.

- The overland flow responses of the hillslope plot were also observed for natural storm events for three years using automatic rainfall recorder and digital water level recorder. Analysis of the measured data revealed that overland flow generation from the hillslope plot is a threshold dependent process. Runoff generation process was found to be primarily controlled by total event rainfall, maximum rainfall intensity, storm duration, and 7 days API. The evaluation of the experimentally established rainfall-runoff relationship for the hillslope plot also showed reasonable agreement for natural storm events.
- To capture the lateral subsurface flow from the hillslope plot, 25 piezometers was installed along five transects. The buildup and recession of

water table in these piezometers were recorded during and after the artificial runoff events. Rapid rise and fall of water table were observed from the piezometer readings. With a very slow matrix flow rate, such rapid response of water table is difficult to describe. The water table response in the piezometers installed along the two sides of the runoff plot was negligible. The movement of water was predominantly along the major surface gradient of the plot. These evidences indicate that the hillslope plot generated rapid subsurface stormflow through its lateral preferential pathways along the direction of the slope with very little sideways dispersion of water flux.

CHAPTER 4 MATHEMATICAL MODELING

This chapter presents simple conceptual modeling approaches for overland flow and subsurface stormflow in a preferential infiltration dominated natural hillslope under high intensity storm events with wet antecedent soil moisture conditions. The main controlling parameters affecting the hydrological response of the hillslope have been identified from the experimental investigations discussed in the previous chapter. The functional relationships developed from the experimental evidences have been used in the modeling concept. Some of the physical parameters, measured from the *in situ* experiments conducted on the hillslope plot, have been used to calibrate the models. The models were parameterized to reproduce the observed surface and subsurface flow behaviors revealed from the field experiments. This provided a basis for characterizing the surface and subsurface hydrological response of the hillslope plot under high intensity storm events.

4.1 Overland Flow Modeling

4.1.1 Description of the model

As mentioned in the previous chapter, accurate practical measurement of overland flow depth on a natural hillslope is difficult. Therefore, mathematical approximation of the overland flow governing equations is considered here to characterize overland flow behavior on the hillslope. The process of overland flow can be defined by approximation of the St. Venant equations of continuity and momentum (Chaudhry, 1993). In the present study, one-dimensional shallow water overland flow equations with diffusive wave approximation were solved using a finite

volume technique (Jain *et al.,* 2005). Neglecting the inertia term, the one-dimensional shallow water flow equations in non-conservation form can be written in vector form as

$$\frac{\partial \mathbf{U}}{\partial t} + \frac{\partial \mathbf{F}}{\partial x} = \mathbf{G} \tag{4.1}$$

in which

$$\mathbf{U} = \begin{pmatrix} h \\ 0 \end{pmatrix}$$

$$\mathbf{F} = \begin{pmatrix} uh \\ h \end{pmatrix}$$

$$\mathbf{G} = \begin{pmatrix} (-f_b) \\ (S_0 - S_f) \end{pmatrix} \tag{4.2}$$

where h is the flow depth (m); u is the depth averaged flow velocity (m/s); x is the distance along flow direction (m); f_b is the steady preferential infiltration rate (m/s); S_0 is the ground slope; and S_f is the friction slope. S_f can be computed from Manning's equation (Chow, 1959). For shallow water overland flow, the Manning's equation can be written as (Chaudhry, 1993)

$$S_f = \frac{n^2 u^2}{h^{4/3}} \tag{4.3}$$

where n is the Manning's roughness coefficient ($m^{-\frac{1}{3}}s$) representing hydraulic resistance to flow.

Before solving equations 4.1-4.3, the two-dimensional flow domain was divided into number of computation cells. Based on elevation and flow depth, one dimensional flow network was established. The finite volume approximation of equations (4.1-4.3) was applied at each computational cell (Jain *et al.,* 2005). The initial condition is $h(x,t=0) = 0$ and the boundary condition at the upstream end is $h(0,t) = h_e$, where h_e is equivalent flow depth (m), which can be computed for a given

inflow discharge, applying Manning's equation for the upstream boundary computational cells.

The overland flow experiments conducted on the hillslope plot revealed that the steady preferential infiltration rate (f_b), is dependent on inflow intensity (i) and degree of vegetation. As the macroporosity of the hillslope was mainly due to the growth of plant roots, change in vegetation density and the resulting changes in root network were closely related to the preferential infiltration rate into the soil. The functional relationships between the preferential infiltration rate and inflow intensity (i) for the site was experimentally established for different vegetation conditions of the plot (Table 3.11).

To simulate the overland flow behavior on the hillslope plot for a particular runoff experiment, the measured inflow intensity and steady preferential infiltration rate have been given as model inputs. The overland flow model computed flow depth and friction slope at each computational cell and the outflow hydrograph at the downstream end of the slope. The value of Manning's roughness coefficient (n) for a particular experiment was approximated by matching the model simulated outflow hydrograph with the outflow hydrograph measured at the downstream end of the slope. The observed and simulated runoff coefficients were also compared (Table 4.1). Initially, starting with an assumed value of n, simulations were carried out to compute the outflow hydrographs. This trial procedure was repeated till the observed and simulated hydrographs were almost identical for a given set of experiment. The least-deviation simulation having similar values of observed and predicted runoff coefficients provided the approximate value of n for the experiment. Similar procedure was followed for all the *in situ* experiments to compute the Manning's roughness coefficients (Fig. 4.1). It is worth noting that the estimated n represents a

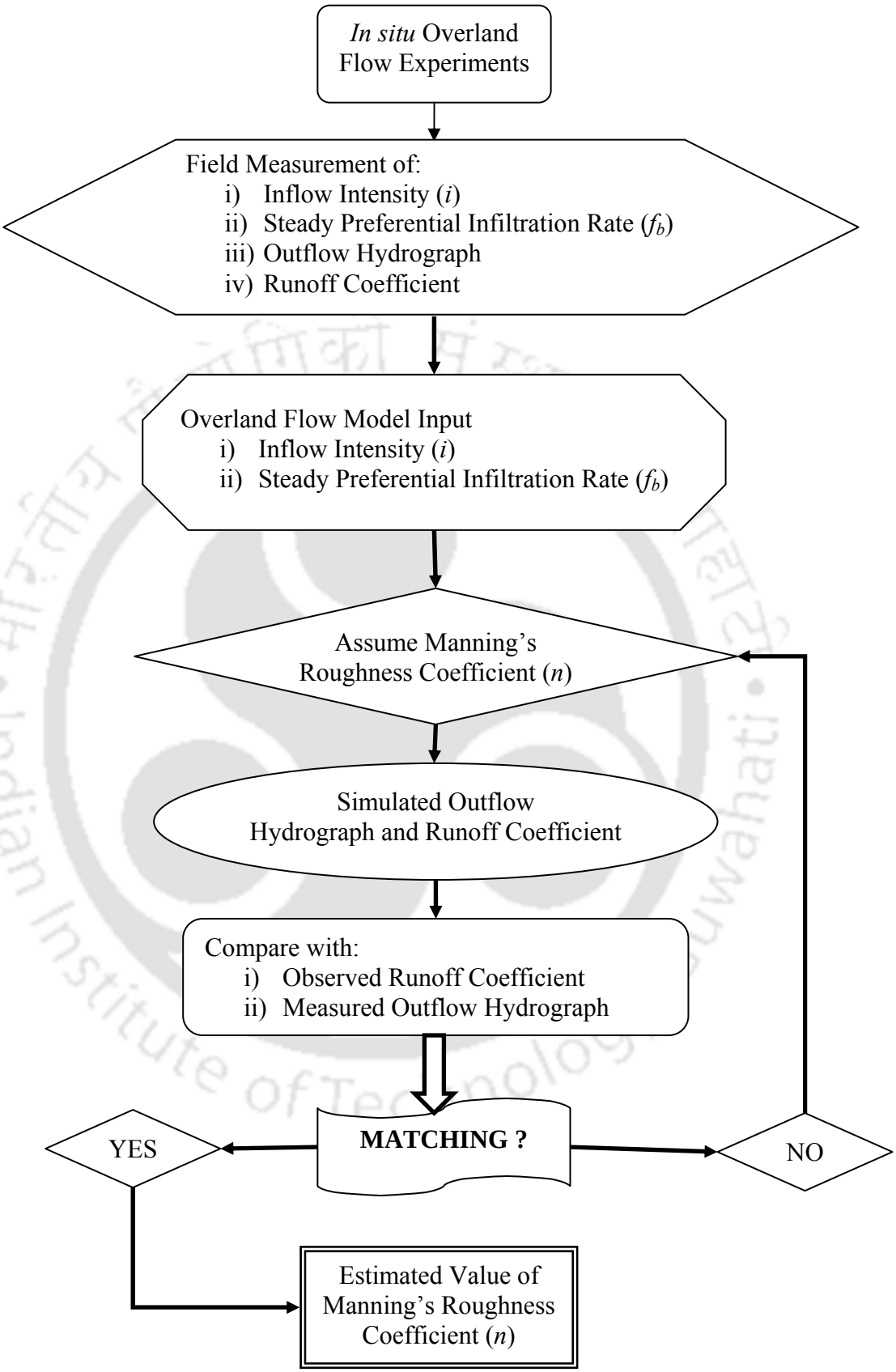

Fig. 4.1 Estimation of Manning's roughness coefficient from model simulations

lumped value of surface roughness for a steady overland flow condition over the hillslope plot.

4.1.2 Overland flow model simulations

The simulated and observed outflow hydrographs obtained for some of the overland flow experiments are shown in Fig. 4.2. The comparison seems to be good and the behavior is similar to the one reported by Lima (1989) and Liu and Singh (2004), which also compared simulated runoff hydrographs with experimental results obtained on a permeable slope. The simulated overland flow depths at various computational time steps were also analyzed. Fig. 4.3(a-c) shows the two dimensional color contour plots of some of the model simulated overland flow depths under steady infiltration conditions of the plot. The simulations showed that the average overland flow depth varied in the range of 3-10 mm with maximum coefficient of variation of about 200% and over 80 percent area of the hillslope, the flow depth was less than 5 mm. These simulated flow depths were also found to be in close agreement with the depths observed during the field experiments. Fig. 4.4 shows the two dimensional plot of flow accumulation over the hillslope plot. The high spatial variation of the overland flow depth was due to the effect of microtopography of the plot, which generally does not have significant effect on the lumped hydrological response from the hillslope (Liu and Singh, 2004).

The values of the Manning's roughness coefficient (n) obtained from model simulations are enumerated in Table 4.1. The variation of n with inflow intensity is shown in Fig. 4.5. It can be observed that Manning's roughness coefficient has a power relation with inflow intensity (Table 4.2). Similar relationship was also reported by Wu *et al.* (1999) on the basis of laboratory experiments. The deviation of the three curves predominantly represents the effect of degree of vegetation in three

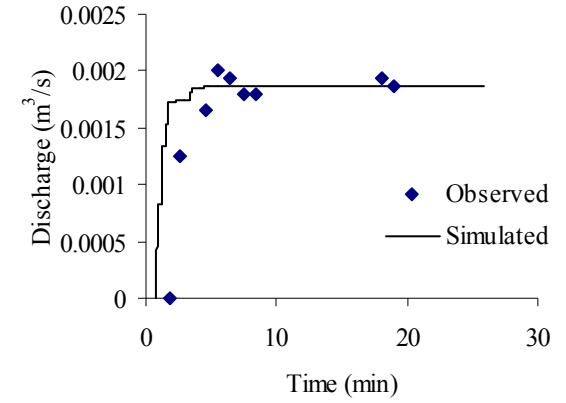

(a) Experiment No. 1

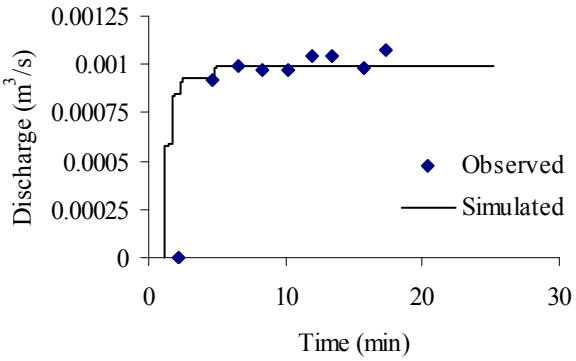

(b) Experiment No. 8

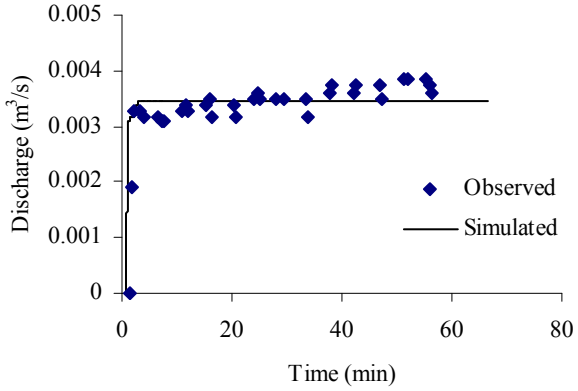

(c) Experiment No. 14

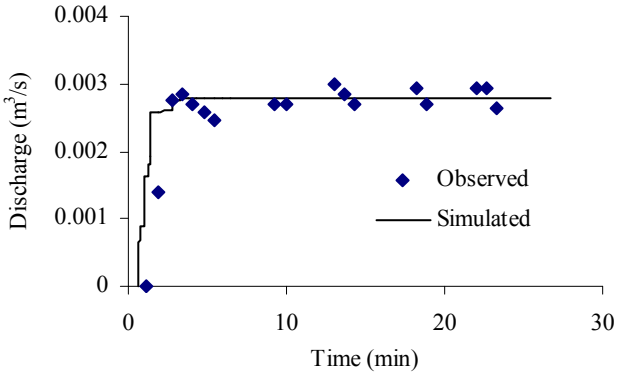

(d) Experiment No. 20

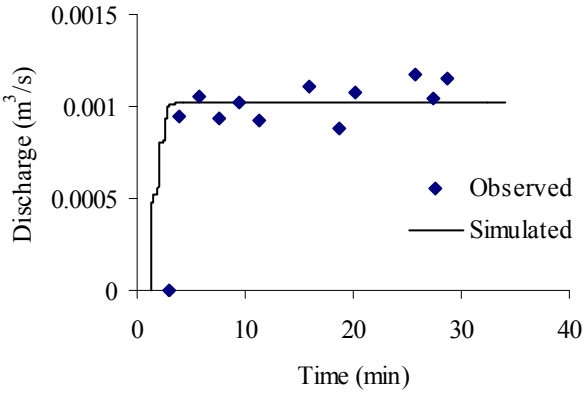

(e) Experiment No. 22

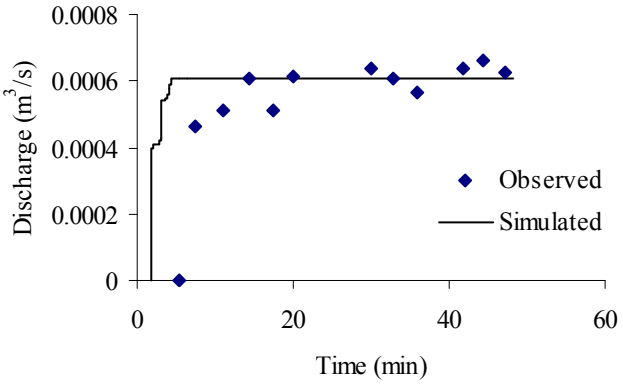

(f) Experiment No. 33

Fig. 4.2(a-f) Observed and overland flow model simulated outflow hydrographs from the hillslope plot for some of the experiemnts

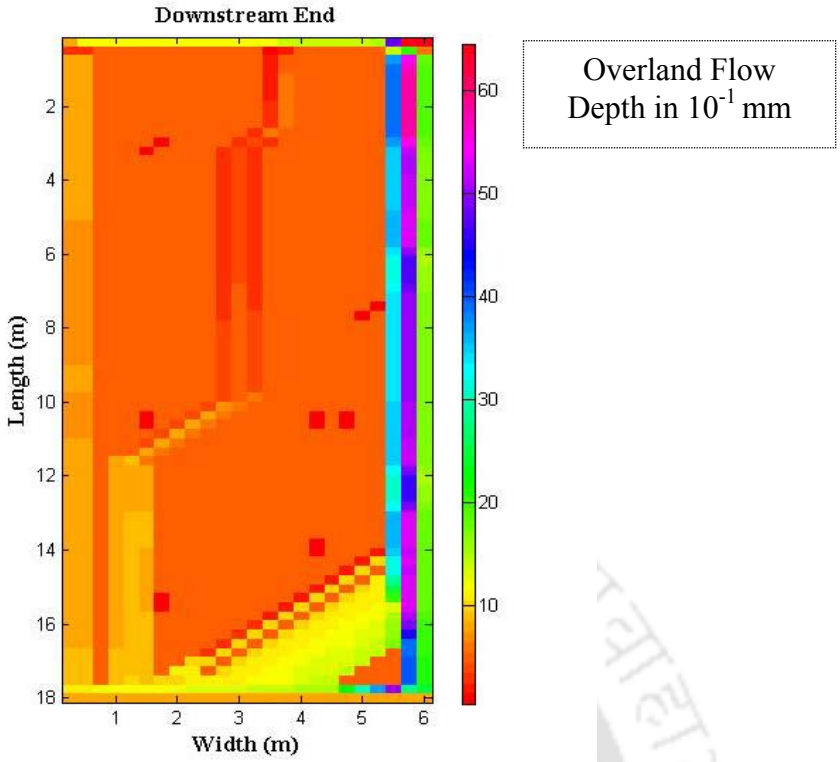

(a) Experiment No. 11 (Inflow intensity 121 mm/hr)

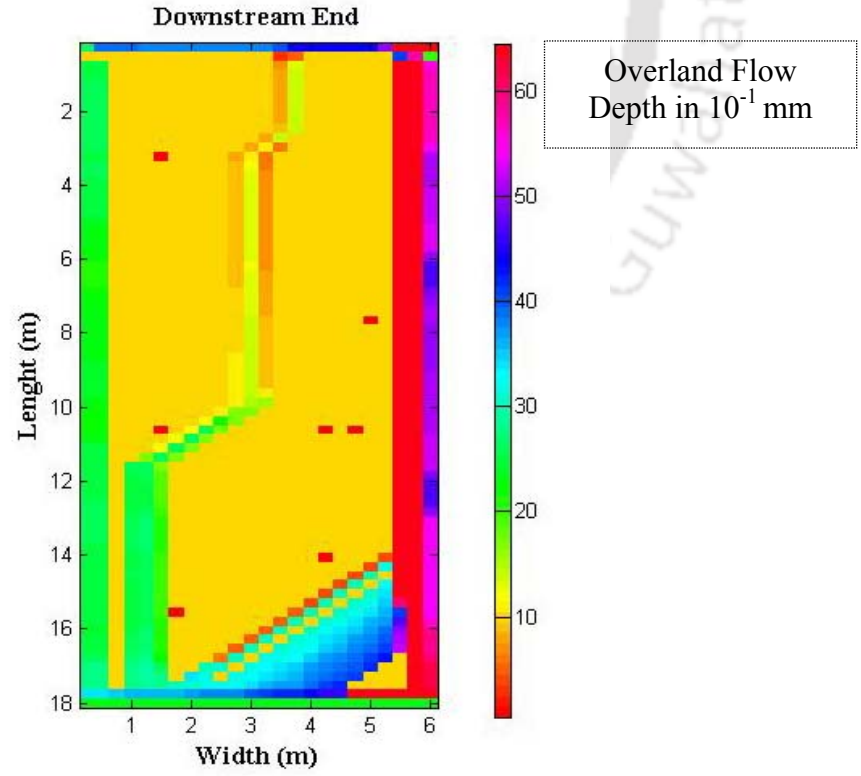

(b) Experiment No. 16 (Inflow intensity 229 mm/hr)

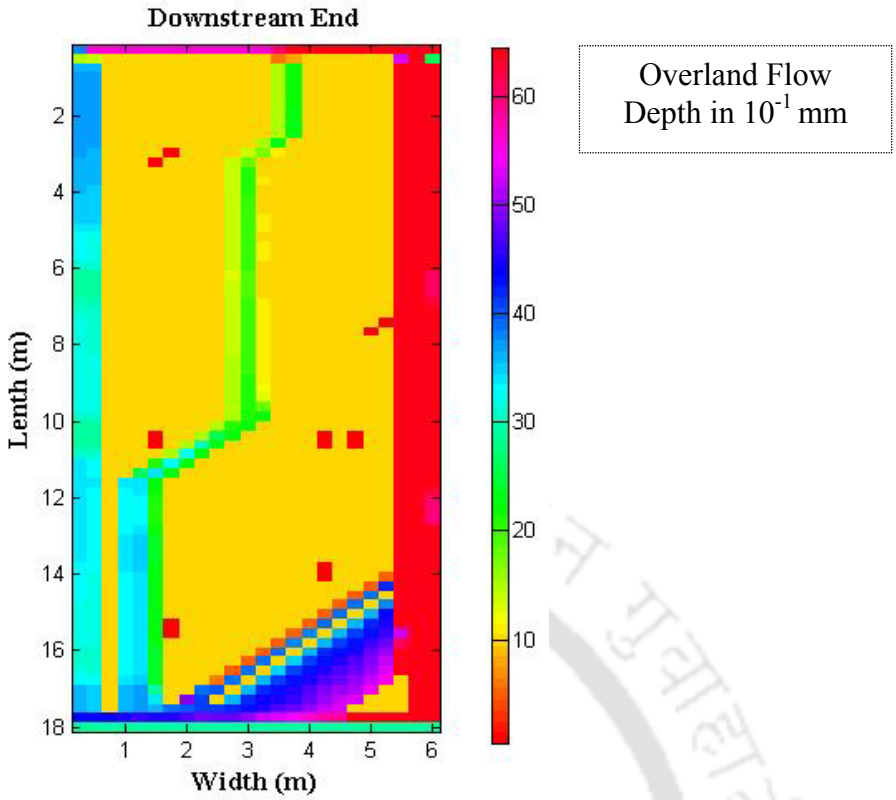

(c) Experiment No. 19 (Inflow intensity 339 mm/hr)

Fig. 4.3(a-c) Variation of simulated overland flow depths for different inflow intensities for moderate vegetation condition of the plot

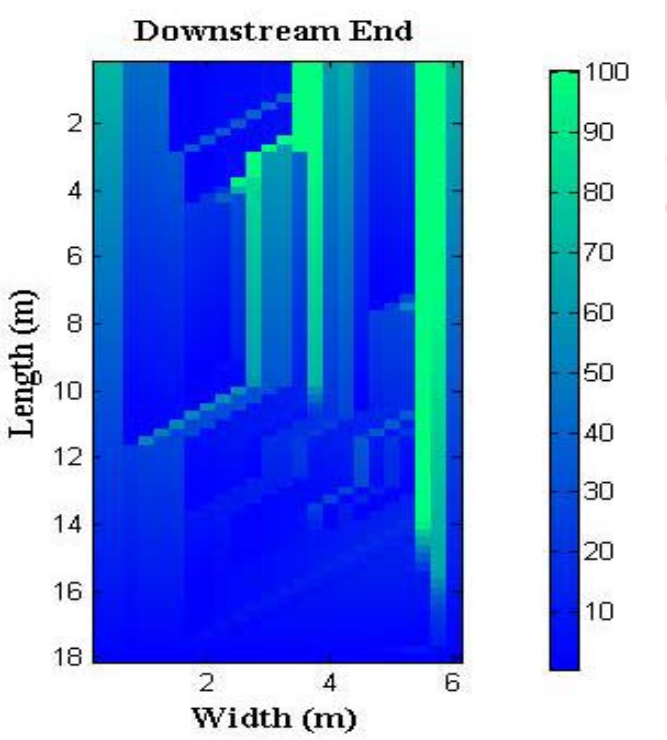

Fig. 4.4 Flow accumulation of the experimental hillslope plot

Table 4.1 Simulations of the overland flow model for the hillslope plot

Experiment No.	*Vegetation Condition*	*Inflow Intensity (mm/hr)*	*Simulated Steady Outflow Rate (mm/hr)*	*Runoff Coefficient*		*Manning's Roughness Coefficient (n)*
				Observed	Simulated	
1	Sparse	128	62	0.49	0.48	0.051
2		59	22	0.44	0.37	0.071
3		115	59	0.52	0.51	0.049
4		167	89	0.54	0.53	0.045
5		361	238	0.61	0.66	0.032
6		85	35	0.49	0.41	0.061
7		136	71	0.51	0.52	0.048
8		72	33	0.49	0.46	0.058
9		158	85	0.53	0.54	0.050
10		79	40	0.54	0.51	0.052
11	Moderate	121	47	0.49	0.39	0.060
12		406	190	0.56	0.47	0.043
13		298	132	0.56	0.44	0.049
14		276	115	0.51	0.42	0.053
15		103	35	0.53	0.34	0.070
16		229	84	0.54	0.37	0.062
17		80	23	0.35	0.29	0.085
18		241	141	0.63	0.59	0.041
19		339	187	0.56	0.55	0.039
20		174	93	0.54	0.53	0.049
21		270	152	0.67	0.56	0.041
22	Dense	132	34	0.15	0.26	0.079
23		190	50	0.12	0.26	0.075
24		300	149	0.42	0.50	0.044
25		310	104	0.21	0.34	0.058
26		87	15	0.01	0.17	0.110
27		214	72	0.20	0.34	0.065
28		95	20	0.08	0.25	0.099
29		305	127	0.30	0.42	0.050
30		89	19	0.06	0.21	0.099
31		91	21	0.09	0.23	0.094
32		134	53	0.27	0.40	0.058
33		97	20	0.04	0.21	0.099
34		184	60	0.21	0.33	0.066

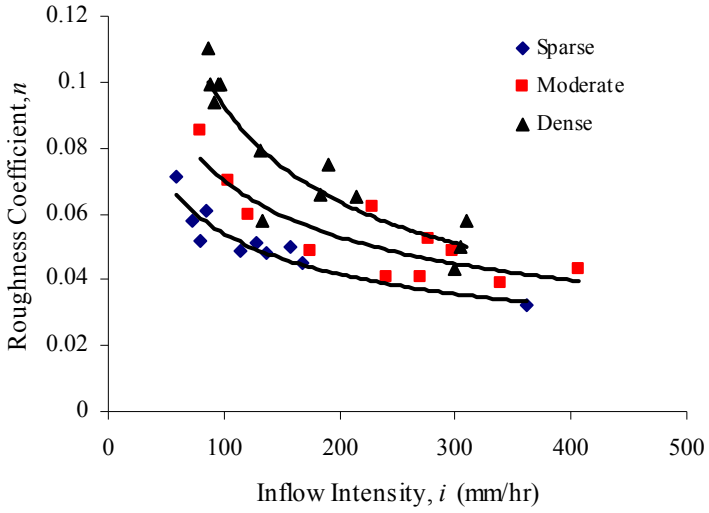

Fig. 4.5 Variation of Manning's roughness coefficient (n) with inflow intensity (i)

Table 4.2 Relationships of n with inflow intensity (i)

Vegetation Density	*Range of n*	*Relationship of n with Inflow Intensity, i*	R^2
Sparse	0.032 – 0.071	$n = 1.1348\ i^{-0.544}$	0.83
Moderate	0.039 – 0.085	$n = 0.3064\ i^{-0.3768}$	0.89
Dense	0.044 – 0.11	$n = 0.4579 i^{-0.4073}$	0.73

different seasons. The resulting higher n for dense vegetation indicates more surface roughness to overland flow. With increasing inflow intensity for a particular type of vegetation degree, Manning's roughness coefficient decreases. These results show that the surface roughness to overland flow decreases with increasing ponding depth, due to increase in flow velocity. However, this decreasing rate of the surface roughness is high at low ponding depth. The surface roughness mentioned here represents a lumped resistance to overland flow caused by soil surface, microtopography, vegetation, etc. From the relationships shown in Figs. 3.29 and

3.31, it can be observed that the curves representing sparse and moderate vegetation are close to each other. But in Fig. 4.5, they are separated from each other. Preferential infiltration rate into the soil is primarily controlled by active macropore network and ponding depth, which is a function of inflow intensity. As preferential infiltration trends for sparse and moderate vegetation are similar, the active macropore flow structure in both the conditions might be of same order. The field measured t_c, representing the travel time of the overland flow during macropore flow initiation, obviously follow the same trend as that of preferential infiltration rate. However, Manning's roughness coefficient depends on the surface roughness and ponding depth under steady preferential infiltration rate. For low overland flow depth, variation of the surface roughness on a vegetated hillslope is mainly characterized by degree of vegetation. Thus, the curves in Fig. 4.5 are well separated for sparse, moderate, and dense vegetation conditions of the plot.

4.2 Modeling Lateral Subsurface Stormflow

To model subsurface stormflow evident in the hillslope, the recent progress in the concept of subsurface flow modeling at the hillslope scale introduced by Fan and Bras (1998), which has been subsequently adopted by some researchers with good success (Troch *et al*., 2002; Rezzoug, *et al*., 2005), has been used. Instead of adopting an effective lateral saturated hydraulic conductivity, actual saturated hydraulic conductivity for soil matrix flow was considered and one new sink term to account for quick lateral macropore flow has been introduced. A physical based numerical solution of the subsurface flow equations was provided to simulate the *in situ* plot scale runoff experiments conducted in the experimental hillslope plot. The proposed model was used (i) to capture the rapid subsurface stormflow evident in the hillslope, (ii) to reflect the contributions of soil matrix and macropores in prompt interflow

occurring immediately after high intensity storm events, and (iii) to provide a surrogate indicator of hydraulically effective or hydrologically active lateral macroporosity of the hillslope. Apart from these, the dependency of effective lateral macroporosity, matrix, and macropore flow rates under varying recharge conditions were also evaluated.

4.2.1 Physical concept of the model

Three characteristic hillslope types: divergent, convergent, and uniform, are commonly used for modeling hillslope flow behavior (Fan and Bras, 1998; Troch *et al*., 2002; Rezzoug *et al*., 2005). In the present investigation the case of a uniform hillslope facet used for *in situ* field experiments was considered for the modeling of rapid subsurface stormflow. The elegant method of converting a three-dimensional hillslope soil mantle into a two-dimensional soil profile proposed by Fan and Bras (1998) has been followed. Fig. 4.6 shows the definition sketch of soil profile and macropore dominated subsurface flow concept of a uniform hillslope facet. The impermeable layer was at some depth below the soil mantle which consists of soil matrix and a population of lateral macropores. The hydraulically effective soil macropores, which gets connectivity throughout the entire length of the slope, were assumed to be distributed in different layers of the soil profile. These lateral macropores were considered as circular pipes of small uniform diameter. From the piezometer and profile probe measurements taken during the field experiments it was evident that, due to high preferential infiltration during extreme rainfall events a temporary water table is formed over the impermeable layer and starts contributing to lateral subsurface stormflow. Apart from the saturated matrix flow, the lateral macropores present below the temporary water table actively contributes to quick interflow mechanism from the hillslope. These macropores were termed as 'hydrologically active macropores'.

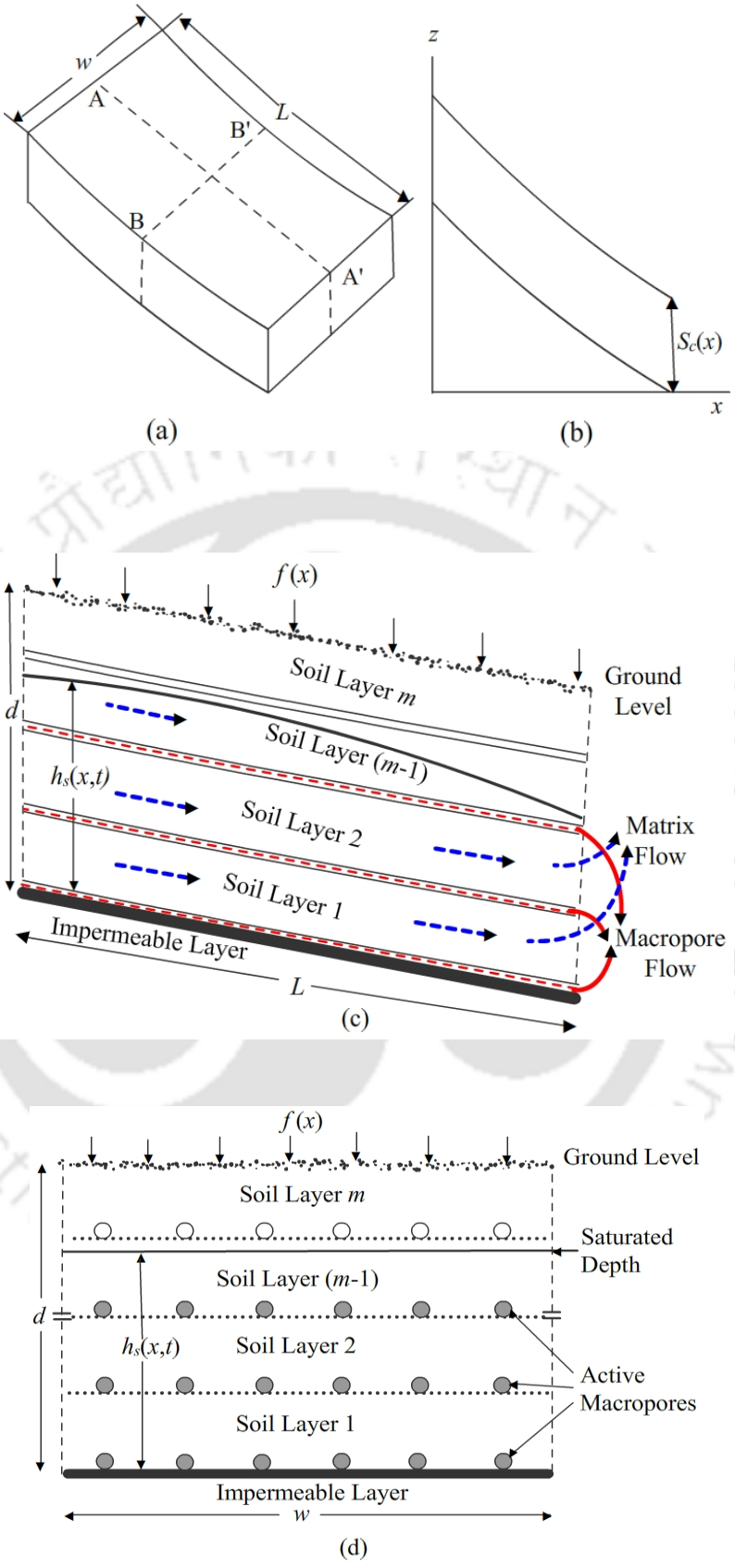

Fig. 4.6 (a-b) Definition sketch of a uniform hillslope and its soil moisture capacity; (c) Section A-A' and (d) section B-B' showing the subsurface formations of the hillslope soil

The amount of water which seeps into the macropores was assumed to be discharged laterally with very high velocity without any interaction with the surrounding soil matrix. This consideration is quite practical as similar flow behavior has been reported by Anderson *et al.* (2008) from the experimental evidence of lateral preferential flow in hillslopes. Thus, the temporary water table buildup and its recession were controlled by recharge as well as the hydraulic conductivity of soil matrix and number and diameter of hydrologically active macropores present within the saturated soil strata.

4.2.2 Mathematical formulation of subsurface stormflow

Soil moisture storage capacity function (Fan and Bras, 1998), $S_c(x)$ for a uniform hillslope facet (Fig. 4.6) can be defined as

$$S_c(x) = w\, d\, \varepsilon \tag{4.4}$$

where w is the width of the hillslope (m), d is the uniform soil depth (m), and ε is the drainable porosity. $S_c(x)$ defines the storage capacity of the hillslope in terms of its drainable pore space.

If $S(x,t)$ is the soil moisture storage at a given flow distance x at any time t, then it can be expressed in the form of continuity equation and Darcy's law. The continuity equation for hillslope subsurface flow considering both soil matrix and macropore flow can be written as

$$\frac{\partial S}{\partial t} + \frac{\partial Q}{\partial x} = f(x,t)w - q(x,t) \tag{4.5}$$

where $f(x,t)$ is the rate of recharge to the saturated layer (m/hr), Q is the subsurface discharge rate through soil matrix (m^3/hr), and $q(x,t)$ is the total discharge rate through the soil macropores per unit length of the hillslope (m^2/hr). Clearly, when the soil is

completely saturated $S(x,t) \geq S_c(x)$. The matrix flow rate Q can be related to the storage $S(x,t)$ through a kinematic form of Darcy's equation given as

$$Q = -k_s \frac{S}{\varepsilon} \frac{\partial z}{\partial x} \tag{4.6}$$

where k_s is the saturated hydraulic conductivity of the soil matrix (m/hr), and z is the bedrock elevation above a datum. Combining equation (4.6) with the continuity equation for a known spatially varying steady recharge rate $[f(x)]$ and assuming no spatial variation of k_s and ε, yields a quasi-linear wave equation

$$a(x)\frac{\partial S}{\partial x} + \frac{\partial S}{\partial t} = c(x,S,t) \tag{4.7}$$

where

$$a(x) = -\frac{k_s}{\varepsilon} z'(x) \tag{4.8}$$

and

$$c(x,S,t) = f(x)w + \frac{k_s S}{\varepsilon} z''(x) - q(x,t) \tag{4.9}$$

Here, $z'(x)$ and $z''(x)$ are first and second derivatives of the bedrock profile curvature function.

4.2.3 Computation of macropore flow

Assuming soil macropores as small diameter circular pipes, the rate of steady groundwater ingression into the macropores can be approximated (Kolymbas and Wagner, 2007) as

$$q = \frac{2\pi k_s h}{\log\left(\frac{2h}{r}\right)} \tag{4.10}$$

where q is the steady rate of water ingression into the macropore per unit length (m^2/hr), r is the radius of the macropore (m), and h is the saturated head over the

macropore (m). As the velocity of water flow through the macropores is expected to be very high, it was assumed that under wet antecedent conditions the water seeping into the macropores are readily discharged laterally without any interaction with the surrounding soil matrix which was either saturated or at its field capacity. Now, let us consider that in a soil profile depth d there are m no. of soil layers of equal thickness with the i^{th} layer containing n_i no. of hydraulically effective connected macropores per unit width of the slope (where i = 1, 2, 3, …… m) located at the bottom of the layer and spaced equally along the width (Fig. 4.6). If at any given time the saturated depth above the impermeable layer is $h_s(x)$ then the saturated head over the macropores can be computed as

$$h_i(x) = h_s(x) - i\,(d/m) + (d/m) \tag{4.11}$$

When the hydraulically effective macropores are below the saturated depth, they are termed as 'hydrologically active macropores' as they actively contribute to prompt lateral subsurface storm runoff from the hillslope. Clearly, when $h_i(x)$ is negative, macropores are above the saturated zone and they are not hydrologically active. Thus, the total lateral flow per unit length of the hydrologically active macropores at a given time can be computed as

$$q(x,t) = \sum_{i=1}^{m} n_i \frac{2\pi k_s h_i(x,t)}{\log\left(2h_i(x,t)/r_{avg}\right)} \tag{4.12}$$

where r_{avg} is the average radius of the soil macropores (m).

4.2.4 Numerical solution of subsurface stormflow

The numerical solution of equation (4.7) was obtained using a finite difference method considering Warming-Beam upwind scheme (Niyogi *et al.*, 2005). The following initial and boundary conditions were invoked.

Initial conditions:

When $t = 0$, at $z = z(x)$, $S = 0$

Boundary conditions:

When $t > 0$, at $x = 0$, $\frac{dS}{dx} = 0$

Fan and Bras (1998) reported that the use of a second-order polynomial bedrock profile function was not suitable to capture the local variations and thus stressed on the necessity of numerical solutions to capture such variations. Therefore, instead of adopting a bedrock profile function, digital elevation data obtained from fine grid topographic survey conducted by a total station were used. However, the bedrock slope along the centroid profile was approximated as that of the surface topography assuming a uniform soil depth. The model computes subsurface storage at different time steps in each grid cell and also gives subsurface lateral flow response at the bottom of the hillslope as saturated matrix flow and lateral preferential flow. At a particular time step the storage within the hillslope can be used to calculate the saturated depth or water table depth over the impermeable layer.

Before conducting the experiments a wet antecedent condition was established in the hillslope soil. Such wet initial condition primed the macropores for rapid initiation of lateral subsurface stormflow. Fifteen runoff experiments (Table 4.6) were conducted which showed the range of average rate of recharge (f_{avg}) from 0.071 – 0.257 m/hr for varying inflow intensities and durations. During all the experiments the water table depth at the piezometers were monitored at regular intervals to capture the buildup and recession of saturated zone above the impermeable layer. The responses of the piezometers located at the two sides of the plot were negligible as the subsurface flow along the length of the slope was dominating. The average saturated depths at five points along the centroid of the plot was approximated by averaging the piezometer readings at a particular transect (Table 4.3). These average depths at different time steps were compared with the model simulated saturated depths.

Table 4.3 Computation of average saturated depth in the piezometers at different transects (Fig. 3.40) for the experiment E-12

Time (hr)	*Water Table Depth in Piezometers of Transect 1 (cm)*						*Water Table Depth in Piezometers of Transect 2 (cm)*						*Water Table Depth in Piezometers of Transect 3 (cm)*					
	1	**2**	**3**	**4**	**5**	Average	**6**	**7**	**8**	**9**	**10**	Average	**11**	**12**	**13**	**14**	**15**	Average
0.00	0.0	0.0	0.0	0.0	0.0	0.0	0.0	0.0	0.0	0.0	0.0	0.0	0.0	0.0	0.0	0.0	0.0	0.0
0.28	1.0	10.0	15.5	0.0	0.0	5.3	1.0	12.5	34.5	16.0	0.0	12.8	2.5	31.5	47.0	23.0	0.0	20.8
0.45	2.5	19.5	28.0	12.0	0.0	12.4	1.5	33.0	54.0	28.0	0.0	23.3	3.0	43.0	67.5	33.5	0.0	29.4
0.70	3.0	25.5	43.0	18.0	0.0	17.9	2.0	35.0	56.0	29.0	0.0	24.4	3.0	56.0	73.0	40.0	0.0	34.4
0.95	2.5	22.5	37.0	16.0	0.0	15.6	1.0	34.0	55.5	29.5	0.0	24.0	2.0	50.0	57.5	31.0	0.0	28.1
1.20	0.0	18.5	29.0	13.5	0.0	12.2	0.0	31.0	45.0	25.0	0.0	20.2	0.0	48.0	53.0	27.0	0.0	25.6
1.45	0.0	13.0	24.5	7.0	0.0	8.9	0.0	25.5	35.0	17.0	0.0	15.5	0.0	27.0	38.0	20.0	0.0	17.0
1.70	0.0	9.5	19.0	5.0	0.0	6.7	0.0	20.5	31.0	14.0	0.0	13.1	0.0	23.5	34.0	18.0	0.0	15.1
1.95	0.0	1.0	2.5	0.0	0.0	0.7	0.0	2.0	4.0	0.5	0.0	1.3	0.0	2.5	4.0	0.0	0.0	1.3

Table 4.3 Continued…

Time (hr)	*Water Table Depth in Piezometers of Transect 4 (cm)*						*Water Table Depth in Piezometers of Transect 5 (cm)*					
	16	**17**	**18**	**19**	**20**	Average	**21**	**22**	**23**	**24**	**25**	Average
0.00	0.0	0.0	0.0	0.0	0.0	0.0	0.0	0.0	0.0	0.0	0.0	0.0
0.28	4.0	41.5	63.5	23.5	0.0	26.5	5.0	53.5	71.0	41.0	0.0	34.1
0.45	6.0	51.5	71.5	44.5	0.0	34.7	5.5	61.0	79.0	51.5	0.0	39.4
0.70	6.0	72.5	87.5	59.0	0.0	45.0	6.0	92.0	94.5	85.0	0.0	55.5
0.95	3.0	53.5	73.5	42.5	0.0	34.5	4.0	72.0	75.5	57.0	0.0	41.7
1.20	2.5	41.0	60.5	31.0	0.0	27.0	2.0	49.5	62.5	38.5	0.0	30.5
1.45	0.0	35.0	43.5	24.0	0.0	20.5	2.0	34.5	49.0	27.0	0.0	22.5
1.70	0.0	27.0	37.5	15.0	0.0	15.9	1.0	31.5	42.0	22.0	0.0	19.3
1.95	0.0	0.5	1.0	0.0	0.5	0.4	0.5	4.5	4.0	0.0	0.0	1.8

4.2.5 Simulations of the subsurface stormflow model

The subsurface stormflow model has been simulated for the experimental hillslope plot using the field data obtained from the runoff experiments. It has been considered that there was a uniform soil depth with d = 1 m, w = 6 m, L = 18 m, average k_s = 0.05 m/hr, and ε = 0.3. From visual observations and the dye tracing experiments conducted with the hillslope soil columns, the presence of dense macropore network throughout the soil profile was evident and the macropores having diameter of 1-2 mm were found to be dominating. Larger diameter macropores were very less in number. These data were used to define a suitable size of soil macropores in the model setup. For numerical solutions the adoption of a uniform grid size of 0.25 m along the longitudinal direction and a time step of 0.05 hour was sufficient to avoid any numerical instability or oscillation. The vertical grid depends on the number of layers defined in the soil profile. The 1 m deep soil profile of the hillslope plot has been subdivided into m no. of vertical layers. The macropores were assumed to be uniformly distributed in these soil layers. With different rates of recharge the number of hydraulically effective macropores in each layer was varied to match the observed and simulated temporal variations of water table in the experimental plot. To obtain a good matching between observed and predicted saturated profiles, a statistical parameter called Performance Index (PI) was used. This index has been given by Lin and Cunningham III (1995) as

$$\text{Performance Index (PI)} = \frac{\sqrt{\sum_{i=1}^{n}(O_i - P_i)^2}}{\sum_{i=1}^{n}|O_i|} \tag{4.13}$$

where O = observed value, P = predicted value, and n = total number of data samples. The lower the value of PI, the better is the prediction. For each experiment the values

of PI were calculated for different time steps and the matching was considered to be acceptable, if the PI for all the time steps were less than 0.1.

4.2.5.1 Design of soil macropore structure through simulations

For each of the fifteen runoff experiments the possible active soil macropore structures were optimized through simulations of the subsurface stormflow model. The procedure has been illustrated here as an example for the experiment E-12. Similar method has been adopted for all the fifteen experiments. Different structures of soil macropores were defined by assuming various combinations of the parameters viz. no. of soil layers (m), no. of hydraulically active connected macropores per unit width of the slope in each layer (N), and average radius of macropores (r_{avg}). These arbitrary structures of soil macropores are shown in Table 4.4. Initially, the simulations were run assuming there are 10 layers in the 1 m deep soil profile (Set I, Set II, Set III, and Set IV). In all these cases the average diameter of macropores were taken as 1.5 mm, which corresponds to the average diameter of the dominating soil macropore size class (1-2 mm). The results of the simulations were analyzed to compare the observed and predicted saturation profile buildup and recession above the impermeable layer. The values of PI were computed for each computational time steps. Table 4.5 shows the values of PI obtained for different soil macropore structures. From these values it is clear that the macropore structure defined in Set III produced the best prediction overall, compared to the other structures. Fig. 4.7 shows the observed and simulated profiles of saturated depth over the impermeable layer at different time steps for the experiment E-12 adopting the macropore structure defined in Set III. The figure depicts that the consideration of 13 hydraulically effective macropores per unit width of the slope in each soil layer was sufficient to capture the observed temporal variations of saturated profile during water table buildup as well as

recession. The predictions were not acceptable if the number of macropores were increased or decreased (Table 4.5). From the simulations it was also possible to compute the no. of hydrologically active macropores at different time steps during the experiment. These are the macropores present below the saturated soil zone and thus actively contribute to lateral subsurface stormflow. Fig. 4.8 shows how the number of hydrologically active macropores varied with time for the experiment E-12, depending on the saturated depth and soil macropore structure. With the increase of

Table 4.4 Random soil macropore structures assumed for the experiment E-12

Macropore Structure	*No. of Soil Layers (m)*	*No. of Connected Macropores per unit Width of the Slope in Each Soil Layer (N)*	*Average Radius of Soil Macropores (r_{avg}), mm*
Set I	10	05	0.75
Set II	10	09	0.75
Set III	10	13	0.75
Set IV	10	20	0.75
Set V	20	06	0.75
Set VI	30	04	0.75
Set VII	10	13	1.50
Set VIII	10	13	3.00

Table 4.5 Values of computed performance index at various time steps for different macropore structures

Time Step (hr)	*Performance Index (PI)*							
	Set I	Set II	Set III	Set IV	Set V	Set VI	Set VII	Set VIII
0.30	0.041	0.052	0.065	0.088	0.055	0.054	0.071	0.090
0.45	0.052	0.039	0.045	0.076	0.036	0.035	0.052	0.077
0.70	0.088	0.034	0.034	0.091	0.026	0.028	0.047	0.088
0.95	0.232	0.113	0.031	0.083	0.071	0.079	0.021	0.078
1.20	0.294	0.119	0.023	0.130	0.064	0.076	0.044	0.128
1.45	0.434	0.184	0.033	0.131	0.115	0.132	0.024	0.131
1.70	0.487	0.188	0.036	0.167	0.117	0.138	0.054	0.166

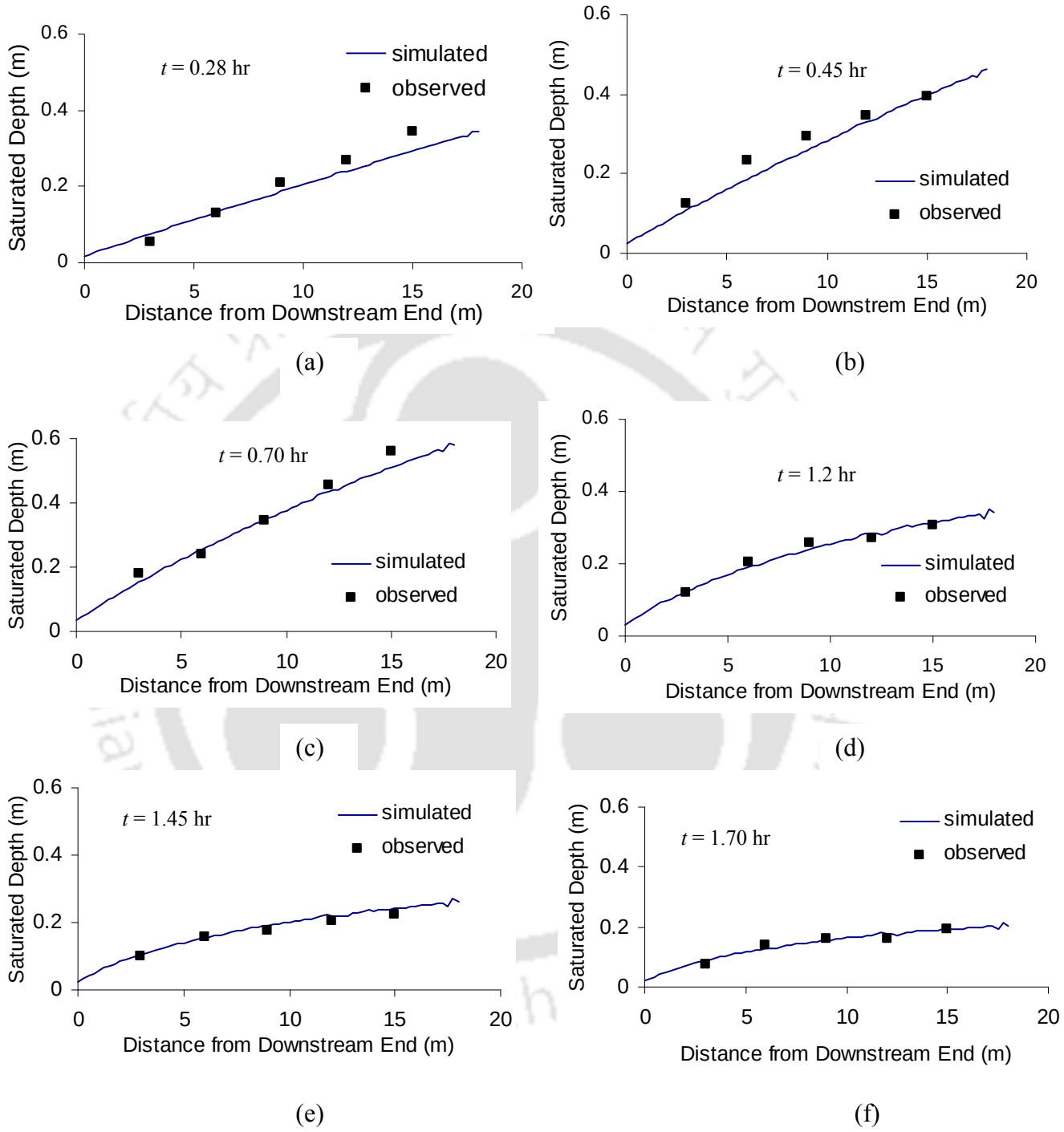

Fig. 4.7(a-f) Observed and simulated temporal variations of saturated depth for Set III of the experiment E-12 with f_{avg}= 0.139 m/hr continued for 0.8 hr

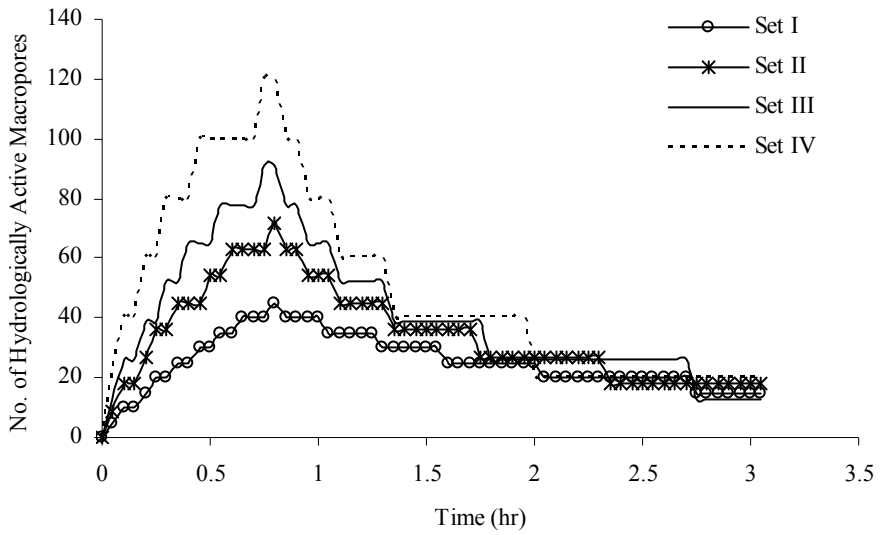

Fig. 4.8 Temporal variations in no. of hydrologically active macropores with different macropore structures for the experiment E-12

macropore density in the soil layers, no. of hydrologically active macropores present below the water table were also increased. This resulted in quick drainage of subsurface water from the hillslope due to higher lateral preferential flow. It is also worth noting that during saturation buildup the water table profile was predominantly controlled by the rate of recharge (up to 0.80 hr for the experiment E-12). During this stage macropore structures did not exhibit significant control over the shape of water table profile. But, during recession phase the water table was lowered primarily due to lateral preferential flow through the hydrologically active macropores. For higher density of connected macropores below the saturated zone, the recession was faster as more macropores were hydrologically active (Fig. 4.8). The PI values in Table 4.5 also reflect that during buildup the predictions for all the macropore structures were acceptable. But, except Set III all other structures failed to capture the recession phase properly. Therefore, the water table recession in the hillslope was critically controlled by the soil macropore structure.

To study the effect of increasing number of layers in the soil profile the macropore structures in Set V and Set VI were defined with 20 and 30 layers, respectively, in the 1 m deep soil profile. The macropore diameter was kept as 1.5 mm. The model simulations showed that in order to have a reasonable comparison with the observed data, the no. of hydraulically effective connected macropores per unit width of the slope in each layer (N) were required to be reduced. In Set III it was necessary to assume 13 macropores in each soil layer. But, with the increase of soil layers in Set V and Set VI, only 6 and 4 macropores in each layer, respectively, were required to have a comparable prediction. Fig. 4.9 depicts the variation in no. of hydrologically active macropores at different time steps for the macropore structures Set III, Set V, and Set VI. From the figure it is clear that regardless of the number of soil layers, the temporal variations in water table profile largely depended on the hydrologically active macroporosity of soil. The distribution of the macropores in a layer did not seem to have a significant effect. Rather, the density of actively flowing macropores present below the saturated zone primarily controlled the subsurface stormflow response from the hillslope.

To study the effect of variation in macropore diameter, macropore structures Set VII and Set VIII were defined. Except the macropore diameters, these structures were exactly similar to Set III, which provided the best predictions. Average macropore diameter of 3 mm and 6 mm were considered for Set VII and Set VIII, respectively. Fig. 4.10 shows the comparison of hydrologically active macroporosity of Set VII and Set VIII with Set III. It can be observed that with the increase of macropore diameter the number of hydrologically active macropores reduced. Considering 13 connected macropores in each soil layer, adoption of 1.5 mm as macropore diameter gave the best results. It can also be noticed that even with 3 mm

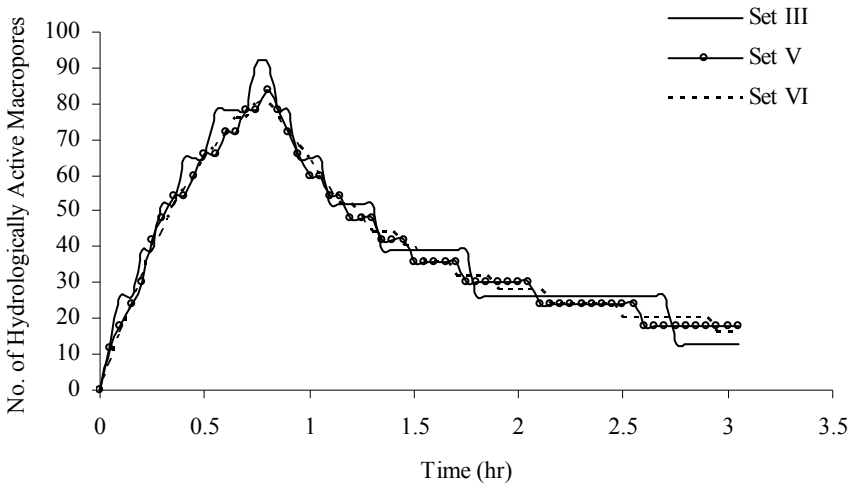

Fig. 4.9 Hydrologically active macropores at different time steps with the macropore structures Set III, Set V, and Set VI for the experiment E-12

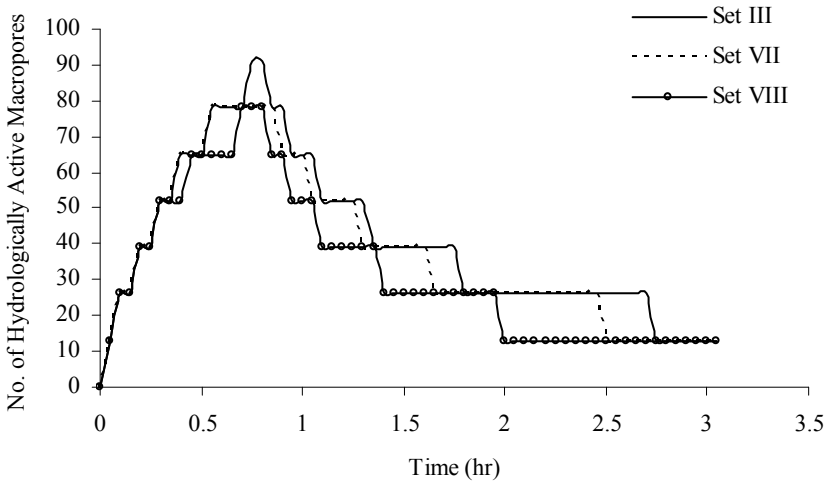

Fig. 4.10 Variation in hydrologically active macropores with time due to change in macropore diameter for the experiment E-12

diameter of macropores (Set VII) the predictions were acceptable (Table 4.5). However, with 6 mm macropore diameter (Set VIII) the predictions were not so good. Clearly, the subsurface stormflow generated from the hillslope depended on macropore diameter. But, it was not a very critical parameter in terms of model predictions. In general, the macropore density in the soil profile was found to be a

more critical parameter compared to the macropore diameter to control the subsurface stormflow generation from the hillslope.

Similar results were obtained from the simulations of the runoff experiments conducted on the hillslope plot. Table 4.6 shows the ranges of PI obtained with the best adopted soil macropore structures defined for the fifteen experiments. The detailed observed and simulated water table depths and the estimated PI values are given in Appendix 1. Another important observation could be made from the model simulations. It was found that all the experiments showed a common trend of increasing the number of hydraulically effective and hydrologically active macropores in soil with the increasing rate of recharge (Table 4.6). This can be attributed to the threshold behavior of preferential flow generation as mentioned by Uchida *et al*. (2005). Water can flow into a macropore if its water entry pressure is exceeded (Ela *et al*., 1992; Li and Ghodrati, 1997; and Weiler and Naef, 2003). Therefore, with lower rates of recharge some of the macropores present in soil might not get sufficient connectivity to become hydraulically effective. But, under high recharge rates the connectivity between those inactive macropores were established to make them hydraulically effective and potentially active for rapid preferential flow generation. Therefore, the experiments showed a good correlation between average rate of recharge (f_{avg}) and maximum number of hydrologically active macropores (N) with a logarithmic functional relationship (Fig. 4.11). The field observations clearly showed very fast buildup and recession of saturated zone above the impermeable layer indicating the occurrence of rapid subsurface stormflow from the hillslope. In most of the cases major portion of subsurface runoff occurred within 2-3 hours from the cessation of recharge. With a very slow matrix flow rate such quick response was not possible and thus it is clear that the lateral preferential flow dominated the storm hydrograph. This typical subsurface runoff pattern seems to be captured properly in

Table 4.6 The details of the subsurface runoff experiments conducted on the hillslope

Experiment No.	*Average Rate of Recharge (f_{avg}) (m/hr)*	*Duration of Recharge (hr)*	*No. of Optimized Hydraulically Effective Macropores per unit Width of the Slope in each of the 10 Soil Layers*	*Range of PI*
E-1	0.184	1.50	15	0.030 – 0.069
E-2	0.079	1.08	06	0.018 – 0.080
E-3	0.257	0.75	20	0.017 – 0.049
E-4	0.071	0.83	05	0.036 – 0.081
E-5	0.090	0.78	08	0.039 – 0.080
E-6	0.109	1.57	10	0.022 – 0.057
E-7	0.195	1.03	18	0.022 – 0.046
E-8	0.076	1.03	05	0.026 – 0.051
E-9	0.135	1.00	12	0.030 – 0.049
E-10	0.123	0.75	11	0.029 – 0.064
E-11	0.126	1.00	11	0.026 – 0.054
E-12	0.139	0.80	13	0.023 – 0.065
E-13	0.176	1.00	16	0.019 – 0.039
E-14	0.110	0.92	10	0.016 – 0.031
E-15	0.106	0.85	09	0.018 – 0.037

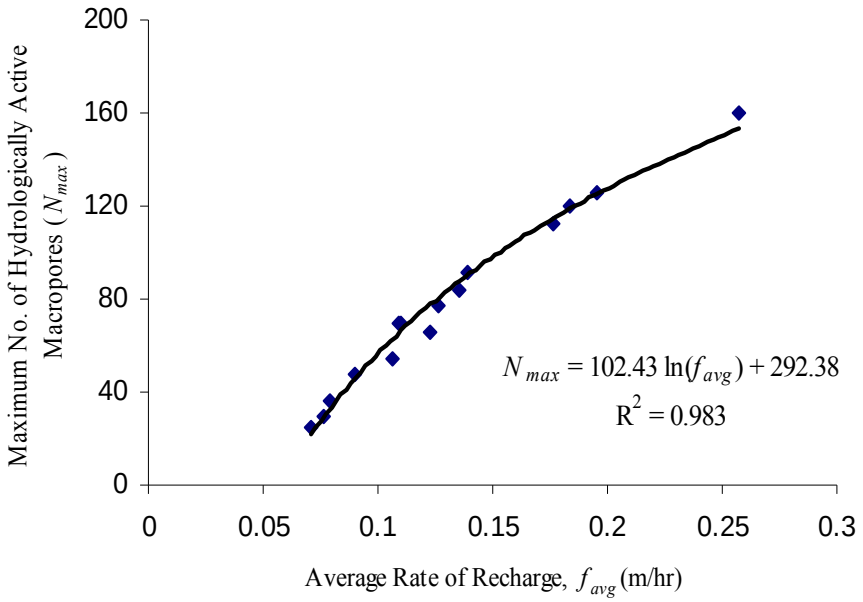

Fig. 4.11 Maximum no. of hydrologically active macropores for different rates of recharge

the model simulations. Fig. 4.12 shows the computed subsurface flow hydrographs of matrix and macropore flow for the experiment E-12. The peak of both the hydrographs occurred immediately after the cessation of recharge. Similar to the other experiments it clearly shows that matrix flow was almost negligible compared to the amount and rate of lateral preferential flow (Sarkar and Dutta, 2009; Sarkar and Dutta, 2011). van Schaik *et al.* (2008) also reported a maximum macropore flow contribution of 80% in total subsurface runoff in semi-arid hillslopes. Fig. 4.13 clearly depicts that preferential flow contributed the major part of prompt interflow occurring immediately after the storm events (within first two hours). With increasing rate of recharge, contribution of macropore flow also increased as a polynomial function. Analysis of the computed subsurface flow hydrographs clearly showed that the peak rate of macropore flow has a good linear correlation with recharge (Fig. 4.14). However, Fig. 4.15 indicates that the peak matrix flow rate has a power relationship with recharge showing comparatively poor correlation. This may be due to the significant domination of preferential flow over matrix flow in the storm hydrograph generated from the hillslope plot.

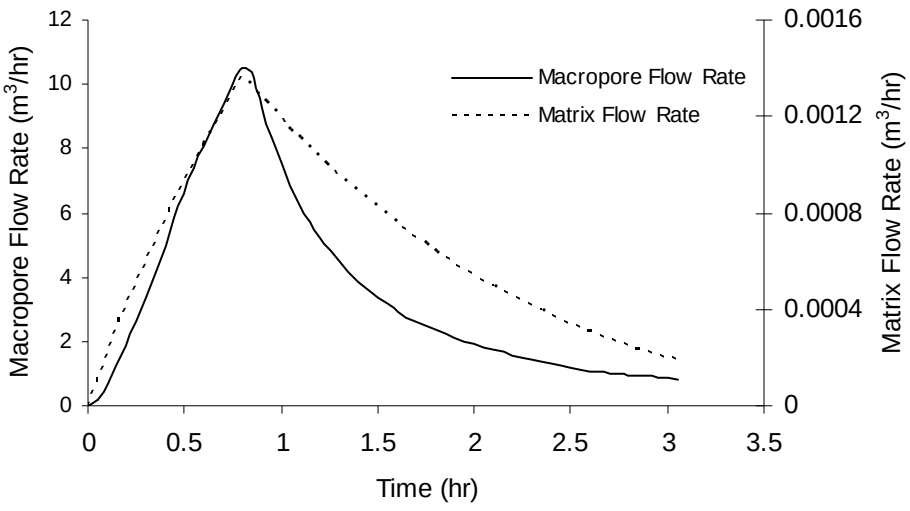

Fig. 4.12 Computed subsurface flow hydrographs through soil matrix and macropores for the experiment E-12

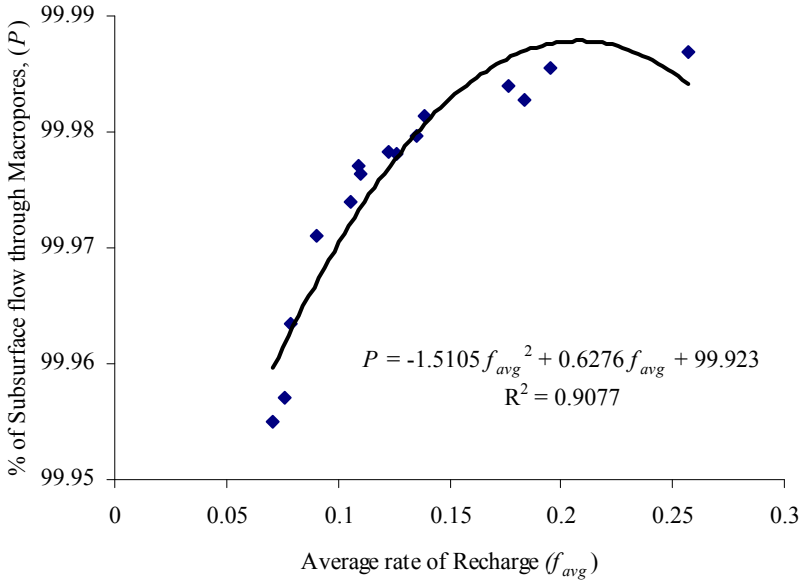

Fig. 4.13 Contribution of preferential flow in subsurface stormflow hydrograph for different rates of recharge

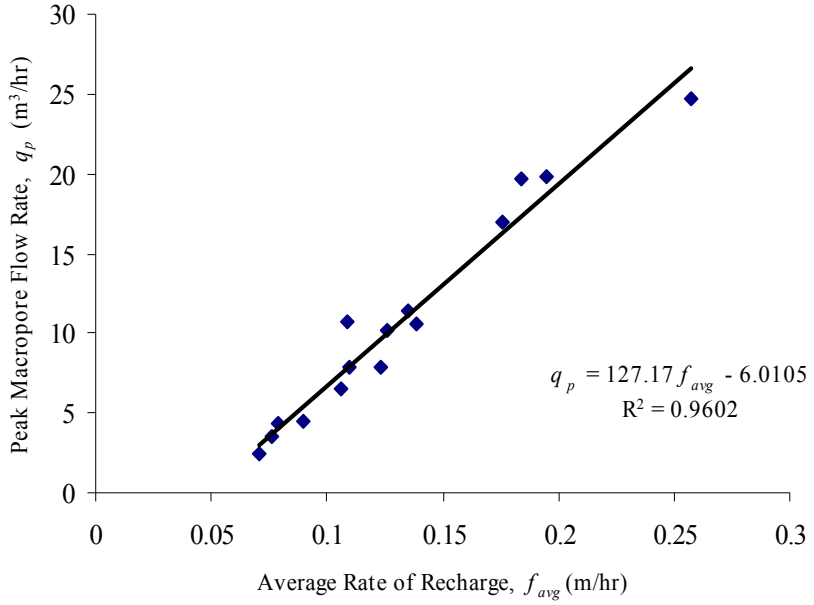

Fig. 4.14 Peak rate of macropore flow as a function of average rate of recharge

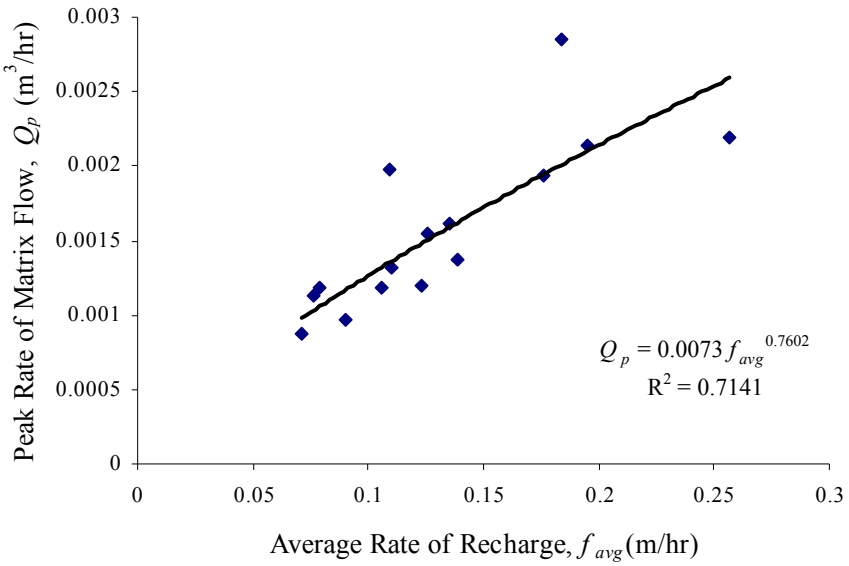

Fig. 4.15 Peak rate of soil matrix flow as a function of average rate of recharge

4.3 Summary of the Chapter

The results obtained from the simulations of the overland flow and subsurface stormflow models can be summarized as follows.

- This chapter presents a physical based conceptual modeling approach for overland flow and subsurface stormflow generation from an initially wet experimental hillslope plot under high intensity artificial runoff events. The functional relationships developed from the *in situ* experimental investigations have been used to calibrate the model parameters.
- The overland flow process on the hillslope plot has been defined by approximating the St. Venant equations of continuity and momentum. The resulting one-dimensional shallow water overland flow equations with diffusive wave approximation were solved using a finite volume technique by defining suitable initial and boundary conditions. Prior to this, from the two-dimensional flow domain one-dimensional flow network was established

based on cell elevation and flow depth. The model computed flow depth and friction slope at each computational cell and the hydrograph at the downstream end of the slope.

- The two most important input parameters of the overland flow model are steady preferential infiltration rate (f_b) and inflow intensity (i). These two parameters were measured from the field experiments conducted on the hillslope plot. For a particular experiment knowing the value of these parameters and the equivalent flow depth (h_e) in the upstream boundary computational cells, the overland flow model was simulated with an assumed value of Manning's roughness coefficient (n). The model simulated outflow hydrograph was then compared with the measured hydrograph at the downstream end of the plot. Using a trial and error method the value of n was varied till the observed flow hydrograph matched with the model simulated hydrograph. This estimated value of n represented a lumped value of surface roughness of soil, vegetation, and microtopography under a steady overland flow condition over the plot.
- The model simulated overland flow behavior on the hillslope was in good agreement with those reported in literature under similar conditions. From model simulations it was found that the average overland flow depth varied in the range of 3-10 mm with maximum coefficient of variation of about 200 percent. Over 80 percent area of the hillslope plot, the flow depth was less than 5 mm. These simulated flow depths reasonably complemented the roughly measured flow depths during the field experiments. The spatial variations in overland flow depth were mainly due to the micro-topographic

variations, which do not have significant effect on the lumped overland flow response from the hillslope.

- The estimated Manning's roughness coefficients were found to be a depth dependent parameter. Manning's n had a power relationship with inflow intensity (i). Similar relationships are also well reported in literature. Manning's n was also found to be closely related to degree of vegetation. Denser vegetation imparted higher surface resistance to result in higher values of n. The estimated n values distinctly represented three vegetation conditions of the plot viz. sparse, moderate, and dense. For shallow overland flow depth, variation of the surface roughness on a vegetated hillslope was mainly characterized by degree of vegetation.
- To model subsurface stormflow from the experimental hillslope plot, the modeling concept of Fan and Bras (1998) has been adopted with some modifications. The present model does not use an effective lateral hydraulic conductivity to represent combined effect of soil matrix and macropore flow. It considers actual saturated hydraulic conductivity for water flow through soil matrix and a new sink term to account for rapid lateral water movement through soil macropores.
- A physical based numerical solution of the subsurface flow equations was provided to capture the rapid subsurface stormflow evident in the hillslope, to reflect the contributions of soil matrix and macropores in prompt interflow occurring immediately after high intensity runoff events, and to provide a surrogate indicator of hydraulically effective or hydrologically active lateral macroporosity of the hillslope. The dependency of effective lateral

macroporosity, matrix, and macropore flow rates under varying recharge conditions were also evaluated.

- Considering the extent of complexity in defining the soil macropore structures and the intricacy of macrpore flow through soil, a number of assumptions were taken to simplify the macropore flow processes. The hydraulically active macropores were assumed to be straight and continuous small pipes of uniform diameter, which are distributed in different soil layers. When these macropores are present below the saturated soil, water seeps into these pores. These macropores were termed as hydrologically active. The water, which seeps into these macropores, has been assumed to be discharged laterally at a very high velocity without any interaction with the surrounding soil matrix. Considering the saturated condition of the surrounding soil matrix this approximation is quite practical.
- For the uniform hillslope experimental plot the three-dimensional soil mantle was converted to a two-dimensional soil profile by defining the storage capacity of the hillslope in terms of its drainable pore space. Instead of adopting a polynomial function to define the bedrock profile, digital elevation data of the experimental plot were used. The bedrock slope along the centroid profile was approximated as that of the surface topography assuming a uniform soil depth of 1 m. Defining proper initial and boundary conditions the numerical solution of the subsurface stromflow equation was obtained using a finite difference method with the Warming-Beam upwind scheme. The model computed subsurface storage at different time steps in each grid cell and also quantified subsurface lateral flow response at the bottom of the hillslope as saturated matrix flow and lateral preferential flow. At a particular time step the

storage within the hillslope can be used to calculate the saturated depth or water table depth over the impermeable layer.

- Fifteen runoff experiments were conducted in the hillslope plot with varying inflow intensities and durations to compute the average rate of recharge (f_{avg}). During these experiments the water table depth in the piezometers were monitored at regular intervals to capture the buildup and recession of saturated zone above the impermeable layer. The responses of the piezometers located at the two sides of the plot were found to be negligible as the subsurface flow along the length of the slope was dominating. The average saturated depths at five points along the cetroid of the plot were approximated by averaging the piezometer readings at the five transects. These average depths at different time steps were compared with the model simulated saturated depths.
- In order to calibrate the model for the experimental hillslope plot simulations were run with different arbitrary structures of soil macropores. For different rates of recharge the number of hydraulically effective macropores in each layer was varied to match the observed and model simulated temporal variations of water table profile in the experimental plot. To ensure a good matching between the observed and predicted saturated profiles, a statistical parameter called Performance Index (PI) was used. Lower value of PI indicated better prediction of the model. For all the experiments the values of PI were calculated at different time steps and if the PI for all the time steps were less than 0.1, the predictions were considered acceptable.
- For all the experiments the soil macropore structures were optimized through simulations of the model with number of arbitrary macropore structures defined by assuming various combinations of the parameters viz. no. of soil

layers (m), no. of hydraulically active connected macropores per unit width of the slope in each layer (N), and average radius of macropores (r_{avg}). The structure, which produced the lowest values of PI for all the computational time steps, was selected as the best possible structure to define soil macroporosity under those specific conditions of the experiment.

- It was observed that the water table recession in the hillslope was critically controlled by the soil macropore structure. During saturation buildup the water table profile was predominantly controlled by the rate of recharge. During this stage macropore structures did not exhibit significant control over the shape and position of the water table. But, once the recharge stopped, the water table was lowered primarily due to lateral preferential flow through the hydrologically active macropores present below the water table. For higher density of macropores below the saturated zone, the recession was faster as more macropores were hydrologically active.

- The distribution of the macropores in different soil layers did not seem to have significant effect. Rather, the density or number of actively flowing macropores present below the saturated zone primarily controlled the subsurface stormflow response from the hillslope. Therefore, increasing the number of soil layers and increasing the number of hydraulically effective macropores per layer without changing the number of soil layers, had similar impacts on model performance.

- Change in macropore diameter was found to have some effect on subsurface stormflow response from the hillslope plot. But, instead of increasing macropore diameter, increasing the number of macropores in the soil layers

showed more prominent effect on subsurface water profile. Therefore, compared to macropore diameter, active macropore density of soil is a more critical parameter for subsurface stormflow generation from the hillslope.

- All the experiments showed a common trend of increasing the number of hydraulically effective and hydrologically active macropores in the soil with increasing rate of recharge. This can be attributed to the threshold behavior of preferential flow generation which states that water can flow into a macropore only if its water entry pressure is exceeded. With lower rates of recharge some of the macropores present in soil might not get sufficient connectivity to become hydraulically effective. But, under higher recharge rates the connectivity between those inactive macropores were established to make them hydraulically effective and potentially active for rapid preferential flow generation. Therefore, a good correlation between average rate of recharge (f_{avg}) and maximum number of hydrologically active macropores (N_{max}) was observed.

- The subsurface model could capture the rapid buildup and recession of saturated zone above the impermeable layer due to the occurrence of subsurface stormflow from the hillslope. In most of the cases major portion of subsurface runoff occurred within 2-3 hours from the cessation of recharge. With a very slow matrix flow rate such quick response was not possible and thus it was clear that the lateral preferential flow dominated the storm hydrograph. The computed subsurface flow hydrographs of matrix and macropore flow showed that the peak of both the hydrographs occurred immediately after the cessation of recharge. The matrix flow was almost negligible compared to the amount and rate of lateral preferential flow from

the experimental hillslope plot. Lateral preferential flow contributed major part of prompt interflow occurring immediately after the storm events. Here it is important to mention that this particular subsurface flow behavior was a specific case for a particular hillslope plot, which had extreme degree of active soil macroporosity. Therefore, the results can not be generalized for all cases of lateral preferential flow generation. Under certain circumstances soil matrix flow may dominate over preferential flow.

- It was also found that with the increasing rate of recharge, contribution of macropore flow increased as a polynomial function. Computed subsurface flow hydrographs showed that the peak rate of macropore flow has a good linear correlation with recharge. However, the peak matrix flow rate has a power relationship with recharge showing comparatively poor correlation. This may be due to the significant domination of preferential flow over matrix flow in the subsurface runoff hydrograph, which was evident in the hillslope plot under investigation.

CHAPTER 5 MODEL APPLICATIONS IN DIFFERENT HILLSLOPE TYPES

This chapter presents a parametric study of the overland flow and subsurface stormflow models. The hydrological responses of different characteristic hillslope types under varying conditions of macropore diameter, rainfall intensity, rainfall duration, sealing of macropores, hillslope profile curvature, relief etc. are analyzed. The sensitivity of some basic controlling parameters of the models has been studied.

5.1 Different Types of Hillslopes

The topographic surface of a hillslope can be approximately defined by a continuous function. Evans (1980) proposed such a bivariate quadratic function, which is the general equation of conic shape given as

$$z = ax^2 + by^2 + cxy + dx + ey + f \tag{5.1}$$

where z is the elevation (m), x is the horizontal distance along the length direction (m), y is the horizontal distance in the direction perpendicular to the length direction (m), and a, b, c, d, e, f are the constants. Following the methods suggested by Evans (1980), hillslope topography can be characterized by the combined curvature in the gradient direction and the width direction, which is perpendicular to the gradient. The curvature in the gradient direction is known as profile curvature and the same in the width direction is known as plan curvature. The profile curvature defines the change in slope angle and thereby controls the change of velocity of water flowing down along the slope curve, whereas the plan curvature reflects the change in aspect angle to influence the divergence or convergence of water flow. Troch *et al.* (2002) used the following form of bivariate quadratic function for defining plan and profile curvatures of the hillslopes

$$z(x) = E + H(1 - x/L)^{\alpha} + \omega y^2 \tag{5.2}$$

where $z(x)$ is the surface topography curvature function, E is the elevation of reference datum (m), H is the relief of the hillslope (m), L is the corresponding slope length (m), α is the exponent which defines profile curvature, ω is the plan curvature parameter, and y is the distance in the width direction from the centre of the slope (m). If $\alpha > 1$, it is a concave profile, $\alpha < 1$ defines a convex profile, and for $\alpha = 1$, the profile is straight. Similarly, when $\omega > 0$, plan curvature is concave, for $\omega < 0$, plan curvature is convex, and for $\omega = 0$, plan curvature becomes straight. Considering different combinations of α and ω, it is possible to define nine possible geometric shapes (Table 5.1) of hillslope topography (Dikau, 1989).

Table 5.1 Different combinations of possible hillslope types

α	ω	Profile Curvature	Plan Curvature
> 1	> 0	Concave	Concave
> 1	0	Concave	Straight
> 1	< 0	Concave	Convex
1	> 0	Straight	Concave
1	0	Straight	Straight
1	< 0	Straight	Convex
< 1	> 0	Convex	Concave
< 1	0	Convex	Straight
< 1	< 0	Convex	Convex

To study the effect of topographical shape on the hydrographs generated at the bottom of the slope, three basic hillslope types, as shown in Table 5.2, were considered. The length of the hillslope plot (L) was taken as 100 m with a uniform

width (w) of 22 m. Total relief between the upslope and downslope points (H) was 20 m. Considering a reference datum of 100 m, uniform grids (2 m × 2 m) were generated for the three selected types of hillslopes (Fig. 5.1). A constant soil depth of 1 m was taken by assuming that the surface profile curvature of the terrain was parallel to the bedrock profile. It is a usual practice to have such an assumption in case the soil depth function is unknown (Troch *et al*., 2002). It was further assumed that the hydrological behavior of the hillslope was identical to that of the experimental hillslope plot and therefore, the relationships derived from the *in situ* experiments on the plot were valid for the new theoretical hillslopes.

Table 5.2 Three selected hillslope types and their plan and profile parameters

Hillslope Type	α	ω	Profile Curvature	Plan Curvature
Type 1	2	0	Concave	Straight
Type 2	1	0	Straight	Straight
Type 3	0.5	0	Convex	Straight

5.2 Overland Flow Behavior on Hillslopes

For simulating the overland flow behavior on the three hillslope types defined in Fig. 5.1 and Table 5.2 it was considered that the theoretical hillslopes have dense vegetation cover and a highly macroporous soil as similar to the experimental plot. Overland flow hydrographs were simulated for five different rainfall intensities: 100 mm/hr, 125 mm/hr, 150 mm/hr, 200 mm/hr, and 300 mm/hr. For all these intensities average preferential infiltration rates (f_b) were calculated from the functional relationship for dense vegetation condition (Table 5.3), which was derived from the *in situ* experiments conducted on the hillslope plot. For the five rainfall intensities the computed values of f_b are given in Table 5.3. The rainfall intensity in excess of the

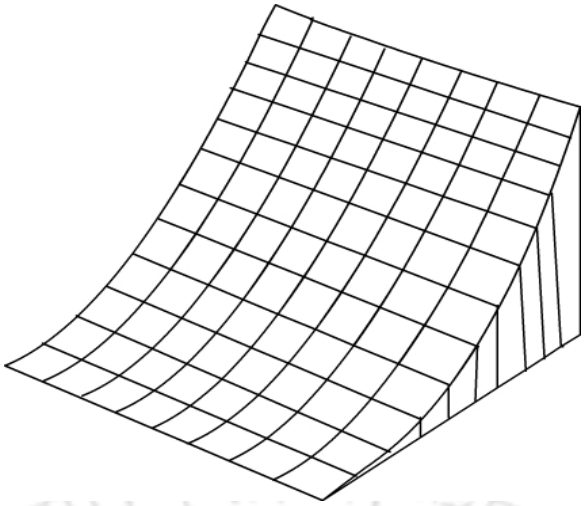

(a) Type 1

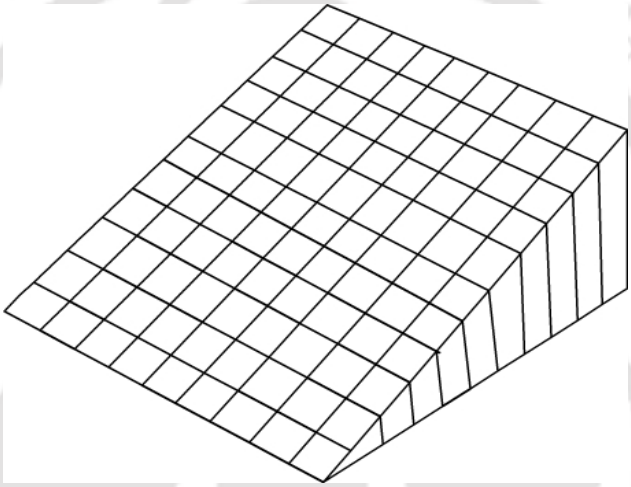

(b) Type 2

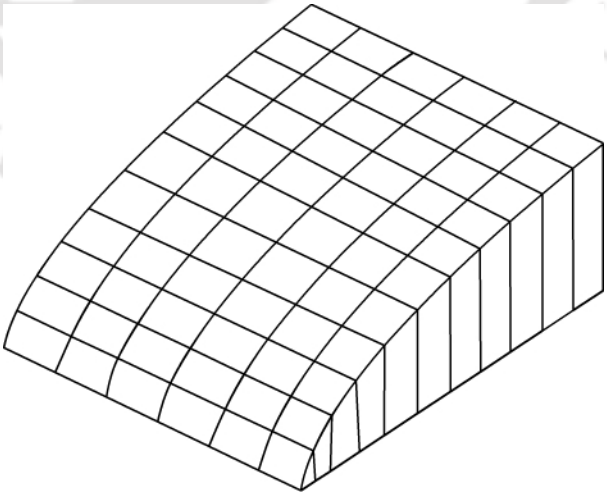

(c) Type 3

Fig. 5.1 (a-c) Three different types of hillslope profiles

Table 5.3 Average preferential infiltration rates for different rainfall intensities

Vegetation Condition	Relationship of f_b with Rainfall Intensity (i)	Rainfall Intensity (mm/hr)	f_b (mm/hr)
Dense	$f_b = 0.6052\, i + 31.737$	100	92
		125	107
		150	123
		200	153
		300	213

value of f_b, generated overland flow from the hillslope and the infiltration excess flow was routed to the outlet of the slope with an average n value of 0.04. The infiltrated water was assumed to be percolated rapidly through the vertical macropores of soil to recharge the saturated zone (i.e. $f_b \approx f_{avg}$), which was present at some depth below the ground surface. In all the simulations the duration of rainfall was taken as 30 minutes. Figs. 5.2, 5.3, and 5.4 show the simulated hydrographs for the Type 1, Type 2, and Type 3 hillslopes, respectively. All the three hillslopes showed the similar shapes of the hydrographs. Discharge at the outlet of the slope gradually increased from zero as contributions from upslope points started reaching the outlet. After some time the discharge reached a maximum value and became constant till the rainfall continued. This was due to the assumed steady rainfall and constant recharge condition of the plot. After the cessation of rainfall, discharge gradually reduced with the reduction of storage within the hillslopes. For all the hilslopes, with increase in rainfall intensity, peak rate of discharge (Q_p) increased and time to peak (t_p) decreased. A relative comparison of the hydrographs generated from the three hillslopes (Table 5.4) clearly shows the effects of profile curvature on the overland flow hydrographs. The peak rate of discharge for a given particular rainfall intensity remained the same for all the

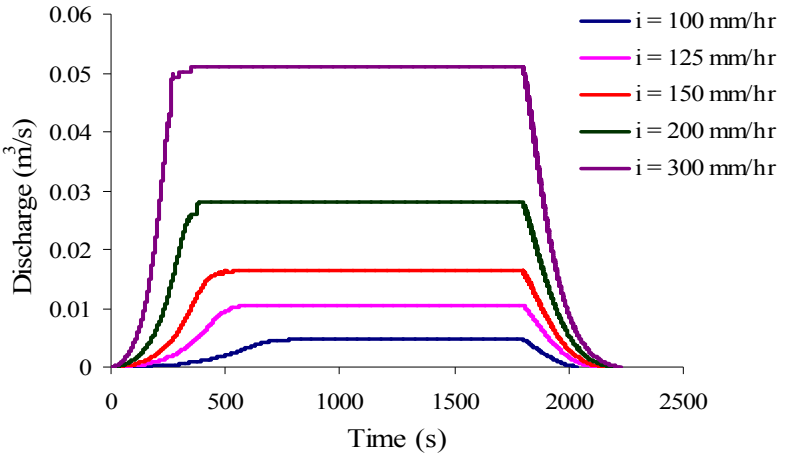

Fig. 5.2 Overland flow hydrographs for the Type 1 hillslope at different intensities

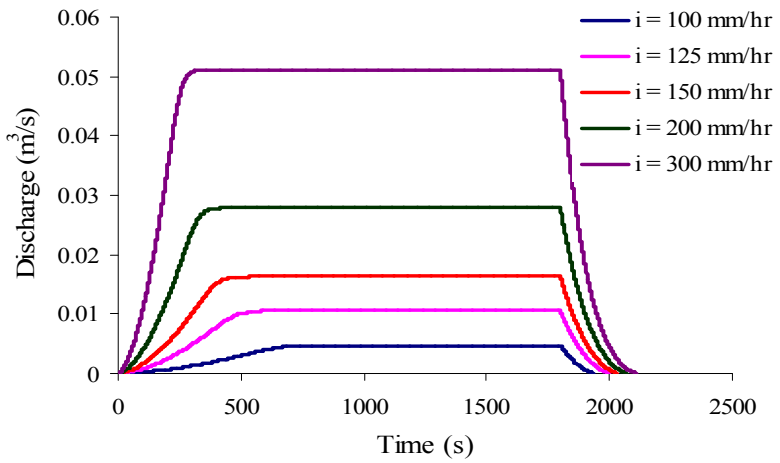

Fig. 5.3 Overland flow hydrographs for the Type 2 hillslope at different intensities

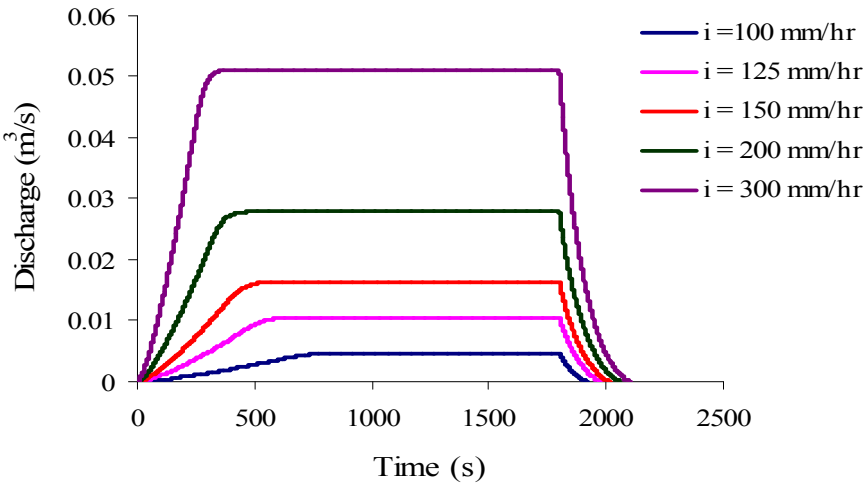

Fig. 5.4 Overland flow hydrographs for the Type 3 hillslope at different intensities

Table 5.4 Comparison of overland flow hydrographs for different hillslope types

Hillslope Type	Rainfall Intensity (mm/hr)	Peak Discharge, Q_p (m^3/s)	Time to Peak, t_p (s)	Time of Recession, t_r (s)
Type 1	100	0.00473	778	217
	125	0.01056	623	315
	150	0.01639	558	351
	200	0.02794	437	394
	300	0.05115	367	428
Type 2	100	0.00473	737	136
	125	0.01056	583	198
	150	0.01639	535	233
	200	0.02794	415	273
	300	0.05115	351	310
Type 3	100	0.00473	820	116
	125	0.01056	653	179
	150	0.01639	603	217
	200	0.02794	466	261
	300	0.05115	395	303

three selected hillslopes. This was expected as a steady rainfall and recharge condition continued for an extended duration over the plot. However, different profile curvatures showed significant effect on time to peak (t_p) and time of recession (t_r). Least values of t_p were obtained for the Type 2 hillslope as in this case the continuous straight slope profile resulted in increasing flow velocity and lower time of concentration. Comparatively higher values of t_p were evident in the Type 1 hillslope. It is because the slope profile was steeper at some of the upslope grids, but after some

distance the steepness of slope was reduced considerably towards the outlet. This resulted in reduction of flow velocity and consequently higher travel time was observed. Type 3 hillslope showed maximum values of t_p as except some grids near the outlet, the elevation difference between most of the upslope grids was very less which resulted in a flatter profile curvature. Similarly, the time of recession (t_r) was also controlled by the hillslope profile curvatures. As recession of flow started after the cessation of rainfall, the storage of water at that particular instant primarily controlled the time of recession. Clearly, Type 3 hillslope has least surface storage due to its convex profile and Type 1 hillslope has maximum storage capacity owing to its concave profile. Therefore, t_r values were least for the Type 3 hillslope and it was maximum for the Type 1 hillslope. Type 2 hillslope exhibited intermediate values of t_r due to its moderate surface storage property.

5.2.1 Effect of relief on overland flow

To study the effect of relief on overland flow hydrographs, keeping the other conditions same the relief of the three types of hillslopes were changed from 20 m to 10 m and the resulting Digital Elevation Models (DEM) were generated. Considering a rainfall intensity of 150 mm/hr overland flow hydrographs were simulated (Fig. 5.5). Comparison between the runoff hydrographs revealed (Table 5.5) that in all three types of hillslopes steady peak outflow conditions was attained. Both t_p and t_r followed the same previous trend for different profiles of the hillslopes. However, due to flattening of the slope the values of t_p and t_r were increased.

5.2.2 Overland flow in non-macroporous soil

To study the effect of soil macroporosity on surface runoff hydrographs, the overland flow model has been simulated for the hillslopes with and without

Table 5.5 Effect of change in relief on overland flow hydrographs for i = 150 mm/hr

Hillslope Type	H = 20 m			H = 10 m		
	Q_p (m^3/s)	t_p (s)	t_r (s)	Q_p (m^3/s)	t_p (s)	t_r (s)
Type 1	0.01639	558	351	0.01639	682	437
Type 2	0.01639	535	233	0.01639	657	287
Type 3	0.01639	653	179	0.01639	743	267

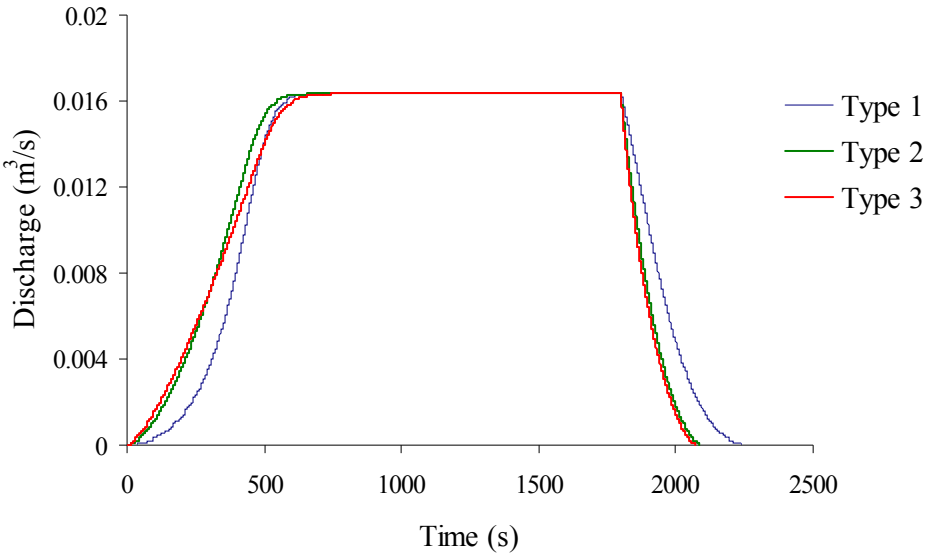

Fig. 5.5 Overland flow hydrographs for H = 10 m and i = 150 mm/hr

preferential pathways. In non-macroporous hillslopes the process of infiltration into the soil matrix, which is governed by the Darcy's law, was approximated by the Green-Ampt equation (Chow et al., 1988). For sandy loam soil of the hillslope, Green-Ampt infiltration parameters were taken as: wetting front soil suction head (ψ) = 0.1101 m, saturated hydraulic conductivity (K_s) = 50 mm/hr, and effective porosity (θ_e) = 0.3. The infiltration excess runoff hydrographs for different rainfall intensities were generated. Figs. 5.6 and 5.7 show some of the simulated hydrographs for the Type 2 and Type 3 hillslopes, respectively. Unlike preferential infiltration dominated

hillslopes, here the build up was slower and steady peak discharge conditions were not attained quickly. Perhaps it was going to take a much longer duration to attain a steady infiltration condition due to a very slow rate of soil matrix flow. Expectedly, the magnitude of peak discharge was much higher (Table 5.6) than that of the preferential infiltration dominated hillslopes. Therefore, non-macroporous or hillslopes with disturbed macropore structures are known to have very high value of runoff coefficients than natural vegetated hillslopes, where high preferential infiltration rates are expected. Most significantly, from the maximum depth of saturated water front propagation below the ground surface (Table 5.6) it was evident that in no case the water front reached up to the impermeable layer to initiate any active subsurface stormflow. Whereas, in macroporous soils the vertical macropores rapidly conveyed the infiltrated water towards the impermeable layer, where a temporary water table build up took place to initiate rapid lateral preferential flow through well connected network of soil macropores.

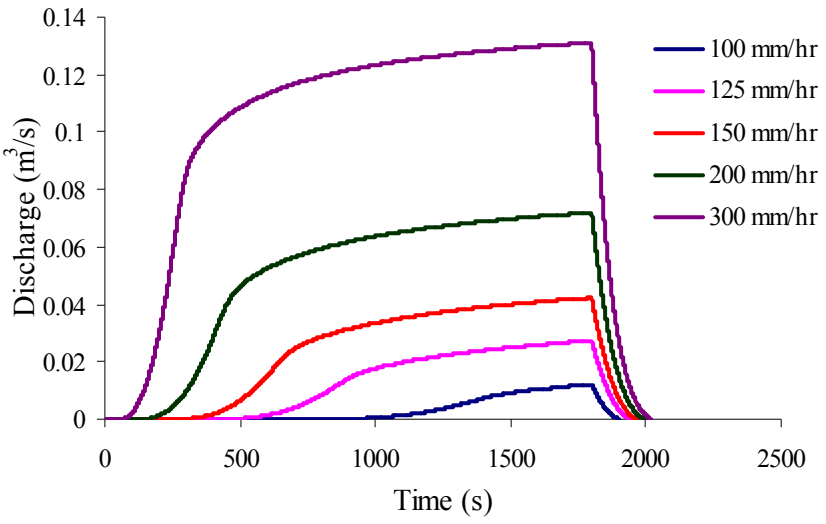

Fig. 5.6 Overland flow hydrographs for non-macroporous soil (Type 2 hillslope)

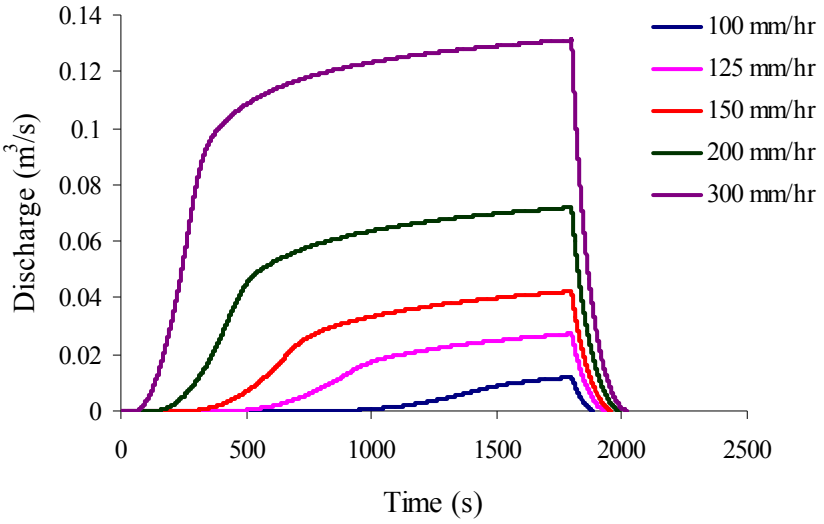

Fig. 5.7 Overland flow hydrographs for non-macroporous soil (Type 3 hillslope)

Table 5.6 Peak discharge and saturated depth for non-macroporous hillslope soils

Hillslope Type	Rainfall Intensity (mm/hr)	Peak Discharge, Q_p (m^3/s)	Depth of Saturated Wetting Front, d_s (m)
Type 1	100	0.01177	0.2079
	125	0.02684	0.2114
	150	0.04158	0.2132
	200	0.07106	0.2152
	300	0.12950	0.2171
Type 2	100	0.01210	0.2022
	125	0.02739	0.2054
	150	0.04224	0.2071
	200	0.07139	0.2091
	300	0.01310	0.2108
Type 3	100	0.01200	0.2012
	125	0.02739	0.2044
	150	0.04235	0.2063
	200	0.07205	0.2085
	300	0.01312	0.2105

5.3 Subsurface Stormflow from Hillslopes

The subsurface stormflow model was used to study the response of different hillslope types under varying intensities of simulated rainfall. The average rate of recharge to the saturated layer was obtained from the same functional relationship used in overland flow simulations assuming $f_{avg} \approx f_b$. It was evident from the discussions in the previous chapter that hydraulically effective macroporosity of the hillslope soil was strongly dependent on rainfall intensity or the rate of recharge. Knowing the values of f_{avg}, the number of hydraulically effective macropores per unit width of the slope (N) that might be present in different soil layers was approximately defined. The experimental based and model calibrated values of N were defined for different rainfall intensities (Table 5.7) assuming that the theoretical hillslope soil has the same order of macroporosity as that of the experimental plot. For simplification in macropore flow routing it was assumed that the macropores have infinite carrying capacity and the water seeping into a macropore is discharged instantaneously to the bottom of the hillslope. This consideration involves some approximation. But, in steep hillslopes the resident time of water in the macropore domain is expected to be very less due to high gradient and piston effect like movement of water through preferential pathways. Figs. 5.8-5.10 depict the hydrographs for macropore flow and Figs. 5.11-5.13 show the matrix flow hydrographs for different types of hillslopes. With increasing intensities of rainfall the contributions of both soil macropores and matrix in subsurface stormflow also increased. In both the cases the peak flow occurred after the cessation of recharge as at this point the saturated depth above the impermeable layer was maximum. However, the magnitude of macropore flow was much higher than the matrix flow rate. The peak discharge through the soil macropores was quite comparable with the peak rate of overland flow. It was also

observed that the bedrock profile curvature did not have significant effect on the macropore flow rate. Macropore flow strongly depended on the number of active connected macropores in soil. Therefore, minor variations in saturated depth owing to different curvatures of bedrock profile were insignificant. However, matrix flow rates were affected by different profile curvatures due to the differences in hydraulic gradient.

An interesting observation can be made from Table 5.8 which enumerates the variations in the build up of saturated profile above the impermeable layer. If the saturated depth becomes more than the depth of soil, saturation excess overland flow will occur. In all the cases it could be observed that the depth of saturated profile were less than the soil depth. Even under the simulated extreme rainfall conditions, saturation excess overland flow was not evident. Therefore, in hillslopes where high macroporosity results in quick vertical as well as lateral transmission of infiltrated water, the process of saturation excess overland flow might not occur in spite of having the saturated soil conditions and high rainfall intensity. However, it is also worth mentioning that saturation excess overland flow was evident for simulations

Table 5.7 Hydraulically effective soil macroporosity for different rainfall intensities

Rainfall Intensity (mm/hr)	f_{avg} (mm/hr)	Number of Hydrulically Effective Macropores per unit Width of Slope in a given Soil Layer (N)
100	92	8
125	107	9
150	123	11
200	153	13
300	213	18

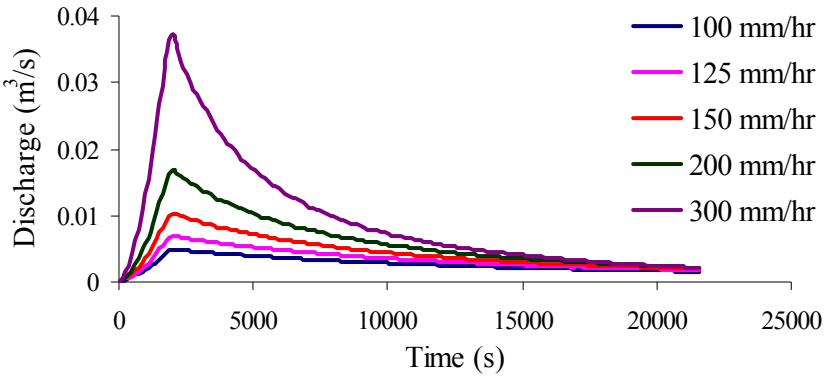

Fig. 5.8 Macropore flow hydrographs for the Type 1 hillslope

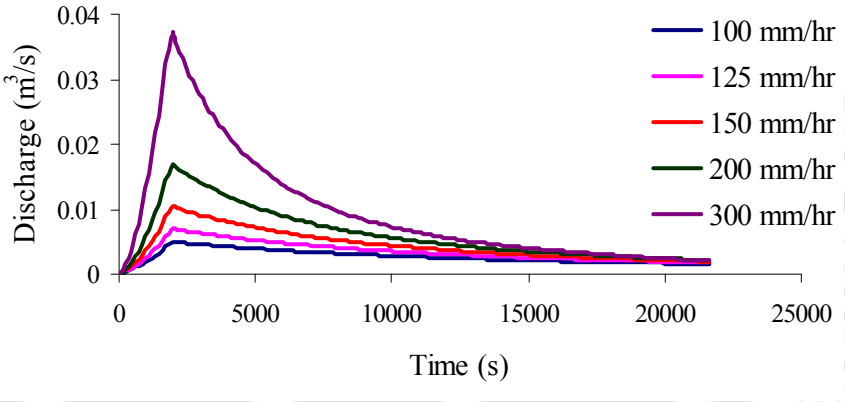

Fig. 5.9 Macropore flow hydrographs for the Type 2 hillslope

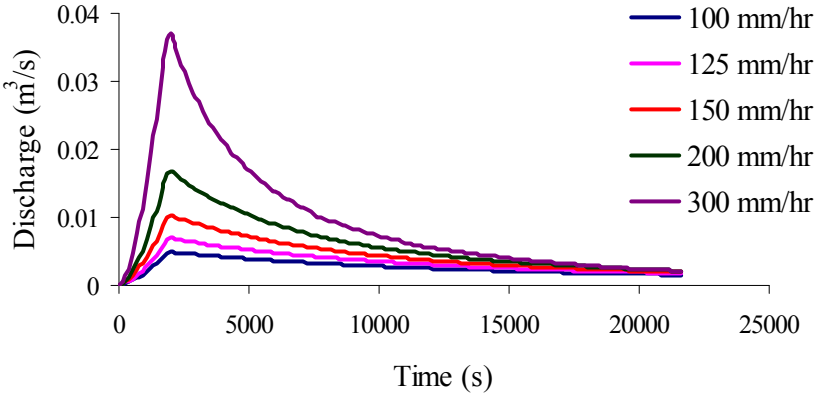

Fig. 5.10 Macropore flow hydrographs for the Type 3 hillslope

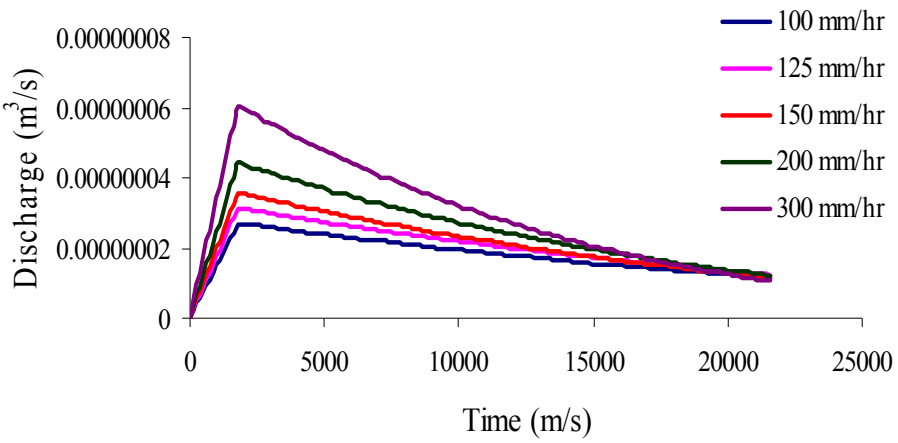

Fig. 5.11 Matrix flow hydrographs for the Type 1 hillslope

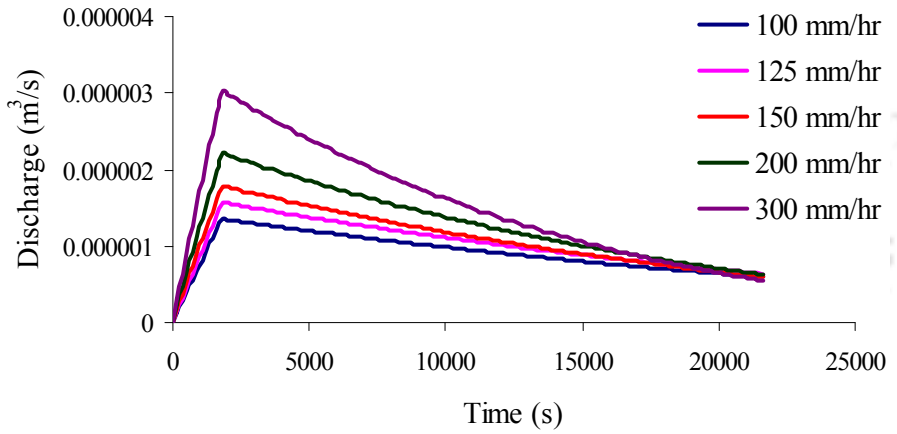

Fig. 5.12 Matrix flow hydrographs for the Type 2 hillslope

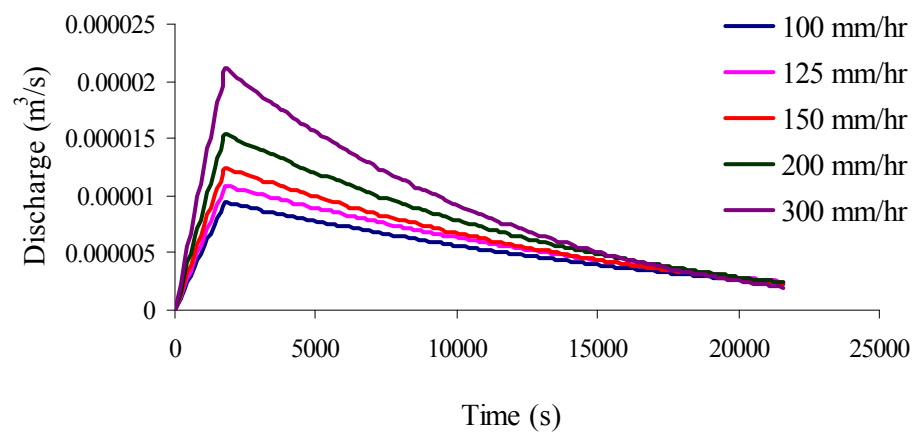

Fig. 5.13 Matrix flow hydrographs for the Type 3 hillslope

with no lateral macroporosity (i.e. $N = 0$) under the influence of prolonged recharge and similar high vertical preferential infiltration rate (Table 5.9). Thus, if the lateral macroporosity of a hillslope is disturbed due to the loss of connectivity, but the vertical macropores are still active to rapidly convey the infiltrated water towards the impermeable layer, saturation excess overland flow might occur.

5.3.1 Effect of relief on subsurface stormflow

To study the effect of relief on subsurface stormflow, the relief of hillslopes along the bedrock profile was changed from 20 m to 15 m. In the present modeling concept as macropore flow is incorporated as a sink term, it is not going to be affected by the variations in relief. However, peak matrix flow rate was found to be decreased with the reduction of relief (Table 5.10).

Table 5.8 Maximum depth of water table above the impermeable bed

Hillslope Type	Rainfall Intensity (mm/hr)	Maximum Depth of Saturated Profile above the Impermeable Bed , h_s, (m)
Type 1	100	0.4182
	125	0.4817
	150	0.5443
	200	0.6609
	300	0.8627
Type 2	100	0.4182
	125	0.4817
	150	0.5443
	200	0.6609
	300	0.8627
Type 3	100	0.4182
	125	0.4817
	150	0.5443
	200	0.6609
	300	0.8627

Table 5.9 Occurrence of saturation excess overland flow with no lateral macropores

Hillslope Type	Rainfall Intensity (mm/hr)	Time at which saturation excess overland flow initiated (hr)		
		Duration of Rainfall (0.75 hr)	Duration of Rainfall (1 hr)	Duration of Rainfall (1.25 hr)
Type 2	100	No flow	No flow	1.15
	125	No flow	1.00	1.00
	150	No flow	0.90	0.90
	200	0.70	0.70	0.70
	300	0.50	0.50	0.50

Table 5.10 Effect of change in relief on matrix flow hydrographs for i = 150 mm/hr

Hillslope Type	H = 20 m	H = 15 m
	$Q_{p(mat)}$ (m^3/s)	$Q_{p(mat)}$ (m^3/s)
Type 1	3.58×10^{-08}	2.67×10^{-08}
Type 2	1.79×10^{-06}	1.34×10^{-06}
Type 3	1.24×10^{-05}	1.00×10^{-05}

5.3.2 Effects of changing lateral macroporosity on subsurface stormflow

The effects of change in macropore diameter (r_{avg}) and number of hydraulically effective macropores per unit width of slope (N) were evaluated. First, keeping the same values of N, the diameters of macropores were doubled. It can be observed from Table 5.11 that doubling the macropore diameter did not change the maximum saturated depth above the impermeable layer (h_s) significantly. Consequently, the increase in macropore flow rate was small. However, keeping

macropore diameter same, if the values of N were increased, the saturated depth changed considerably resulting in higher macropore flow. It is an important observation that macropore diameter is not a critical parameter of the model. In the process of characterization of soil macroporosity, macropore diameter of 1.5 mm was selected for model simulations from the dominating macropore size groups 1-2 mm and 3-4 mm. Here, the selection of 2 mm or 3 mm diameter would not have changed the macropore flow rate significantly. But, the selection of N is much more critical as it can have pronounced effect on macropore flow. For different soil and hydro-geologic conditions the value of N can change for different land use or land cover and management practices as well as for varying rainfall intensities. Therefore, experimental data should be analyzed carefully in order to define the lateral macroporosity of soil under different physical and hydro-geologic conditions of hillslopes.

Table 5.11 Effect of change in soil macroporosity on subsurface flow

Hillslope Type	Rainfall Intensity (mm/h)	r_{avg} = 0.00075 m		r_{avg} = 0.0015 m		r_{avg} = 0.00075 m	
		N_a	h_s (m)	N_a	h_s (m)	N_a	h_s (m)
Type 2	100	8	0.418229	8	0.416035	12	0.409466
	125	9	0.481692	9	0.47858	14	0.468101
	150	11	0.544342	11	0.539856	17	0.524805
	200	13	0.660877	13	0.653944	20	0.630256
	300	18	0.862673	18	0.848814	27	0.804413

5.4 Summary of the Chapter

This chapter outlined a parametric study of the overland flow and subsurface stormflow models for theoretical hillslopes having lateral and vertical macroporosity

similar to the experimental hillslope plot. Some important findings of this chapter can be summarized as follows:

- The plan and profile curvatures of a hillslope facet can be defined by a bivariate quadratic function. With different combinations of plan and profile curvature parameters it is possible to define nine geometric shapes of hillslope topography. To study the effect of topographical shape on the hydrographs generated at the bottom of the slope, three basic hillslope types, all having straight plan curvatures and with concave (Type 1), straight (Type 2), and convex (Type 3) profile curvatures, were considered.
- The length and width of the theoretical hillslopes were taken as 100 m and 22 m, respectively. Assuming a total relief of 20 m, uniform grids (2 m × 2 m) were generated for the three selected types of hillslopes with a datum of 100 m. A constant soil depth of 1 m was taken by assuming the surface profile curvature parallel to the bedrock profile. It was further assumed that the soil macropore structure of the hillslope was identical to that of the experimental hillslope plot and therefore, the relationships derived from the *in situ* experiments on the hillslope plot were valid for the theoretical hillslopes. A dense vegetation condition over the hillslopes was assumed.
- Overland flow hydrographs were simulated for five different rainfall intensities: 100 mm/hr, 125 mm/hr, 150 mm/hr, 200 mm/hr, and 300 mm/hr. Average preferential infiltration rates (f_b) were calculated from the experimentally derived functional relationship for dense vegetation condition of the hillslope plot.
- The overland flow hydrographs for all the three hillslopes had similar shapes. Discharge at the outlet of the slope gradually increased from zero to reach a

maximum value and remained constant till the rainfall continued. This was due to the assumed steady rainfall and constant recharge condition of the plot. Gradual recession of flow occurred after the cessation of rainfall. Higher rainfall intensities produced greater peak with lesser time to peak.

- Comparison of the overland flow hydrographs showed the effects of profile curvature on time to peak (t_p) and time of recession (t_r). Least values of t_p were evident for the Type 2 hillslope. Comparatively higher values of t_p were observed in the Type 1 hillslope, whereas in Type 3 hillslope maximum values of t_p were evident. After cessation of rainfall the surface storage of water at a particular instant primarily controlled the time of recession. Type 3 hillslope had least surface storage due to its convex profile and Type 1 hillslope had maximum storage due to its concave profile. Therefore, t_r values were least for the Type 3 hillslope and it was maximum for the Type 1 hillslope. Type 2 hillslope showed intermediate values of t_r due to its moderate surface storage capacity.
- To study the effect of relief on overland flow hydrographs, keeping the other prameters same the total relief of the three theoretical hillslopes were reduced by 50% and the resulting DEMs were generated. Similar natures of overland flow hydrographs were evident for all three types of hillslopes. However, due to flattening of the slope the values of time to peak and time of recession were increased.
- The effect of soil macroporosity on overland flow was studied by comparing the simulated surface runoff hydrographs from macroporous and non-macroporous hillslope soils. In non-macroporous hillslope soils Green-Ampt equation was used to describe the process of infiltration of water into the

homogeneous soil matrix, which follows the Darcy's principle. Assuming a sandy loam soil, the Green-Ampt infiltration parameters were defined. For non-macroporous hillslope soils the steady peak discharge conditions were not attained quickly due to a very slow rate of soil matrix flow. The magnitude of peak discharge was much higher than that of the preferential infiltration dominated hillslopes. Therefore, non-macroporous soils or hillslopes with disturbed macropore structures produce higher runoff coefficients than undisturbed vegetated hillslopes. It was also observed that in non-macroporous soils the saturated water front never reached the impermeable layer to initiate any water table buildup for lateral subsurface stormflow generation. Whereas, in macroporous soils the vertical macropores rapidly conveyed the infiltrated water towards the impermeable layer, where a temporary water table build up took place to initiate rapid lateral preferential flow through well connected network of lateral soil macropores.

- The subsurface stormflow response of the three theoretical hillslopes was analyzed from the model simulations. For different rainfall intensities the average rate of recharge to the saturated layer was approximated as $f_{avg} \approx f_b$ and based on recharge the number of hydraulically effective macropores per unit width of the slope in each soil layer was defined assuming that the theoretical hillslopes had similar macroporosity as that of the experimental hillslope plot. The macropores were assumed to have infinite conductance and thus the resident time of water in the macropore domain was negligible.
- The matrix and macropore flow hydrographs showed that with increasing rainfall intensities the contributions of both matrix and macropore flows in subsurface stormflow increased. The peak of both the hydrographs occurred

immediately after the cessation of recharge. The macropore flow rates were much higher than soil matrix flow rates. Macropore flow rates were comparable with the overland flow rates from the hillslopes.

- The macropore flow rates were not affected significantly by the bedrock profile curvatures. But, the soil matrix flow rates were influenced by profile curvatures due to changes in hydraulic gradient. In highly macroporous hillslopes even under extreme recharge conditions saturation excess overland flow was not evident due to rapid vertical and lateral transmission of infiltrated water. Saturation excess overland flow occurred only under the conditions of prolonged recharge with very high rates of vertical water movement with no active lateral macroporosity of soils. Therefore, hillslopes with disturbed lateral macroporosity might generate saturation excess overland flow. Soil macropore flow was unaffected by the change of hillslope relief, but the matrix flow rates were found to be decreased due to reduction in relief.
- Doubling the macropore diameter did not affect the saturated depth of water above the impermeable layer and the macropore flow rates significantly. However, keeping the diameter same any change in the number of hydraulically active macropores showed considerable influence on macropore flow rates. Therefore, compared to macropore diameter the number of connected soil macropores was a more sensitive parameter of the subsurface stormflow model.

CHAPTER 6 SUMMARY AND CONCLUSIONS

6.1 Summary

The present research work was undertaken in the Brahmaputra river basin of India to understand and conceptualize the hydrological response of a typical hillslope plot having extremely high degree of active soil macroporosity. On the hillslope plot more than 50 experiments were conducted over the years with artificial runoff events as well as by monitoring natural storm events. With the help of detailed instrumentation in the plot the surface and subsurface hydrological behaviors of the hillslope were captured. The analysis of the detailed experimental data led to some understanding of the critical hydrological processes prevailing in the hillslope. In fact, the experimental results showed some extreme flow conditions which are very rare and therefore, are not frequently reported in literature. The experimental understandings were extended to develop physical based numerical models to conceptualize the surface and subsurface flow processes of the hillslope plot. The field experimental data were used in semi-distributed hydrological models to characterize overland flow and subsurface stormflow.

The hillslope plot (18 m × 6 m) selected for the study had undisturbed natural vegetation consisting of close growing grasses and shrubs. The vegetation showed seasonal dynamics with sparse, moderate, and dense conditions. A detailed topographic survey was conducted on the hillslope with a uniform grid of 0.25 m, by a total station of (±5 mm +2 ppm) accuracy to generate the Digital Elevation Model (DEM) of the hillslope plot. The average slope in the main sloping direction was 20 percent. The analysis of soil samples collected from the hillslope plot revealed a two layer soil formation with a coarse soil layer overlaying a fine textured soil layer. An

impermeable layer was found at about 1 m depth below the ground level. The average saturated hydraulic conductivity of the soil matrix was 50 mm/hr. Considering the rainfall patterns and physical conditions of the hillslopes of northeast India, a sheet flow generation system was designed for the hillslope plot to capture the overland flow and subsurface stormflow characteristics. Using the sheet flow generation system steady overland flow conditions could be generated with varying storm durations (15 -120 minutes) and wide range of inflow intensities (50-406 mm/hr). The plot was instrumented with profile probe soil moisture meter and 25 piezometers installed along five transects of the plot to keep track of subsurface moisture conditions and temporary water table buildup and recession above the impermeable layer. The depth of the piezometers was extended up to the impermeable layer (1 m) from the ground surface. Measurements of water table in all the piezometers and profile probe locations were taken before, during, and after the runoff experiments.

Double ring infiltrometer tests conducted at different locations of the hillslope plot showed significant effect of scale on infiltration. The irregular patterns of infiltration in dry soils indicated the presence of highly active macropores in the hillslope soil. Under wet soil conditions, a near steady infiltration condition could be attained. The point infiltration data of the plot, measured under wet antecedent conditions, were used to define a linear function to represent the spatial variation of infiltration along the length of the hillslope plot. Plot scale runoff experiments conducted with the sheet flow generation system provided a spatially averaged steady preferential infiltration rate for the hillslope plot. The runoff plot experimental data also indicated that under initially wet soil conditions a steady infiltration condition could be attained over the hillslope plot after some time.

To characterize macroporosity of the hillslope soil, undisturbed soil columns were collected from the plot. Dye tracing experiments were conducted in the laboratory with the soil columns. Subsequent digital image processing techniques were used to derive quantitative information about total number of macropores, depth distribution of macropores, maximum and minimum size of macropores, and volume density in terms of stained path width with depth as an explanatory variable. The presence of high macroporosity throughout the soil profile was clearly evident. The 1-4 mm diameter macropores were found to be dominating. More precisely, the 1-2 mm diameter macropores, mostly developed by the plant roots, dominated the soil profile.

Using the profile probe soil moisture sensor, spatial and temporal variations in soil moisture distribution in the hillslope plot were monitored. It was found that during and after the runoff events, soil moisture contents at different depths remained fairly constant. The constant moisture profile of the hillslope soil indicated the attainment of steady infiltration/recharge condition over the plot. It was also observed that once wetted, the topsoil remained at field capacity for the next 2-3 days. Thus, from early monsoon storms the hillslope soil becomes saturated and then remains at field capacity for a prolonged period. This creates a favorable condition for triggering subsurface stormflow under subsequent storm events. Soil moisture content readings in the lower soil layer also showed rapid buildup and recession of saturated zone above the impermeable bed to indicate the occurrence of subsurface stormflow from the hillslope.

On the hillslope plot 34 artificial runoff experiments were conducted in three different seasons to study the effect of natural vegetation (sparse, moderate, and dense) on overland flow behavior. Under wet antecedent moisture conditions, the outflow hydrographs measured at the downstream end of the slope attained a constant

discharge within a very short time. This represented a steady infiltration condition of the plot. The steady preferential infiltration rate (f_b), was found to be dependent on inflow intensity (i) and degree of vegetation. The values of f_b were computed from the *in situ* field experiments knowing the inflow and outflow hydrographs. All the experimental studies revealed that the preferential infiltration rate (50-250 mm/hr) was much higher than the average saturated hydraulic conductivity of the soil matrix (50 mm/hr). As the macroporosity of the hillslope soil was mainly due to the growth of plant roots, vegetation density was found to be closely related to preferential infiltration rate. Dense vegetation on the hillslope allowed higher preferential infiltration due to active macropore network developed by the plant roots. The functional relationships between i and f_b for the plot were experimentally established for the three vegetation conditions. Time of concentration (t_c) of the plot was also expressed as a function of inflow intensity. These experimentally developed functional relationships are valid for wet antecedent soil moisture conditions and high intensity storm events occurring for a prolonged period.

The overland flow response of the hillslope under natural sotrm events were also monitored using an automatic rainfall recorder and a digital water level recorder. The measurements were stored in a data logger with an observation time interval of 5 minutes. The three year (2008-2010) rainfall-runoff data for the plot were analyzed. The observations revealed that the overland flow generation from the hillslope plot was a threshold dependent process. A favorable combination of rainfall depth, storm duration, maximum intensity, and 7 days Antecedent Precipitation Index (API) primarily controlled the runoff generation process from the hillslope. The relationship between inflow intensity (i) and preferential infiltration rate (f_b), which was developed from the artificial runoff experiments, was also evaluated for the runoff generating

natural storm events. It was found that the relationship could capture the observed peak of the hydrographs and total runoff volume reasonably well.

The piezometer readings taken during and after the artificial runoff experiments were analyzed to study the process of water table buildup and recession above the impermeable layer. The water table depths measured in the piezometers installed along the two sides of the plot were negligible. The subsurface water movement was predominantly along the major surface gradient of the plot. Very rapid fluctuation of water table during buildup and recession was evident. The hillslope soil matrix with a very slow hydraulic conductivity (50 mm/hr) was not capable of producing such sharp fluctuations of saturate profile. These evidences clearly indicated the presence of highly active lateral preferential pathways in the hillslope soil which generated rapid lateral subsurface stormflow from the plot.

The physical understandings of the surface and subsurface flow processes of the hillslope plot evident from the *in situ* experimental results were extended to develop conceptual models for overland flow and subsurface stormflow. The functional relationships derived form the field experiments were used to calibrate the model parameters. The basic input data for the models were also measured from the *in situ* experiments.

The process of overland flow was defined by approximation of the St. Venant equations of continuity and momentum. One-dimensional shallow water overland flow equations with diffusive wave approximation were solved using a finite volume technique. The two-dimensional flow domain was divided into number of computational cells. Based on elevation and flow depth, one dimensional flow network was established. The model was used to compute flow depth and friction slope at each computational cell and the overland flow hydrograph at the downstream

end of the slope. The main input parameters of the model were inflow intensity, preferential infiltration rate, and equivalent depth at the upstream boundary computational cells. The first two parameters were measured from field experiments and the equivalent depth was computed from the known inflow intensity applying the Manning's equation. The model was simulated with an assumed value of Manning's roughness coefficient (n) and the resulting outflow hydrograph was compared with the measured outflow hydrograph. Using a hit and trial method the value of n was varied till a best matching between the observed and simulated hydrographs were obtained. The estimated n represented a lumped surface resistance to flow due to soil roughness, vegetation, and microtopography. The Manning's n was was found to be a depth dependent parameter. The variation of n with inflow intensity clearly showed that Manning's roughness coefficient has a power relation with inflow intensity. Manning's n was also dependent on vegetation density. Higher vegetation density yielded higher values of n. For shallow overland flow on hillslopes the surface roughness was mainly characterized by degree of vegetation. The analysis of the simulated overland flow depths at various computational time steps showed that the average overland flow depth varied in the range of 3-10 mm with maximum coefficient of variation of 200 percent. Over 80 percent area of the plot the flow depth was less than 5 mm.

Subsurface stormflow from the hillslope plot was modeled using the basic concept introduced by Fan and Bras (1998). The model considered actual saturated hydraulic conductivity of soil for matrix flow and a new sink term to account for rapid macropore flow. A number of assumptions were taken to simplify the rather complex soil macropore structures. In the model, the hydraulically effective connected lateral macropores were defined as small diameter straight pipes of uniform diameter. These

macropores were assumed to be distributed evenly in different soil layers. If these macropores are present below the saturated soil, water seeps into these pores and macropore flow initiates. The water flowing through the macropore domain was assumed to be discharged to the bottom of the slope at a very high velocity without any interaction with the surrounding saturated soil matrix. The actively flowing connected macropores present below the saturated soil were termed as 'hydrologically active macropores'.

The uniform hillslope plot used for the *in situ* field experiments was considered for the modeling of subsurface stormflow. The three-dimensional hillslope soil mantle was converted to a two-dimensional soil profile consisting of its drainable pore spaces. The bedrock slope along the centroid profile was approximated from the surface topography assuming a uniform soil depth of 1 m. A kinematic form of Darcy's equation was combined with the continuity equation for hillslope subsurface flow considering both soil matrix and macropore flow. The resulting quasi-linear wave equation was solved using a finite difference method considering the Warming-Beam upwind scheme. The physical based numerical solution of the subsurface flow equations was used to capture the rapid buildup and recession of the water table observed from the runoff experiments. The model was used (1) to capture the rapid subsurface stormflow evident in the hillslope, (2) to reflect the contributions of soil matrix and macropores in prompt interflow occurring immediately after the high intensity runoff events, and (3) to provide a surrogate indicator of hydraulically effective lateral macroporosity of the hillslope. Apart from these, the dependency of effective lateral macroporosity, matrix, and macropore flow rates under varying recharge conditions were also analyzed.

Additional fifteen runoff experiments were conducted in the hillslope plot with varying intensities and durations to study the subsurface stormflow behavior. The average rate of recharge was computed from these experiments. Due to high preferential infiltration during the runoff events a temporary water table was formed over the impermeable layer. The piezometer readings were used to capture the water table fluctuations. The average saturated depths at five points along the centroid of the plot were approximated from the piezometer readings along the five transects.

To calibrate the model for the hillslope plot, simulations were run with different macropore structures defined by number of soil layers (m), number of hydraulically active connected macropores per unit width of the slope in each layer (N), and average radius of macropores (r_{avg}). The model computed subsurface water storage within the hillslope soil and the saturated depths above the impermeable layer at different time steps. For a particular experiment the observed and model simulated water table profiles were compared for different macropore structures. A statistical parameter called Performance Index (PI) was used to ensure good comparison between the observed and simulated data. The macropore structure, which produced PI values less than 0.1 for all the computational time steps, was considered to be the most suitable one to describe the macroporosity of the hillslope soil.

The model simulations showed that the water table buildup in the hillslope was mainly controlled by the rate of recharge. However, the recession phase was critically controlled by the soil macropore structure. The distribution of macropores in different soil layers did not have significant effect on subsurface stormflow. The density of macropores in soil had prominent effect on the recession pattern of water table. At any given instant, the number of actively flowing macropores present below the saturated soil primarily controlled the spatial and temporal variations of water

table. Higher density of macropores below the saturated zone resulted in faster recession of water table. Change in macropore diameter did not have significant effect on subsurface stormflow. Therefore, macropore density was clearly a more critical parameter than macropore diameter.

All the simulated experiments showed the common trend of increasing the number of hydraulically effective and hydrologically active macropores in soil with increasing rate of recharge. This can be attributed to the threshold behavior of preferential flow generation. Water can flow into a macropore if its water entry pressure is exceeded. Therefore, with lower rates of recharge some of the macropores present in soil might not get sufficient connectivity to become hydraulically effective. But, under higher recharge rates the connectivity between those inactive macropores was established to make them hydraulically effective and potentially active for rapid preferential flow generation. Therefore, the experiments showed a good correlation between average rate of recharge (f_{avg}) and maximum number of hydrologically active macropores (N_{max}).

The simulated hydrographs of soil matrix flow and macropore flow were compared. The peak of the hydrographs occurred immediately after the cessation of recharge. The matrix flow was almost negligible compared to the amount and rate of lateral preferential flow from the experimental hillslope plot. Lateral preferential flow contributed major part of prompt interflow occurring immediately after the storm events. The subsurface flow behavior evident in the hillslope under investigation was a specific case of extreme degree of active soil macroporosity. Therefore, the results should not be generalized for all conditions of lateral preferential flow generation. Under certain circumstances soil matrix flow may dominate over preferential flow. It was also found that with the increasing rate of recharge, contribution of macropore

flow increased as a polynomial function. Computed subsurface flow hydrographs showed that the peak rate of macropore flow has a good linear correlation with recharge.

To study the effect of topographical shape on the runoff hydrographs, three basic hillslope types (Type 1, Type 2, and Type 3) were considered. The length of the theoretical hillslope plot (L) was taken as 100 m with a uniform width (w) of 22 m. Total relief between the upslope and downslope points (H) was 20 m. Uniform grids (2 m × 2 m) were generated for the three types of hillslopes. A constant soil depth of 1 m was taken by assuming that the surface profile curvature of the terrain was parallel to the bedrock profile. It was further assumed that the hydrological behavior of macropores in the theoretical hillslopes was identical to that of the experimental plot and therefore, the relationships derived from the *in situ* experiments were also valid for the theoretical hillslopes.

Overland flow hydrographs were simulated for five different rainfall intensities: 100 mm/h, 125 mm/h, 150 mm/h, 200 mm/h, and 300 mm/h. For all these intensities average preferential infiltration rate (f_b) was calculated from the functional relationship for dense vegetation condition, which was derived from the hillslope plot experiments. The infiltrated water was assumed to be rapidly conveyed through the vertical macropores of soil to recharge the saturated zone (i.e. $f_b \approx f_{avg}$), which gradually builds up above the impermeable layer. In all the simulations the duration of the storm events was taken as 30 minutes. Comparison of the resulting overland flow hydrographs revealed the following facts:

- For all the hilslopes, with increasing rainfall intensity, peak rate of discharge (Q_p) increased and time to peak (t_p) decreased.

- Different profile curvatures showed significant effect on t_p and time of recession (t_r). Least values of t_p were obtained for the Type 2 hillslope. Comparatively higher values of t_p were evident in Type 1 hillslope and Type 3 hillslope showed maximum values of t_p.
- The time of recession was mainly controlled by the storage property of the hillslope profile curvatures. The values of t_r were least for Type 3 hillslope and it was maximum for Type 1 hillslope. Type 2 hillslope exhibited intermediate values of t_r due to its moderate surface storage capacity.
- To study the effect of relief on overland flow hydrographs, keeping the other conditions same the reliefs of the three hillslopes were reduced from 20 m to 10 m. Though all three types of hillslopes showed similar steady peak outflow conditions, but the values of t_p and t_r were increased due to flattening of the slope.
- To study the effect of macroporosity on overland flow hydrographs, the overland flow model was simulated for the hillslopes without any preferential pathways. In non-macroporous hillslopes the process of infiltration into the soil matrix, which is governed by the Darcy's law, was approximated by the Green-Ampt equation. The magnitude of peak overland flow discharge was found to be much higher than that of the preferential infiltration dominated hillslopes. Therefore, if the macroporosity of a natural hillslope soil is disturbed, the overland flow rate should increase considerably. Most significantly, from the maximum depth of saturated water front propagation in soil it was evident that in no case the water front reached up to the impermeable layer to start the water table buildup for the initiation of subsurface stormflow from the hillslope.

The subsurface stormflow model was used to study the response of different hillslope types under varying rainfall intensities. Knowing the values of f_{avg}, the number of hydraulically effective macropores per unit width (N) that might be present in different soil layers was defined. The simulated subsurface flow hydrographs lead to the following observations:

- With increasing intensities of rainfall the contributions to subsurface stormflow through soil macropores and matrix increased. In both the cases the peak flow occurred after the cessation of recharge as at this point the saturated depth above the impermeable layer was maximum. The magnitude of macropore flow was much higher than the matrix flow rate. Under high intensity storm events the peak rate of discharge through the soil macropores was quite comparable with that of the overland flow rate.
- In all the cases it was observed that the depths of saturated profile above the impermeable layer were less than the soil depth. Even under the simulated extreme rainfall conditions, saturation excess overland flow was not evident. Therefore, in hillslopes where high macroporosity results in quick vertical as well as lateral transmission of infiltrated water, the process of saturation excess overland flow might not occur in spite of having high intensity rainfall under saturated soil conditions.
- The change in macropore diameter did not have significant effect on macropore flow rate. But keeping macropore diameter same if the values of N were increased, the saturated depth changed considerably resulting in higher macropore flow. For different soil and hydro-geologic conditions the value of N can change for different land use, land cover, and management practices as well as under different rainfall intensities. Saturation excess overland flow was

found to occur when the process of vertical preferential infiltration remained unaffected, but the connectivity of the lateral macropores was lost (i.e. $N \approx 0$). Thus, in case of high vertical macroporosity and comparatively less active lateral preferential flow, saturation excess overland flow may occur. Therefore, the parameter N was found to be very critical and it should be defined in the model with careful analysis and interpretation of experimental data on soil macroporosity.

6.2 Major Conclusions

The following major conclusions were drawn from the present investigation:

- The dye infiltration tests revealed that the hillslope had very high degree of macroporosity in the soil profile. In the vegetated hillslope plot, soil macropores of 1-2 mm diameter, developed mainly by the plant roots were dominating.
- Due to the presence of high macroporosity in the soil, point measurements of infiltration showed wide spatial variations within the hillslope plot. Steady infiltration condition could only be attained after a long time. The plot scale measurements of infiltration using a sheet flow generation system could capture the steady infiltration behavior of the plot within a relatively shorter time. This can be attributed to the effect of scale on infiltration in a macroporous hillslope soil.
- The spatio-temporal variations of soil moisture profile in the hillslope plot showed that after being wetted the moisture content in the topsoil (up to 40 cm depth) remained fairly constant for a prolonged duration.
- The artificial runoff experiments conducted on the hillslope plot under wet antecedent conditions showed steadiness in outflow rates and topsoil moisture

contents. These observations indicated the attainment of steady preferential infiltration conditions over the macropore dominated hillslope plot.

- Artificial runoff experiments conducted on the hillslope plot showed that at the hillslope scale, the relationships between inflow intensity and preferential infiltration rate was almost linear. However, the relationships varied for different degrees of vegetation.
- Observation of overland flow response under natural storm events revealed that overland flow generation from the hillslope plot was a threshold dependent process. Runoff generation process was primarily controlled by total event rainfall, maximum rainfall intensity, storm duration, and 7 days API. The evaluation of the experimentally established relationship between preferential infiltration rate and rainfall intensity for the hillslope plot showed reasonable agreement with the infiltration behavior under natural storm events.
- The measurement of water table depths in the piezometers installed at the hillslope plot showed rapid buildup and recession of water table over the impermeable layer. The subsurface water flux dominated along the major surface gradient of the plot with insignificant lateral flux component.
- The simulation of overland flow model for the hillslope plot showed that the average flow depth varied in the range of 3-10 mm and over 80% area of the plot the flow depth was less than 5 mm. The spatial variations in overland flow depth were mainly due to the micro-topographic variations.
- The Manning's roughness coefficients estimated from the model simulations showed a power relation with inflow intensity. Manning's *n* also varied with degree of vegetation. In a preferential infiltration dominated hillslope, for

shallow overland flow depths, variation of surface roughness was mainly characterized by the degree of vegetation.

- The subsurface stormflow model was simulated to optimize the active soil macropore structures of the hillslope plot under different rates of recharge.
- It was found that the rapid buildup and recession behavior of the water table was primarily controlled by the active lateral preferential flow pathways.
- The hydraulically effective or hydrologically active lateral macroporosity and peak rates of matrix and macropore flow were found to be controlled primarily by the rate of recharge. Maximum number of hydrologically active macropores had a logarithmic functional relationship with the rate of recharge.
- In the experimental hillslope plot the contribution of macropore flow in total subsurface stormflow was significantly high.
- Effects of different topographical shapes and bedrock profiles on surface and subsurface flow hydrographs were significant.
- In non-macroporous soils subsurface stormflow is expected to be very slow and in case of medium and low permeability soils it may not occur at all.
- Even under wet antecedent conditions hillslope soils having very high lateral macroporosity, may not produce any saturation excess overland flow under high intensity storm events.
- The impact of change in lateral macroporosity owing to different land use and management practices may be significant. It was found that if the connectivity of the lateral macropores is disturbed, saturation excess overland flow might be evident, if the vertical soil macropores remain active under extreme storm events.

- The present investigation provides an insight to the dominating hydrological processes, their interdependence, and their extremities in a hillslope through *in situ* experiments and physical based hydrological modeling approach.

6.3 Scopes for Future Research

The present investigation outlined an experimental and physically based semi-distributed hydrological modeling approach for evaluating the hydrological response of a macropore dominated natural hillslope. Some approximations and assumptions taken in this study simplified the complexity of the problem. Even with such simplifications the results obtained from this study were encouraging. In Brahmaputra river basin, where the hillslopes are characterized by high degree of soil macroporosity and the area receives extreme rainfall events frequently during the monsoon season, rapid lateral preferential flow is the major source of storm runoff. Therefore, flash floods in rivers are a common problem encountered in the Brahmaputra river basin. Till date very few experimental data are available to investigate such critical hydrological events of the region at the process level. Especially, the remote areas of northeast India are still not well developed from the socio-economic point of view. The process of acquiring data from these regions by installing state of art instruments still remains as a great challenge to the hydrologists and researchers working in the area. In such situations, the simplified experimental techniques illustrated in this study should be useful for collecting hydrological information, identification of the critical hydrological processes, and their modeling. Obviously, the research work presented in this thesis is not exhaustive. An effort has been made to identify and bring out the critical hydrological processes, prevailing in the vast hillslopes of northeast India, in front of the scientific community. Several hydrological issues of the region are still left to be addressed. There are vast scopes

for future work in the present field of research, which will improve and enhance our understanding and conceptualization of this complex hydrological problem. Some specific aspects that can be targeted for future research are:

- Similar plot scale field experiments conducted in different hillslopes of the region should give better insight to the extremities of the hydrological processes. The present study can be used to compare the results obtained from other locations and thus the extent of validity of the present experimental relationships can be further established with more confidence.
- Incorporating the component of vertical macropore flow the overland flow and subsurface stormflow model can be coupled.
- In macropore domain flow routing concept can be improved by considering the effects of curvature, flow regime, and different flow geometries.
- Better instrumentation can be used to have more accurate quantitative data on soil macropore structures, macropore flow velocity, subsurface geological formations etc. These should provide a more clear understanding of the macropore flow processes.
- Finally, the simplifying assumptions taken in the model development can be improved by incorporating more realistic physical definition of the complex flow processes. Efforts are also to be made to extend the modeling concept from plot scale to watershed scale.

APPENDIX 1

Table A-1 Observed and predicted values of water table depth above impermeable layer for different experiments conducted on the hillslope plot

Experiment No.	Time (hr)	Distance from Downstream End (m)	Water Table Depth (m)		Performance Index (PI)
			Observed	Predicted	
E-1	0.21	3	0.1069	0.0679	
		6	0.1085	0.1195	
		9	0.2153	0.1695	0.0696
		12	0.2369	0.2193	
		15	0.2575	0.2676	
	0.55	3	0.1825	0.1622	
		6	0.2721	0.2711	
		9	0.4036	0.3684	0.0301
		12	0.4710	0.4603	
		15	0.5830	0.5436	
	0.97	3	0.2150	0.2291	
		6	0.4358	0.3590	
		9	0.5047	0.4670	0.0370
		12	0.5609	0.5617	
		15	0.6589	0.6452	
	1.30	3	0.2850	0.2596	
		6	0.5037	0.3926	
		9	0.5458	0.4985	0.0481
		12	0.5868	0.5887	
		15	0.6915	0.6677	
	1.63	3	0.3093	0.2588	
		6	0.4176	0.3770	
		9	0.4498	0.4669	0.0335
		12	0.5813	0.5422	
		15	0.5928	0.6065	
	1.88	3	0.2039	0.1978	
		6	0.3143	0.2713	
		9	0.3354	0.3216	0.0339
		12	0.3617	0.3617	
		15	0.4251	0.3932	

Table A-1 continued…

	2.13	3	0.1311	0.1558	
		6	0.2039	0.2051	
		9	0.2304	0.2375	0.0374
		12	0.2706	0.2621	
		15	0.3141	0.2807	
	2.46	3	0.0875	0.1192	
		6	0.1481	0.1538	
		9	0.1875	0.1747	0.0507
		12	0.1727	0.1898	
		15	0.1908	0.2006	
E-2	0.25	3	0.0083	0.0377	
		6	0.0703	0.0664	
		9	0.1048	0.0951	0.0806
		12	0.1381	0.1236	
		15	0.1718	0.1518	
	0.46	3	0.0810	0.0661	
		6	0.1461	0.1163	
		9	0.1520	0.1651	0.0572
		12	0.2370	0.2136	
		15	0.2903	0.2610	
	0.66	3	0.1237	0.0931	
		6	0.1683	0.1618	
		9	0.2358	0.2284	0.0360
		12	0.3157	0.2930	
		15	0.3394	0.3556	
	0.91	3	0.1304	0.1242	
		6	0.2359	0.2129	
		9	0.3164	0.2963	0.0286
		12	0.4037	0.3760	
		15	0.4393	0.4519	
	1.25	3	0.1401	0.1387	
		6	0.2561	0.2318	
		9	0.3151	0.3153	0.0237
		12	0.4036	0.3923	
		15	0.4370	0.4622	

Table A-1 continued...

	1.50	3	0.1391	0.1271	
		6	0.2173	0.2084	
		9	0.2705	0.2785	0.0181
		12	0.3550	0.3402	
		15	0.4061	0.3947	
	1.75	3	0.1097	0.1169	
		6	0.2133	0.1890	
		9	0.2675	0.2475	0.0290
		12	0.2845	0.2985	
		15	0.3407	0.3419	
	2.00	3	0.0833	0.1079	
		6	0.1561	0.1718	
		9	0.2425	0.2214	0.0367
		12	0.2540	0.2646	
		15	0.2951	0.2997	
E-3	0.16	3	0.0602	0.0713	
		6	0.1050	0.1251	
		9	0.1713	0.1776	0.0499
		12	0.2433	0.2292	
		15	0.3150	0.2800	
	0.33	3	0.1204	0.1496	
		6	0.2340	0.2529	
		9	0.3788	0.3480	0.0429
		12	0.4520	0.4366	
		15	0.5770	0.5194	
	0.58	3	0.2371	0.2176	
		6	0.3408	0.3474	
		9	0.5200	0.4581	0.0326
		12	0.5609	0.5555	
		15	0.6818	0.6425	
	0.80	3	0.2606	0.2260	
		6	0.3706	0.3442	
		9	0.4708	0.4380	0.0292
		12	0.5057	0.5164	
		15	0.6174	0.5839	

Table A-1 continued…

	0.91	3	0.2038	0.1967	
		6	0.2900	0.2892	
		9	0.3775	0.3582	0.0250
		12	0.4523	0.4131	
		15	0.4652	0.4588	
	1.25	3	0.1158	0.1274	
		6	0.1718	0.1748	
		9	0.2037	0.2044	0.0174
		12	0.2283	0.2265	
		15	0.2323	0.2436	
	1.41	3	0.1047	0.1078	
		6	0.1206	0.1449	
		9	0.1600	0.1683	0.0397
		12	0.2017	0.1847	
		15	0.1950	0.1966	
E-4	0.16	3	0.0050	0.0207	
		6	0.0389	0.0364	
		9	0.0491	0.0521	0.0815
		12	0.0602	0.0679	
		15	0.0926	0.0836	
	0.30	3	0.0591	0.0407	
		6	0.0875	0.0716	
		9	0.1258	0.1026	0.0595
		12	0.1323	0.1332	
		15	0.1700	0.1636	
	0.50	3	0.0853	0.0664	
		6	0.1290	0.1167	
		9	0.1584	0.1658	0.0459
		12	0.2422	0.2145	
		15	0.2468	0.2622	
	0.75	3	0.1258	0.0970	
		6	0.1740	0.1683	
		9	0.2453	0.2375	0.0362
		12	0.3353	0.3047	
		15	0.3575	0.3698	

Table A-1 continued…

	0.91	3	0.1330	0.1073	
		6	0.2044	0.1846	
		9	0.2496	0.2583	0.0372
		12	0.3262	0.3294	
		15	0.3640	0.3975	
	1.08	3	0.0975	0.1021	
		6	0.1850	0.1733	
		9	0.2396	0.2393	0.0381
		12	0.3453	0.3021	
		15	0.3495	0.3608	
	1.50	3	0.0800	0.0930	
		6	0.1294	0.1532	
		9	0.1904	0.2073	0.0558
		12	0.3028	0.2575	
		15	0.3130	0.3016	
	1.83	3	0.0700	0.0857	
		6	0.1080	0.1379	
		9	0.1856	0.1850	0.0436
		12	0.2197	0.2258	
		15	0.2500	0.2619	
E-5	0.16	3	0.0150	0.0259	
		6	0.0550	0.0456	
		9	0.0690	0.0653	0.0809
		12	0.1050	0.0851	
		15	0.1209	0.1049	
	0.33	3	0.0607	0.0583	
		6	0.1125	0.1029	
		9	0.1305	0.1464	0.0604
		12	0.2317	0.1892	
		15	0.2358	0.2317	
	0.50	3	0.1022	0.0812	
		6	0.1326	0.1419	
		9	0.2426	0.2008	0.0463
		12	0.2618	0.2577	
		15	0.3251	0.3135	

Table A-1 continued...

	0.66	3	0.1240	0.1029	
		6	0.1416	0.1774	
		9	0.2431	0.2488	0.0434
		12	0.3495	0.3173	
		15	0.3958	0.3828	
	0.91	3	0.1513	0.1174	
		6	0.2049	0.1989	
		9	0.2682	0.2724	0.0398
		12	0.3845	0.3409	
		15	0.4151	0.4048	
	1.25	3	0.0600	0.1014	
		6	0.1698	0.1664	
		9	0.1838	0.2202	0.0630
		12	0.2843	0.2692	
		15	0.3433	0.3114	
	1.66	3	0.0550	0.0873	
		6	0.1245	0.1369	
		9	0.1568	0.1780	0.0518
		12	0.2152	0.2119	
		15	0.2378	0.2409	
E-6	0.21	3	0.0463	0.0411	
		6	0.0650	0.0724	
		9	0.1023	0.1037	0.0247
		12	0.1280	0.1346	
		15	0.1600	0.1652	
	0.55	3	0.1043	0.1047	
		6	0.1400	0.1801	
		9	0.2418	0.2522	0.0383
		12	0.3046	0.3215	
		15	0.3953	0.3873	
	0.96	3	0.1867	0.1607	
		6	0.2800	0.2671	
		9	0.3513	0.3620	0.0254
		12	0.4767	0.4486	
		15	0.5093	0.5279	

Table A-1 continued…

	1.30	3	0.2038	0.1971	
		6	0.3144	0.3161	
		9	0.4513	0.4169	0.0239
		12	0.5417	0.5062	
		15	0.5915	0.5850	
	1.63	3	0.2340	0.2227	
		6	0.3451	0.3452	
		9	0.4782	0.4462	0.0236
		12	0.5733	0.5341	
		15	0.6028	0.6119	
	1.88	3	0.2033	0.1881	
		6	0.2647	0.2786	
		9	0.3490	0.3474	0.0226
		12	0.4356	0.4041	
		15	0.4600	0.4516	
	2.30	3	0.1230	0.1464	
		6	0.2055	0.2065	
		9	0.2308	0.2487	0.0313
		12	0.2740	0.2815	
		15	0.3265	0.3068	
	2.46	3	0.1090	0.1338	
		6	0.1718	0.1872	
		9	0.2375	0.2223	0.0349
		12	0.2667	0.2500	
		15	0.2708	0.2714	
	2.88	3	0.0623	0.1043	
		6	0.1466	0.1413	
		9	0.1625	0.1652	0.0573
		12	0.1817	0.1827	
		15	0.2049	0.1953	
E-7	0.18	3	0.0550	0.0709	
		6	0.1335	0.1247	
		9	0.1706	0.1766	0.0382
		12	0.2377	0.2278	
		15	0.3046	0.2777	

Table A-1 continued…

0.35	3	0.1032	0.1169	
	6	0.2415	0.1998	
	9	0.2988	0.2777	0.0464
	12	0.3850	0.3518	
	15	0.4580	0.4222	
0.56	3	0.1352	0.1644	
	6	0.2714	0.2723	
	9	0.4051	0.3681	0.0273
	12	0.4506	0.4549	
	15	0.5490	0.5343	
0.85	3	0.2370	0.2141	
	6	0.3469	0.3352	
	9	0.5069	0.4363	0.0393
	12	0.5707	0.5244	
	15	0.5935	0.6026	
1.10	3	0.2457	0.2187	
	6	0.3685	0.3278	
	9	0.4256	0.4139	0.0256
	12	0.5037	0.4865	
	15	0.5585	0.5493	
1.35	3	0.1448	0.1629	
	6	0.2246	0.2282	
	9	0.2500	0.2751	0.0339
	12	0.3057	0.3107	
	15	0.3706	0.3401	
1.68	3	0.1036	0.1123	
	6	0.1426	0.1509	
	9	0.1975	0.1756	0.0395
	12	0.2154	0.1932	
	15	0.2155	0.2066	
2.18	3	0.0733	0.0722	
	6	0.0888	0.0923	
	9	0.1086	0.1036	0.0225
	12	0.1133	0.1121	
	15	0.1280	0.1184	

Table A-1 continued…

E-8	0.25	3	0.0400	0.0366	
		6	0.0544	0.0643	
		9	0.0963	0.0920	0.0350
		12	0.1259	0.1197	
		15	0.1378	0.1471	
	0.50	3	0.0967	0.0711	
		6	0.1253	0.1249	
		9	0.1533	0.1772	0.0414
		12	0.2406	0.2292	
		15	0.2863	0.2801	
	0.75	3	0.1025	0.1040	
		6	0.1595	0.1798	
		9	0.2192	0.2533	0.0518
		12	0.3751	0.3248	
		15	0.3870	0.3938	
	1.08	3	0.1353	0.1374	
		6	0.2643	0.2337	
		9	0.3496	0.3236	0.0269
		12	0.4057	0.4087	
		15	0.5080	0.4885	
	1.33	3	0.1532	0.1278	
		6	0.2471	0.2137	
		9	0.3090	0.2911	0.0336
		12	0.3580	0.3619	
		15	0.4066	0.4257	
	1.50	3	0.1333	0.1225	
		6	0.1763	0.2031	
		9	0.2613	0.2740	0.0297
		12	0.3283	0.3376	
		15	0.4153	0.3943	
	1.80	3	0.1042	0.1128	
		6	0.1638	0.1845	
		9	0.2175	0.2437	0.0312
		12	0.2917	0.2965	
		15	0.3444	0.3417	

Table A-1 continued…

	2.08	3	0.0900	0.1044	
		6	0.1313	0.1678	
		9	0.2170	0.2183	0.0394
		12	0.2667	0.2629	
		15	0.3048	0.2996	
E-9	0.16	3	0.0300	0.0383	
		6	0.0850	0.0676	
		9	0.1040	0.0968	0.0425
		12	0.1263	0.1258	
		15	0.1500	0.1545	
	0.36	3	0.0767	0.0849	
		6	0.1342	0.1480	
		9	0.2363	0.2092	0.0484
		12	0.3098	0.2684	
		15	0.3358	0.3261	
	0.66	3	0.1333	0.1433	
		6	0.2175	0.2418	
		9	0.3501	0.3319	0.0305
		12	0.4518	0.4157	
		15	0.5089	0.4933	
	0.83	3	0.1804	0.1737	
		6	0.2436	0.2864	
		9	0.4586	0.3853	0.0491
		12	0.5062	0.4747	
		15	0.5905	0.5557	
	1.08	3	0.1507	0.1789	
		6	0.2458	0.2828	
		9	0.4071	0.3680	0.0394
		12	0.4508	0.4411	
		15	0.4750	0.5043	
	1.58	3	0.1304	0.1242	
		6	0.2075	0.1833	
		9	0.2371	0.2240	0.0304
		12	0.2407	0.2565	
		15	0.2747	0.2817	

Table A-1 continued…

	1.91	3	0.0802	0.1024	
		6	0.1370	0.1463	
		9	0.1843	0.1761	0.0379
		12	0.2133	0.1978	
		15	0.2054	0.2141	
E-10	0.16	3	0.0378	0.0351	
		6	0.0750	0.0617	
		9	0.1096	0.0885	0.0644
		12	0.1273	0.1151	
		15	0.1586	0.1415	
	0.50	3	0.0967	0.1075	
		6	0.1530	0.1846	
		9	0.2452	0.2582	0.0404
		12	0.3510	0.3290	
		15	0.4259	0.3963	
	0.75	3	0.1357	0.1486	
		6	0.2462	0.2497	
		9	0.3746	0.3416	0.0328
		12	0.4563	0.4266	
		15	0.5392	0.5052	
	1.00	3	0.1262	0.1263	
		6	0.2308	0.2045	
		9	0.2725	0.2705	0.0297
		12	0.3485	0.3270	
		15	0.3564	0.3766	
	1.25	3	0.1233	0.1085	
		6	0.1521	0.1714	
		9	0.2075	0.2194	0.0321
		12	0.2650	0.2604	
		15	0.2759	0.2939	
	1.46	3	0.1052	0.0973	
		6	0.1308	0.1494	
		9	0.1723	0.1892	0.0324
		12	0.2200	0.2206	
		15	0.2370	0.2467	

Table A-1 continued…

	1.91	3	0.0500	0.0768	
		6	0.0913	0.1122	
		9	0.1360	0.1388	0.0627
		12	0.1788	0.1597	
		15	0.1713	0.1754	
E-11	0.25	3	0.0500	0.0584	
		6	0.1229	0.1030	
		9	0.1463	0.1465	0.0368
		12	0.1750	0.1895	
		15	0.2395	0.2321	
	0.41	3	0.0983	0.0902	
		6	0.1347	0.1568	
		9	0.2638	0.2212	0.0544
		12	0.3242	0.2834	
		15	0.3482	0.3438	
	0.66	3	0.1428	0.1370	
		6	0.2454	0.2313	
		9	0.3751	0.3189	0.0360
		12	0.4096	0.4008	
		15	0.4883	0.4775	
	0.91	3	0.1662	0.1737	
		6	0.2643	0.2859	
		9	0.4054	0.3853	0.0312
		12	0.5065	0.4752	
		15	0.5991	0.5571	
	1.16	3	0.1575	0.1678	
		6	0.2573	0.2655	
		9	0.3453	0.3454	0.0270
		12	0.4569	0.4140	
		15	0.4663	0.4733	
	1.33	3	0.1217	0.1464	
		6	0.2440	0.2246	
		9	0.3053	0.2854	0.0326
		12	0.3588	0.3348	
		15	0.3657	0.3760	

Table A-1 continued…

	1.58	3	0.1037	0.1245	
		6	0.1741	0.1866	
		9	0.1963	0.2304	0.0411
		12	0.2732	0.2659	
		15	0.2904	0.2935	
	1.83	3	0.0833	0.1071	
		6	0.1263	0.1568	
		9	0.1800	0.1906	0.0476
		12	0.2180	0.2161	
		15	0.2393	0.2363	
E-12	0.28	3	0.0533	0.0753	
		6	0.1284	0.1321	
		9	0.2097	0.1869	0.0649
		12	0.2683	0.2406	
		15	0.3425	0.2930	
	0.45	3	0.1242	0.1084	
		6	0.2333	0.1859	
		9	0.2942	0.2597	0.0453
		12	0.3471	0.3303	
		15	0.3937	0.3974	
	0.70	3	0.1796	0.1531	
		6	0.2414	0.2557	
		9	0.3435	0.3481	0.0342
		12	0.4538	0.4328	
		15	0.5588	0.5106	
	0.95	3	0.1575	0.1488	
		6	0.2416	0.2380	
		9	0.2800	0.3119	0.0310
		12	0.3492	0.3759	
		15	0.4175	0.4310	
	1.20	3	0.1210	0.1228	
		6	0.2047	0.1899	
		9	0.2580	0.2404	0.0234
		12	0.2713	0.2818	
		15	0.3056	0.3153	

Table A-1 continued…

	1.45	3	0.0983	0.1031	
		6	0.1572	0.1546	
		9	0.1741	0.1914	0.0332
		12	0.2052	0.2196	
		15	0.2258	0.2425	
	1.70	3	0.0741	0.0883	
		6	0.1376	0.1272	
		9	0.1585	0.1557	0.0357
		12	0.1583	0.1769	
		15	0.1925	0.1928	
E-13	0.25	3	0.0783	0.0794	
		6	0.1318	0.1389	
		9	0.2035	0.1964	0.0198
		12	0.2411	0.2527	
		15	0.2965	0.3073	
	0.45	3	0.1335	0.1319	
		6	0.2406	0.2240	
		9	0.3063	0.3092	0.0340
		12	0.3492	0.3888	
		15	0.4383	0.4635	
	0.70	3	0.1558	0.1810	
		6	0.2800	0.2959	
		9	0.4505	0.3955	0.0399
		12	0.5282	0.4843	
		15	0.5875	0.5645	
	0.95	3	0.1903	0.2160	
		6	0.3688	0.3383	
		9	0.5063	0.4402	0.0380
		12	0.5560	0.5291	
		15	0.5890	0.6082	
	1.20	3	0.1961	0.1786	
		6	0.2608	0.2625	
		9	0.3504	0.3255	0.0313
		12	0.4153	0.3770	
		15	0.4364	0.4192	

Table A-1 continued…

	1.36	3	0.1350	0.1536	
		6	0.2043	0.2190	
		9	0.2815	0.2664	0.0305
		12	0.3046	0.3028	
		15	0.3595	0.3322	
	1.61	3	0.1200	0.1211	
		6	0.1500	0.1684	
		9	0.1825	0.1986	0.0288
		12	0.2288	0.2215	
		15	0.2473	0.2395	
	1.86	3	0.1040	0.0982	
		6	0.1380	0.1318	
		9	0.1500	0.1539	0.0272
		12	0.1800	0.1699	
		15	0.1975	0.1817	
E-14	0.30	3	0.0600	0.0608	
		6	0.1084	0.1072	
		9	0.1305	0.1524	0.0316
		12	0.1900	0.1970	
		15	0.2419	0.2409	
	0.55	3	0.1247	0.1057	
		6	0.2036	0.1817	
		9	0.2509	0.2544	0.0226
		12	0.3252	0.3241	
		15	0.3905	0.3905	
	0.80	3	0.1322	0.1430	
		6	0.2364	0.2410	
		9	0.3457	0.3307	0.0161
		12	0.4156	0.4138	
		15	0.5088	0.4906	
	1.05	3	0.1700	0.1523	
		6	0.2436	0.2490	
		9	0.3386	0.3323	0.0206
		12	0.4287	0.4065	
		15	0.4565	0.4726	

Table A-1 continued…

	1.30	3	0.1633	0.1311	
		6	0.2296	0.2075	
		9	0.2825	0.2694	0.0318
		12	0.3250	0.3208	
		15	0.3533	0.3649	
	1.55	3	0.1026	0.1139	
		6	0.1820	0.1764	
		9	0.2110	0.2226	0.0165
		12	0.2617	0.2612	
		15	0.2947	0.2921	
E-15	0.30	3	0.0650	0.0590	
		6	0.1289	0.1041	
		9	0.1438	0.1481	0.0368
		12	0.2034	0.1916	
		15	0.2384	0.2345	
	0.55	3	0.0933	0.1031	
		6	0.1566	0.1780	
		9	0.2464	0.2497	0.0341
		12	0.3525	0.3189	
		15	0.3955	0.3853	
	0.80	3	0.1351	0.1407	
		6	0.2363	0.2384	
		9	0.3456	0.3282	0.0379
		12	0.4733	0.4123	
		15	0.4898	0.4906	
	1.05	3	0.1063	0.1324	
		6	0.1951	0.2177	
		9	0.2934	0.2917	0.0267
		12	0.3617	0.3574	
		15	0.4051	0.4154	
	1.30	3	0.1117	0.1165	
		6	0.1643	0.1872	
		9	0.2500	0.2441	0.0288
		12	0.3083	0.2930	
		15	0.3530	0.3343	

Table A-1 continued…

1.55	3	0.1033	0.1035	
	6	0.1599	0.1624	
	9	0.2031	0.2073	0.0218
	12	0.2667	0.2452	
	15	0.2775	0.2762	
1.80	3	0.1017	0.0930	
	6	0.1358	0.1415	
	9	0.1750	0.1790	0.0184
	12	0.2133	0.2082	
	15	0.2423	0.2320	

REFERENCES

Abdul, A.S. and Gillham, R.W. (1984). "Laboratory studies of the effects of of the capillary fringe on streamflow generation." *Water Resour. Res.*, 20, 691-698.

Abrahams, A. D., Parsons, A. J., and Hirsch, P. J. (1992). "Field and laboratory studies of resistance to interrill overland flow on semi-arid hillslopes, southern Arizona." *Overland flow,* A. J. Parsons and A. D. Abrahams, eds., UCL Press, University College London, London, 1-23.

Adams, R., Parkin, G., Rutherford, J.C., Ibbitt, R.P. and Elliott, A.H. (2005). "Using a rainfall simulator and a physically based hydrological model to investigate runoff processes in a hillslope." *Hydrological Processes,* 19, 2209-2223.

Afyuni, M.M., Cassel, O.K., and Robarge, W.P. (1993). "Effect of landscape position on soil water and corn silage yield." *Soil Sci. Soc. Am. J.*, 57, 1573-1580.

Alaoui, A. and Goetz, B. (2008). "Dye tracer and infiltration experiments to investigate macropore flow." *Geoderma*, 144(1-2), 279-286.

Anderson, A.E., Weiler, M., Alila, Y. and Hudson, R.O. (2008). "Dye staining and excavation of a lateral preferential flow network." *Hydrol. Earth Syst. Sci. Discuss.,* 5, 1043-1065.

Anderson, A.E., Weiler, M., Alila, Y. and Hudson, R.O. (2009). "Subsurface flow velocities in a hillslope with lateral preferential flow." *Water Resour. Res.*, 45, W11407, doi: 10.1029/2008WR007121.

Anderson, A.E., Weiler, M., Alila, Y. and Hudson, R.O. (2010). "Piezometric response in zones of a watershed with lateral preferential flow as a first-order control on subsurface flow." *Hydrological Processes*, 24(16), 2237-2247.

Bachmair, S., Weiler, M., and Nützmann, G. (2009). "Controls of land use and soil structure on water movement: Lessons for pollutant transfer through the unsaturated zone." *Journal of Hydrology,* 369, 241-252.

Bachmair, S., Weiler, M., and Nützmann, G. (2010). "Benchmarking of two dual-permeability models under different land use and land cover." *Vadose Zone Journal*, 9(2), 226-237.

Batlle-Aguilar, J., Schneider, S., Pessel, M., Tucholka, P., Coquet, Y., and Vachier, P. (2009). "Axisymetrical infiltration in soil imaged by noninvasive electrical resistivimetry." *Soil Sci. Soc. Am. J.*, 73, 510-520.

Beckers, J., and Alila, Y. (2004). "A model of rapid preferential hillslope runoff contributions to peak flow generation in a temperate rain forest watershed." *Water Resour. Res.,* 40, W03501, doi:10.1029/2003WR002582.

Beven, K. (1981). "Kinematic subsurface stormflow." *Water Resour. Res.*, 17(5), 1419-1424.

Beven, K. (1982). "On subsurface stormflow: Predictions with simple kinematic theory for saturated and unsaturated flows." *Water Resour. Res.*, 18(6), 1627-1633.

Beven, K.J. (2000a). *Rainfall–Runoff Modelling*, John Wiley & Sons Ltd., Chichester, England.

Beven, K. J. (2000b). "Uniqueness of place and process representations in hydrological modeling." *Hydrol. Earth Syst. Sci.,* 4, 203– 213.

Beven, K.J., and Clarke, R.T. (1986). "On the variation of infiltration into a homogeneous soil matrix containing a population of macropores." *Water Resour. Res.,* 22(3), 383-388.

Beven, K. and Germann, P. (1981). "Water flow in soil macropores, 2, A combined flow model." *J. Soil Sci.*, 32, 15-29.

Beven, K. and Germann, P. (1982). "Macropores and water flow in soils." *Water Resour. Res.*, 18(5), 1311-1325.

Beven, K.J. and Kirkby, M.J. (1979). "A physically based, variable contributing area model of basin hydrology." *Hydrology Science Bulletin*, 24, 43–69.

Blake, G., Schlichting, E., and Zimmermann, U. (1973). "Water recharge in a soil with shrinkage cracks." *Soil Sci. Soc. Am. Proc.*, 37, 669-672.

Bouma, J. and Dekker, L.W. (1978). "A case study on infiltration into dry clay soil, 1, Morphological observations." *Geoderma*, 20, 27-40.

Bouma, J., Dekker, L.W., and Haans, J.C.F.M. (1980). "Measurement of depth to water table in a heavy clay soil." *Soil Sci.*, 130(5), 264-270.

Bouma, J., Jongerius, A., Boersma, O., Jager, A., and Schoonderbeek, D. (1977). "The function of different types of macropores during saturated flow through four swelling soil horizons." *Soil Sci. Soc. Am. J.*, 41, 945-950.

Bouma, J., Jongerius, A., and Schoonderbeek, D. (1979). "Calculation of saturated hydraulic conductivity of some pedal clay soils using morphometric data." *Soil Sci. Soc. Am. J.*, 43, 261-264.

Bouma, J. and Wosten, J.H.L. (1979). “”Flow patterns during extended saturated flow in two undisturbed swelling clay soils with different macro structures.” *Soil Sci. Soc. Am. J.*, 43, 16-22.

Brewer, R. (1964). *Fabric and Mineral Analysis of Soils*, John Wiley, New York.

Bronstert, A. (1999). “Capabilities and limitations of detailed hillslope hydrological modelling.” *Hydrological Processes*, 13, 21-48.

Bronstert, A., and Plate, E.J. (1997). “Modelling of runoff generation and soil moisture dynamics for hillslopes and micro-catchments.” *Journal of Hydrology,* 198, 177-195.

Brooks, E.S. (2003). “Distributed hydrologic modeling of the eastern Palouse.” Ph.D. dissertation, University of Idaho, Moscow.

Bullock, P. and Thomasson, A.J. (1979). “Rothamsted studies of soil structure, 2, measurement and characterisation of macroporosity by image analysis and with data from water retention measurements, *J. Soil Sci.*, 30(3), 391-414.

Burt, T.P. and Butcher, D.P. (1985). “Topographic controls of soil moisture distributions.” *J. Soil Sci.*, 36, 469-486.

Buttle, J.M. and McDonald, D.J. (2000). “Soil macroporosity and infiltration characteristics of a forest podzol.” *Hydrological Processes*, 14(5), 831-848.

Calver, A., Kirkby, M.J. and Weyman, D.R. (1972). “Modelling hillslope and channel flow,” in Chorley, R.J. (Ed.), *Spatial Analysis in Geomorphology*, Methuen, London, 197-218.

Cattle, S.R., Koppi, A.J., and McBratney, A.B. (1994). “The effect of cultivation on the properties of a Rhodoxeralf from the wheat/sheep belt of New South Wales.” *Geoderma*, 63, 215-225.

Chaudhry, M.H. (1993). *Open channel flow*, Prentice Hall, Englewood Cliffs, N.J.

Chen, C.L. (1975). “Laboratory studies of the resistance coefficient for sheet flow over natural turf surfaces.” *Urban storm runoff inlet hydrograph study,* Vol. 2, Utah Water Res. Lab., Utah State University, Logan, Utah.

Chen, L., Liu, Q. Q., and Li, J. C. (2001). “Runoff generation characteristics in typical erosion regions on the Loess Plateau.” *Int. J. Sediment Res.,* 16(4), 473-485.

Chow, V.T. (1959). *Open-channel hydraulics,* McGraw-Hill, New York.

Chow, V.T., Maidment, D.R., and Mays, L.W. (1988). *Applied Hydrology*, McGraw Hill, Inc., 140-147.

Christiansen, J.S., Thorsen, M., Clausen, T., Hansen, S., and Refsgaard, J.C. (2004). "Modelling of macropore flow and transport processes at catchment scale." *Journal of Hydrology,* 299(1-2), 136-158.

Dagan, G. (1986). "Statistical theory of groundwater flow and transport: Pore to laboratory, laboratory to formation, and formation to regional scale." *Water Resour. Res.*, 22, S120–S134.

DeVries, J. and Chow, T.L. (1978). "Hydrologic behavior of a forested mountain soil in coastal British Columbia." *Water Resour. Res.*, 14(15), 935-942.

Dikau, R. (1989). "The application of a digital relief model to landform analysis in geomorphology." In Raper, J. (Ed.) *Three dimensional applications in geographical information systems*, Taylor and Francis, London, 51-77.

Droogers, P., Stein, A., Bouma, J., and de Boer, G. (1998). "Parameters for describing soil macroporosity derived from staining patterns." *Geoderma*, 83, 293-308.

Duguid, J.O. and Lee, P.C.Y. (1977). "Flow in fractured porous media." *Water Resour. Res.*, 13(3), 558-566.

Dunne, T. and Black, R.D. (1970). "An experimental investigation of runoff production in permeable soils." *Water Resour. Res.*, 6, 478-490.

Ehlers, W. (1975). "Observations on earthworm channels and infiltration on tilled and untilled loose soil." *Soil Sci.*, 119(2), 242-249.

Ela, S.D., Gupta, S.C., and Rawls, W.J. (1992). "Macropore and surface seal interactions affecting water infiltration into soils." *Soil Sci. Soc. Am. J.,* 56, 714-721.

Elçi, A. and Molz, F.J. (2009). "Identification of lateral macropore flow in a forested riparian wetland through numerical simulation of a subsurface tracer experiment." *Water, Air, & Soil Pollution*, 197(1-4), 149-164.

Emmett, W. W. (1970). *The Hydraulics of Overland Flow on Hillslopes.* U.S.Geological Survey Professional Paper No. 662-A U.S. Govt. Printing Office, Washington D.C.

Evans, I.S. (1980). "An integrated system of terrain analysis and slope mapping." *Z Geomorph NF Suppl-Bd*, 36, 274-295.

Faeh, A.O., Scherrer, S., and Naef, F. (1997). "A combined field and numerical approach to investigate flow processes in natural macroporous soils under extreme precipitation." *Hydrol. Earth Syst. Sci.,* 1, 787–800.

Famiglietti, J.S., Rudnicki, J.W., and Rodell, M. (1998). "Variability in surface moisture content along a hillslope transect: Rattlesnake Hill, Texas." *Journal of Hydrology*, 210, 259-281.

Fan, Y. and Bras, R.L. (1998). "Analytical solutions to hillslope subsurface storm flow and saturated overland flow." *Water Resour. Res.*, 34(4), 921-927.

Fisher, J.C. (1997). "A one-dimensional model of subsurface hillslope flow." Technical Report, US Forest Service Redwood Science Laboratory.

Fletcher, P.W. (1952). "The hydrologic function of forest soils in watershed management." *J. Forestry*, 50, 359-362.

Flury, M., Flühler, H., Jury, W.A., and Leuenberger, J. (1994). "Susceptibility of soils to preferential flow of water." *Water Resour. Res.*, 30, 1945-1954.

Foody, G.M., Campbell, N.A., Trodd, N.M., and Wood, T.F. (1992). "Derivation and applications of probabilistic measures of class membership from the maximum-likelihood classification." *Photogrammetric Engineering and Remote Sensing*, 58(9), 1335-1341.

Forrer, I., Kasteel, R., Flurry, M., and Flühler, H. (1999). "Longitudinal and lateral dispersion in an unsaturated field soil." *Water Resour. Res.*, 35(10), 3049-3060.

Francis, C.F., Thornes, J.B., Romero Diaz, A., Lopez Bermudez, F., and Fisher, G.C. (1986). "Topographic control of soil moisture, vegetation cover and land degradation in a moisture stressed Mediterranean environment." *Catena*, 13, 211–225.

Freer, J., Mcdonnell, J., Beven, K.J., Brammer, D., Burns, D., Hooper, R.P., and Kendal, C. (1997). "Topographic controls on subsurface storm flow at the hillslope scale for two hydrologically distinct small catchments." *Hydrological Processes*, 11, 1347-1352.

Gerke, H.H., and van Genuchten, M.T. (1993). "A dual-porosity model for simulating the preferential movement of water and solutes in structured porous media." *Water Resour. Res.,* 29(2), 305-319.

German-Heins, J. and Flury, M. (2000). "Sorption of Brilliant Blue FCF in soils affected by pH and ionic strength." *Geoderma*, 97, 87-101.

Germann, P. (1981). "Untersuchungen über den Boden wasserhaushalt inn Einzugsgebiet Rietholzbach." *Mitt. Versuchanst. Wasserbau Hydrol. Glaziologie ETH Zurich*, 51, 133 pp.

Germann, P. and Beven, K. (1985). "Kinematic wave approximation to infiltration into soils with sorbing macropores." *Water Resour. Res.*, 21(7), 990-996.

Germann, P.F. and Beven, K. (1986). "A distribution function approach to water flow in soil macropores based on kinematic wave theory." *Journal of Hydrology*, 83, 173-183.

Germann, P., Pierce, R.S., and Beven, K. (1986). "Kinematic wave approximation to the initiation of subsurface storm flow in a sloping forest soil." *Adv. Water Resour.,* 9, 70-76.

Ghodrati, M., Chendorain, M., and Chang, Y.J. (1999). "Characterization of macropore flow mechanism in soil by means of a split macropore column." *Soil Sci. Soc. Am. J.*, 63, 1093-1101.

Ghodrati, M. and Jury, W.A. (1990). "A field study using dyes to characterize preferential flow of water." *Soil Sci. Soc. Am. J.*, 54(6), 1558-1563.

Gómez-Plaza, A., Martínez-Mena, M., Albaladejo, J., and Castillo, V.M. (2001). "Factors regulating spatial distribution of soil water content in small semiarid catchments." *Journal of Hydrology*, 253, 211-226.

Govindaraju, R. S., Kavvas, M. L., and Tayfur, G. (1992). "A simplified model for two dimensional overland flows." *Adv. Water Resour.,* 15, 133-141.

Graham, C.B. and McDonnell, J.J. (2010). "Hillslope threshold response to rainfall: (2) Development and use of a macroscale model." *Journal of Hydrology*, 393, 77-93.

Graham, C.B., Woods, R.A., and McDonnell, J.J. (2010). "Hillslope threshold response to rainfall: (1) A field based forensic approach." *Journal of Hydrology*, 393, 65-76.

Gregory, K.J. and Walling, D.E. (1973). *Drainage Basin Form and Process: A Geomorphological Approach*, Arnold, London, 456 pp.

Green, W.H. and Ampt, G.A. (1911). "Studies on soil physics: I. Flow of air and water through soils." *Journal of Agricultural Science*, 4(1), 1-24.

Hawley, M.E., Jackson, T.J., and McCuen, R.H. (1983). "Surface soil moisture variation on small agricultural watersheds." *Journal of Hydrology*, 62, 179–200.

Haws, N.W., Liu, B., Boast, C.W., Rao, P.S.C., Kladivko, E.J., and Franzmeier, D.P. (2004). "Spatial variability and measurement scale of infiltration rate on an agricultural landscape." *Soil Sci. Soc. Am. J.*, 68, 1818-1826.

Helmers, M.J. and Eisenhauer, D.E. (2006). "Overland flow modeling in a vegetative filter considering non-planar topography and spatial variability of soil hydraulic properties and vegetation density." *Journal of Hydrology*, 328, 267-282.

Helvey, J.D., Hewlett, J.D., and Douglass, J.E. (1972). "Predicting soil moisture in the southern Appalachians." *Soil Sci. Soc. Am. Proc.*, 36, 954-959.

Herbst, M. and Diekkruger, B. (2003). "Modelling the spatial variability of soil moisture in a micro-scale catchment and comparison with field data using geostatistics." *Physics and Chemistry of the Earth,* Parts A/B/C, 28(6-7), 239-245.

Hewitt, J.S. and Dexter, A.R. (1980). "Effects of tillage and stubble management on the structure of a swelling soil." *J. Soil Sci.*, 31(2), 203.

Hewlett, J.D. and Hibbert, A.R. (1963). "Moisture and energy conditions within a sloping soil mass during drainage." *J. Geophys. Res.*, 68(4), 1081-1087.

Hirsch, P. J. (1992). "Hydraulic resistance to overland flow on semi-arid hillslopes: A physical simulation." PhD dissertation, Dept. of Geography, State Univ. of New York at Buffalo, Buffalo, N.Y.

Holtan, H.N. (1961). "A concept for infiltration estimates in watershed engineering." Agricultural Research Service, United States Department of Agriculture.

Hoogmoed, W.D. and Bouma, J. (1980). "A simulation model for predicting infiltration into cracked clay soil." *Soil Sci. Soc. Am. J.*, 44, 458-461.

Horton, R.E. (1933). "The role of infiltration in the hydrologic cycle." *Trans. Am. Geophys. Union*, 14, 446-460.

Huggins, L.F. and Monke, E.J. (1966). *The mathematical solution of the hydrology of small watersheds*, Technical report No. 1, Water Resources Research Centre, Purdue University, West Lafayette, Indiana – 130p.

Hursh, C.R. and Brater, E.F. (1941). "Separating storm hydrographs from small drainage areasinto surface and subsurface flow." *Trans. Am. Geophys. Union*, 863-870.

Hutchinson, D.G. and Moore, R.D. (2000). "Throughflow variability on a forested hillslope underlain by compacted glacial till." *Hydrol. Processes*, 14(10), 1751-1766.

Jain, M.K., Kothyari, U.C., and Ranga Raju, K.G.R. (2005). "GIS based distributed model for soil erosion and rate of sediment outflow from catchments." *Journal of Hydraulic Engineering,* 131(9), 755-769.

Jarvis, N.J. (1989). "A simple empirical model for root water uptake." *Journal of Hydrology*, 107, 57-72.

Jones, J.A.A. (1971). "Soil piping and stream channel initiation." *Water Resour. Res.*, 7(3), 602-610.

Jones, J.A.A. (1997). "Pipe flow contributing areas and runoff response." *Hydrological Processes,* 11, 35-41.

Jones, J.A.A. and Connelly, L.I. (2002). "A semi distributed simulation model for natural pipeflow." *Journal of Hydrology*, 262, 28-49.

Kadlec, R.H. (1990). "Overland flow in wetlands: Vegetation resistance." *Journal of Hydrologic Engineering.,* ASCE, 116(5), 691-706.

Karmaker, T. and Dutta, S. (2010). "Generation of synthetic hydrographs for a large river basin." *Journal of Hydrology*, 381, 287-296.

Kienzler, P. and Naef, F. (2006). "How geophysical methods can contribute to subsurface storm flow investigations." *Geophysical Research Abstracts*, Vol. 8, 03135.

Kirkby, M.J. (1969). "Infiltration, throughflow and overland flow," in Chorley, R.J. (Ed.), *Water, Earth and Man*, Methuen, London, Ch. 5.1, 215-227.

Kirkby, M. J., (Ed.) (1978). *Hillslope Hydrology*, Wiley-Interscience, New York.

Kirkby, M.J. and Chorley, R.J. (1967). "Throughflow, overland flow and erosion." *Bull. Intern. Assoc. Sci. Hydrology*, 12, 5-21.

Kissel, D.E., Ritchie, J.T., and Burnett, E. (1973). "Chloride movement in undisturbed swelling clay soil." *Soil Sci. Soc. Am. Proc.*, 37, 21-24.

Kitahara, H. (1993). "Characteristics of pipe flow in forested slopes." *IAHS Publication* 212, 235-242.

Kitahara, H., Shimizu, A., and Mashima, Y. (1988). "Characteristics of pipe flow in a subsurface soil layer of a gentle hillside." *J. Japan For. Soc.*, 70, 318-323.

Knapp, B.J. (1973). "A system for the field measurement of soil water movement." *Tech. Bull. Brit. Geomorph. Res. Gp.*, No. 9, 26 pp.

Kolymbas, D. and Wagner, P. (2007). "Groundwater ingress to tunnels – The exact analytical solution." *Tunnelling and Underground Space Technology,* 22, 23-27.

Kostiakov, A.N. (1932). "On the dynamics of the coefficients of water percolation in the soils and on the necessity of studying it from a dynamic point of view for the purpose of amelioration." *Transaction of the 6th Com. Int. Soc. Soil Sci.,* Moscow, Part A: 15-21.

Kroes, J.G., van Dam, J.C., Groenendijk, P., Hendriks, R.F.A., and Jacobs, C.M.J. (2008). *SWAP version 3.2. Theory description and user manual*. Alterra Report 1649, Alterra, Wageningen, Netherlands.

Larsbo, M. and Jarvis, N. (2003). "Macro 5.0. A model of water flow and solute transport in macroporous soil. Technical description, Studies in Biogeophysical Environment, Emergo, 6, 48 pp.

Larsson, M.H., and Jarvis, N.J. (1999). "Evaluation of a dual-porosity model to predict field-scale solute transport in a macroporous soil." *Journal of Hydrology,* 215, 153-171.

Lauren, J.G., Wagenet, R.J., Bouma, J., and Wosten, J.H.M. (1988). "Variability of saturated hydraulic conductivity in a glossaquic hapludalf with macropores." *Soil Sci*., 145, 20–28.

Léonard, J., Perrier, E., and de Marsily, G. (1999). "A model for simulating the influence of a spatial distribution of large circular macropores on surface runoff." *Water Resour. Res.,* 37(12), 3217-3225.

Li, Y., and Ghodrati, M. (1997). "Preferential transport of solute through soil columns containing constructed macropores." *Soil Sci. Soc. Am. J.,* 61, 1308-1317.

Ligon, J.T., Wilson, T.V., Allen, J.F., and Singh, U.P. (1977). "Tracing vertical translocation of soil moisture." *J. Hydraul. Div. Am. Soc. Civ. Eng.*, 103(HY 10), 1147-1158.

Lima, J. L. M. P. (1989). "Overland flow under rainfall: Some aspects related to modeling and conditioning factors." PhD thesis, Agricultural Univ. Wageningen, Wageningen, The Netherlands.

Lin, Y., and Cunningham III, G.A. (1995). "A new approach to fuzzy-neural system modeling." *IEEE Transactions on Fuzzy Systems*, 3(2), 190-197.

Lischeid, G., Alewell, C., Bittersohl, J., Gottlein, A., Jungnickel, C., Lange, H., Mandersheid, B., Moritz, K., Ostendorf, B., and Sager, H. (1998). "Investigating soil and groundwater quality at different scales in a forested catchment: The Waldstein case study." *Nutr. Cycling Agroecosyst.*, 50,109–118.

Liu, Q. Q., Chen, L., Li, J.C., and Singh, V.P. (2004). "Two-dimensional kinematic wave model of overland-flow." *Journal of Hydrology*, 291(1-2), 28-41.

Liu, Q. Q. and Singh, V. P. (2004). "Effect of microtopography, slope length and gradient, and vegetation cover on overland flow through simulation." *Journal of Hydrologic Engineering*, ASCE, 9(5), 375-382.

Lull, H.W. and Reinhart, K.G. (1955). *Soil moisture measurement*, U.S.D.A. Southern For. Exp. Sta., New Orleans, LA., Occas. Paper No. 140.

Luxmoore, R.J. (1981). "Micro-, meso- and macroporosity od soil." *Soil Sci. Soc. Am. J.*, 45, 671 pp.

Marshall, T.J. (1959). "Relations between water and soil." *Tech. Comm. 50*, Commonwealth Bur. Soils, Harpenden, U.K.

McDonald, P.M. (1967). "Diposition of soil moisture held in temporary storage in large pores." *Soil Sci.*, 103(2), 139-143.

McDonnell, J. (1990). "A rationale for old water discharge trough macropores in a steep, humid catchment." *Water Resour. Res.*, 26(11), 2821-2832.

Merril, C.R. (1990). "Gel-staining techniques", In Deutscher M P (Ed.) *Guide to protein purificatio. methods in enzymology,* Academic press Inc.,Volume 182.

Miller, J.D. and Gaskin, G.J. (1997). "The development and application of the ThetaProbe soil water sensor.", *MLURI Technical Note*.

Montgomery, D.R., Dietrich, W.E., Torres, R., Anderson, S.P., Heffner, J.T., and Loague, K. (1997). "Hydrologic response of a steep, unchanneled valley to natural and applied rainfall." *Water Resour. Res.*, 33(1), 91-109.

Moore, I.D., Burch, G.J., Mackenzie, D.H. (1988). "Topographic effects on the distribution of surface water and the location of ephemeral gullies." *Trans. Am. Soc. Agric. Eng.*, 31, 1098–1107.

Morris, C. and Mooney, S.J. (2004). "A high-resolution system for the quantification of preferential flow in undisturbed soil using observations of tracers." *Geoderma*, 118, 133-143.

Mosley, M.P. (1979). "Streamflow generation in a forested watershed, New Zealand." *Water Resour. Res.*, 15(4), 795-806.

Mosley, M.P. (1982). "Subsurface flow velocities through selected forest soils, South Island, New Zealand." *Journal of Hydrology*, 55, 65-92.

Muskat, M. (1946). *The Flow of Homogeneous Fluids through Porous Media*, J.W. Edwards Inc., Ann Arbor, Mich., 1976 pp.

Natsch, A., Keel, Ch., Troxler, J., Zala, M., von Albertini, N., and Défago, G. (1996). "Importance of preferential flow and soil management in vertical transport of a biocontrol strain of pseudomonas fluorescens in structured field soil." *Applied and Environmental Microbiology*, 62(1), 33-40.

Návar, J., Turton, D.J. and Miller, E.L. (1995). "Estimating macropore and matrix flow using the hydrograph separation procedure in an experimental forest plot." *Hydrological Processes*, 9(7), 743-753.

Negi, G.C.S. (2001). "The need for micro-scale and meso-scale hydrological research in the Himalayan mountains." *Environmental Conservation*, 28(2), 95-98.

Negishi, J.N., Sidle, R.C., Ziegler, A.D., Noguchi, S., Abdul Rahim, N. (2008). "Contribution of intercepted subsurface flow to road runoff and sediment transport in a logging-disturbed tropical catchment." *Earth Surface Processes and Land Forms*, 33(8), 1174-1191.

Negishi, J.N., Ziegler, A.D., Noguchi, S., Sidle, R.C., and Rahim, N.A. (2004). "Storm flow generation in a tropical headwater zero-order basin in Peninsular Malaysia." Proceedings of the workshop of the International Union of Forest Research Organizations (IUFRO), Forest Hydrology Working Group, 10-12 July, 2004, Kota Kinabalu, Sabah, Malaysia, 111-114.

Nelson, W.R. and Baver, L.D. (1940). "Movement of water through soils in relation to the nature of the pores."*Soil Sci. Soc. Am. Proc.*, 5, 69-76.

Niyogi, P., Chakraborty, S.K., and Laha, M.K. (2005). *Introduction to Computational Fluid Dynamics,* pp. 118-121, Pearson Education (Singapore) Pte. Ltd., Indian Branch, Delhi, India.

Noguchi, S., *et al.* (1999). "Morphological characteristics of macropores and the distribution of preferential flow pathways in a forested slope segment." *Soil Sci. Soc. Am. J.*, 63(5), 1413-1423.

Nyberg, L. (1996). "Spatial variability of water content in the covered catchment at Gardsjon, Sweden." *Hydrological Processes*, 10, 89–103.

Öhrström, P., Persson, M., Albergel, J., Zante, P., Nasri, S., Berndtsson, R., and Olsson, J. (2002). "Field-scale variation of preferential flow as indicated from dye coverage." *Journal of Hydrology*, 257, 164-173.

Olsen, P.A. and Børresen, T. (1997). "Measuring differences in soil properties in soils with different cultivation practices using computer tomography." *Soil and Tillage Research*, 44(1-2)**,** 1-12.

Omoti, U. and Wild, A. (1979). "Use of fluorescent dyes to mark the pathways of solute movement through soils under leaching conditions, 2. field experiments." *Soil Sci.*, 128(2), 98-104.

Parr, J.F. and Bertrand, A.R. (1960). "Water infiltration into soil." *Adv. Agronomy*, 12, 311-363.

Perillo, C.A., Gupta, S.C., Nater, E.A., and Moncrief, J.F. (1999). "Prevalence and initiation of preferential flow paths in a sandy loam argillic horizon." *Geoderma*, 89, 307-331.

Perret, J., Prasher, S.O., Kantzas, A. and Langford, C. (1999). "Three-dimensional quantification of macropore in undisturbed soil cores." *Soil Sci. Soc. Am. J.*, 63, 1530-1543.

Petch, R.A. (1988). "Soil saturation patterns in steep, convergent hillslopes under forest and pasture vegetation." *Hydrological Processes*, 2, 93-103.

Peters, D.L., *et al.* (1995). "Runoff production in forested, shallow soil, Canadian Shield Basin." *Water Resour. Res.*, 31(5), 1291-1304.

Philip, J.R. (1957). "The theory of infiltration, 1. The infiltration equation and its solution." *Soil Sci.*, 83, 345-357.

Quisenberry, V.L. and Phillips, R.E. (1976). "Percolation of surface-applied water in the field." *Soil Sci. Soc. Am. J.*, 40, 484–489.

Rajot, J. L., Léonard, J., and Perrier, E. (2004). "Biological macropores effect on runoff and infiltration: a combined experimental and modelling approach." *Agriculture, Ecosystems & Environment*, 104(2), 277-285.

Ranken, D.W. (1974). "Hydrologic properties of soil and subsoil on a steep forested slope." Masters Thesis, Oreg. State Univ., Corvallis.

Ray, C., Ellsworth, T.R., Valocchi, A.J., and Boast, C.W. (1997). "An improved dual porosity model for chemical transport in macroporous soils." *Journal of Hydrology,* 193, 270-292.

Reeves, M.J. (1980). "Recharge of the English chalk, A possible mechanism." *Eng. Geol.*, 14(4), 231-240.

Rezzoug, A., Schumann, A., Chifflard, P., and Zepp, H. (2005). "Field measurement od soil moisture dynamics and numerical simulation using the kinematic wave approximation." *Adv. Water Resour.*, 28, 917-926.

Richards, R. A. (1931). "Capillary conduction of liquid through porous media." *Physics 1*, 318-333.

Roberge, J. and Plamondon, A.P. (1987). "Snowmelt runoff pathways in a boreal forest hillslope: The role of pipe throughflow." *Journal of Hydrology*, 95(1-2), 39-54.

Rogowski, A.S. and Weinrich, B.E. (1981). "Modeling water flux on stripmined land." *Trans. Am. Soc. Agr. Eng.*, 24(4), 935-940.

Roessel, B.W.P. (1950). "Hydrologic problems concerning the runoff in headwater regions." *Trans. Am. Geophys. Union*, 31, 431-442.

Ruan, H. and Illangasekare, T.H. (1998). "A model to couple overland flow and infiltration into macroporous vadose zone." *Journal of Hydrology,* 210, 116-127.

Sarkar, R. and Dutta, S. (2009). "An experimental and modelling investigation of macropore dominated subsurface stormflow in vegetated hillslopes of northeast India." In Yilmaz, K.K, Yucel, I., Gupta, H.V., Wagener, T., Yang, D., Savenije, H., Neale, C., Kunstmann, H., and Pomeroy, J. (Eds.), *New approaches to hydrological prediction in data-sparse regions*, *International Association of Hydrological Sciences* (IAHS) *Publication* 333, 145-152.

Sarkar, R. and Dutta, S. (2011). "Field investigation and modeling of rapid subsurface stormflow through preferential pathways in a vegetated hillslope of northeast India: Case Study.", *Journal of Hydrologic Engineering*, Accepted Manuscript (In Press), doi:10.1061/(ASCE)HE.1943-5584.0000431.

Sarkar, R., Dutta, S., and Panigrahy, S. (2008a). "Effect of scale on infiltration in a macropore dominated hillslope". *Current Science,* 94(4), 490-494.

Sarkar, R., Dutta, S., and Panigrahy, S. (2008b). "Characterizing overland flow on a preferential infiltration dominated hillslope: Case study." *Journal of Hydrologic Engineering*, 13(7), 563-569.

Scanlan, C. and Hinz, C. (2007). "A conceptual model to quantify plant root induced changes in soil hydraulic conductivity and water retention." International Annual Meetings of ASA-CSSA-SSSA, 4-8 November, 2007, New Orleance, Louisiana.

Scanlon, T.M., Raffensperger, J.P., and Hornberger, G.M. (2000). "Shallow subsurface storm flow in a forested headwater catchment: Observations and modeling using a modified TOPMODEL." *Water Resour. Res.*, 36(9), 2575–2586.

Schaap, M.G. (1999). *Rosetta Users Manual,* Soil Salinity Laboratory, Agricultural Research Service, United States Department of Agriculture (USDA).

Schaap, M.G., Leij, F.J., and van Genuchten M.Th. (1998). "Neural network analysis for hierarchical prediction of soil water retention and saturated hydraulic conductivity." *Soil Sci. Soc. Am. J.* 62:847-855

Scherrer, S., Naef, F., Faeh, A.O., and Cordery, I. (2006). " Formation of runoff at the hillslope scale during intense precipitation." *Hydrol. Earth Syst. Sci. Discuss.,* 3, 2523-2558.

Scotter, D.R. (1978). "Preferential solute movement through larger soil voids, 1, Some computations using simple theory." *Aust. J. Soil Res.*, 16, 257-267.

Shougrakpam, S., Sarkar, R., and Dutta, S. (2010). "An experimental investigation to characterise soil macroporosity under different land use and land covers of northeast India". *Journal of Earth System Science*, 119(5), 655-674.

Sidle, R.C., *et al.* (1995). "Seasonal hydrologic response at various spatial scales in a small forested catchment, Hitachi-Ohta, Japan." *Journal of Hydrology*, 168(1-4), 227-250.

Sidle, R.C., Tsuboyama, Y., Noguchi, S., Hosoda, I., Fujieda, M., and Shimizu, T. (2000). "Storm-flow generation in steep forested headwaters: a linked hydrogeomorphic paradigm." *Hydrological Processes,* 14, 369-385.

Sidle, R.C., *et al.* (2001). "A conceptual model of preferential flow systems in forested hillslopes: Evidence of self-organization." *Hydrol. Processes*, 15(10), 1675-1692.

Singh, A.K. (2006). "Subsurface stormflow in steep hillslopes." M.Tech Thesis, Department of Civil Engineering, IIT Guwahati, Assam, India.

Singh, V. P., Sharma, N. and Ojha, C. S. P. (2004). *The Brahmaputra Basin Water Resources*, Kluwer Academic Publishers, Netherlands.

Sloan, P.G. and Moore, I.D. (1984). "Modeling subsurface stormflow on steeply sloping forested watersheds." *Water Resour. Res.*, 20(12), 1815-1822.

Sloan, P.G., Moore, I.D., Coltharp, G.B., and Eigel, J.D. (1983). "Modeling surface and subsurface stormflow on steeply-sloping forested watersheds." Research Report No. 142, University of Kentucky, Water Resources Research Institute, Lexington, Kentucky, 131 pp.

Smettem, K.R.J., Chittleborough, D.J., Richards, B.G. & Leaney, F.W. (1991). "The influence of macropores on runoff generation from a hillslope soil with a contrasting textural class." *Journal of Hydrology*, 122, 235-252.

Smith, R.E. and Hebbert, R.H.B. (1983). "Mathematical simulation of Interdependent surface and subsurface hydrologic processes." *Water Resour. Res.*, 19(4), 987-1001.

Soja, R. and Starkel, L. (2007). "Extreme rainfalls in Eastern Himalaya and southern slope of Meghalaya Plateau and their geomorphologic impacts." *Geomorphology,* 84(2007), 170-180.

Stauffer, F. and Dracos, T. (1986). "Experimental and numerical study of water and solute infiltration in layered porous media." *Journal of Hydrology*, 84, 9-34.

Steenhuis, T.S., *et al.* (1988). "Preferential flow influences on drainage of shallow sloping soils." *Agric. Water Manage.*, 14(1-4), 137-151.

Stoeckeler, J.H. and Curtis, W.R. (1960). "Soil moisture regime in south-western Wisconsin as affected by aspect and forest type." *J. Forestry*, 58(11), 892-896.

Subramanya, K. (1999). *Engineering Hydrology,* Tata McGraw-Hill Publishing Company Limited, New Delhi, India.

Tang, J., Zhang, B., Gao, C., and Zepp, H. (2011). "Subsurface lateral flow from hillslope and its contribution to nitrate loading in the streams during typical storm events in an agricultural catchment." *Hydrol. Earth Syst. Sci. Discuss.*, 8, 4151-4193.

Tani, M. (1997). "Runoff generation processes estimated from hydrological observations on a steep forested hillslope with a thin soil layer." *Journal of Hydrology*, 200(1-4), 84-109.

Terajima, T., *et al.* (2000). "Morphology, structure and flow phases in soil pipes developing in forested hillslopes underlain by a Quaternary sand-gravel formation, Hokkaaido, northern main island in Japan." *Hydrol. Processes,* 14(4), 713-726.

Ticehurst, J.L., Cresswell, H.P., and Jakeman, A.J. (2003). "Using a physically based model to conduct a sensitivity analysis of subsurface lateral flow in south-east Australia." *Environmental Modelling & Software,* 18, 729-740.

Troch, P., van Loon, E., and Hilberts, A. (2002). "Analytical solutions to a hillslope-storage kinematic wave equation for subsurface flow." *Adv. Water Resour.*, 25, 637-649.

Trojan, M.D., and Linden, D.R. (1992). "Microrelief and rainfall effects on water and solute movement in earthworm borrows." *Soil Sci. Soc. Am. J.,* 56, 727-733.

Tromp-van Meerveld, I. and Weiler, M. (2008). "Hillslope dynamics modeled with increasing complexity." *Journal of Hydrology*, 361, 24-40.

Tromp-van Meerveld, H.J. and McDonnell, J.J. (2006a). "Threshold relations in subsurface stormflow: 1. A 147-storm analysis analysis of the Panola hillslope." *Water Resour. Res.,* 42, W02410, doi:10.1029/2004WR003778.

Tromp-van Meerveld, H.J. and McDonnell, J.J. (2006b). "Threshold relations in subsurface stormflow: 2. The fill and spill hypothesis." *Water Resour. Res.,* 42, doi:10.1029/2004WR003778.

Tsihrintzis, V.A. (2001). "Discussion on 'Variation of roughness coefficients on submerged and unsubmerged vegetation' by Wu, Fu-Chun., Shen, H.W. and Chou, Yi-Ju. (1999)." *Journal of Hydraulic Engineering*, 127(3), 241–245.

Tsuboyama, Y., *et al.* (1994). "Flow and solute transport through the soil matrix and macropores of a hillslope segment." *Water Resour. Res.*, 30(4), 879-890.

Tsukamota, Y. (1961). "An experiment on subsurface flow." *J. Japanese Soc. Forestry*, 43, 61-68.

Tsutsumi, D., *et al.* (2005). "Development of a simple lateral preferential flow model with steady state application in hillslope soils." *Water Resour. Res.,*41, W12420, doi: 10.1029/2004WR003877.

Uchida, T., Kosugi, K., and Mizuyama, T. (1999). "Runoff characteristics of pipe flow and effects of pipeflow on rainfall-runoff phenomena in a mountainous watershed." *Journal of Hydrology*, 222(1-4), 18-36.

Uchida, T., Kosugi, K.I., and Mizuyama, T. (2002). "Effects of pipe flow and bedrock groundwater on runoff generation in a steep headwater catchment in Ashiu, central Japan." *Water Resour. Res.,* 38(7), 1119, doi: 10.1029/2001WR000261.

Uchida, T., Tromp-van Meerveld, I., and McDonnell, J. J. (2005). "The role of lateral pipe flow in hillslope runoff response: An intercomparison of non-linear hillslope response." *Journal of Hydrology,* 311, 117– 133.

Vadivelu, S., Sen, T. K., Bhaskar, B. P., Baruah, U., Sarkar, D., Maji, A. K., and Gajbhiye, K. S. (2004). *Soil series of Assam*, Technical Bulletin, NBSS Publ. 101, National Bureau of Soil Survey and Land Use Planning, Indian Council of Agricultural Research, India.

van Genuchten, M.T. (1980). "A closed-form equation for predicting hydraulic conductivity of unsaturated soils." *Soil Sci. Soc. Am. J.,* 44, 892-898.

van Schaik, N.L.M.B. (2009). "Spatial variablity of infiltration patterns related to site characteristics in semi-arid watershed." *Catena*, 78, 36-47.

van Schaik, N.L.M.B. (2010). *The role of macropore flow from PLOT to catchment scale*: *A study in a semi-arid area*, Netherlands Geographical Studies 390.

van Schaik, N.L.M.B., Schnabel, S., and Jetten, V.G. (2008). "The influence of preferential flow on hillslope hydrology in semi-arid watershed (in the Spanish Dehesas)." *Hydrological Processes*, 22, 3844-3855.

van Schaik, N.L.M.B., Hendriks, R.F.A., and van Dam, J.C. (2010). "Parameterization of macropore flow using dye-tracer infiltration patterns in the SWAP model." *Vadose Zone Journal*, 9(1), 95-106.

van Stiphout, T.P.J, van Lanen, H.A.J., Boersma, O.H., and Bouma, J. (1987). "The effect of bypass flow and internal catchment of rain on the water regime in a clay loam grassland soil." *Journal of Hydrology,* 95, 1-11.

Van't Woudt, B.D. (1955). "On a hillside moisture gradient in volcanic ash soil, New Zealand." *Trans. Am. Geophys. Union*, 36(3), 419-424.

Venkatesh, B., Lakshman, N., Purandara, B.K., and Reddy, V.B. (2011). "Analysis of observed soil moisture patterns under different land covers in Western Ghats, India." *Journal of Hydrology,* 397, 281-294.

Vertessy, R.A. and Elsenbeer, H. (1999). "Distributed modeling of storm flow generation in an Amazonian rain forest catchment: Effects of model parameterization." *Water Resour. Res.*, 35(7), 2173-2187.

Vogel, T., Brezina, J., Dohnal, M., and Dusek, J. (2010a). "Physical and numerical coupling in dual-continuum modeling of preferential flow." *Vadose Zone Journal*, 9(2), 260-267.

Vogel, T., Sanda, M., Dusek, J., Dohnal, M., Votrubova, J. (2010b). "Using oxygen-18 to study the role of preferential flow in the formation of hillslope runoff." *Vadose Zone Journal*, 9(2), 252-259.

Wagenet, R.J. (1998). "Scale issues in agroecological research chains." *Nutr. Cycling Agroecosyst.*, 50, 23–34.

Wahl, N.A., Buczko, U., Bens, O., and Hüttl, R.F. (2003). "Infiltration capacity and macroporosity of a silty-loamy soil under different tillage systems." *Geophysical Research Abstracts*, 5, 05326.

Wakahama, G. (1974). "The role of meltwater densification processes of snow and rain", in *Snow Mechanics*, Proceedings of the Grindelwald Symposium, Int. Assoc. Sci. Hydrol., Washington, D.C., 66-72.

Walter, M.T., Steenhuis, T.S., Mehta, V.K., Thongs, D., Zion, M., and Schneiderman, E. (2002). "Refined conceptualization of TOPMODEL for shallow subsurface flows." *Hydrological Processes*, 16, 2041–2046

Wang, G.T., Chen, S.L., Boll, J., Stockle, C.O., and McCool, D.K. (2002). "Modelling overland flow based on Saint-Venant equations for a discretized hillslope system." *Hydroloical Processes,* 16, 2409-2421.

Wang, K., Zhang, R., and Yasuda, H. (2006). "Characterizing heterogeneity of soil water flow by dye infiltration experiments." *Journal of Hydrology*, 328, 559-571.

Weibel, E.R. (1979). *Stereological methods*, *Vol. 1 Practical methods for biological morphometry*, Academic Press, London.

Weiler, M. (2001). "Mechanisms controlling macropore flow during infiltration: Dye tracer experiments and simulations." Ph.D Thesis, Swiss Federal Institute of Technology, Zurich, Switzerland.

Weiler, M. (2005). "An infiltration model based on flow variability in soil macropores: development, sensitivity analysis and applications." *Journal of Hydrology*, 310, 294-315.

Weiler, M., McDonnell, J.J., Tromp-van Meerveld, I., and Uchida, T. (2005). *Subsurface stormflow*, Encyclopedia of Hydrological Sciences.

Weiler, M. and Flühler, H. (2004). "Inferring flow types from dye patterns in macroporous soils." *Geoderma*, 120(1–2), 137–153.

Weiler, M. and McDonnell, J. (2004). "Virtual experiments: a new approach for improving process conceptualization in hillslope hydrology." *Journal of Hydrology*, 285(1-4), 3-18.

Weiler, M., and McDonnell, J.J. (2007). "Conceptualizing lateral preferential flow and flow networks and simulating the effects on gauged and ungauged hillslopes." *Water Resour. Res.,* 43, W03403, doi:10.1029/2006WR004867.

Weiler, M., and Naef, F. (2003). "An experimental tracer study of the role of macropores in infiltration in grassland soils." *Hydrologic Processes,* 17(2), 477-493.

Weiler, M., Naef, F., and Leibundgut, C. (1998). **"**Study of runoff generation on hillslopes using tracer experiments and a physically based numerical hillslope model." *IAHS Publication* 248, 353-360.

Weyman, D.R. (1973). "Measurements of the downslope flow of water in soil." *Journal of Hydrology*, 20, 267-288.

Whalley, W.R. (1993). "Considerations on the use of time-domain reflectometry for measuring soil water content." *J. Soil Sci.*, 44, 1-9.

Whipkey, R.Z. (1965). "Subsurface stormflow from forested slopes." *Bull. Intern. Assoc. Sci. Hydrology*, 10(3), 74-85.

Whipkey, R.Z. (1969). "Storm runoff from forested catchments by subsurface routes." *Publ. Internat. Assoc. Sci. Hydrology*, 85(2), 773-779.

Wilkins, D.E., Buchele, W.F., and Lovely, W.G. (1977). "A technique to index soil pores and aggregates larger than 20 μm." *Soil Sci. Soc. Am. J.*, 41(1), 139-170.

Wu, Fu-Chun., Shen, H.W. and Chou, Yi-Ju. (1999). "Variation of roughness coefficients for unsubmerged and submerged vegetation." *Journal of Hydraulic Engineering,* 125(9), 934-942.

Yeakley, J.A., Swank, W.T., Swift, L.W., Hornberger, G.M., and Shugart, H.H. (1998). "Soil moisture gradients and controls on a southern Appalachian hillslope from drought through recharge." *Hydrol. Earth Sys. Sci.*, 2(1), 41-49.

Zehe, E. and Flühler, H. (2001). "Slope scale variation of flow patterns in soil profiles." *Journal of Hydrology*, 247, 116-132.

Zehe, E., Maurer, T., Ihringer, J., and Plate, E. (2001). "Modeling water flow and mass transport in a loess catchment." *Phys. Chem. Earth* (B), 26(7-8), 487-507.

Zhang, G.P., Savenije, H.H.G., Fenicia, F., and Pfister, L. (2006). "Modelling subsurface storm flow with the Representative Elementary Watershed (REW) approach: Application to the Alzette River Basin." *Hydrol. Earth Syst. Sci.*, 10, 937–955.

Ziegler, A.D., Giambelluca, T.W., Tran, L.T., Vana, T.T., Nullet, M.A., Fox, J., Vien, T.D., Pinthong, J., Maxwell, J.F., and Evett, S. (2004). "Hydrological consequences of landscape fragmentation in mountainous northern Vietnam: evidence of accelerated overland flow generation." *Journal of Hydrology*, 287(1–4), 124–146.

LIST OF RELEVANT PUBLICATIONS

Research papers in peer reviewed Journals/Books:

1. **Rupak Sarkar**, Subashisa Dutta and Sushma Panigrahy(2008). "Characterizing Overland Flow on a Preferential Infiltration Dominated Hillslope: Case Study", ***Journal of Hydrologic Engineering*** **(ASCE)**, Vol. 13, No. 7, 563-569.

2. Sudipta Kumar Mishra, **Rupak Sarkar**, Subashisa Dutta and Sushma Panigrahy (2008). "A Physically Based Hydrological Model for Paddy Agriculture Dominated Hilly Watersheds in Tropical Region". ***Journal of Hydrology*** **(Elsevier),** Vol. 357, 389-404.

3. **Rupak Sarkar,** Subashisa Dutta and Sushma Panigrahy (2008). "Effect of scale on infiltration in a macropore dominated hillslope". ***Current Science***, Vol. 94, No. 4, 490-494.

4. **Rupak Sarkar** and Subashisa Dutta (2009). "An experimental and modelling investigation of macropore dominated subsurface stormflow in vegetated hillslopes of northeast India." In Yilmaz, K.K, Yucel, I., Gupta, H.V., Wagener, T., Yang, D., Savenije, H., Neale, C., Kunstmann, H., and Pomeroy, J. (Eds.) *New approaches to hydrological prediction in data-sparse regions*, ***International Association of Hydrological Sciences*** **(IAHS)** ***Publication*** **333**, 145-152.

5. Sangeeta Shougrakpam, **Rupak Sarkar**, and Subashisa Dutta (2010). "An experimental investigation to characterise soil macroporosity under different land use and land covers of northeast India". ***Journal of Earth System Science*** **(Springer)**, Vol. 119, No. 5, 655-674.

6. **Rupak Sarkar** and Subashisa Dutta (2011). "Field investigation and modeling of rapid subsurface stormflow through preferential pathways in a vegetated hillslope of northeast India: Case Study.", ***Journal of Hydrologic Engineering*** **(ASCE)**, Article in Press, (doi: 10.1061/(ASCE)HE.1943-5584.0000431).

International Conferences/Workshops:

1. **Rupak Sarkar**, Subashisa Dutta and Sushma Panigrahi (2006). "Hydrological Response of Hillslopes in the Brahmaputra Basin: An Experimental and Modeling Investigation", In *An International Perspective on Environmental and Water Resources,* December 18-20, 2006, New Delhi, India. Organized by: Environmental and Water Resources Institute **(EWRI) of ASCE** and **IIT Kanpur, INDIA.**
2. **Rupak Sarkar,** Animesh Singh**,** Subashisa Dutta and Sushma Panigrahy (2007). "Characterising Subsurface Stormflow in a Preferential Flow Dominated Natural Hillslope", In *International Workshop on Integrated Water Resources Management* – **(IWRM-2007)**, February 5-7, 2007, Bangalore, India. Organized by: Karnataka Environment Research Foundation.
3. **Rupak Sarkar** and Subashisa Dutta (2008). "An experimental and modeling investigation on macropore dominated subsurface storm flow in vegetated hillslopes of North-East India." In International Workshop on *Agricultural Ecosystem and Sustainable Development in Brahmaputra Basin.* Assam, India. Organized by: Gauhati University, Guwahati, Assam and Centre for Southeast Asian Studies, Kyoto University, Japan on 19-20th December, 2008.

National Conferences:

1. Subashisa Dutta and **Rupak Sarkar** (2006). "Subsurface Stormflow Study for Hydrological Extremities Management in North-Eastern India", In the National Conference *NEGeo-2006 – Developing North East Geospatially.* September 21-22, 2006, Guwahati, India
2. **Rupak Sarkar,** Shyamal Ghosh, Subashisa Dutta and Sushma Panigrahy (2007). "Subsurface Stormflow in A Preferential Infiltration Dominated Natural Hillslope in Brahmaputra River Basin", XXVI National Seminar on Hydrology on *Rainfall Versus Water Resources in North-East India.* Organized by: Association of Hydrologists of India in association with Department of Geography, North-Eastern Hill University, 26 - 28th October, 2007, Shillong, India.